Novel Anion-bound Borates as Lubricant Additives

Katherine Mary Shaw, MSci (Hons)

Thesis submitted to the University of Nottingham for the degree of

Doctor of Philosophy

October 2016

Declaration

The work described in this thesis was carried out at the University of Nottingham between October 2012 and June 2016, under the supervision of Dr Deborah L. Kays. All of the work is my own unless stated to the contrary, and has not previously been submitted for any degrees at this or any other university.

Katherine M Shaw

Abstract

Effective anti-wear lubricant additives are highly desirable in order to improve the performance and lifetime of automotive engines and transmission systems, whilst keeping in line with environmental standards. Although there has been recent research interest into the use of additives containing both boron and phosphorus, the field is rather underdeveloped and there is much scope for further exploration of this area. To this end, this thesis describes the synthesis and anti-wear testing of a series of novel phosphate-bound borate potential lubricant additives.

An investigation into pyroborate compounds, a key building block of these additives, is presented. The synthesis of a range of known and novel pyroborates is reported, and $(3\text{-MeOcatB})_2O$ is crystallographically characterised. Analysis of the Lewis acidity of these species *via* the Gutmann-Beckett method is discussed, revealing loss of acidity when alkyl substituents and nitrogen donor atoms are introduced. A preliminary DFT study of $(catB)_2O$, $(3\text{-MeOcatB})_2O$, $(Naph\text{-}1,2\text{-}O_2B)_2O$, $(Ph\{NH\}_2B)_2O$ and $(pinB)_2O$ indicates that Lewis acidity depends on both the size and energy of the empty p_z orbitals on the boron centres only in the case of alkoxy-donor species.

The synthesis of a range of novel four-coordinate bis-borate species *via* a largely solvent-free methodology is reported and the crystallographic analysis of a selection of these compounds is presented. A preliminary study indicates very weak conductivity of these species, due to lack of solubility and large ionic radii. This presents a starting point for the further variation of such species for electrochemical applications.

The use of short-chain anion-bound pyroborate species as models for longer-chain additive compounds is discussed. The synthesis of a range of model species is reported, and a study of their solution-phase behaviour carried out by NMR spectroscopy. The

anion-binding behaviour of a selection of these species is discussed and the binding strength of $(catB)_2O$ and (3-MeO$catB_2O$) with several anions compared. The extension of this methodology to long-chain analogues is presented, highlighting the hydrolytic stability and scalability offered by such species.

The screening of the lubricant suitability of a range of long-chain phosphate-bound borate species is discussed, with attention paid to hydrolytic stability and oil-solubility. The testing of the suitable additives under engine oil and driveline conditions is presented, and the resulting wear scar diameters, coefficients of friction and contact potentials discussed. This offers insight into the structure-performance relationship at play in these systems, indicating structural motifs to be avoided in the design of these additives. The comparison of the performance of these compounds with existing anti-wear additives is presented, with many of these novel phosphate-bound species offering superior anti-wear activity, particular those of lower molecular weight. Further testing of the high-performing additive $\{HN^nBu_3\}\{[(4\text{-}PIB_{1000}catB)_2O][H^nBuPO_4]\}$ in both engine oils and driveline tests indicates the strong promise of these compounds as a new family of lubricant additives.

Acknowledgements

First and foremost I would like to thank my supervisor Debbie for her support, advice and encouragement throughout my PhD, and for giving me so much ownership of the project. I'd also like to thank Prof. Neil Champness for his supervision and advice in the final stage of my PhD.

Thank you to everyone at Lubrizol Corp. who were involved with my project, particularly Ed Sampler and Nicolas Nouvel for their time and significant input, Sam Kilsby for help with alkyl catechol synthesis, Mark McGuiness for his continued helpful advice, and Zahra Hussain and John Durham for HFRR measurements. I am also extremely grateful to Lubrizol Corp. for the funding of my PhD project.

Many thanks go to all members of the Kays group, past and present, for their help, support and friendship, especially Helen, whose friendship has been invaluable during this time. I'd like to thank the Liddle and Champness groups, for the fun and help they've provided, and my other friends in the School, particularly Kev and Jeremy, who've helped keep me sane. Thank you to Nic Pearce for running DFT calculations, Lyndsey Knight for solid-state NMR, Steven Maxwell-Hogg for conductivity measurements and Lixu Yang for her extremely helpful discussions on NMR titrations. I am also grateful to my project student Anna, who contributed to this work.

Thanks go to the technical and stores staff at the University of Nottingham, particularly Shaz, Adrienne and Kev for NMR support, Graeme, Mick and Ben for mass spectrometry, Sandy and especially Will for their assistance and patience with X-ray crystallography, Mark Guyler for helping us to keep the lab running, and Sue for vital daily tea and friendly chats. Thank you also to Stephen Boyer, of London Metropolitan University, for elemental analyses, the EPSRC National Mass Spectrometry Facility,

Swansea, for additional mass spectrometry measurements and MEDAC Ltd for air-sensitive ICP analysis.

I'd like to thank my family for their support, particularly my mum who has listened to my random phone calls every week.

Finally, I'd like to not only thank but dedicate this thesis to my wonderful husband, Ryan, whose unconditional love, support and patience keeps me going.

Much of this work is covered in a patent entitled ‘LUBRICATING COMPOSITIONS COMPRISING AN ANTI-WEAR/FRICTION MODIFYING AGENT’, filed in March 2015 and awaiting publication.

Contents

Declaration ii

Abstract iii

Acknowledgements v

Contents viii

List of Figures xiv

List of Schemes xix

List of Tables xxi

Abbreviations xxiv

Chapter I – Introduction 1

1.1 Friction and Lubrication 2

1.2 Base Oils 4

1.3 Engine Oil and Driveline Lubricants 9

1.4 Lubricant Additives 11

1.4.1 Detergents and Dispersants 12

1.4.2 Antioxidants 15

1.4.3 Wear and Anti-wear Additives 18

1.4.3.1 Phosphorus-containing Anti-wear Additives 23

1.4.3.2 Boron-containing Anti-wear Additives 31

1.4.3.2.1 Inorganic Boron Additives 31

1.4.3.2.2 Organic Borate Additives 34

1.4.3.3 Additives Containing Both Boron and Phosphorus 39

1.5 Aims of this Research 43

Chapter II – General Experimental Techniques 44

2.1 Manipulation of Air-sensitive Compounds 45

2.2 Physical Measurements 47

2.2.1 NMR Spectroscopy 47

2.2.2 Mass Spectrometry 47

2.2.3 Elemental Microanalysis 48

2.2.4 ICP-OES Analysis 48

2.2.5 UV/vis Spectroscopy 48

2.2.6 X-ray Crystallography 49

2.2.7 Computational Chemistry 49

2.2.8 Conductivity 50

2.3 Preparation of Solvents and Reagents 51

2.4 Preparation of Precursors 52

2.4.1 General Procedure for the Synthesis of Mono-alkyl 52

Phosphate Esters

2.4.2 General Procedure for the Synthesis of Ammonium Phosphates 55

Chapter III – Pyroborate Compounds 66

3.1 Introduction 67

3.2 Experimental 74

3.2.1 General Procedure for the Synthesis of PIB Catechols 74

3.2.2 General Procedure for the Synthesis of Straight-chain Alkyl Catechols 75

3.2.3 General Procedure for the Synthesis of Pyroborate Esters 77

3.2.4 Lewis Acidity Determination 86

3.3 Results and Discussion 87

3.3.1 Synthesis of Pyroborate Compounds 87

3.3.2 Lewis Acidity of Pyroborate Compounds 95

3.3.3 Computational Chemistry 98

3.4 Conclusions 102

3.5 Future Work 104

Chapter IV – Four-coordinate Bis-borate Compounds 106

4.1 Introduction 107

4.2 Experimental 112

4.2.1 General Procedure for the Synthesis of Ammonium Bis-borates 112

4.3 Results and Discussion 122

4.3.1 Synthesis of Four-coordinate Bis-borate Compounds 122

4.3.2 Crystallographic Analysis 125

4.3.3 Conductivity Study 139

4.4 Conclusions 142

4.5 Future Work 144

Chapter V – Anion-binding Studies 146

5.1 Introduction 147

5.2 Experimental 154

5.2.1 Synthesis 154

5.2.2 NMR Binding 172

5.3 Results and Discussion 174

5.3.1 Short-chain Model Anion-bound Borate Compounds 174

5.3.1.1 Studies into Dihydrogen Phosphate Model Compound 174

5.3.1.2 Synthesis and Studies into *n*-Butylphosphate-bound Model Compound 184

5.3.1.3 Synthesis of Alkylphosphate-bound Model Compounds 197

5.3.1.4 Synthesis of Other Anion-bound Model Compounds 203

5.3.2 Anion Binding Studies of Model Compounds 207

5.3.2.1 Binding Stoichiometry 208

5.3.2.1.1 Binding Stoichiometry of Alkylphosphates 208

5.3.2.1.2 Binding Stoichiometry of Other Anions 212

5.3.2.2 NMR Titrations 213

5.3.3 Synthesis of Long-chain Anion-bound Compounds 216

5.4 Conclusions 222

5.5 Future Work 225

Chapter VI – Anti-wear Testing of Additives 227

6.1 Introduction 228

6.2 Experimental 232

6.3 Results and Discussion 233

6.3.1 Screening of Compounds for Lubricant Suitability 233

6.3.2 Single Component HFRR Testing 236

6.3.2.1 Engine Oil Single Component Testing 237

6.3.2.1.1 Wear 237

6.3.2.1.2 Friction 240

6.3.2.1.3 Contact Potential 242

6.3.2.2 Driveline Single Component Testing 246

6.3.2.2.1 Wear 246

6.3.2.2.2 Friction 250

6.3.2.2.3 Contact Potential 252

6.3.3 Further Engine Oils Testing 255

6.3.4 Fully Formulated Driveline HFRR Testing 257

6.4 Conclusions 261

6.5 Future Work 264

Chapter VII – Global Conclusions 266

7.1 Global Conclusions 267

Appendix I – Crystallography Data Tables 273

Appendix II – Job Plot and NMR Titration Data 276

Appendix III – Anti-wear Testing Data 302

References 320

List of Figures

Figure 1.1 Simplistic diagram of a shaft in a bore when (a) static and (b) running under hydrodynamic lubrication regime. 3

Figure 1.2 Boundary lubrication regime. 4

Figure 1.3 Generalised Stribeck curve showing typical lubrication regimes. 5

Figure 1.4 General structures of synthetic (a) diesters, (b) phthalates and (c) polyolesters. 8

Figure 1.5 Generic structure of (a) detergent and (b) dispersant additives. 12

Figure 1.6 General representation of lubricant detergent reverse micelle containing calcium carbonate. 14

Figure 1.7 Schematic representation of the range of wear coefficient (K) exhibited under different wear regimes. 19

Figure 1.8 Mechanism of adhesive wear from formation of slip lines (a) to generation of wear particles (c) to transfer of wear debris (d). 21

Figure 1.9 General structure of ZDDPs. 24

Figure 1.10 Structure of the tri-para isomer of tricresyl phosphate (TCP). 25

Figure 1.11 Alternative models of TCP adsorption and reaction on steel. 26

Figure 1.12 The structure of a long-chain phosphoric acid used as an anti-wear additive. 27

Figure 1.13 Structures of diphosphate additives (a) HDP and (b) DDP. 28

Figure 1.14 Structures of thiophosphates tested for anti-wear performance. 28

Figure 1.15 The structure of lithium molybdophosphate additive. 29

Figure 1.16 Structures of (a) choline bis(2-ethylhexyl) phosphate and (b) choline dibutyl dithiophosphate. 30

Figure 1.17 The crystal structure of hexagonal boron nitride. 31

Figure 1.18 Surface damage (%) using different lubricants on a steel surface. 32

Figure 1.19 Lamellar structure of boric acid. 33

Figure 1.20 The general structure of Schiff base-containing borate esters. 34

Figure 1.21 The general structure of heterocylic-containing borate esters. 35

Figure 1.22 The general structure of thiodiazole-containing borate esters. 36

Figure 1.23 Structure of benzothiazole-containing anti-wear additive, highlighting stabilisation via conjugation into empty p_z orbital on boron. 37

Figure 1.24 Variation in wear scar diameter for different concentrations of a boron-containing thiophosphite (BTP) additive and an analogous boron-free additive (TP). 37

Figure 1.25 Tri(hydroxymethyl)propane borate esters. 38

Figure 1.26 Structure of borophosphate glass. 39

Figure 1.27 Structure of DOB-DTP. 40

Figure 1.28 Structure of phosphate/borate compound based on soybean lecithin. 41

Figure 1.29 Structure of orthoborate-phosphonium ionic liquids. 42

Figure 2.1 Schlenk line apparatus. 45

Figure 3.1 (a) The structure of pyroboric acid and (b) alkenyl pyroborate compound used as a fuel additive to lower carburettor deposits. 67

Figure 3.2 Example of an amido pyroborate used as a fuel/lubricant additive. 69

Figure 3.3 Bonding model for three-coordinate borate compounds. 69

Figure 3.4 Hydrolytically stable ammonium pyroborate lubricant additive. 70

Figure 3.5 Catalytic cycle for the formation of boryl silyl ethers in the reaction of $(pinB)_2O$ and hydrosilanes. 71

Figure 3.6 The molecular structure of **[3]**, $(3\text{-MeOcatB})_2O$. 90

Figure 3.7 Side-on view of the molecular structure of **[3]**, illustrating the deviation from planarity. 91

Figure 3.8 DFT Calculated optimised structure of **[5]**, indicating high degree of twist in the molecule. 98

Figure 3.9 DFT Calculated Molecular Orbital Energies for LUMOs (**[11]**, **[1]** and **[3]**), LUMO+1 (**[13]**), LUMO+2 (**[5]**) and LUMO+4 (**[10]**). 99

Figure 3.10 Electron-deficient catechol species to be used in future work. 104

Figure 4.1 Example of a four-coordinate borate-containing anti-wear additive. 107

Figure 4.2 The structures of (a) LiMOB and (b) LBDOB. 109

Figure 4.3 Fluorescent four-coordinate bis-borate compound which selectively binds chloride. 110

Figure 4.4 The molecular structure of **[18]**, $[HNEt_3][cat_2B]$. 126

Figure 4.5 The molecular structure of **[19]**, $[HN^nBu_3][cat_2B]$. 126

Figure 4.6 The molecular structure of $[HN^nBu_3][3\text{-}MeOcat_2B]$ **[26]** (left) and $[HNEt_3][Br_4cat_2B]$ **[28]** (right). 127

Figure 4.7 Packing of anionic portion of [28], showing possible Br···Br contacts. 128

Figure 4.8 The molecular structure of **[32]**, 129

Figure 4.9 The molecular structure of **[33]**, 129

Figure 4.10 Anion components of **[18]**, **[19]**, **[26]**, **[32]** and **[33]**, showing degree of bending away from approximate D_{2d} symmetry. 136

Figure 4.11 The asymmetric unit of the solid-state structure of **[21]**, $[H_3N^nBu][cat_2B]$. 137

Figure 4.12 Possible further variation in catechol species. 144

Figure 4.13 Possible further variation in amine. 145

Figure 5.1 Indolocarbazole compounds which bind anions through hydrogen bonds. 148

Figure 5.2 A macrocyclic compound which selectively binds $H_2PO_4^-$. 149

Figure 5.3 Ammonium boranes for used for sensing (a) CN^- and (b) F^-. 151

Figure 5.4 Heteronuclear bidentate receptors which effectively bind F^-. 152

Figure 5.5 Dialuminium compound which is able to complex NO_3^-. 153

Figure 5.6 Pyroborate anion-bound compounds. 153

Figure 5.7 Molecular structure of **[36]**, $[N^nBu_4][cat_2B]$. 176

Figure 5.8 $^{11}B\{^1H\}$ NMR spectra resulting from gradual addition of $(catB)_2O$ to $[N^nBu_4][H_2PO_4]$. 178

Figure 5.9 $^{31}P\{^1H\}$ NMR spectra resulting from gradual addition of $(catB)_2O$ to $[N^nBu_4][H_2PO_4]$. 179

Figure 5.10 $^{11}B\{^1H\}$ NMR spectra resulting from gradual addition of $[N^nBu_4][H_2PO_4]$ to $(catB)_2O$. 179

Figure 5.11 $^{31}P\{^1H\}$ NMR spectra resulting from gradual addition of $[N^nBu_4][H_2PO_4]$ to $(catB)_2O$. 181

Figure 5.12 $^{11}B\{^1H\}$ NMR spectra resulting from gradual addition of $[N^nBu_4][H_2PO_4]$ to $(catB)_2O$ – above 1 equivalents. 182

Figure 5.13 $^{31}P\{^1H\}$ NMR spectra resulting from gradual addition of $[N^nBu_4][H_2PO_4]$ to $(catB)_2O$ – above 1 equivalents. 183

Figure 5.14 ^1H NMR spectra of **[37]** at 25 °C and −70 °C. 187

Figure 5.15 $^{31}P\{^1H\}$ NMR spectra of **[37]** at 25 °C and −70 °C. 189

Figure 5.16 $^{11}B\{^{1}H\}$ NMR spectra of **[37]** between 25 °C and −70 °C. 189

Figure 5.17 $^{11}B\{^{1}H\}$ NMR spectra of **[37]** at 25 °C and 50 °C. 191

Figure 5.18 Solid-state NMR spectrum of **[37]**. 192

Figure 5.19 $^{11}B\{^{1}H\}$ NMR spectra of **[38]** at 25 °C and −70 °C. 199

Figure 5.20 $^{11}B\{^{1}H\}$ NMR spectra of **[45]** at 25 °C and 50 °C. 202

Figure 5.21 Representative Job plot, indicating the location of maxima for a variety of binding stoichiometries. 209

Figure 6.1 Simplified diagram of HFRR setup. 229

Figure 6.2 Typical “bad” (top), “marginal” (middle) and “good” (bottom) fuels tested by HFRR. 230

Figure 6.3 Structure of control compound **[56]**. 237

Figure 6.4 Average engine oil wear scar diameter (μm) of tested compounds. 238

Figure 6.5 Average engine oil coefficient of friction of tested compounds. 241

Figure 6.6 Average engine oil contact potential (%) of tested compounds. 244

Figure 6.7 Average driveline wear scar diameter (μm) of tested compounds. 248

Figure 6.8 Average driveline coefficient of friction of tested compounds. 250

Figure 6.9 Average driveline contact potential (%) of tested compounds. 252

Figure 6.10 Structures of model compound **[37]** and its PIB_{1000} analogue **[53]**. 255

Figure 6.11 Antioxidancy of **[53]**. 256

Figure 6.12 Microcoker test results for **[53]**. 256

Figure 6.13 Hot tube test results for **[53]**. 257

Figure 6.14 Average fully formulated driveline wear scar diameters (μm). 258

Figure 6.15 Average fully formulated driveline coefficients of friction. 258

Figure 6.16 Average fully formulated driveline contact potentials (%). 260

List of Schemes

Scheme 1.1 General synthesis of PAOs from α-olefins. 6

Scheme 1.2 Synthesis of overbased detergent additives. 13

Scheme 1.3 Synthesis and structures of mono-, bis- and tris-succinimide dispersant molecules. 15

Scheme 1.4 Oxidation chain reaction. 16

Scheme 1.5 Antioxidant mechanism for hindered phenol antioxidants. 17

Scheme 1.6 Regeneration of aminic antioxidant from phenolic antioxidant. 17

Scheme 1.7 General synthesis of ZDDPs. 25

Scheme 3.1 Reactions of diphenyldiboroxane. 67

Scheme 3.2 Diboroxane-containing FLP in activation of CO_2. 72

Scheme 3.3 Formation of VAPOL BOROX catalyst from pyroborate precatalyst. 72

Scheme 3.4 Synthesis of pyroborate esters. 88

Scheme 3.5 Synthesis of alkyl catechols. 89

Scheme 3.6 Modification of o-phenylenediamine. 104

Scheme 3.7 Possible synthetic route to dimeric pyroborate species. 105

Scheme 4.1 Synthesis of bis-borate compounds. 122

Scheme 4.2 Potential synthesis of lithium bis-borate species. 145

Scheme 5.1 Attempted synthesis of dihydrogen phosphate-bound compound. 174

Scheme 5.2 Reactions of triphenylborate and suggested reaction products. 184

Scheme 5.3 Attempted syntheses of proposed catechol-free borate-phosphates. 186

Scheme 5.4 Synthesis of model compound **[37]**. 186

Scheme 5.5 Possible formation of fluorinated compound upon reaction with TMAF. 194

Scheme 5.6 Synthesis of Model Anion-bound Borate Compounds. 195

Scheme 5.7 Synthesis of long-chain phosphate-bound borate compounds. 216

Scheme 5.8 Possible synthesis of a family of novel borate-phosphate species. 226

Scheme 6.1 Synthesis of shorter-chain catechols. 265

List of Tables

Table 1.1 Lubrication regimes in automotive engines. 10

Table 1.2 Typical lubricant composition of petrol and diesel engines oils. 10

Table 1.3 Typical composition of automatic transmission fluid. 11

Table 2.1 Variable $^{31}P\{^{1}H\}$ chemical shifts for H_3PO_4 peak in mono-alkyl phosphate ester spectra. 52

Table 3.1 Selected bond lengths and angles for **[3]**. 90

Table 3.2 Lewis acidity values of tested pyroborate compounds. 96

Table 3.3 DFT Calculated molecular orbital diagrams for LUMOs (**[11]**, **[1]** and **[3]**), LUMO+1 (**[13]**), LUMO+2 (**[5]**) and LUMO+4 (**[10]**). 100

Table 3.4 Bond lengths (Å) and angles (°) obtained through X-ray diffraction analysis and DFT calculations. 101

Table 4.1 Selected bond lengths (Å) and angles (°) for bis-borate compounds. 134

Table 4.2 Approximate deviations of anion from D_{2d} symmetry. 135

Table 4.3 Selected bond lengths (Å) and angles (°) for **[21]**. 138

Table 4.4 Hydrogen bond distances (Å) for **[21]**. 139

Table 4.5 Conductivity results for bis-borate compounds. 140

Table 5.1 Selected bond lengths (Å) and angles (°) for **[36]**, $[N^{n}Bu_4][cat_2B]$. 176

Table 5.2 Model anion-bound borate compounds. 196

Table 5.3 Comparison of line widths at half height $\nu_{1/2}$ (Hz) of $^{11}B\{^{1}H\}$ signals of different borate species ($\delta B \approx 14$ ppm). 198

Table 5.4 Binding constants (M^{-1}) for the binding of various anions to pyroborates **[1]** and **[3]**. 214

Table 5.5 Long-chain phosphate-bound borate compounds. 217

Table 6.1 Parameters for anti-wear testing of compounds. 232

Table 6.2 Screening of suitability of compounds as lubricant additives. 235

Table 6.3 Temperature at which film breakdown occurs at 200 g load. 245

Abbreviations

Ac	acetyl
AC	alternating current
AFM	atomic force microscopy
AN	acid number
AO	anti-oxidant
APCI	atmospheric pressure chemical ionisation
Ar	aromatic (NMR)
AW	anti-wear
Bn	benzyl
bn	billion
BOROX	chiral boroxinate
br	broad (NMR)
BTP	boron-containing thiophosphite additive
Bu	butyl
Cat	$O_2C_6H_4$-1,2
CCD	charge-coupled device
CIF	crystallographic information file
d	doublet (NMR)
DBPo	dibutylphosphonate
dd	double doublet (NMR)
DDP	1,5-dihydroxynaphthylene bis(diphenyl phosphate)
DFT	density functional theory
DL	driveline
DNA	deoxyribonucleic acid
DOB-DTP	S-di-n-octoxyboron-O,O′-di-n-octyldithiophosphate
DP	degree of polymerisation
EDS	energy dispersive X-ray spectroscopy
EHL	elastohydrodynamic lubrication
EI	electron impact ionisation
EO	engine oil
EO	ethylene oxide
EP	extreme pressure
ESI	electrospray ionisation
Et	ethyl
FLP	frustrated Lewis pair
GMO	glycerol mono-oleate
h-BN	hexagonal boron nitride
HDP	hydroquinone bis(diphenyl)phosphate
HFRR	high frequency reciprocating rig
HL	hydrodynamic lubrication
ICP-OES	inductively coupled plasma optical emission spectroscopy
ISO	international organization for standardization

LBDOB	[1,2-benzenediolato(2-)-O,O-oxalato]borate
LC-MS	liquid chromatography-mass spectrometry
LiMOB	lithium (malonato oxalate) borate
LUMO	lowest unoccupied molecular orbital
LZ	Lubrizol
m	multiplet (NMR)
MALDI-TOF	matrix assisted laser desorption/ionisation-time of flight
Me	methyl
Modtc	molybdenum dithio-carbamate
MS	mass spectrometry
M_w	molecular weight
Naph	naphthyl, $C_{10}H_7^-$
NMR	nuclear magnetic resonance
Oct	octyl, octect (NMR)
PAG	polyalkylglycol
PAO	polyalphaolefin
PDSC	pressure differential scanning calorimetry
Ph	phenyl
phen	phenanthroline, $C_{12}H_8N_2$
PIB	polyisobutylene
PIBSA	polyisobutylene succinic anhydride
pin	$O_2C_2Me_4$
PO	propylene oxide
ppm	parts per million
PPN	bis(triphenylphosphine)iminium
Pr	propyl
q	quartet (NMR)
qC	quaternary carbon (NMR)
quin	quintet (NMR)
rms	root mean squared
RNA	ribonucleic acid
rpm	revolutions per minute
s	singlet (NMR)
SBN	single-layer boron nitride
SEM	scanning electron microscopy
sept	septet (NMR)
sext	sextet (NMR)
t	triplet (NMR)
TBAF	tetrabutylammonium fluoride
TCP	tricresylphosphate
td	triple of doublets (NMR)
TEM	transmission electron microscopy
Tf	triflate
THF	tetrahydrofuran
TMAF	tetramethylammonium fluoride

TMS	trimethylsilane
TP	boron-free thiophosphite additive
UV/vis	ultraviolet/visible
v.br	very broad (NMR)
VANOL	3,3′-diphenyl-2,2′-bi-1-naphthol
VAPOL	2,2′-diphenyl-3,3′-(4-biphenanthrol)
XANES	X-ray absorption near edge structure
XPS	X-ray photoelectron spectroscopy
ZDDP	zinc dialkyldithiophosphate
δ	chemical shift (NMR)
$\nu_{1/2}$	line width at half height

Chapter I

Introduction

1. Introduction

1.1 Friction and Lubrication

Although friction is vital for many aspects of our daily lives, such as walking on the ground or driving a car along a road, it presents a significant challenge within a variety of fields, particularly those of industrial chemistry and engineering, as it wastes energy and reduces efficiency. Indeed, it has been reported that almost a third of the power generated by an automobile is lost *via* friction.[1] The cost of friction has been known to be significant since as early as 1966, when the so-called "Jost Report" estimated that over £500 million per annum could be saved in the UK by the effective use of tribological advances and lubrication technologies.[2] More recently, it has this year been estimated that the cost of friction and wear in China alone is upwards of ¥58 billion (£6.3 billion) a year.[3] The use of lubricating fluids to reduce the friction between two surfaces has been known since Ancient Egyptian times, as hieroglyphs have been discovered which depict slaves using a liquid, presumably water, to aid the movement of stone blocks.[4] Following this, oils and greases have been used to lubricate carriage bearings and machinery from the middle ages to the Industrial Revolution, when the effect of friction on machinery was more significant than ever.[5] All modern machines require lubricants, as the power generated by such equipment involves significant metal to metal contact, leading to the formation of high levels of friction, which must be overcome for work to be carried out.

Several lubrication regimes have been established since the late nineteenth century, when Reynold first proposed the mechanism of hydrodynamic lubrication.[6] Under this regime thick films of lubricant are present between two metal surfaces, typically a rotating shaft in a bore, lowering friction by keeping the two components well

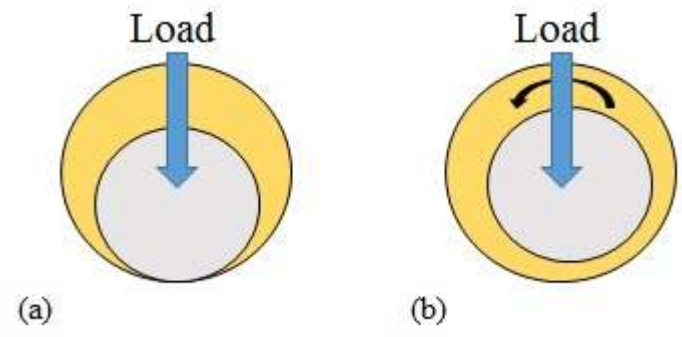


Figure 1.1 Simplistic diagram of a shaft in a bore when (a) static and (b) running under hydrodynamic lubrication regime.

separated (Figure 1.1). For this regime, lubricant viscosity must be controlled carefully, in order to achieve sufficient film thickness at high temperatures, whilst reducing pressure between the oil and the surfaces.

However, under high loads and low viscosities, the hydrodynamic lubrication regime does not apply, as the film thickness becomes so low that metal-to-metal contact occurs. This is particularly prevalent during the start-up and stopping of automotive engines, and is known as boundary lubrication. In this case, the tips of surface roughness (asperities) make contact and adhere to one another, leading to increased pressure between the surfaces (Figure 1.2). Bowden and Tabor have described this situation as "Switzerland inverted upon Austria, with only the mountain peaks in contact".[7] When this mechanism occurs, the nature of the surface films formed by the lubricant fluid is of vital importance, and is key to the reduction of friction between the two surfaces. Consequently, the viscosity of the fluid is of less importance during boundary lubrication than in other regimes, and the tribochemistry of the lubricant is significant.

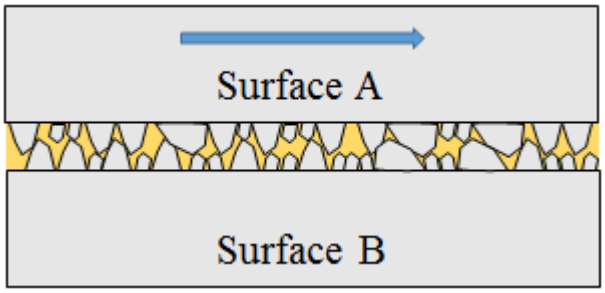


Figure 1.2 Boundary lubrication regime.

The range of lubrication mechanisms was completed by Dowson and Higginson, who demonstrated that extreme loading between contacts caused a plastic deformation of the materials together with a pressure-induced enhanced viscosity of the lubricant.[8] This is known as elastohydrodynamic lubrication, and higher loads than predictable may be carried by the contacts. Between this and boundary lubrication, there is also the mixed lubrication regime, which involves a mixture of the two and includes the period when friction begins to decrease as viscosity of the lubricant increases. These different regimes have been brought together in the so-called Stribeck curve, which demonstrates how friction between two contacts varies with viscosity, sliding speed and load (Figure 1.3).[5, 9] This may be used both to theoretically predict the behaviour of a lubricant under a particular set of conditions,[10] or used experimentally to indicate which lubrication mechanism is taking place in a system.[11]

1.2 Base Oils

The backbone of every lubricating fluid is the base oil, or mixture of base oils, which make up the bulk of its composition and which may be used to control the viscosity, fluidity and stability of the lubricant. Such base oils can be split into two broad categories: mineral and synthetic. Petroleum-derived mineral base oils, produced

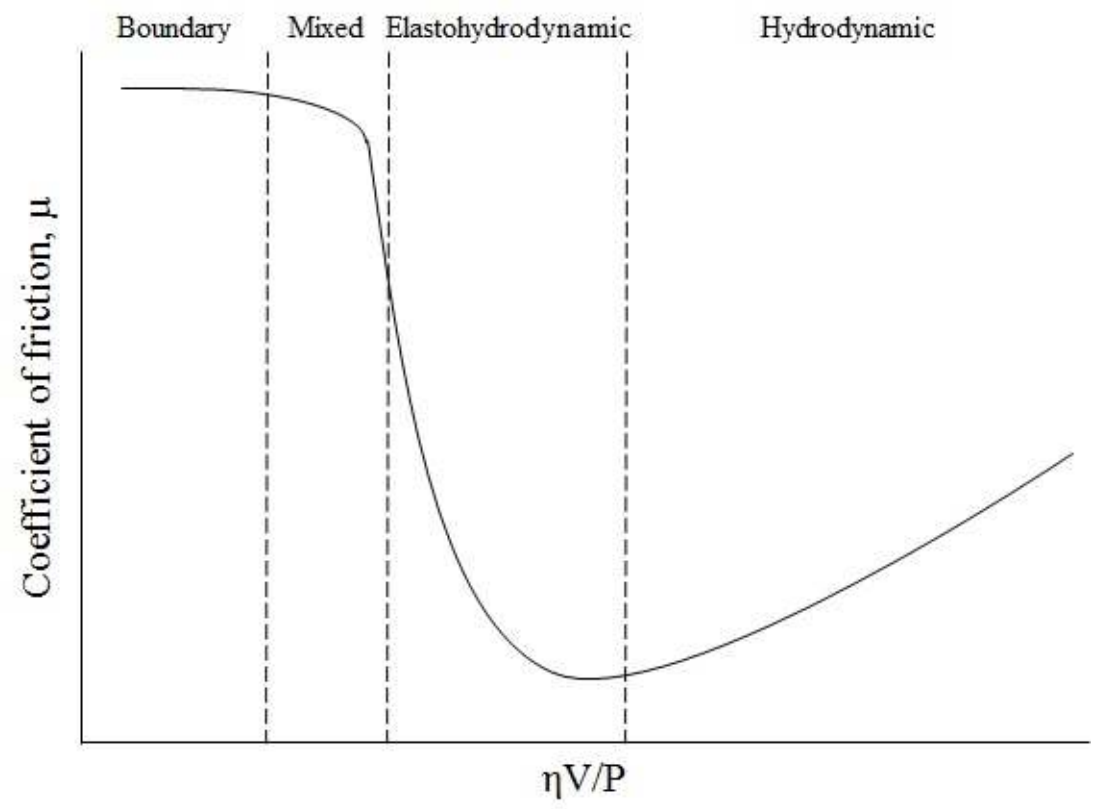
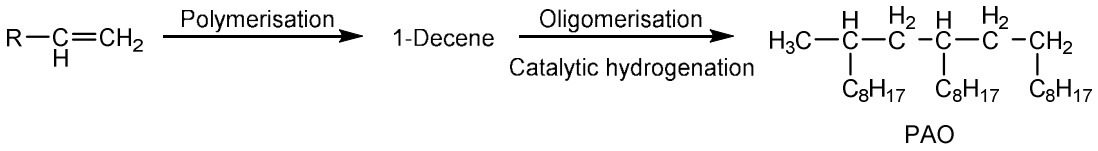


Figure 1.3 Generalised Stribeck curve showing typical lubrication regimes. η = fluid viscosity, V = sliding velocity, P = load.

from the refinement of crude oil, make up the majority of all base oils, being produced on a scale of 40 million tons and accounting for 97 % of all lubricants.[12] This is because mineral oils perform well, are easily available and are low-cost compared with their synthetic counterparts.[5] They are obtainable as by-products in the production of kerosene, but often need refinement due to the vast mixture of hydrocarbons present in the oil initially, which costs a great deal of energy. These include advantageous branched, paraffinic hydrocarbons and unwanted aromatic molecules and waxes, which must all be separated in a multi-step process. Moreover, the inherent mixture of compounds present in mineral oils leads to a limit in performance, as they are not tailored to their end use, and the engineering characteristics of each mineral oil are generally fixed once a certain viscosity has been reached.[13]

Although synthetic base oils have been investigated since the early 1930s,[14] due to their high cost they were not of commercial significance until after World War II, when the development of synthetic lubricant technology was necessary for military aero-engine performance over increasing temperature ranges.[5] Since this time, performance-driven synthetic oils have been developed for applications including aviation, space, military and high-performance industrial equipment.[9]

Polyalphaolefins (PAOs) are synthetic oils comprised of hydrogenated oligomers synthesised from C_8-C_{12} α-olefins which offer lubricant characteristics similar to highly refined paraffinic mineral oils.[15] They offer advantages over mineral oils due to their more narrowly defined molecular weight range, lower pour points, higher flash points, higher viscosity and lower volatility at high temperatures. Because of these superior properties, PAO-based lubricants have not only found popularity in the automotive industry, but have found niche uses in food grade applications, cosmetics, refrigeration, textiles, dielectric fluids, brake fluids and shock absorption.[16] In most cases, PAOs are synthesised from 1-decene, which may be firstly prepared *via* the polymerisation of other α-olefins (Scheme 1.1). This is then polymerised and hydrogenated to give the final saturated PAO.



Scheme 1.1 General synthesis of PAOs from α-olefins.[9]

Although the complex mixture of aromatic compounds found in mineral base oils are undesirable, synthetic alkylated aromatic hydrocarbons with well-defined structures

are useful in many specialist applications due to their excellent solvency and low pour-points, making them particularly useful in low-temperature applications such as in arctic machinery. Furthermore, their good thermal stability and compatibility with fluorinated hydrocarbons has seen the widespread use of alkylated aromatics as refrigerator oils.[5]

Polyisobutenes (PIBs), synthesised *via* the polymerisation of relatively inexpensive isobutene by-products of crude oil refinement, are an alternative synthetic base oil. They offer lower temperature stability than PAOs, which can be advantageous in high-temperature applications, where they decompose to gases, leaving no unwanted oily residues or deposits.[13] They are also highly compatible with mineral oils, providing mixtures with good metal wetting properties and improved film strength.[5] Furthermore, PIBs are well-established as viscosity modifiers, and can be blended with mineral and other synthetic oils to increase viscosity whilst providing the additional benefits of low toxicity and low cost.[17]

Prior to the early 19th century, most lubricants took the form of natural fatty acid esters found in sperm oil, lard oil and vegetable oils such as rapeseed oil. It is unsurprising, then, that synthetic esters have received significant interest as base oils, and have found use in engine oils, two-stroke oils, compressor oils and aviation lubricants.[5] This may be attributed to the many advantages offered by synthetic ester oils, including stability at extreme temperatures, high viscosity, low volatility and good compatibility with additives and other base oils.[18] Furthermore, the inherent biodegradability of synthetic esters has led to them being utilised in forestry

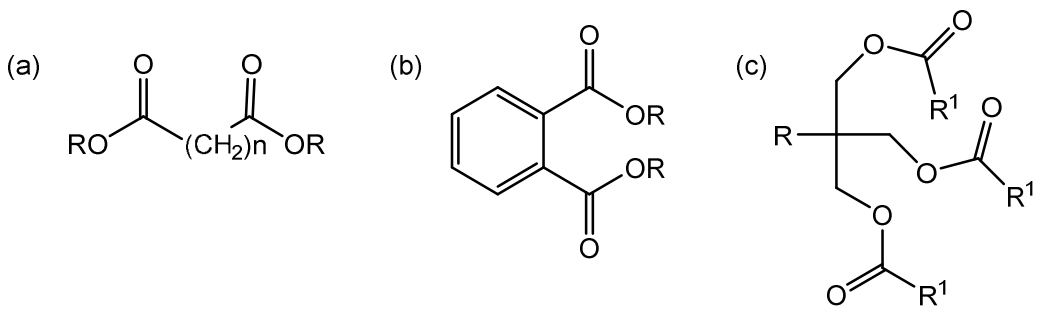


Figure 1.4 General structures of synthetic (a) diesters, (b) phthalates and (c) polyolesters.

and agricultural applications.[9] These esters may be constructed from a variety of alcohols and acids to give well-defined products of known composition and properties, and may generally by split into three categories: diesters, phthalates and polyolesters (Figure 1.4).

Polalkylglycols (PAGs) are another popular synthetic base oil, which are synthesised from alcohols and reactive alkylene oxides, typically ethylene or propylene oxide (EO/PO) to give the polymeric PAG.[5] Varying the initiating alcohol and quantities of alkylene oxide gives a vast range of PAGs with differing physical and tribological properties. For instance, random copolymerisation of EO and PO provides water soluble PAGs which have found use in fire-resistant hydraulic fluids and water-based metalworking fluids.[19] PAG structures may be finely tuned in order to provide a product with the desired properties, which is not possible with traditional hydrocarbon-based synthetic oils. This affords base oils with anti-wear and extreme pressure (EP) properties, high viscosities, low pour points, good thermal stability and low flash points.[5, 9] Furthermore, PAGs generally exhibit low toxicity and have found use as food grade lubricant oils.

Trialkyl or triaryl phosphate esters, of the general formula $O=P(OR)_3$, were originally commercialised as anti-wear additives (*vide infra*), but have since found use as synthetic base oils, particularly due to their excellent fire-resistant properties.[13] Indeed, US military-specified fire-resistant hydraulic fluid MIL-H-19457 is based on trixylenyl phosphate. The chemical, and hence lubrication, properties of phosphate esters can be varied considerably *via* the choice of substituents, and their inherent low pour-points have led to their use in low-temperature applications.[5] However, phosphate esters are more expensive than traditional base fluids, and so their performance must outweigh the higher cost of this base oil.

1.3 Engine Oil and Driveline Lubricants

There is a vast range of commercial lubricants used today, including industrial, automotive, driveline (transmission), aviation, spacecraft and marine lubricants, which must be tailored to suit their specific application. Automotive engine oils, constituting approximately 60 % of the total world lubricants and fluids, must carry out several functions in addition to reducing friction between moving parts: providing seals to cylinders, cooling the engine and transporting unwanted deposits and debris to the oil filter.[9] Engine oils are subjected to a wide range of temperatures and lubrication regimes, and so these lubricants must possess properties which meet all of these needs (Table 1.1). Engine oil lubricants typically comprise of a base oil, a package of additives and a viscosity modifier, and the relative quantities of these depend on whether the engine in use is petrol or diesel (Table 1.2).

Driveline lubricating fluids operate in the transmission system of an automobile, including the gear box, clutch, axles and propeller shaft. The different designs of gears and their operating parameters make each system unique, providing an extremely

challenging environment for lubricants. Furthermore, the transmission system contains several components which must all be protected by a single oil. The key property of any driveline fluid is its friction-reducing performance, to ensure effective gear changes with minimal slippage and maximum torque output.[5] Furthermore, the lubricant must remove heat efficiently from the moving parts, protect gears and bushings, operate at extreme temperatures, be non-corrosive, stable to oxidation, compatible with all seals and resist high shearing forces in the gears and bearings. Therefore, driveline lubricants, particularly for more complex automatic transmissions, are often highly complex formulations containing up to twenty additives (Table 1.3).

Table 1.1 Lubrication regimes in automotive engines.[9]

Components	Lubrication Regime	Related Oil Properties
Bearings, bushings	Hydrodynamic	Oil viscosity
Gears, piston rings, liners	Hydrodynamic-boundary	Oil viscosity, anti-wear and EP additives
Cam, valve train	Mixed to boundary	Anti-wear and EP additives

Table 1.2 Typical lubricant composition of petrol and diesel engines oils.[5]

Components	Petrol and diesel	Diesel Only
Base oil	78 %	85 %
Additive package	12 %	8 %
Viscosity modifier	10 %	7 %

Table 1.3 Typical composition of automatic transmission fluid.[5]

Additives	Treat rates	Function
Dispersants	2-6 %	Cleanliness, friction and wear
Detergents	0.1-1%	Cleanliness, friction, corrosion and wear
Anti-oxidants	0.3-1 %	Oil thickness, prevent varnish/deposits
Anti-wear	0.1-0.5 %	Protection of gears
Friction modifiers	0.2-1.5 %	Control shift feel and durability of clutch
Corrosion inhibitor	0.03-0.5 %	Prevent rust, pitting and wear
Antifoam	50-400 ppm	Prevent excessive foaming
Seal swell agent	0.3-1.5 %	Combats seal cracking
Viscosity modifier	2-15 %	Improve viscosity and shear stability
Base oils	80-95 %	Oxidative stability and low-temperature fluidity

1.4 Lubricant Additives

The additives incorporated into lubricants are vital for efficient performance and are where a variety of chemistries may be utilised to carry out a multitude of functions. The additive package not only improves the overall performance and efficiency of the engine, but extends the lifetime of the lubricant, leading to fewer oil changes, which is greater value for consumers and better for the environment.

1.4.1 Detergents and Dispersants

The purpose of detergent and dispersant additives is to maintain cleanliness within the lubricant and protect engine parts from destructive deposits and agglomerations of dirt. Generally, these additives are comprised of a long hydrocarbon tail which imparts oil solubility to the molecule, and a polar head group which in the case of detergents is usually salted with a metal counterion, typically calcium, magnesium or zinc (Figure 1.5).[5] Dispersants differ in structure from detergents as they usually include additional bridging 'hook' group between the head and tail, consisting of typically either maleic anhydride or phenol.

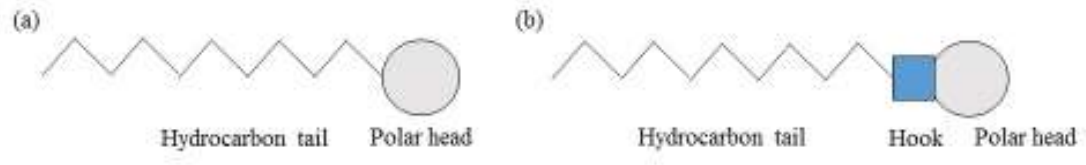
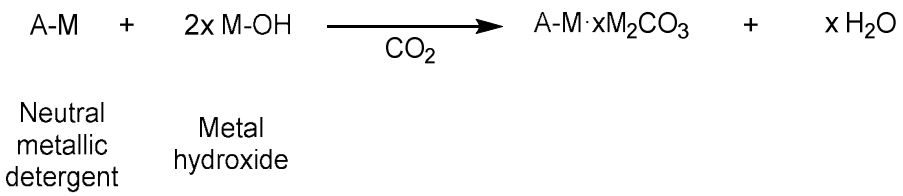


Figure 1.5 Generic structure of (a) detergent and (b) dispersant additives.

One of the key functions of detergents is the neutralisation of acidic products formed in the combustion of the fuel and through degradation of the lubricant. These include organic carboxylic acids, formed from the fuel and lubricants themselves, and inorganic acids such as H_2SO_4, HCl, and HNO_3, formed when the gases produced in the combustion process react with water in the system.[20] This may be achieved by 'overbasing' the detergents – incorporating many equivalents of metal hydroxide into the detergent, which is then converted to metal carbonate (Scheme 1.2). The metal carbonate formed during the reaction is contained as nanoparticles in reverse micelles, assembled as the polar head groups interact with the carbonate core



Scheme 1.2 Synthesis of overbased detergent additives, where M is a monovalent metal.

and the hydrophobic tail points out into the oil (Figure 1.6). This allows the metal carbonate to be dispersed throughout the lubricant in an oil-soluble form. Detergents also function by interacting with the metal surfaces within the engine *via* their polar head groups, forming a protective film which keeps the surfaces clean and prevents the agglomeration of deposits and corrosion.[21] Various organic surfactants may be used as detergents, but the most common are long chain carboxylic acids, alcohols, glycols, phenates, sulfonates, salicylates or phosphonates.[22]

Modern engines are often used for short distance, start-stop travel, leading to lower operating temperatures, incomplete combustion and more viscous lubricants.[21] This in turn generates two unwanted deposits within the lubricating oil – soot and sludge. Soot is typically formed in diesel engines due to incomplete combustion of the fuel, and can build up to give particles which thicken the oil and cause wear between metal surfaces within the engine.[5, 23] Sludge is formed in petrol engines and is generally finer than soot. It is generated through thermal oxidation and reaction of the lubricant oil with blowby gases from partially burned fuel. Both of these deposits are detrimental to the engine's performance, and dispersants work to hinder agglomeration of soot and sludge and intersperse the particles throughout the oil.

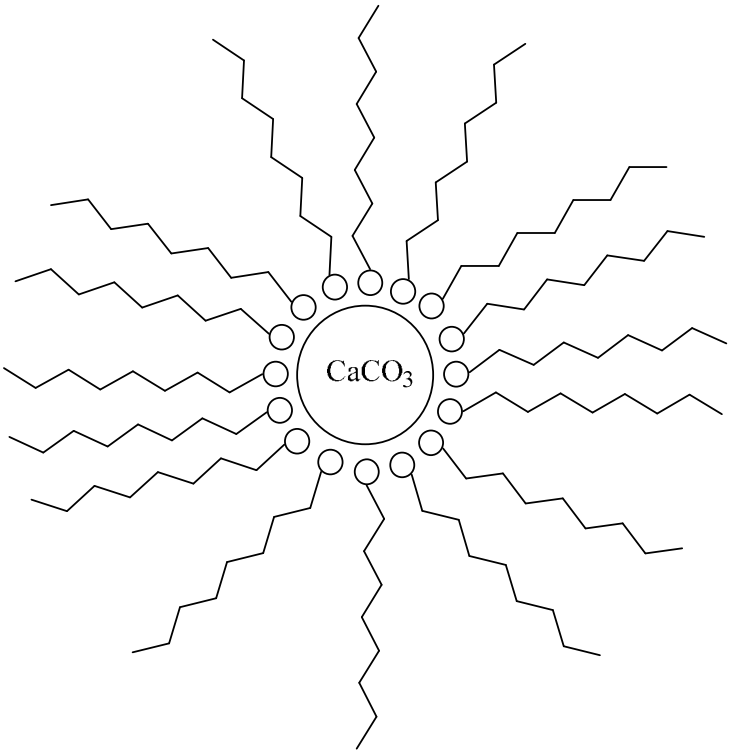
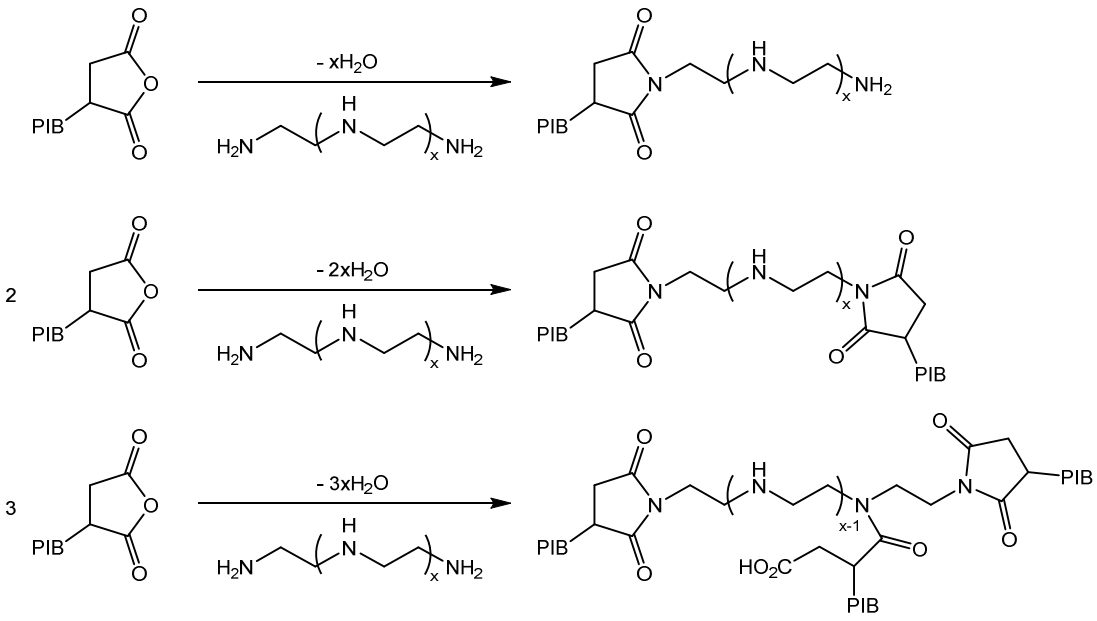


Figure 1.6 General representation of lubricant detergent reverse micelle containing calcium carbonate.

This is typically achieved through two mechanisms: steric and electrostatic stabilisation. To provide a steric barrier to aggregation, the polar head group adsorbs onto the deposit surface and the long hydrocarbon tail provides a physical barrier between the particles, preventing them from combining and increasing in size. Electrostatic stabilisation is achieved when deposit particles containing acidic functional groups react with basic amine dispersants and become negatively charged. The repulsion between these charged species prevents the agglomeration and build-up of deposits.

One of the most commercially successful dispersants are succinimides, which were first introduced almost fifty years ago.[24] These are typically synthesised through the reaction of polyisobutylene succinic anyhydride (PIBSA) with a polyamine, which

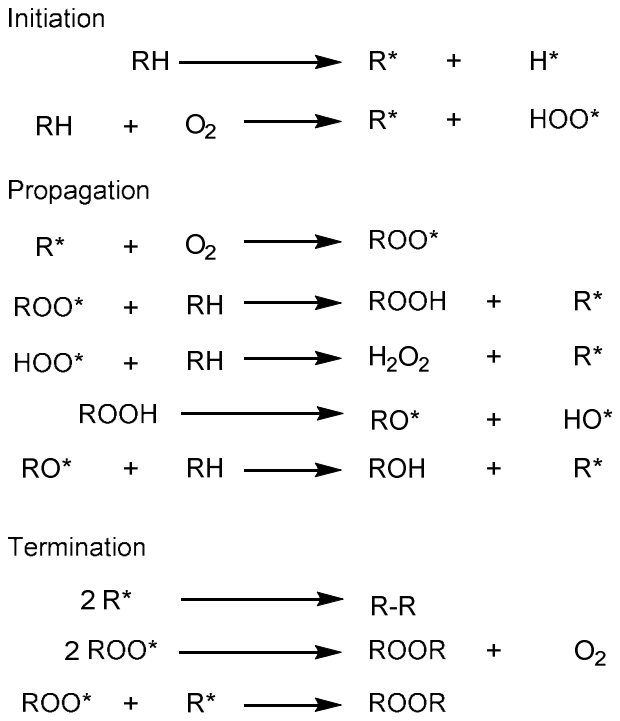


Scheme 1.3 Synthesis and structures of mono-, bis- and tris-succinimide dispersant molecules.[5]

gives mono-, bis- or tris-succinimides, depending on the ratio of amine to PIBSA used (Scheme 1.3).[5] It has been reported that the more secondary amines present within the succinimide dispersant, the better anchoring to the deposit particle, resulting in a more efficient dispersant.[25]

1.4.2 Antioxidants

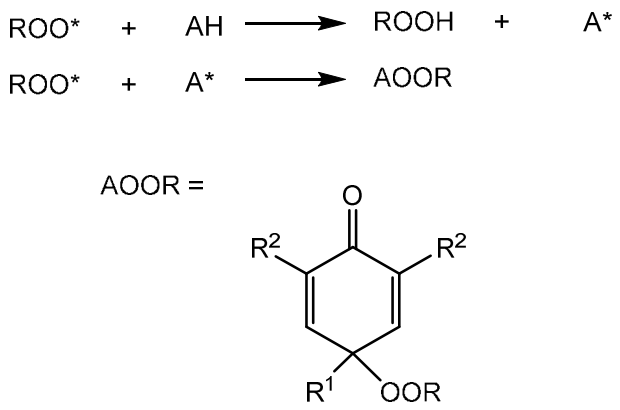
Oxidative degradation of lubricant oils takes place during engine operation due to the high operating temperatures, presence of air and reactive metal surfaces which accelerate the free radical chain reaction (Scheme 1.4).[9] This causes corrosion and oil thickening, and produces unwanted sludge and debris.[26] In order to minimise this, antioxidants must be added to the lubricant which deactivate the free radicals formed and decompose hydroperoxides. The most commonly used free radical scavengers are hindered phenols and aromatic amines.



Scheme 1.4 Oxidation chain reaction.[9]

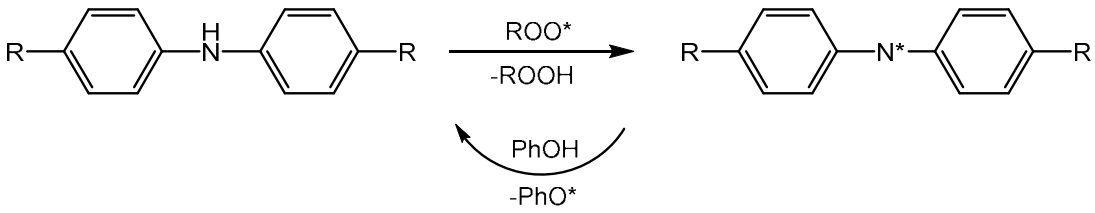
Hindered phenols such as 2,6-di-*tert*-butyl-4-methylphenol compete with the propagation step of the oxidation chain reaction, reacting with peroxy radicals to remove them from the oxidation process (Scheme 1.5).[27] Steric hindrance in both ortho positions is necessary to prevent hydrogen abstraction by the phenoxy radical, allowing it to react with another peroxy radical to form the stable cyclohexadione peroxide.

Secondary aromatic amines also work by competing with the propagation step of the oxidation mechanism, but once the aminic proton is abstracted the resulting radical disproportionates and continues to react to give polyconjugated products.[27] This leads to depletion of the antioxidant, which may be counteracted *via* regeneration using a phenolic antioxidant (Scheme 1.6). The phenoxy radical formed can then go on to further deactivate the oxidation of the lubricant. This synergism has been used to great effect, and both types of antioxidant are often used in lubricant packages.[28]



Scheme 1.5 Antioxidant mechanism for hindered phenol antioxidants, where A = antioxidant, R = hydrocarbon from lubricant, R^1/R^2 = alkyl group.

As the hot metal surfaces in contact with the lubricant have been shown to accelerate the formation of oxidation products,[26, 28] metal passivators are often included in the lubricant formulation. These usually take the form of alkylated benzotriazoles, which form a layer on the metal surface, inhibiting the catalysis of the oxidation reaction.[9]



Scheme 1.6 Regeneration of aminic antioxidant from phenolic antioxidant.[27]

1.4.3 Wear and Anti-wear Additives

One of the most vital types of compound in a lubricant package are anti-wear additives. There are many definitions of wear, but a broad definition which incorporates every situation is "damage to a surface, generally involving progressive loss of material, due to relative motion between that surface and a contacting surface or substance".[29] The process of wear presents significant challenges to tribologists, engineers and chemists alike. For instance, the operating conditions which lead to wear occurring are very different to those under which metals are mechanically tested for properties such as tensile strength and hardness, and so surfaces undergoing wear may respond very differently to as expected. Furthermore, the distances and thicknesses of films involved in wear are extremely small (10 nm-10 μm), and timescales are in the order of microseconds, meaning wear processes are difficult to analyse and measure. Surfaces interact at local high spots, known as asperities, leading to high levels of strain, high transient local temperatures and extreme local conditions. Therefore, wear mechanisms are complex and often involve a mixture of mechanical and chemical processes. These are yet to be modelled accurately, as there is a plethora of different properties to be considered. Indeed, even the difficulties in the description of wear particles and their shapes have stimulated a great deal of research.[30]

The Archard equation is often used as a starting point for describing wear, as it is the simplest possible assumption of the relation of wear and load (Equation 1). The wear coefficient, K, may be used to approximate and describe the wear regime taking place (Figure 1.7).[30] These different wear regimes often involve significantly different mechanisms of material loss. With metal surfaces, 'severe' wear is usually associated with large particles of metallic debris, whereas 'mild' wear leads to the

$$(1)\ Q = KW/H$$

Equation 1. The Archard equation describing the volume of material removed during a wear process (Q) to the normal load (W). K = wear coefficient, H = hardness of surface.

loss of fine metal oxide particles. As lubrication is introduced to the system, the rate of wear drops by several orders of magnitude and reduces further as the lubricant film thickness increases from boundary, elastohydrodynamic to hydrodynamic regimes (Figure 1.7).

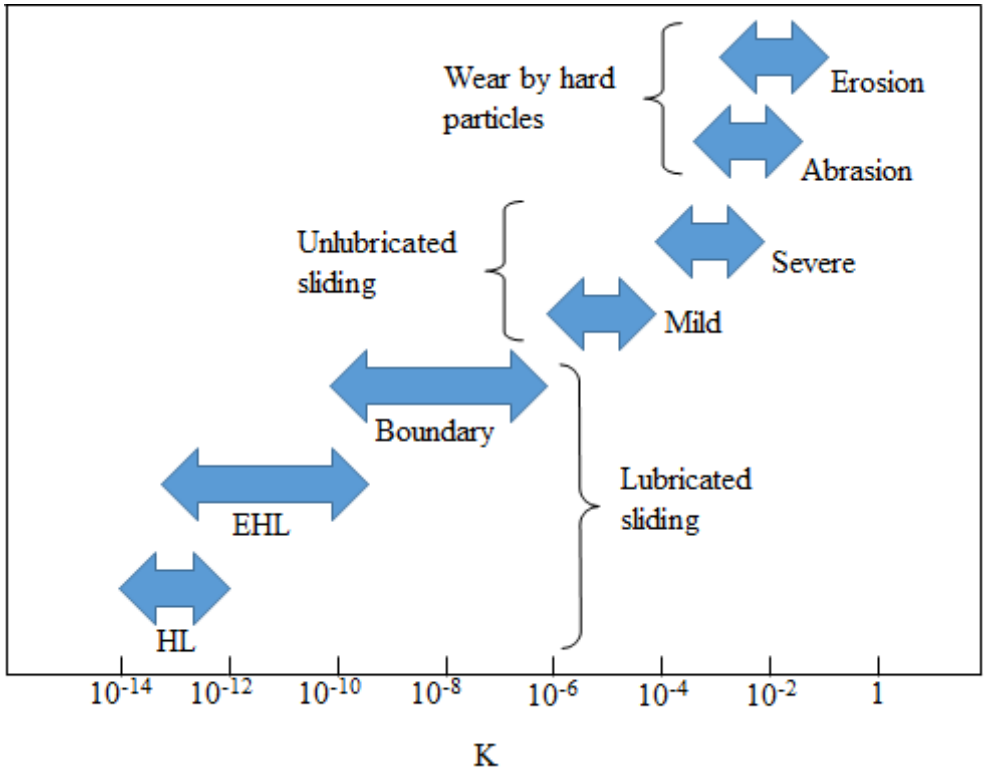


Figure 1.7 Schematic representation of the range of wear coefficient (K) exhibited under different wear regimes. HL = hydrodynamic lubrication, EHL = elastohydrodynamic lubrication.[30]

The process of wear is normally split into four mechanisms: adhesive wear, abrasive wear, contact fatigue and corrosive wear. Adhesive wear involves contact between two or more asperities, resulting in atomic bonding between the metal surfaces and plastic deformation.[31] This deformation has been found to depend on the contact area between the surfaces, and the wear coefficient can vary between 10^{-4} and 10^{-3} depending on surface roughness, surface energies and contact environment.[32] Furthermore, molecular dynamics simulations have found that during adhesive wear asperity-asperity shear leads to large increases in local temperature of up to 3400 K, which can lead to local melting.[31] Adhesive wear has proven difficult to model, as the nature and degree of wear depends heavily on the pressures involved, and there is often a "running-in" period at the beginning of a test, where wear is initially high, but the resulting effect on the surface can vary depending on the materials and conditions involved.[33]

A recent study by Mishina and Hase describes the use of Atomic Force Microscopy (AFM) to allow the formation of a more detailed adhesive wear mechanism.[34] It was discovered that plastic deformation at the asperity contacts causes 'slip lines' within the metal surfaces, and tiny wear particles form where these lines cross (Figure 1.8). These particles then grow in size and are transferred from the surface as wear debris. Furthermore, it was found that chemisorbed lubricant films slow down this process by preventing direct contact between the asperity surfaces. The number of wear particles per unit area was found to increase with increased adhesion force between the surfaces, with iron-iron contacts displaying the largest adhesive forces in the study, and so the highest number of wear particles. Adhesive wear can be minimised by using metal surfaces which do not bond together easily, improving the formation of additive layers (*vide infra*) or increasing oil film thickness.[5]

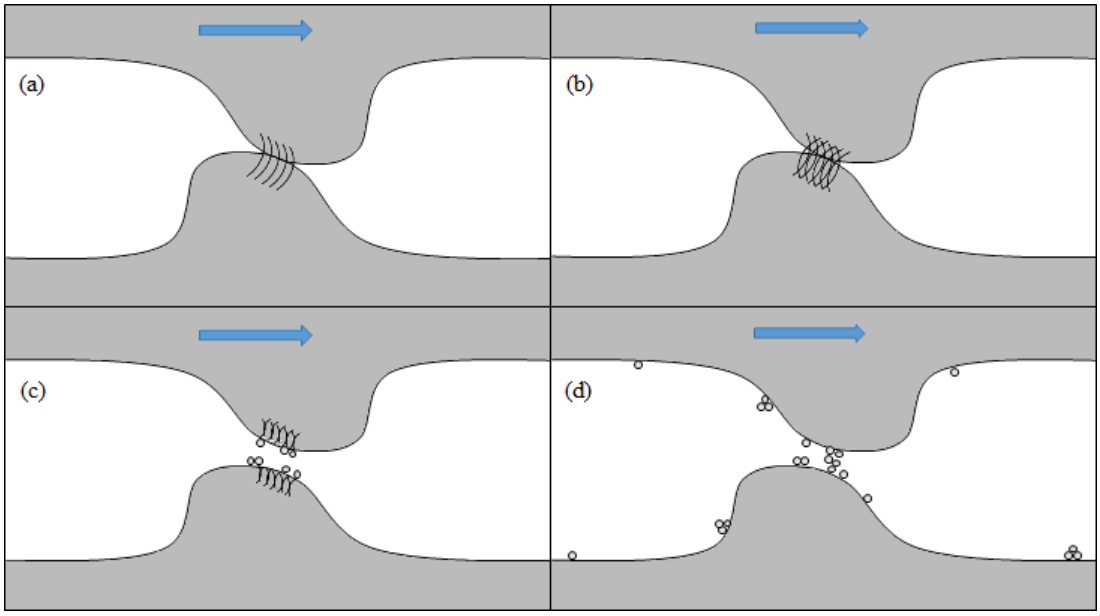


Figure 1.8 Mechanism of adhesive wear from formation of slip lines (a) to generation of wear particles (c) to transfer of wear debris (d).

Abrasive wear occurs when a hard surface rubs against a softer surface, removing material from the asperities. In lubricated systems, this is generally a third-body process, with abrasive particles such as silica from dust contamination wearing away the metal surfaces.[9] This may go on to generate metallic abrasive debris which can cause further wear damage. As adhesive wear is able to produce metallic wear particles, it is possible for a transition from an adhesive to an abrasive wear mechanism to occur. Abrasive wear is generally minimised through careful choice of surface material properties, such as hardness and roughness, but effective oil filtration can also remove harmful abrasive particles from the system.[5, 9]

Corrosive wear occurs through the attack of chemical species on the metal surface, resulting in the removal of material. This can be beneficial if carried out by EP or anti-wear additives to form low-shear-strength lubricant films between the surfaces, but uncontrolled corrosion by harmful acidic products within the oil can severely damage

the mechanical parts, not only by the removal of material but by exposing fresh metal surfaces to attack. These corrosive species may be oxygen, water, carbon dioxide, sulfur compounds from within the lubricant (especially prevalent in diesel engines), acidic combustion products (*e.g.* oxyacids of nitrogen and sulfur) and acidic products from oxidative degradation of the oil.[5] This mechanism of wear may be limited *via* the use of overbased detergents (*vide supra*) and by the careful choice of anti-wear and EP additives which do not excessively react with the metal surfaces they come into contact with.

Contact fatigue causes pitting of the metal surfaces, and occurs under the surface at points of high stress. Once this has initiated, propagation throughout the material occurs until a structural weakness is encountered. The material then cracks through to the surface, where breakages are levelled out to triangular pits by the hydraulic action of the lubricant under contact pressure.[5] Although this mechanism of wear originates under the metal surface, it may be limited by reducing levels of stress between the surfaces *via* effective lubrication.

Anti-wear additives work to reduce local stress by removing the asperities or forming a layer on the surface which sufficiently distributes the stress throughout the material.[35] They mainly act during the thin film (boundary) lubrication regime, which is particularly significant during starting and stopping automotive engines, and they primarily reduce adhesive wear by preventing metal-to-metal contact. Therefore, successful formation of a film on the metal surface is key to the performance of these additives.

Under boundary lubrication conditions, additive films may form *via* four main mechanisms: adsorption by van der Waals forces, formation of high viscosity layers,

thin reacted layers/smoothing and thick reacted inorganic layers. For adsorption *via* van der Waals interactions, additives must contain a polar end, such as alcohols, esters and carboxylic acids, which attaches to the metal. A non-polar end points out into the oil solution, forming a shear strength layer which reduces friction and wear.

High viscosity layers of greater than 10 μm thickness may be formed when oil components react in the presence of reactive metal surfaces. This gives a hydrodynamic effect, even at slow speeds. However, these films can be ineffective under higher loads.

When oil components attack metal surfaces, they may form thin reacted films which smooth the surface roughness, reducing adhesion.[5] This usually requires moderate temperatures. At high temperatures and loads, additives can react with metal surfaces to form thicker inorganic films, such as sulfides, which work to reduce adhesion between the sliding surfaces. However, they must be quickly reformed to prevent them from scuffing the metal surface. For either mechanism, a minimum surface must be maintained for friction and wear to be controlled.

1.4.3.1 Phosphorus-containing Anti-wear Additives

Although several classes of anti-wear additive have been developed over the decades, by far the most prevalent are zinc dialkyldithiophosphates (ZDDPs), the general structure of which is shown in Figure 1.9. This class of molecule has been used successfully as both an antioxidant and anti-wear additive since the first patent was filed for such use in 1941.[36] Following this, research into ZDDP and the use of this class of compounds as an additive has grown rapidly.[37]

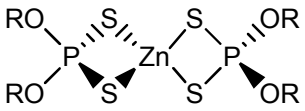
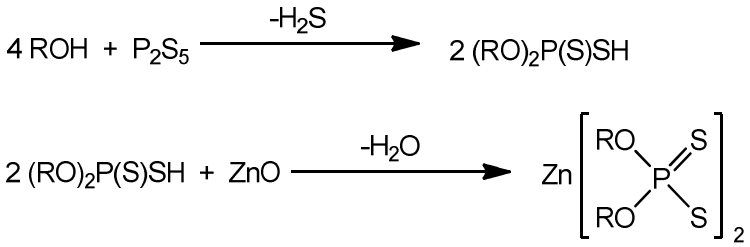


Figure 1.9 General structure of ZDDPs.

ZDDPs may contain either aryl or alkyl groups, and are synthesised from primary or secondary alcohols.[38] Phosphorus pentasulfide is reacted with an alcohol to give a dialkyldithiophosphoric acid which is then neutralised with zinc oxide to give the resulting ZDDP compound (Scheme 1.7).[39] Although the mechanism of ZDDP film formation is still not definitively known, it has been suggested that it is likely to involve cross-linking between zinc phosphates on metal surfaces.[40] Indeed, XPS and XANES analysis has revealed that ZDDP films have a graded structure with a hard outer layer of zinc polyphosphates and an inner bulk of shorter chain iron and zinc phosphates.[41] However, this has been found to differ for aryl ZDDPs, which produce films containing polyphosphates throughout their entirety.[38]

Despite semi-empirical quantum chemistry calculations on model ZDDP compounds suggesting that varying the alkyl substituent on the thiophosphate moiety had little effect on the bond lengths and angles, and so reactivity, of the ZDDP,[42] studies have found that short, branched alkyl chains groups can be more reactive than longer substituents, leading to better anti-wear performance.[5] Furthermore, there is an inverse relationship between thermal stability and anti-wear potency of ZDDPs, which suggests films are formed *via* thermal degradation of the additives.

Despite the success of ZDDP, the existence of zinc, sulfur and particularly phosphorus has been found to foul catalytic exhaust converters and poison the catalyst, reducing the life of the emission system.[43] For this reason, limits are being



Scheme 1.7 General synthesis of ZDDPs.

put in place worldwide to limit sulfur and especially phosphorus concentrations in motor oils.[44] Therefore, in order to limit overall phosphorus content and so prevent unwanted damage to car engines, a more efficient class of anti-wear additive than ZDDP is desirable so that a lower concentration of phosphorus can be used. It has been suggested that it is not only the phosphorus but the zinc which is detrimental to combustion engines in ZDDP, and it has been found that mixtures of ZDDP and metal-free phosphorus-containing additives have similar anti-wear performance and are less detrimental to catalytic convertors than ZDDP alone.[45]

Organic phosphate esters have been used extensively as anti-wear additives for a similar length of time to ZDDPs, with such use being reported as early as 1940.[46] These additives typically take the form of tricresyl phosphate (TCP), one of ten isomers of which is shown in Figure 1.10. It has been proposed that these

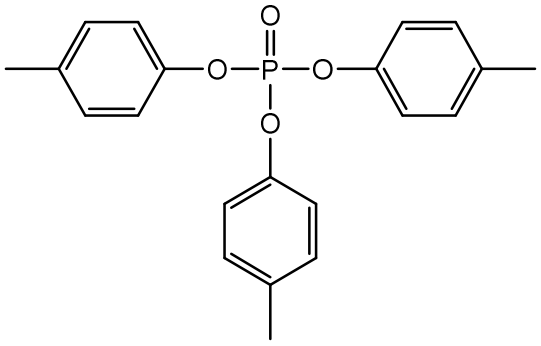


Figure 1.10 Structure of the tri-para isomer of tricresyl phosphate (TCP).

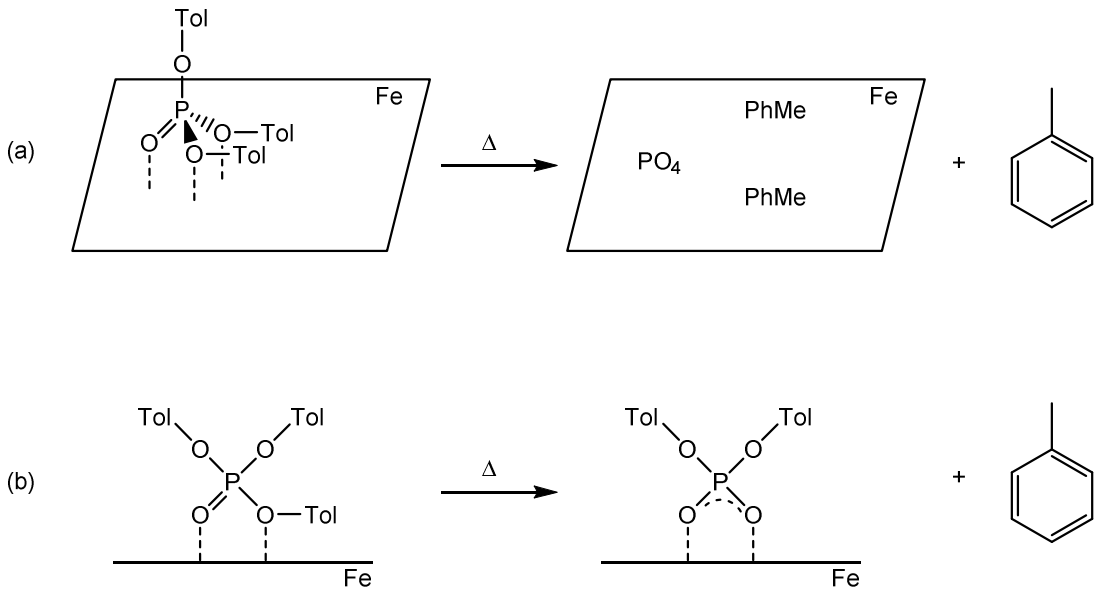


Figure 1.11 Alternative models of TCP adsorption and reaction on steel.[47]

compounds decompose on steel surfaces to form a protective film of iron phosphate, with two mechanisms being suggested for the adsorption and subsequent breakdown of TCP (Figure 1.11).[47] Similarly, trilaurylphosphate has been found to decompose to form films of three different forms of iron phosphate: $FeFe_4(PO_4)_3(OH)_5$, $Fe_3(PO_4)_2$ and $FePO_4$.[48]

Ren *et al.* tested the long-chain phosphoric acid shown in Figure 1.12, and found it to be a very effective anti-wear additive in water-based lubricants.[49] XANES analysis showed that the phosphorus component of the protective film which was formed during testing comprised of phosphate or polyphosphate. Furthermore, Minami and Mitsumune reported the use of dibutylphosphonate (DBPo) as an anti-wear additive in several vegetable oils, and a decrease in wear was measured for each oil with the addition of DBPo.[50]

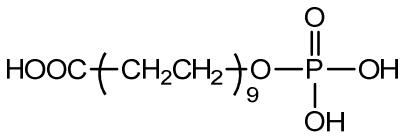


Figure 1.12 The structure of a long-chain phosphoric acid used as an anti-wear additive.[49]

In more recent work, phosphate esters have been synthesised which include N-containing heterocycles, as this motif has also shown promise in lubrication tests.[51] For instance, Feng and co-workers have reported the anti-wear testing of several benzimidazolyl phosphates which outperformed TCP in the reduction of both friction and wear, and increased the thermal stability of the base oil.[52]

Recent work has also focused on the utilisation of diphosphate molecules which bridge two phosphorus centres with an aryl group as anti-wear additives, with hydroquinone bis(diphenyl)phosphate (HDP)[53] and 1,5-dihydroxynaphthylene bis(diphenyl phosphate) (DDP)[54] (Figure 1.13) both showing good friction- and wear-reducing properties. Indeed, HDP exhibited better anti-wear and EP properties than TCP, through the formation of a boundary lubrication film comprised of FeOOH, Fe_2O_3, $FePO_4$ and polyether compounds. Similarly, DDP led to a film composed of FeOOH, Fe_3O_4 and $FePO_4$.

This idea has been extended further by Wang *et al*. in 2016, who demonstrated the high-performance anti-wear properties of 'treelike' polymeric phosphates grafted onto graphene oxide nanosheets.[55] This combined the good anti-wear activity of phosphate esters with the thermal and mechanical stability of graphene oxide, with the tribological properties of the composite being attributed to the formation of a boundary film composed of FeO, Fe_2O_3, $FePO_4$ and C-O-C and P-O components.

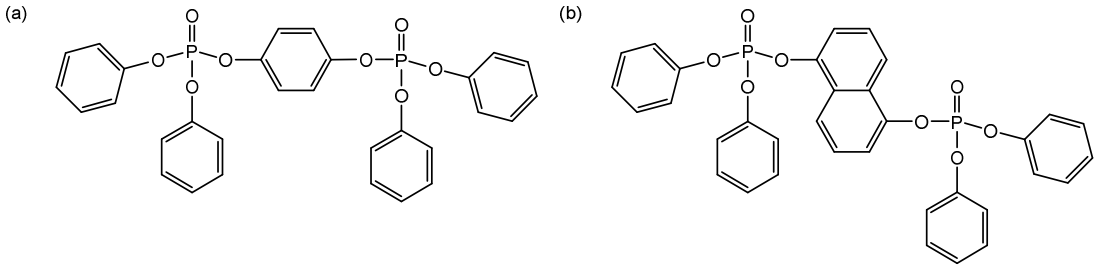


Figure 1.13 Structures of diphosphate additives (a) HDP[53] and (b) DDP.[54]

The incorporation of sulfur into phosphate additives has also been successfully investigated. For instance, Schumacher *et al*. reported the anti-wear performance of a variety of phosphates and thiophosphates of the structures shown in Figure 1.14.[56] It was found that the concentration of phosphorus was key to the performance of these compounds, with structural variation having very little effect on their anti-wear activity.

Kasrai *et al.* showed that similar mono- and dithiophosphates showed anti-wear activity, which could be attributed to the formation of thick iron(II) polyphosphate films during wear testing.[57] Furthermore, a combination of diisopropyl phosphite and triphenyl thiophosphate reported by Jiang and Yang produced a synergistic friction-reducing and anti-wear effect on sliding steel against Al_2O_3 ceramics.[58]

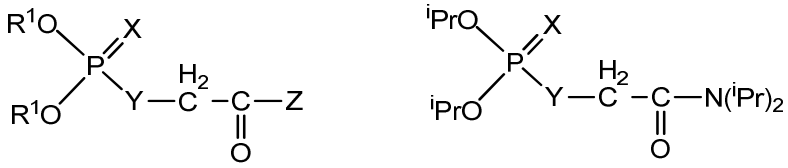


Figure 1.14 Structures of thiophosphates tested for anti-wear performance. X, Y = O, S, Z = OR^2, $N(R^3)_2$, R^1 = alkyl, cycloalkyl, aryl, R^2, R^3 = alkyl, cycloalkyl.[56]

Inorganic components have been combined with organophosphorus motifs in order to produce effective lubricant materials. An example of this was reported by Li and co-workers in 2014, who synthesised lanthanum trifluoride nanoparticles capped by tri-*n*-butylphosphate.[59] This kept the size of the nanoparticles small, and the combination of both components led to significantly reduced friction and wear on steel surfaces in paraffin oil. It is postulated that this worked *via* the LaF_3 core being released during the test and adsorbing onto the steel surface, whilst the tri-*n*-butylphosphate formed a tribofilm on rubbed steel surfaces and so lowered friction.

Phosphorus-containing lubricant additives do not necessarily have to contain an organic component at all, and one example of such a purely inorganic additive is the lithium molybdophosphate additive shown in Figure 1.15, which was reported to improve lubricant properties and stability in railway plastic greases.[60] Furthermore, a mixture of sodium polyphosphate and potassium dihydrogen phosphate greatly reduced the friction coefficient between rolling steel surfaces by melting and forming a uniform film on the metal surface at elevated temperatures.[61]

Ionic liquids have received intense research interest in recent years for their lubricating properties.[62] For example, a report in 2014 by Zhang and co-workers highlighted the excellent tribological performance of lithium-containing ionic liquids.[63] Consequently, recent advances in phosphorus-containing lubricant additives have focused on ionic liquids. For example, Qu *et al*. reported that

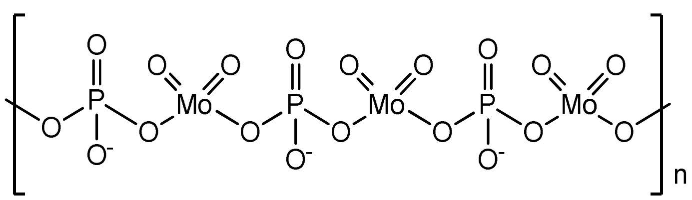


Figure 1.15 The structure of lithium molybdophosphate additive.[60]

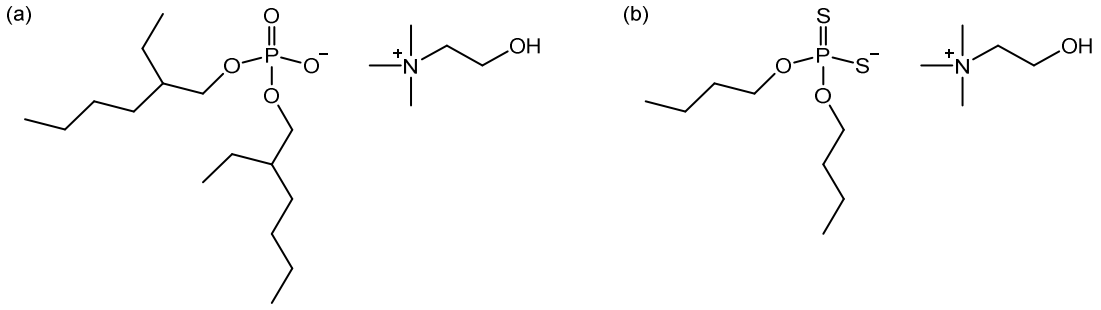


Figure 1.16 Structures of (a) choline bis(2-ethylhexyl) phosphate and (b) choline dibutyl dithiophosphate.[64]

phosphonium organophosphate ionic liquid additives outperformed traditional ammonium phosphate anti-wear additives and phosphonium ionic liquids with other counteranions, with the phosphorus present in the tribofilm originating entirely from the anionic component.[65] Similar results by Battez and co-workers in 2016 indicated that the incorporation of an organophosphate anion in phosphonium ionic liquids led to superior anti-wear performance, due to the reactivity of the phosphate moiety.[66] Furthermore, quaternary ammonium phosphate ionic liquids have been found to have better EP, anti-wear and friction-reducing properties than ZDDP in PAOs.[67] The additives decomposed to polyphosphate during testing, and the degree of polymerisation was found to play a key role in their performance. Likewise, choline bis(2-ethylhexyl) phosphate and choline dibutyl dithiophosphate (Figure 1.16) formed iron polyphosphate films during anti-wear testing in a similar mechanism to that postulated for ZDDP.[64]

1.4.3.2 Boron-containing Anti-wear Additives

1.4.3.2.1 Inorganic Boron Additives

Inorganic boron compounds have been studied for use in lubricants for several decades, particularly in the form of hexagonal boron nitride, *h*-BN.[68] *h*-BN has a lamellar, crystalline structure similar to that of graphite (Figure 1.17), having an inter-layer distance of 3.33 Å compared to the 3.35 Å inter-layer distance of graphite.[69]

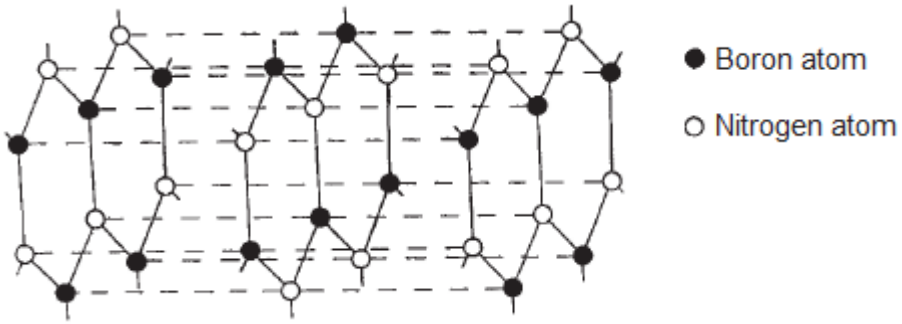


Figure 1.17 The crystal structure of hexagonal boron nitride.[69]

These physical similarities have prompted a great deal of interest in this material as an alternative to solid graphite lubrication.[70] For instance, Pawlak *et al.* have demonstrated that adding *h*-BN to a grease-based lubricant improved the anti-wear performance, so much so that it surpassed the performance of a commercial lubricant (Militec-4).[71] This is shown graphically in Figure 1.18. Furthermore, Zhang and co-workers reported the use of a nanocomposite material containing single-layer boron nitride (SBN) and a polyamide which showed significant anti-wear and friction-reducing activity in dry sliding tests.[72]

Due to the similarities in structure between h-BN and graphite, it has been used in conjunction with graphite as an anti-wear composite. For example, Chen *et al*. found

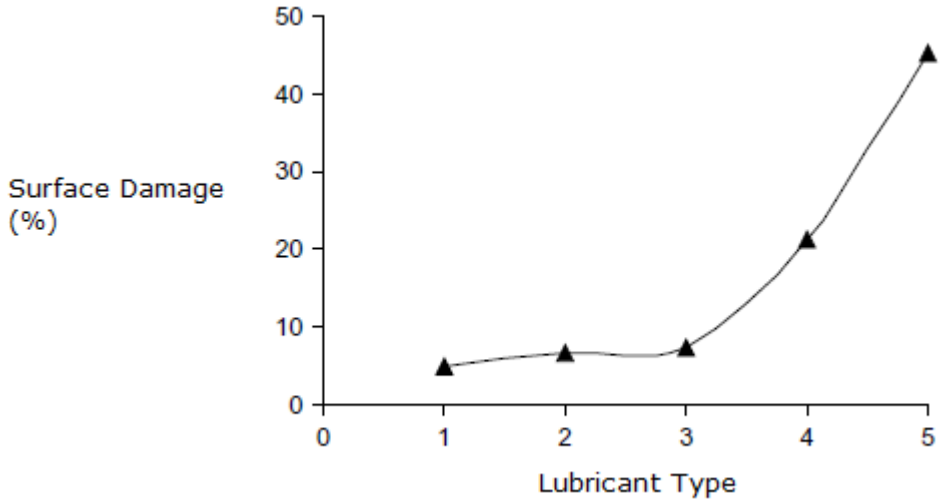


Figure 1.18 Surface damage (%) using different lubricants on a steel surface: 1 = grease + 10 wt. % h-BN, 2 = grease + 5 wt. % h-BN, 3 = grease only, 4 = Militec-4, 5 = dry.[71]

that the addition of small amounts of *h*-BN to graphite lubricants stabilised the friction and wear properties of the resulting composite on a copper surface.[73]

h-BN has also been investigated for its use in composites with other inorganic lubricant materials for anti-wear and friction-reducing performance, such as Si_3N_4-based ceramics,[74] nickel alloys,[75] nickel-based composites with nano-silver,[76] nickel-chromium composites[77] and ferroboron coatings.[78] Furthermore, *h*-BN has been used in combination with carbon[79] and carbon nitride[80] films in order to reduce wear and corrosion, and boron carbon nitride films under ionic liquid lubrication have proved effective in reducing both friction and wear.[81]

Boron nitride has also been investigated for its use in biological lubricant applications, with Pawlak *et al.* demonstrating the use of *h*-BN as an additive in Vaseline in order to reduce friction and wear in the lubrication of prosthetic joints.[82] Similarly, in 2013 it was reported that adding boron to a cobalt-chromium alloy in metal-on-metal hip

joint replacements significantly decreased wear, highlighting the potential for such materials in medical applications.[83] Furthermore, *h*-BN has been found to be a very efficient lubricant in tabletting technology.[84]

Boric acid has also been utilised as a solid lubricant due to its lamellar structure which allows layers of the substance to be sheared and slide relative to one another, providing lubricity (Figure 1.19).[85] Furthermore, as boric acid is environmentally benign, it has been postulated as an additive for green lubricants.[86] Indeed, boric acid mixed with canola oil was found to exhibit excellent anti-wear properties, offering a potentially natural and non-toxic lubricant system in brake valves.[87] However, it has been found that boric acid performs better during room temperature applications, as elevated temperatures lead to dehydration of the material to boric oxide (B_2O_3).[88]

Inorganic metal borates have also been investigated for their use as anti-wear additives. For example, Hu *et al.* reported excellent anti-wear properties of nanoscale titanium and zinc borate additives.[89],[90] Following this, zinc borate emulsions have

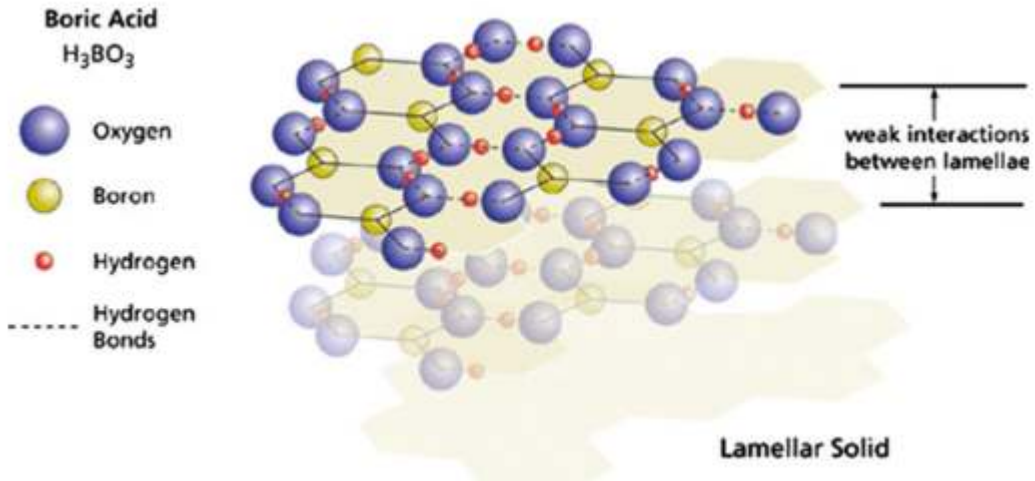


Figure 1.19 Lamellar structure of boric acid.[85]

been found to lower both friction and wear as particles could be kept well separated and dispersed throughout the lubricating oil.[91] Moreover, Normand *et al.* found that micellar calcium borate proved to be an effective anti-wear additive *via* the formation of a borate glass layer on rubbing steel surfaces.[92] This additive was found to perform even better when combined with ZDDP to form a phosphate-borate glass. Similarly, potassium triborate has been used in conjunction with ZDDP to give a composite with excellent anti-wear properties.[93]

1.4.3.2.2 Organic Borate Additives

Organic three-coordinate borate esters have generated great interest for their anti-wear use for several decades, due to their known oxidation stability, good anti-wear and friction-reducing properties, and compatibilities with engine parts.[94] For example, tribenzyl borate was studied by Kreuz *et al.* for its anti-wear properties, and the tribofilms formed during testing were found to contain boron, ferrous iron and organic components.[95] Furthermore, Junbin reported good anti-wear properties of a nitrogen-containing borate ester, which existed as the borate ester on the rubbing surface under mild conditions, and a mixture of the borate ester and boron nitride under harsher conditions.[96] Similarly, borate esters containing Schiff bases

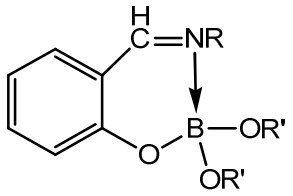


Figure 1.20 The general structure of Schiff base-containing borate esters,

R = C_4H_{19}, C_8H_{17}, $C_{12}H_{25}$, $C_{18}H_{37}$, R' = $C_{16}H_{33}$.[97]

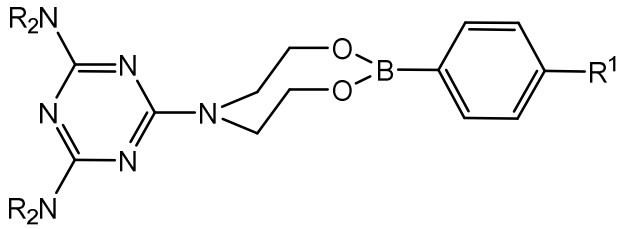


Figure 1.21 The general structure of heterocylic-containing borate esters,

$$R = 2\text{-}EtC_6H_{12},\ R^1 = C_{12}H_{25}.$$[98]

demonstrated better friction-reducing and anti-wear properties than ZDDP *via* the formation of layers containing adsorbed borate ester and B_2O_3 (Figure 1.20).[97]

Furthermore, these compounds possessed good hydrolytic stability due to the extra intramolecular co-ordination of nitrogen to the empty p_z orbital of the boron centre, forming a stable six-membered ring structure. Similarly, Yao *et al.* found that the incorporation of *N,N*-dialkylaminoethyl groups into borate esters gave good hydrolytic stability of the resulting compounds *via* the formation of a five-membered ring structure.[94] It has also been reported that benzotriazole-containing borate esters, which also include intramolecular donation from nitrogen atoms, have good anti-wear properties on steel surfaces.[99]

Further examples of nitrogen-containing borate esters being studied for their tribological performance have been reported in recent years. One example is the work reported by Ren and co-workers in 2014, in which heterocyclic borate esters were synthesised which exhibited both high hydrolytic stability and promising anti-wear performance (Figure 1.21).[98] This has since been expanded to incorporate additional sulfur and oxygen bridging atoms into the compounds, which displayed excellent anti-wear performance due to the formation of inorganic borate, iron oxide and iron sulfate/sulfide films.[100] Jiu *et al*. have also reported the use of borate

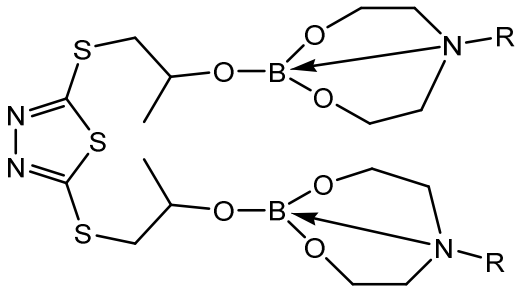


Figure 1.22 The general structure of thiodiazole-containing borate esters,

$$R = C_{18}H_{37}$$ [101]

additives based around a similar diethanolamine centre which show good tribological performance and enhanced biodegradability.[102]

Moreover, in 2014 Zhao *et al*. reported the synthesis and tribological testing of a thiodiazole-containing borate ester, with an additional nitrogen atom located in the cyclic borate motif providing additional stabilisation to the boron centre (Figure 1.22).[101] The borate ester performed very well in anti-wear testing, with it exhibiting a reduction in wear comparable to that of ZDDP at 1.0 wt % concentration. Furthermore, blends of the borate with ZDDP provided a synergistic effect, with the mixture outperforming ZDDP and the borate additive alone. This was postulated to be due to the formation of iron sulfide and iron sulfate in the tribofilm. Similarly, a recent report by Li and co-workers describes the synthesis of a benzothiazole-containing borate ester which exhibited better anti-wear performance than ZDDP, *via* the formation of a film containing B_2O_3, FeS, Fe_3O_4, $FeSO_4$ and organic nitrogen-containing compounds.[103] Furthermore, the compound exhibited good hydrolytic stability, thought to be caused by a combination of conjugation from the neighbouring phenyl ring into the boron centre and steric protection from the two benzothiazole groups (Figure 1.23).

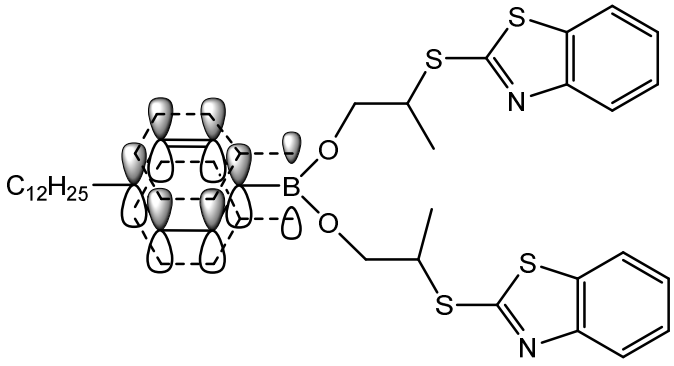


Figure 1.23 Structure of benzothiazole-containing anti-wear additive, highlighting stabilisation via conjugation into empty p_z orbital on boron.[103]

Disulfide borates have been found to be effective in reducing both friction and wear, and have been proposed to be suitable replacements for sulfurised olefins in lubricants.[104] Sun *et al.* also incorporated nitrogen into such additives by synthesising *S*-hydroxyethyl-*N,N*-dialkyl dithiocarbamate borates, which offered

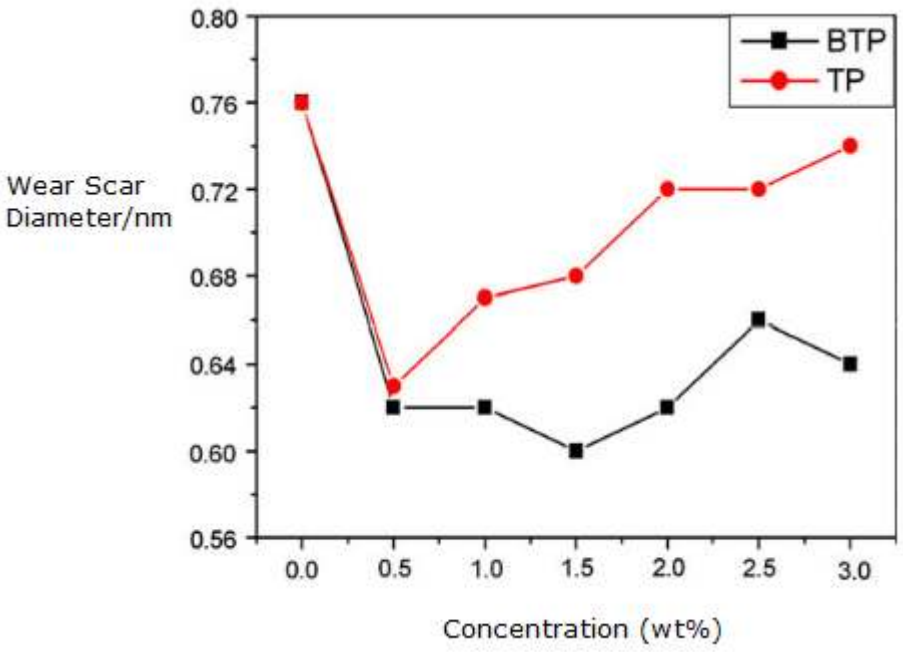


Figure 1.24 Variation in wear scar diameter for different concentrations of a boron-containing thiophosphite (BTP) additive and an analogous boron-free additive (TP).[105]

superior hydrolytic stability than alkyl borate esters and excellent friction- and wear-reducing properties when used as additives in PAOs.[106] This was further developed by Wang and co-workers, who designed a boron-containing thiophosphite additive, with boron, sulfur and phosphorus being the 'active elements', and nitrogen existing in the form of a linking amine group.[105] An analogous boron-free additive was also synthesised and tested, and proved to be a much less efficient anti-wear additive, suggesting that boron must play a key role in the anti-wear mechanism of this additive (Figure 1.24).

It has been reported that tri(hydroxymethyl)propane borate esters containing nitrogen (Figure 1.25) have good anti-wear properties and thermal stability in rapeseed oil, and it was found that increasing the length of the alkyl substituent improved the anti-wear performance of the compound.[107] Similarly, Shah *et al.* reported that the use of longer alkyl chains in alkylborate-dithiocarbamates improved their anti-wear performance and stability.[108] The mechanism of tribofilm formation for such three-coordinate borate esters has been suggested to be *via* the formation of a borate glass.

As for the phosphorus-containing anti-wear additives discussed above, there have been several recent studies investigating the efficacy of boron-containing ionic liquids as lubricant additives. For instance, Khatri and co-workers have described a series of di[bis(salicyalto)borate] ionic liquids which were found to be non-corrosive, possess high thermal stability, and good friction- and wear-reducing properties.[109] Their performance was attributed to the inherent polarity of the ionic

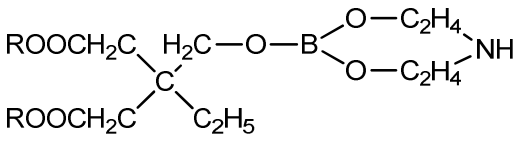


Figure 1.25 Tri(hydroxymethyl)propane borate esters. R = C_7H_{15}, $C_{17}H_{33}$.[107]

liquids leading to efficient formation of a boron-rich film. Furthermore, a patent filed in 2012 describes the use of a variety of four-coordinate borate ionic liquids with several long-chain countercations for use as lubricant additives which exhibited excellent anti-wear performance.[110]

1.4.3.3 Additives Containing Both Boron and Phosphorus

Due to the promising anti-wear properties of boron-containing additives and the known good performance of successful phosphorus-containing anti-wear additives such as ZDDP, additives containing a combination of boron and phosphorus have become of significant interest. Many studies have focused on combining simple boron-containing additives with ZDDP to enhance performance whilst lowering the amount of phosphorus required in the lubricant. For example, Cholakov and co-workers found that a significant amount of ZDDP can be replaced with a borate additive derived from 1,2-hydro-oxystearic acid, alkylphenol, boric acid and triethanolamine to provide a synergetic mixture with similar anti-wear performances to mixtures containing ZDDP alone.[111] Similarly, Varlot *et al.* found that partially replacing ZDPP with calcium borate provided an efficient anti-wear additive mixture.[112] Analysis by TEM and XPS found that the tribofilm comprised of borophosphate glass (Figure 1.26), which was molten under lubricating conditions.

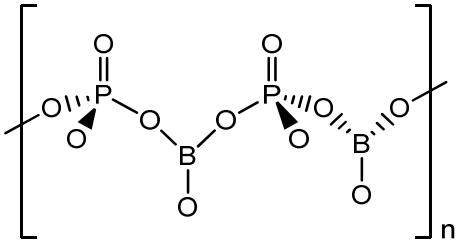


Figure 1.26 Structure of borophosphate glass.[112]

Furthermore, calcium borate was used in conjunction with ZDDP and molybdenum dithio-carbamates (Modtc) in a ternary system which, although no anti-wear improvement was seen, allowed for improved friction-reducing properties.[113]

Antzutkin *et al.* investigated the use of *S*-di-*n*-octoxyboron-*O,O'*-di-*n*-octyldithiophosphate (DOB-DTP) (Figure 1.27) as a lubricant additive, which proved to have better anti-wear and friction-reducing properties than ZDDP.[114] DOB-DTP further improved upon ZDDP as levels of friction were kept stable throughout testing for a range of concentrations. It was postulated that protective films were formed *via* the sulfur atoms binding to the metal surface, which was followed by decomposition into an inorganic layer containing phosphorus, sulfur, oxygen and boron.

Following this, a series of similar alkylborate-thiophosphates containing an ethylene linker between the thiophosphate and borate components were reported to have good anti-wear properties and high thermal stability.[115] This thermal stability was seen to increase with increasing alkyl chain length, and lower friction coefficients than for ZDDP were reported, suggesting that this class of additive could be considered as an efficient environmentally-friendly replacement for ZDDP.

An effective and environmentally friendly boron and phosphorus-containing additive was reported by Liu *et al*. in 2012 which was derived from soybean lecithin, a mixture of various phospholipids (Figure 1.28).[116] The compound was found to be

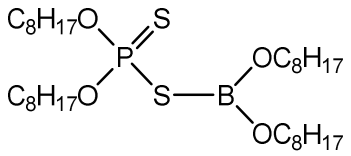


Figure 1.27 Structure of DOB-DTP.[114]

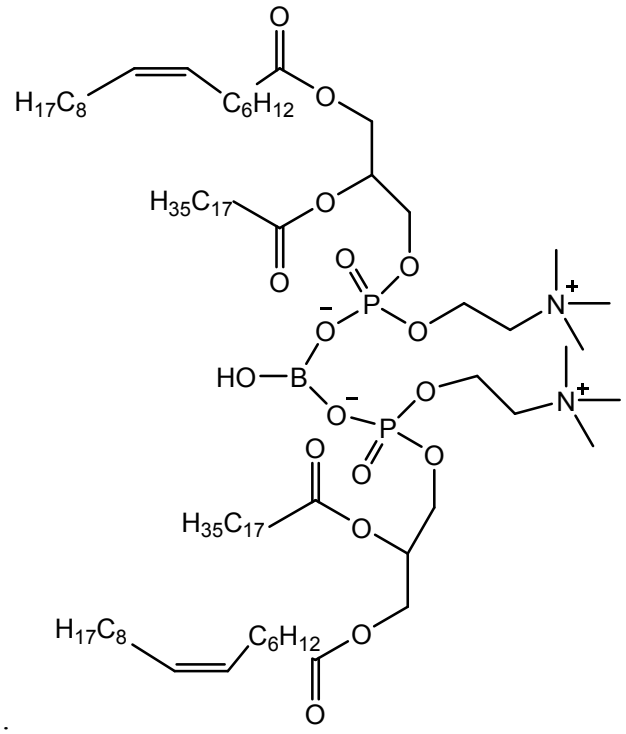


Figure 1.28 Structure of phosphate/borate compound based on soybean lecithin.[116]

hydrolytically stable and showed good anti-wear and friction-reducing performance in synthetic base oils. Furthermore, the steric hindrance offered by the long alkyl chains on the lecithin components led to excellent hydrolytic stability. SEM and XPS analysis revealed that the good performance of these species could be attributed to the formation of reaction films comprised of Fe_2O_3, iron polyphosphates, organic amines and boron nitride.

Phosphorus and boron have also been combined as ionic liquid lubricant additives, with Antzutkin and co-workers having reported the use of orthoborate-phosphonium ionic liquids as potential anti-wear additives for steel-aluminium contacts (Figure 1.29).[117] The compounds were designed to have good hydrolytic stability due to the chelating effect of the diol ligands on the boron centre. Furthermore, these compounds were found to have low melting points, high viscosities and excellent anti-wear and

friction-reducing performances, making them attractive options for environmentally benign anti-wear oil additives. Furthermore, Totolin *et al*. have reported the use of phosphonium phosphate additives in alkylborane imidazole ionic liquids which showed effective friction reduction and good anti-wear properties when tested on steel-steel contacts.[118]

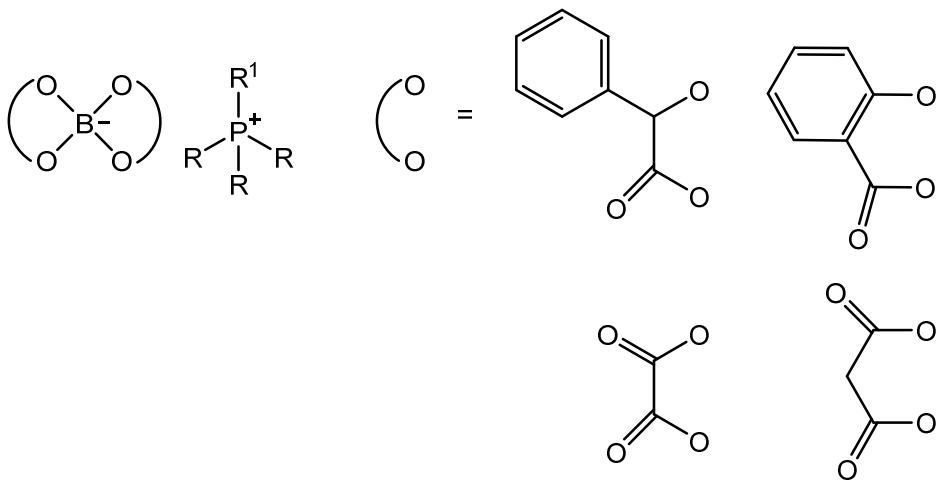


Figure 1.29 Structure of orthoborate-phosphonium ionic liquids. R = C_4H_9, C_6H_{13}, R^1 = C_8H_{17}, $C_{14}H_{29}$.[117]

1.5 Aims of this Research

High performing anti-wear additives are a genuine need if lubricants are to provide sufficient protection of automotive parts to increase engine efficiency and lower fuel consumption whilst causing minimal environmental impact. Although boron and phosphorus-containing anti-wear additives have received significant attention in recent years, with the examples put forth in this chapter highlighting their promising tribological properties, compounds containing both of these elements have not yet been fully explored for their anti-wear use. There is much scope for the synthesis of new classes of additives to be undertaken, involving further structural variation than what has been carried out thus far. Therefore, this project will involve the synthesis of a novel library of compounds containing both borate and phosphate components and the subsequent screening for their lubricant additive suitability and anti-wear performance.

Initial studies will focus on the synthesis and properties of three- and four-coordinate borate species, before the incorporation of anionic phosphate species is considered. Short-chain compounds will act as models for longer-chain analogues to be tested for their anti-wear performance, and investigations into their chemical behaviour will be carried out. Systematic variation in the structural components of the tested compounds will probe the relationship between the chemical structure and anti-wear performance of these species.

Chapter II
General Experimental Techniques

2.1 General Experimental Techniques

2.1.1 Manipulation of Air-sensitive Compounds

Due to the air and moisture-sensitivity of the model compounds synthesised in these studies, it was necessary that their manipulation be carried out under a strictly anaerobic and anhydrous environment. This ensures minimal hydrolysis of the desired products and is achieved through the utilisation of standard Schlenk line and glove box techniques.

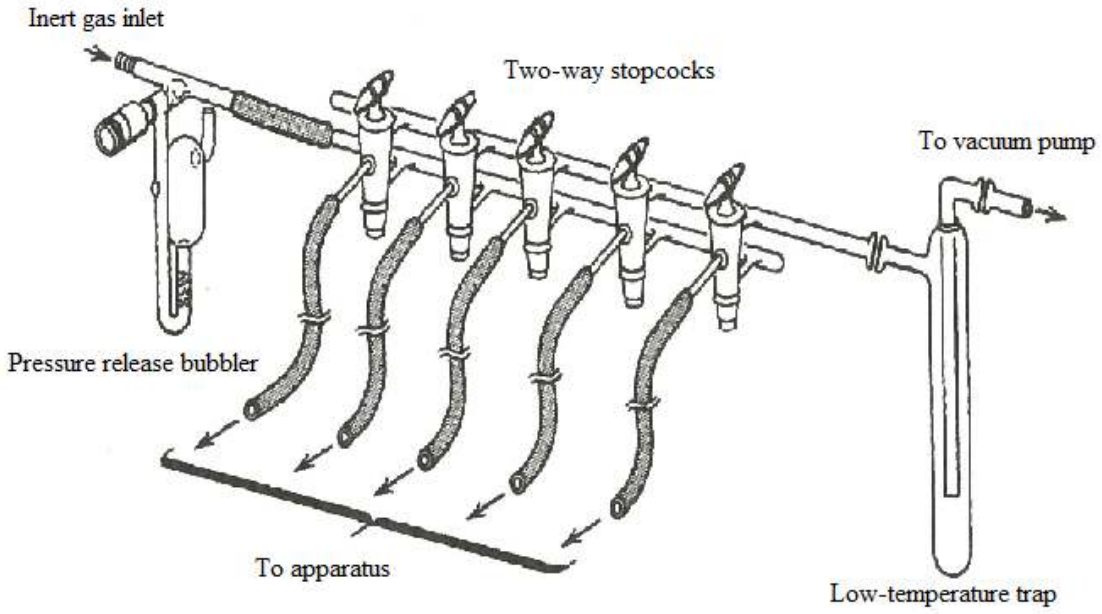


Figure 2.1 Schlenk line apparatus.

In order to maintain an inert atmosphere with the exclusion of air whilst handling both solids and liquids, a Schlenk line apparatus was used (Figure 2.1). This consisted of a heavy-walled pyrex glass manifold containing two-way glass stop-cocks connected to an argon gas cylinder and a dynamic vacuum (~10^{-4} mbar) achieved using an Edwards RV5 rotary vane two-stage mechanical vacuum pump in-line with an Edwards Pirani10 thermal conductivity vacuum gauge. A liquid nitrogen-cooled low-

temperature trap was used for the capture of volatiles from the Schlenk line to prevent contamination and damage to the vacuum pump.

Several thick-walled glass vessels such as Schlenk tubes and ampoules containing Young's taps were attached to the Schlenk line *via* flexible portex tubing and exposed to either the inert gas or vacuum through the stopcocks. Ground glass joints were lightly lubricated with Dow Corning high vacuum grease in order to prevent leaks. Typically, hot glassware was assembled and connected to the Schlenk line and evacuated such that a vacuum of *ca*. 10^{-3} mbar was achieved and flame dried under a continuous vacuum using a Bunsen burner. Once cooled to room temperature, the glassware was subjected to three refill and evacuation cycles, ensuring that an anaerobic and anhydrous atmosphere was achieved. Liquids and solutions were transferred between vessels *via* stainless steel cannulae and glass syringes through rubber septa.

An MBraun UNIlab glove box consisting of a stainless steel construction fitted with a strengthened viewing panel and neoprene gloves was used for storage of anhydrous materials and dry NMR solvents and for carrying out NMR titrations under an inert atmosphere. This inert atmosphere inside the glove box was maintained by the continuous recirculation of N_2 through a copper-based catalyst in order to keep trace O_2 and H_2O levels under 0.1 ppm. Equipment and apparatus were admitted through an ante-chamber using four pump-and-fill cycles in order to minimise the admission of air in to the glove box.

2.2 Physical Measurements

2.2.1 NMR Spectroscopy

Samples of air-sensitive compounds were prepared under an inert atmosphere using glove box techniques and Young's tap-modified borosilicate glass NMR tubes. All NMR data were collected on Bruker DPX300, DPX400, AV400, AV(III)400, AV(III)400HD or AV(III)500 spectrometers. NMR data for PIB_{550} catechol and PIB_{1000} catechol were collected by Lubrizol Corp. at Hazelwood, Derbyshire. Chemical shifts are quoted in ppm relative to neat TMS (^{1}H, $^{13}C\{^{1}H\}$), $BF_3{\cdot}OEt_2$ ($^{11}B\{^{1}H\}$) and H_3PO_4 ($^{31}P\{^{1}H\}$). Residual solvent signals were used as internal references for ^{1}H and $^{13}C\{^{1}H\}$ NMR measurements, and ^{1}H and ^{13}C assignments were confirmed with the use of ^{1}H-^{1}H and ^{1}H-^{13}C correlation experiments where necessary. Solid-state NMR data was acquired on a Bruker Avance III spectrometer operating at 600.13 MHz using a 2.5 mm, TriGamma ^{1}HXY probe. The Magic angle spinning rate was set to 20 kHz and a pulse sequence incorporating a phase cycled composite pulse, suitable for the suppression of background signals, was used to acquire the data.

2.2.2 Mass Spectrometry

Samples for air-sensitive mass spectrometry were prepared under an inert atmosphere in sealed glass capillary tubes. EI-MS measurements were carried out by Dr Mick Cooper at the University of Nottingham using a Bruker Apex4 FTMS using a heptacosafluorotributylamine calibrant, or at the EPSRC National Mass Spectrometry Service Centre using a perfluorotributyl high resolution MS reference, on a Finnigan MAT 95 XP double focussing mass spectrometer. ESI-MS measurements were performed as highly diluted sample solutions in methanol at the University of Nottingham using an automated LC-MS system, based on a Bruker MicroTOF

instrument, with a sodium formate calibrant. ESI-MS data for PIB_{550} catechol and PIB_{1000} catechol was collected by Lubrizol Corp. at Hazelwood. MALDI-TOF MS measurements were performed at the University of Nottingham using a Bruker Ultraflex MALDI TOF mass spectrometer.

2.2.3 Elemental Microanalysis

Air-sensitive elemental analysis samples were prepared under an inert atmosphere in glass ampoules and sealed under argon using Schlenk line techniques. Elemental microanalyses were carried out by Mr Stephen Boyer at the Microanalysis Service, London Metropolitan University.

2.2.4 ICP-OES Analysis

Air-sensitive ICP-OES samples were prepared under an inert atmosphere in glass ampoules and sealed under argon using Schlenk line techniques. ICP-OES analysis was carried out by MEDAC Ltd and ICP-OES analysis of oil-soluble samples was also carried out by the Lubrizol Corporation to verify these results.

2.2.5 UV/vis Spectroscopy

UV/vis spectroscopy samples were prepared as solutions of known concentration in a Young's tap modified 10 mm quartz cell in an inert atmosphere, using glove box techniques. UV/vis spectra were recorded on a Perkin Elmer Lamda 750 UV/vis spectrophotometer, over a wavelength range of 200-1100 nm.

2.2.6 X-ray Crystallography

Under a flow of nitrogen, crystals suitable for analysis by X-ray diffraction were quickly removed from the crystallisation vessel and covered in YR-1800 perfluoropolyether oil. Crystals were mounted on a polymer-tipped dual-stage glass

fibre MiTeGen MicroMount™ and cooled rapidly in a cold stream of nitrogen using an Oxford Cryostreams open flow cryostat.[119] Single crystal X-ray diffraction data were collected on either an Agilent SuperNova Atlas CCD diffractometer (mirror-monochromated Cu-K_α radiation source; λ = 1.54184 Å; ω scans), or an Agilent GV1000 Atlas CCD diffractometer (mirror-monochromated Cu-K_α radiation source; λ = 1.54184 Å; ω scans). Absorption corrections were applied using an analytical numerical method (CrysAlis Pro).[120] Non-H atoms were located using direct methods[121] or charge flipping.[122] Hydrogen atoms were placed and refined using a geometric riding model. Crystal structures were solved and refined using the Olex2 software package,[123] and CIF-checked in conjunction with Prof. Alexander Blake and Dr William Lewis of the School of Chemistry. Single crystal X-ray diffraction data for **[19]** was collected at the Diamond Light Source, beamline I19, and processed using the xia2 software package.[124] Crystal data can be found in Appendix I.

2.2.7 Computational Chemistry

Density Functional Theory (DFT) calculations were performed using Gaussian 03 software with the B3LYP exchange-correlation function.[125] Geometry optimisations were performed for all molecules in the gas phase without solvent effects, with geometry optimisations recognised as local minima by frequency calculations. Molecular orbital diagrams were generated using Molekel 4.2 software.[126] All calculations were carried out on the University of Nottingham's High Performance Computer by Mr Nicolas Pearce and Dr Jonathan McMaster.

2.2.8 Conductivity

AC impedance conductivities were measured using a CH 760 potentiostat in a frequency range from 1 Hz to 100 KHz with a cell containing two paralleled silver wires. The cell constant was 9.26 m^{-1} and was calibrated using a 0.117 M aqueous KCl solution. The volume of liquid within the cell was kept constant between measurements (2 mL).

2.3 Preparation of Solvents and Reagents

Toluene and benzene were dried *via* heating at reflux for three days over potassium metal, distillation and storage in ampoules over a potassium mirror. Dichloromethane and acetonitrile were dried *via* heating at reflux for three days over calcium hydride, distillation and storage in ampoules over 4 Å molecular sieves. *Iso*-Hexane was passed through activated 4 Å molecular sieves and stored over a potassium mirror. All solvents were degassed *in vacuo* before use using Schlenk line techniques. $CDCl_3$ and CD_2Cl_2 were dried over calcium hydride at 85 °C for five days before being vacuum-transferred to a sealed ampoule and degassed with three freeze-pump-thaw cycles before use.

Triethylphosphine oxide was dried *via* heating at 60 °C under a continuous flow of argon. Tetra-*n*-butylammonium acetate, tetra-*n*-butylammonium benzoate, tetra-*n*-butylammonium methanesulfonate and tetra-*n*-butylammonium nitrate were dried *via* the azeotropic removal of water in refluxing benzene. Tetra-*n*-butylammonium dihydrogen phosphate was dried *in vacuo* at 60 °C overnight. Triethylamine and tri-*n*-butylamine were stored over 4 Å molecular sieves prior to use.

Tridecyl alcohol (containing C_{11}-C_{14} *iso*-alcohols, but C_{13}-rich), 1-dodecene, a mixture of C_{16}-C_{18} alpha olefins, 550 M_w and 1000 M_w broad polydispersity polyisobutylene (PIB_{550}/PIB_{1000}), glycerol mono-oleate and FAX-5 filter aid were provided by the Lubrizol Corporation. All other reagents were commercially available and used as received.

2.4 Preparation of Precursors

2.4.1 General Procedure for the Synthesis of Mono-alkyl Phosphate Esters

Under an argon atmosphere, an alcohol was added to polyphosphoric acid (DP = 4) with overhead stirring at 300 rpm. The reaction mixture was heated at 85 °C with stirring at 300 rpm for 3 h before being allowed to cool to room temperature, giving the products as oils in typically a 3:1 ratio with H_3PO_4.

$H_2{}^nBuPO_4$ and H_3PO_4 are known species, but NMR data in $CDCl_3$ has not been reported. The values reported for residual H_3PO_4 contained in mono-alkyl phosphate esters was found to be variable (Table 2.1), which may be due to varying concentrations of phosphoric acid within the sample, and differing hydrogen bonding interactions between the acid and the various mono-alkyl phosphate species, as phosphoric acid has been found to exhibit different NMR properties in different concentrations.[127]

Table 2.1 Variable $^{31}P\{^1H\}$ chemical shifts for H_3PO_4 peak in mono-alkyl phosphate ester spectra.

H_3PO_4-containing Species	**δ_P**
$H_2{}^nBuPO_4$	−0.24
$H_2{}^nOctPO_4$	−0.70
$H_2(2\text{-}EtC_6H_{12})PO_4$	1.28
$H_2OleylPO_4$	−0.09
$H_2(C_{13}H_{27})PO_4$	−0.30

$H_2{}^nBuPO_4$

Synthesised from *n*-butanol (100 mL, 1.09 mol) and polyphosphoric acid (148 g, 0.36 mol); 229 g of $H_2{}^nBuPO_4$ and residual H_3PO_4 (yellow oil, 98 %). ^{1}H NMR (300.13 MHz, 298K, $CDCl_3$): δ = 9.89 (2H, s, O-*H*), 9.30 (1H, s, O-*H*), 9.19 (1H, s, O-*H*), 4.07 (2H, q, ^3J = 7 Hz, CH_2), 1.67 (2H, quin, ^3J = 8 Hz, CH_2), 1.42 (2H, sext, ^3J = 8 Hz, CH_2, 0.94 (3H, t, ^3J = 7 Hz, CH_3). ^{13}C{^{1}H} NMR (75.47 MHz, 298K, $CDCl_3$): δ = 68.1 (*C*H_2), 32.0 (*C*H_2), 18.5 (*C*H_2), 13.5 (*C*H_3). ^{31}P{^{1}H} NMR (121.49 MHz, 298K, $CDCl_3$): δ = 1.42 ($H_2{}^n$Bu*P*O_4), −0.24 (H_3PO_4). MS (ESI negative mode) Expected: 154.0395, Found: 153.0317 ($M-H^-$).

$H_2{}^iBuPO_4$

Synthesised from *iso*-butanol (201 mL, 2.18 mol) and polyphosphoric acid (247 g, 0.73 mol): 311 g of $H_2{}^iBuPO_4$ and residual H_3PO_4 (orange oil, 93 %). ^{1}H NMR (400.13 MHz, 298K, $CDCl_3$): δ = 9.70 (2H, s, O-*H*), 9.20 (1H, s, br, O-*H*), 3.82 (2H, t, ^3J = 6 Hz, CH_2), 1.97 (1H, sept, ^3J = 6 Hz, C*H*), 0.95 (6H, d, ^3J = 6 Hz, CH_3). ^{13}C{^{1}H} NMR (100.61 MHz, 298K, $CDCl_3$): δ = 74.0 (d, ^2J = 5 Hz, P-*C*H_2), 28.8 (d, ^3J = 7 Hz, P-*C*H), 18.5 (*C*H_3). ^{31}P{^{1}H} NMR (161.98 MHz, 298K, $CDCl_3$): δ = 1.26. MS (ESI negative mode) Expected: 154.0395, Found: 153.0317 ($M-H^-$).

$H_2{}^nOctPO_4$

Synthesised from *n*-octanol (172 mL, 1.09 mol) and polyphosphoric acid (147 g, 0.36 mol); 287 g of $H_2{}^nOctPO_4$ and residual H_3PO_4 (yellow oil, 99 %). ^{1}H NMR (300.13 MHz, 298K, $CDCl_3$): δ = 10.74 (2H, s, O-*H*), 9.73 (1H, s, br, O-*H*), 4.09 (2H, q, ^3J = 8 Hz, CH_2), 1.71 (2H, m, ^3J = 8 Hz, CH_2), 1.31 (10H, m, br, CH_2), 0.91 (3H, t, ^3J = 8 Hz, CH_3). ^{13}C{^{1}H} NMR (100.61 MHz, 298K, $CDCl_3$): δ = 68.6 (d, ^2J = 6 Hz, P-*C*H_2),

31.8 (CH$_2$), 30.0 (d, ^3J = 10 Hz, P-CH$_2$), 29.2 (CH$_2$), 29.2 (CH$_2$), 25.3 (CH$_2$), 22.6 (CH$_2$), 14.1 (CH$_3$). ^{31}P{^{1}H} NMR (121.49 MHz, 298K, CDCl$_3$): δ = −0.70 (H$_3P$O$_4$), −0.88 (H^{n}Oct$P$O$_4$). MS (ESI negative mode) Expected: 210.1021, Found: 209.0930 (M−H$^-$).

H$_2$(2-EtC$_6$H$_{12}$)PO$_4$

Synthesised from 2-ethylhexanol (170 mL, 1.09 mol) and polyphosphoric acid (144 g, 0.36 mol); 283 g of H$_2$(2-EtC$_6$H$_{12}$)PO$_4$ and residual H$_3$PO$_4$ (pale orange oil, 99 %). ^{1}H NMR (300.13 MHz, 298K, CDCl$_3$): δ = 10.61 (2H, s, br, O-H), 9.63 (1H, s br, O-H), 3.98 (2H, m, CH_2), 1.59 (1H, m, CH), 1.18-1.50 (8H, m, overlapping CH_2 peaks), 0.90 (6H, m, overlapping CH_3 peaks). ^{13}C{^{1}H} NMR (75.47 MHz, 298K, CDCl$_3$): δ = 70.4 (CH$_2$), 39.9 (CH), 29.7 (CH$_2$), 28.8 (CH$_2$), 23.0 (CH$_2$), 22.9 (CH$_2$), 14.0 (CH$_3$), 10.8 (CH$_3$). ^{31}P{^{1}H} NMR (121.49 MHz, 298K, CDCl$_3$): δ = 1.61 (H$_2$(2-EtC$_6$H$_{12}$)PO$_4$), 1.28 (H$_3P$O$_4$). MS (ESI negative mode) Expected: 210.1021 Found: 209.0922 (M−H$^-$), 210.0963 (M$^-$).

H$_2$OleylPO$_4$

Synthesised from oleyl alcohol (317 mL, 1.20 mol) and polyphosphoric acid (163 g, 0.40 mol); 163 g of H$_2$OleylPO$_4$, residual H$_3$PO$_4$, and a small quantity of HOleyl$_2$PO$_4$ (orange/brown highly viscous oil, 49 %). ^{1}H NMR (300.13 MHz, 298K, CDCl$_3$): δ = 9.71 (5H, s, br, O-H), 5.39 (1H, t, ^3J = 3 Hz, CH), 4.05 (1H, m, CH), 1.98 (3H, m, br, CH_2), 1.67 (3H, m, br, CH_2), 1.27 (22H, s, br, overlapping CH_2 peaks), 0.89 (3H, t, ^3J = 6 Hz, CH_3). ^{13}C{^{1}H} NMR (75.47 MHz, 298K, CDCl$_3$): δ = 130.3 (CH), 129.9 (CH), 68.2 (CH$_2$), 32.6 (CH$_2$), 31.9 (CH$_2$), 30.2 (CH$_2$), 30.1 (CH$_2$), 29.7 (CH$_2$), 29.7 (CH$_2$), 29.6 (CH$_2$), 29.6 (CH$_2$), 29.5 (CH$_2$), 29.4 (CH$_2$), 29.2 (CH$_2$), 27.2 (CH$_2$), 24.9 (CH$_2$), 22.7 (CH$_2$), 14.1 (CH$_3$). ^{31}P{^{1}H} NMR (121.49 MHz, 298K, CDCl$_3$): δ = 0.89

($H_2Oleyl\mathit{P}O_4$), 0.76 ($HOleyl_2\mathit{P}O_4$), −0.09 ($H_3\mathit{P}O_4$). MS (ESI negative mode) Expected: 348.2429, Found: 347.2347 ($M-H^-$).

$H_2(C_{13}H_{27})PO_4$

From tridecyl alcohol (240 g, 1.20 mol) and polyphosphoric acid (163 g, 0.40 mol); 284 g of $H_2(C_{13}H_{27})PO_4$ (orange oil, 85 %). ^{1}H NMR (300.13 MHz, 298K, $CDCl_3$): δ = 10.81 (3H, s, br, O-*H*), 9.46 (2H, s, br, O-*H*), 4.08 (2H, m, br, CH_2), 0.97-1.92 (16H, m, br, overlapping C*H* and CH_2 peaks), 0.59-0.95 (15H, m, br, overlapping CH_3 peaks). $^{13}C\{^1H\}$ NMR (75.47 MHz, 298K, $CDCl_3$): δ = 68.9 (*C*H_2), 66.9 (*C*H_2), 37/0 (*C*H), 34.7 (*C*H), 29.4 (*C*H_2), 28.3 (*C*H_2), 26.7 (*C*H_2), 23.1 (*C*H_2), 22.7 (*C*H_2), 19.2 (*C*H_3), 14.4 (*C*H_3), 14.1 (*C*H_3), 12.2 (*C*H_3), 11.4 (*C*H_3). $^{31}P\{^1H\}$ NMR (121.49 MHz, 298K, $CDCl_3$): δ = 1.48 ($H_2(C_{13}H_{27})\mathit{P}O_4$), −0.30 ($H_3\mathit{P}O_4$). (ESI negative mode) Expected: 280.1803, Found: 279.1731 ($M-H^-$).

2.4.2 General Procedure for the Synthesis of Ammonium Phosphates

The amine of choice was added to an appropriate mono- or di-alkyl phosphate. The reaction mixture was stirred at room temperature until the observed exotherm subsided and the mixture became viscous and homogenous (20-50 min). Due to the high melting point of dodecylamine, the reaction to synthesise $[C_{12}H_{25}NH_3][H(2\text{-}EtC_6H_{12})PO_4]$ was carried out in dichloromethane (100 mL) for 16 h, and volatiles removed *in vacuo* to give the desired product in typically a 3:1 ratio with the dihydrogen phosphate analogue.

$[HN^nBu_3][H^nBuPO_4]$

Synthesised from tri-*n*-butylamine (10.2 mL, 42.6 mmol) and $H_2{}^n BuPO_4$ (6.57 g, 42.6 mmol); 13.7 g of $[HN^nBu_3][H^nBuPO_4]$ and residual $[HN^nBu_3][H_3PO_4]$ (colourless

highly viscous oil, 96 %). ^{1}H NMR (300.13 MHz, 298K, $CDCl_3$): δ = 10.27 (2H, s, br, N-*H*/O-*H*), 3.85 (2H, m, α-C*H*$_2$ of phosphate), 2.89 (6H, m, α-C*H*$_2$ of ammonium), 1.63 (8H, m, overlapping C*H*$_2$ peaks), 1.32 (8H, m, overlapping C*H*$_2$ peaks), 0.90 (9H, t, ^{3}J = 7 Hz, C*H*$_3$ of ammonium), 0.84 (3H, t, ^{3}J = 7 Hz, C*H*$_3$ of phosphate). ^{13}C{^{1}H} NMR (75.47 MHz, 298K, $CDCl_3$): δ = 64.6 (*C*H$_2$), 51.5 (*C*H$_2$), 32.8 (*C*H$_2$), 25.0 (*C*H$_2$), 20.1 (*C*H$_2$), 19.0 (*C*H$_2$), 13.8 (*C*H$_3$), 13.6 (*C*H$_3$). ^{31}P{^{1}H} NMR (121.49 MHz, 298K, $CDCl_3$): δ = 2.47 ($H_2PO_4^-$), 2.10 (H^nBuPO_4). MS (ESI negative mode): Expected: 339.254, Found: 339.2005 (M^-). MS (ESI positive mode): 186.2246 ($[HN^nBu_3]^+$).

[(2-EtC$_6$H$_{12}$)$_2$NH$_2$][H^{n}BuPO$_4$]

Synthesised from bis(2-ethylhexyl)amine (10.3 mL, 34.4 mmol) and $H_2{}^nBuPO_4$ (6.35 g, 34.3mmol); 14.5 g of $[(2\text{-}EtC_6H_{12})_2NH_2][H^nBuPO_4]$ (colourless highly viscous oil, 99 %). ^{1}H NMR (400.13 MHz, 298K, $CDCl_3$): δ = 9.97 (2H, s, N-*H*), 9.06 (1H, s, O-*H*), 3.86 (2H, m, α-C*H*$_2$ of phosphate), 2.81 (4H, m, α-C*H*$_2$ of ammonium), 1.75 (2H, sept, ^{3}J = 8 Hz, C*H*), 1.40 (20H, m, overlapping C*H*$_2$ peaks), 0.89 (15H, m, overlapping C*H*$_3$ peaks). ^{13}C{^{1}H} NMR (100.61 MHz, 298K, $CDCl_3$): δ = 65.3 (*C*H$_2$), 49.5 (*C*H$_2$), 35.0 (*C*H), 32.7 (*C*H$_2$), 30.3 (*C*H$_2$), 28.4 (*C*H$_2$), 23.3 (*C*H$_2$), 22.9 (*C*H$_2$), 18.9 (*C*H$_2$), 14.0 (*C*H$_2$), 13.8 (*C*H$_3$), 10.1 (*C*H$_3$). ^{31}P{^{1}H} NMR (121.49 MHz, 298K, $CDCl_3$): δ = 1.57 (H_3PO_4), 1.35 (H^nBuPO_4). MS (ESI positive mode): 242.2830 ($[(2\text{-}EtC_6H_{12})_2NH_2]^+$)

[HNEt$_3$][H^{n}BuPO$_4$]

Synthesised from triethylamine (10.0 mL, 71.7 mmol) and $H_2{}^nBuPO_4$ (11.0 g, 71.7 mmol); 18.3 g of $[HNEt_3][H^nBuPO_4]$ (yellow highly viscous oil, quant.). ^{1}H NMR (300.13 MHz, 298K, $CDCl_3$): δ = 9.67 (1H, s, br, N-*H*), 3.89 (2H, m, α-C*H*$_2$ of phosphate), 3.04 (6H, q, ^{3}J = 7 Hz, α-C*H*$_2$ of ammonium), 1.60 (2H, m, β-C*H*$_2$ of

phosphate), 1.38 (2H, m, γ-CH_2 of phosphate), 1.30 (9H, t, ^3J = 7 Hz, CH_3 of ammonium), 0.89 (3H, t, ^3J = 7 Hz, CH_3 of phosphate). $^{13}C\{^1H\}$ NMR (75.47 MHz, 298K, $CDCl_3$): δ = 64.8 (*C*H_2), 45.3 (*C*H_2), 32.8 (*C*H_2), 19.0 (*C*H_2), 13.9 (*C*H_3), 8.54 (*C*H_3). $^{31}P\{^1H\}$ NMR (121.49 MHz, 298K, $CDCl_3$): δ = 2.47 (H_3PO_4), 2.17 (H^nBuPO_4). MS (ESI negative mode): Expected: 255.1599, Found: 255.2341 (M^-).

[HN^{n}Bu$_3$][^{n}Bu$_2$PO$_4$]

Synthesised from tri-*n*-butylamine (10.0 mL, 42.1 mmol) and $H^nBu_2PO_4$ (8.85 g, 42.1 mmol); 16.6 g of $[HN^nBu_3][^nBu_2PO_4]$ (colourless oil, quant.) ^1H NMR (300.13 MHz, 298K, $CDCl_3$): δ = 13.29 (1H, s, br, N-*H*), 3.85 (4H, q, ^3J = 6 Hz, α-CH_2 of phosphate), 2.90 (6H, m, α-CH_2 of ammonium), 1.63 (10H, m, overlapping CH_2 peaks), 1.37 (10H, m, overlapping CH_2 peaks), 0.95 (9H, t, ^3J = 7 Hz, CH_3 of ammonium), 0.89 (6H, t, ^3J = 7 Hz, CH_3 of phosphate). $^{13}C\{^1H\}$ NMR (75.47 MHz, 298K, $CDCl_3$): δ = 65.0 (*C*H_2), 51.5 (*C*H_2), 32.9 (*C*H_2), 25.1 (*C*H_2), 20.2 (*C*H_2), 19.0 (*C*H_2), 13.8 (*C*H_3), 13.6 (*C*H_3). $^{31}P\{^1H\}$ NMR (121.49 MHz, 298K, $CDCl_3$): δ = 0.89. MS (ESI negative mode): 209.0944 ($[^nBu_2PO_4]^-$). MS (ESI positive mode): 186.2234 ($[HN^nBu_3]^+$).

[(2-EtC$_6$H$_{12}$)$_3$NH][H^{n}BuPO$_4$]

Synthesised from tris(2-ethylhexyl)amine (23.5 mL, 54.2 mmol) and $H_2{}^nBuPO_4$ (8.34 g, 54.2 mmol); 27.1 g of $[(2\text{-}EtC_6H_{12})_3NH][H^nBuPO_4]$ (colourless viscous oil, 98 %). ^1H NMR (300.13 MHz, 298K, $CDCl_3$): δ = 8.50 (3H, s, br, N-*H*/O-*H*), 3.89 (1H, m, α-CH_2 of phosphate), 2.41 (4H, m, α-CH_2 of ammonium), 1.20-1.64 (31H, m, br, overlapping C*H* and CH_2 peaks), 0.89 (21H, m, overlapping CH_3 peaks). $^{13}C\{^1H\}$ NMR (75.47 MHz, 298K, $CDCl_3$): δ = 65.4 (*C*H_2), 59.5 (*C*H_2), 36.2 (*C*H), 32.7 (*C*H_2), 31.2 (*C*H_2), 28.6 (*C*H_2), 24.4 (*C*H_2), 23.1 (*C*H_2), 18.9 (*C*H_2), 14.0 (*C*H_3), 13.7 (*C*H_3), 10.5 (*C*H_3). $^{31}P\{^1H\}$ NMR (121.49 MHz, 298K, $CDCl_3$): δ = 0.92 (H^nBuPO_4), 0.44

(H_3PO_4). MS (ESI negative mode): 153.0316 ($[H^nBuPO_4]^-$). MS (ESI positive mode): 354.4105 ($[(2\text{-}EtC_6H_{12})_3NH]^+$).

[$H_2N^nBu_2$][H^nBuPO_4]

Synthesised from di-*n*-butylamine (10.0 mL, 58.7 mmol) and $H_2{}^nBuPO_4$ (12.3 g, 58.7 mmol); 13.0 g of [$H_2N^nBu_2$][H^nBuPO_4] (colourless oily solid, 94 %). ^{1}H NMR (300.13 MHz, 298K, $CDCl_3$): δ = 9.17 (1H, s, br, O-*H*), 7.10 (3H, s, br, N-*H*), 3.91 (2H, m, α-C*H*$_2$ of phosphate), 2.91 (4H, m, α-C*H*$_2$ of ammonium), 1.73 (4H, m, β-C*H*$_2$ of ammonium), 1.62 (2H, m, β-C*H*$_2$ of phosphate), 1.39 (6H, m, C*H*$_2$), 0.93 (9H, m, overlapping C*H*$_3$ peaks). ^{13}C{^{1}H} NMR (75.47 MHz, 298K, $CDCl_3$): δ = 65.6 (*C*H$_2$), 46.3 (*C*H$_2$), 32.5 (*C*H$_2$), 27.3 (*C*H$_2$), 20.0 (*C*H$_2$), 18.8 (*C*H$_2$), 13.7 (*C*H$_3$), 13.6 (*C*H$_3$). ^{31}P{^{1}H} NMR (121.49 MHz, 298K, $CDCl_3$): δ = 1.40 (H_3PO_4), 1.20 (H^nBuPO_4). MS (ESI negative mode): 153.0322 ($[H^nBuPO_4]^-$). MS (ESI positive mode): 130.1597 ($[H_2N^nBu_2]^+$).

[H_3N^nBu][H^nBuPO_4]

Synthesised from 1-butylamine (10.0 mL, 58.7 mmol) and $H_2{}^nBuPO_4$ (12.3 g, 58.7 mmol): 19.6 g of [H_3N^nBu][H^nBuPO_4] (colourless, sticky solid, 99 %). ^{1}H NMR (300.13 MHz, 298K, $CDCl_3$): δ = 8.05 (2H, s, br, O-*H*), 7.25 (3H, s. br N-*H*), 3.85 (2H, m, br, α-C*H*$_2$ of phosphate), 2.91 (s, br, α-C*H*$_2$ of ammonium), 1.70 (2H, m, br, C*H*$_2$), 1.60 (2H, m, br, C*H*$_2$), 1.39 (4H, m, br, overlapping C*H*$_2$ peaks), 0.93 (6H, m, br, overlapping C*H*$_3$ peaks). ^{13}C{^{1}H} NMR (75.47 MHz, 298K, $CDCl_3$): δ = 65.3 (*C*H$_2$), 39.5 (*C*H$_2$), 32.70 (*C*H$_2$), 32.70 (*C*H$_2$), 29.4 (*C*H$_2$), 19.8 (*C*H$_2$), 16.9 (*C*H$_2$), 13.7 (*C*H$_3$), 13.6 (*C*H$_3$). ^{31}P{^{1}H} NMR (121.49 MHz, 298K, $CDCl_3$): δ = 0.07. MS (ESI negative mode): 153.0317 ($[H^nBuPO_4]^-$).

[HN^{n}Bu$_3$][H^{i}BuPO$_4$]

Synthesised from tri-*n*-butylamine (10.0 mL, 42.1 mmol) and H$_2$^{i}BuPO$_4$ (6.48 g, 42.1 mmol); 14.2 g of [HN^{n}Bu$_3$][H^{i}BuPO$_4$] (off-white oil, 99 %). ^{1}H NMR (300.13 MHz, 298K, $CDCl_3$): δ = 9.70 (1H, s, br, N-*H*), 3.66 (2H, t, ^{3}J = 6 Hz, α-C*H*$_2$ of phosphate), 2.92 (6H, m, α-C*H*$_2$ of ammonium), 1.88 (1H, sept, ^{3}J = 6 Hz, C*H*), 1.66 (6H, m, β-C*H*$_2$ of ammonium), 1.35 (6H, m, γ-C*H*$_2$ of ammonium), 0.93 (9H, t, ^{3}J = 7 Hz, C*H*$_3$ of ammonium), 0.89 (6H, d, ^{3}J = 6 Hz, C*H*$_3$ of phosphate). ^{13}C{^{1}H} NMR (75.47 MHz, 298K, $CDCl_3$): δ = 71.3 (*C*H$_2$), 51.5 (*C*H$_2$), 29.3 (*C*H), 25.0 (*C*H$_2$), 20.1 (*C*H$_2$), 19.1 (*C*H$_3$). 13.7 (*C*H$_3$). ^{31}P{^{1}H} NMR (121.49 MHz, 298K, $CDCl_3$): δ = 2.49 (H$_3$*P*O$_4$), 2.17 (H^{i}Bu*P*O$_4$). MS (ESI negative mode): 153.0318 ([H^{i}BuPO$_4$]$^{-}$). MS (ESI positive mode): 186.2227 ([HN^{n}Bu$_3$]$^{+}$).

[HN^{n}Bu$_3$][H^{n}OctPO$_4$]

Synthesised from tri-*n*-butylamine (10.0 mL, 42.0 mmol) and H$_2$^{n}OctPO$_4$ (8.81 g, 42.0 mmol); 15.3 g of [HN^{n}Bu$_3$][H^{n}OctPO$_4$] (yellow oil, 92 %). ^{1}H NMR (400.13 MHz, 298K, $CDCl_3$): δ = 9.43 (2H, s, br, N-*H*/O-*H*), 3.85 (2H, m, ^{3}J = 8 Hz, C*H*$_2$), 2.91 (6H, m, ^{3}J = 4 Hz, C*H*$_2$), 1.51-1.72 (8H, m, overlapping C*H*$_2$ peaks), 1.29-1.39 (8H, m, overlapping C*H*$_2$ peaks), 1.13-1.28 (8H, m, overlapping C*H*$_2$ peaks), 0.91 (9H, t, ^{3}J = 8 Hz, overlapping C*H*$_3$ peaks), 0.83 (3H, t, ^{3}J = 8 Hz, C*H*$_3$). ^{13}C{^{1}H} NMR (100.61 MHz, 298K, $CDCl_3$): δ = 65.2 (*C*H$_2$), 51.5 (*C*H$_2$), 31.8 (*C*H$_2$), 30.8 (*C*H$_2$), 29.3 (*C*H$_2$), 25.8 (*C*H$_2$), 25.0 (*C*H$_2$), 22.6 (*C*H$_2$), 20.1 (*C*H$_2$), 14.1 (*C*H$_3$), 13.6 (*C*H$_3$). ^{31}P{^{1}H} NMR (161.92 MHz, 298K, $CDCl_3$): δ = 2.26 (H$_3$*P*O$_4$), 1.96 (H^{n}Oct*P*O$_4$). MS (ESI negative mode): 209.0965 ([H^{n}OctPO$_4$]$^{-}$). MS (ESI positive mode): 186.2222 ([HN^{n}Bu$_3$]$^{+}$).

[(2-EtC$_6$H$_{12}$)$_2$NH$_2$][H^{n}OctPO$_4$]

Synthesised from bis(2-ethylhexyl)amine (10.0 mL, 33.2 mmol) and $H_2{}^nOctPO_4$ (6.98 g, 33.2 mmol); 15.0 g of $[(2\text{-}EtC_6H_{12})_2NH_2][H^nOctPO_4]$ (yellow oil, 99 %). ^{1}H NMR (400.13 MHz, 298K, $CDCl_3$): δ = 9.02 (1H, s, br, N-*H*/O-*H*), 6.57 (3H, s, br, N-*H*/O-*H*), 3.86 (2H, m, ^3J = 8 Hz, C*H*$_2$), 2.73-2.93 (4H, m, C*H*$_2$), 1.75 (2H, m, C*H*), 1.18-1.67 (28H, m, overlapping C*H*$_2$ peaks), 0.90 (15H, t, ^3J = 8 Hz, overlapping C*H*$_3$ peaks). ^{13}C{^{1}H} NMR (100.61 MHz, 298K, $CDCl_3$): δ = 65.8 (*C*H$_2$), 49.4 (*C*H$_2$), 35.0 (*C*H), 31.9 (*C*H$_2$), 30.3 (*C*H$_2$), 30.2 (*C*H$_2$), 29.4 (*C*H$_2$), 29.3 (*C*H$_2$), 28.4 (*C*H$_2$), 25.8 (*C*H$_2$), 23.3 (*C*H$_2$), 22.9 (*C*H$_2$), 22.7 (*C*H$_2$), 14.1 (*C*H$_3$), 10.2 (*C*H$_3$). ^{31}P{^{1}H} NMR (161.92 MHz, 298K, $CDCl_3$): δ = 1.51 (H^nOct*P*O_4), 1.47 (H_3*P*O_4). MS (ESI negative mode): 209.0965 ($[H^nOctPO_4]^-$). MS (ESI positive mode): 242.2841 ($[(2\text{-}EtC_6H_{12})_2NH_2]^+$).

[HN^{n}Bu$_3$][H(2-EtC$_6$H$_{12}$)PO$_4$]

Synthesised from tri-*n*-butylamine (10.0 mL, 42.0 mmol) and $H_2(2\text{-}EtC_6H_{12})PO_4$ (8.81 g, 42.0 mmol); 17.0 g of $[HN^nBu_3][H(2\text{-}EtC_6H_{12})PO_4]$ (colourless oil, quant.) ^{1}H NMR (300.13 MHz, 298K, $CDCl_3$): δ = 9.23 (3H, s, br, N-*H*/O-*H*), 3.78 (2H, oct, *J* = 6 Hz, C*H*$_2$), 2.93 (8H, quin, *J* = 6 Hz, overlapping C*H*$_2$ peaks), 1.66 (8H, m, overlapping C*H*$_2$ peaks), 1.17-1.55 (18H, m, br, overlapping C*H* and C*H*$_2$ peaks), 0.93 (12H, t, ^3J = 6 Hz, C*H*$_3$). 0.85 (6H, ^3J = 6 Hz, C*H*$_3$). ^{13}C{^{1}H} NMR (75.47 MHz, 298K, $CDCl_3$): δ = 67.5 (*C*H$_2$), 51.5 (*C*H$_2$), 40.3 (*C*H), 30.1 (*C*H$_2$), 29.1 (*C*H$_2$), 25.0 (*C*H$_2$), 23.3 (*C*H$_2$), 23.1 (*C*H$_2$), 20.1 (*C*H$_2$), 14.1 (*C*H$_3$), 13.7 (*C*H$_3$), 11.0 (*C*H$_3$). ^{31}P{^{1}H} NMR (121.49 MHz, 298K, $CDCl_3$): δ = 2.35 (H(2-EtC$_6$H$_{12}$)*P*O$_4$), 2.34 (H_3*P*O_4). MS (ESI negative mode): 209.0938 ($[H(2\text{-}EtC_6H_{12})PO_4]^-$). MS (ESI positive mode): 186.2216 ($[HN^nBu_3]^+$).

[(2-EtC$_6$H$_{12}$)$_2$NH$_2$][H(2-EtC$_6$H$_{12}$)PO$_4$]

Synthesised from bis(2-ethylhexyl)amine (10.0 mL 33.2 mmol) and H_2(2-EtC_6H_{12})PO_4 (6.97 g, 33.2 mmol); 15.2 g of [(2-EtC_6H_{12})$_2NH_2$][H(2-EtC_6H_{12})PO_4] (colourless oil, quant.). ^{1}H NMR (300.13 MHz, 298K, $CDCl_3$): δ = 9.12 (4H, s, br, N-*H*/O-*H*), 3.74 (2H, oct, *J* = 6 Hz, C*H*$_2$), 2.81 (4H, oct, *J* = 6 Hz, C*H*$_2$), 1.74 (2H, quin, *J* = 6 Hz, C*H*$_2$), 1.16-1.60 (25H, m, br, overlapping C*H* and C*H*$_2$ peaks), 0.88 (18H, m, overlapping C*H*$_3$ peaks). ^{13}C{^{1}H} NMR (75.47 MHz, 298K, $CDCl_3$): δ = 67.7 (*C*H$_2$), 49.1 (*C*H$_2$), 40.3 (*C*H), 35.0 (*C*H), 30.2 (*C*H$_2$), 30.0 (*C*H$_2$), 29.0 (*C*H$_2$), 28.5 (*C*H$_2$), 25.4 (*C*H$_2$), 23.24 (*C*H$_2$), 23.1 (*C*H$_2$), 22.7 (*C*H$_2$), 14.1 (*C*H$_3$), 14.1 (*C*H$_3$), 10.9 (*C*H$_3$), 10.1 (*C*H$_3$). ^{31}P{^{1}H} NMR (121.49 MHz, 298K, $CDCl_3$): δ = 1.75 (H(2-EtC_6H_{12})*P*O_4), 1.67 (H_3PO_4). MS (ESI negative mode): 209.0938 ([H(2-EtC_6H_{12})PO_4]$^-$). MS (ESI positive mode): 242.2846 ([(2-EtC_6H_{12})$_2NH_2$]$^+$).

[(2-EtC$_6$H$_{12}$)$_3$NH][H(2-EtC$_6$H$_{12}$)PO$_4$]

Synthesised from tris(2-ethylhexylamine) (10.0 mL, 23.1 mmol) and H_2(2-EtC_6H_{12})PO_4 (4.86 g, 23.1 mmol); 10.8 g of [(2-EtC_6H_{12})$_3$NH][H(2-EtC_6H_{12})PO_4] (colourless oil, 83 %). ^{1}H NMR (300.13 MHz, 298K, $CDCl_3$): δ = 9.39 (2H, s, br, N-*H*/O-*H*), 3.82 (2H, m, α-C*H*$_2$ of phosphate), 2.59 (6H, s, br, α-C*H*$_2$ of ammonium), 1.14-1.73 (36H, m, br, overlapping C*H* and C*H*$_2$ peaks), 0.88 (24H, m, overlapping C*H*$_3$ peaks). ^{13}C{^{1}H} NMR (75.47 MHz, 298K, $CDCl_3$): δ = 68.2 (*C*H$_2$), 59.1 (*C*H$_2$), 40.1 (*C*H), 35.7 (*C*H), 31.3 (*C*H$_2$), 29.9 (*C*H$_2$), 29.0 (*C*H$_2$), 28.6 (*C*H$_2$), 24.4 (*C*H$_2$), 23.2 (*C*H$_2$), 23.1 (*C*H$_2$), 23.0 (*C*H$_2$), 14.1 (*C*H$_3$), 14.1 (*C*H$_3$), 10.9 (*C*H$_3$), 10.4 (*C*H$_3$). ^{31}P{^{1}H} NMR (121.49 MHz, 298K, $CDCl_3$): δ = 2.08 (H(2-EtC_6H_{12})*P*O_4), −0.15 (H_3PO_4). MS (ESI negative mode): 209.0942 ([H(2-EtC_6H_{12})*P*O_4]$^-$). MS (ESI positive mode): 354.4097 ([(2-EtC_6H_{12})$_3$NH]$^+$).

[(2-EtC$_6$H$_{12}$)NH$_3$][H(2-EtC$_6$H$_{12}$)PO$_4$]

Synthesised from 2-ethylhexylamine (10.0 mL, 61.0 mmol) and $H_2(2\text{-}EtC_6H_{12})PO_4$ (12.8 g, 61.0 mmol); 20.4 g of $[(2\text{-}EtC_6H_{12})NH_3][H(2\text{-}EtC_6H_{12})PO_4]$ (colourless oil, quant.). ^{1}H NMR (300.13 MHz, 298K, $CDCl_3$): δ = 7.99 (3H, s, br, N-*H*), 3.70 (2H, m, α-C*H*$_2$ of phosphate), 2.76 (2H, m, C*H*$_2$ of ^{n}butylammonium), 1.68 (1H, sept, ^3J = 6 Hz, C*H*), 1.20-1.55 (17H, m, br, overlapping C*H* and C*H*$_2$ peaks), 0.88 (12H, m, overlapping C*H*$_3$ peaks). ^{13}C{^{1}H} NMR (75.47 MHz, 298K, $CDCl_3$): δ = 67.7 (*C*H$_2$), 42.2 (*C*H$_2$), 42.2 (*C*H$_2$), 40.3 (*C*H), 37.6 (*C*H), 30.2 (*C*H$_2$), 30.0 (*C*H$_2$), 29.1 (*C*H$_2$), 28.5 (*C*H$_2$), 23.3 (*C*H$_2$), 23.1 (*C*H$_2$), 23.0 (*C*H$_2$), 22.9 (*C*H$_2$), 14.1 (*C*H$_3$), 14.0 (*C*H$_3$), 10.9 (*C*H$_3$), 10.1 (*C*H$_3$). ^{31}P{^{1}H} NMR (121.49 MHz, 298K, $CDCl_3$): δ = 0.07. MS (ESI negative mode): 209.0949 ($[H(2\text{-}EtC_6H_{12})PO_4]^-$). MS (ESI positive mode): 130.1624 ($[(2\text{-}EtC_6H_{12})NH_3]^+$).

[HN^{n}Bu$_3$][(2-EtC$_6$H$_{12}$)$_2$PO$_4$]

Synthesised from tri-*n*-butylamine (10.0 mL, 42.1 mmol) and $H_2(2\text{-}EtC_6H_{12})PO_4$ (14.5 mL, 42.1 mmol); 21.8 g of $[HN^nBu_3][(2\text{-}EtC_6H_{12})_2PO_4]$ (colourless oil, quant.). ^{1}H NMR (300.13 MHz, 298K, $CDCl_3$): δ = 13.22 (1H, s, br, N-*H*), 3.74 (4H, m, α-C*H*$_2$ of phosphate), 2.93 (6H, m, α-C*H*$_2$ of ammonium). 1.67 (6H, m, β-C*H*$_2$ of ammonium), 1.20-1.57 (24H, m, br, overlapping C*H* and C*H*$_2$ peaks), 0.95 (9H, t, ^3J = 7 Hz, C*H*$_3$ of ammonium), 0.86 (12H, t, ^3J = 7 Hz, C*H*$_3$ of phosphate). ^{13}C{^{1}H} NMR (75.47 MHz, 298K, $CDCl_3$): δ = 67.9 (*C*H$_2$), 51.5 (*C*H$_2$), 40.4 (*C*H), 30.1 (*C*H$_2$), 29.0 (*C*H$_2$), 25.1 (*C*H$_2$), 23.3 (*C*H$_2$), 23.1 (*C*H$_2$), 20.2 (*C*H$_2$), 14.1 (*C*H$_3$), 13.7 (*C*H$_3$), 11.0 (*C*H$_3$). ^{31}P{^{1}H} NMR (121.49 MHz, 298K, $CDCl_3$): δ = 0.91. MS (ESI negative mode): 321.2199 ($[(2\text{-}EtC_6H_{12})_2PO_4]^-$). MS (ESI positive mode): 186.2211 ($[HN^nBu_3]^+$).

[C$_{12}$H$_{25}$NH$_3$][H(2-EtC$_6$H$_{12}$)PO$_4$]

Synthesised from dodecylamine (5.50 g, 28.5 mmol) and $H_2(2\text{-}EtC_6H_{12})PO_4$ (6.00 g, 28.5 mmol); 11.0 g of $[C_{12}H_{25}NH_3][H(2\text{-}EtC_6H_{12})PO_4]$ (oily white solid, 97 %). ^{1}H NMR (300.13 MHz, 298K, $CDCl_3$): δ = 7.90 (2H, s, br, O-*H*/N-*H*), 7.69 (2H, s, br, O-*H*/N-*H*), 3.78 (2H, m, br, α-C*H*$_2$ of phosphate), 2.89 (2H, m, br, α-C*H*$_2$ of ammonium), 1.12-1.82 (25H, m, br, overlapping C*H* and C*H*$_2$ peaks), 0.89 (9H, m, br, overlapping C*H*$_3$ peaks). ^{13}C{^{1}H} NMR (100.61 MHz, 298K, $CDCl_3$): δ = 68.2 (*C*H$_2$), 40.1 (*C*H$_2$), 40.0 (*C*H$_2$), 39.9 (*C*H), 31.9 (*C*H$_2$), 29.9 (*C*H$_2$), 29.7 (*C*H$_2$), 29.4 (*C*H$_2$), 29.0 (*C*H$_2$), 27.6 (*C*H$_2$), 26.9 (*C*H$_2$), 23.2 (*C*H$_2$), 23.0 (*C*H$_2$), 22.7 (*C*H$_2$), 14.1 (*C*H$_3$), 10.8 (*C*H$_3$).^{31}P{^{1}H} NMR (121.49 MHz, 298K, $CDCl_3$): δ = 0.48. MS (ESI negative mode): 209.0948 ($[H(2\text{-}EtC_6H_{12})PO_4]^-$). MS (ESI positive mode): 186.2206 ($[C_{12}H_{25}NH_3]^+$).

[(2-EtC$_6$H$_{12}$)$_2$NH$_2$][HOleylPO$_4$]

Synthesised from bis(2-ethylhexyl)amine (18.9 mL, 62.8 mmol) and $H_2OleylPO_4$ (21.9 g, 62.8 mmol); 19.6 g of $[(2\text{-}EtC_6H_{12})_2NH_2][HOleylPO_4]$ (orange, viscous oil, quant.). ^{1}H NMR (300.13 MHz, 298K, $CDCl_3$): δ = 9.34 (2H, s, br, N-*H*), 8.64 (1H, s, br, O-*H*), 5.38 (1H, s, br, O-*H*), 3.87 (2H, q, ^3J = 7 Hz, α-C*H*$_2$ of phosphate), 2.84 (4H, s, br, α-C*H*$_2$ of ammonium), 1.97 (2H, s, br, C*H*$_2$), 1.76 (2H, m, br, C*H*), 1.10-1.69 (38H, m, br, overlapping C*H* and C*H*$_2$ peaks), 0.90 (15H, m, overlapping C*H*$_3$ peaks). ^{13}C{^{1}H} NMR (75.47 MHz, 298K, $CDCl_3$): δ = 130.3 (H*C*=*C*H), 65.9 (*C*H$_2$), 49.8 (*C*H$_2$), 35.1 (*C*H), 32.6 (*C*H$_2$), 31.9 (*C*H$_2$), 30.7 (*C*H$_2$), 30.6 (*C*H$_2$), 30.2 (*C*H$_2$), 30.1 (*C*H$_2$), 29.7 (*C*H$_2$), 29.5 (*C*H$_2$), 29.4 (*C*H$_2$), 29.1 (*C*H$_2$), 28.4 (*C*H$_2$), 28.3 (*C*H$_2$), 25.7 (*C*H$_2$), 23.3 (*C*H$_2$), 23.2 (*C*H$_2$), 22.8 (*C*H$_2$), 22.7 (*C*H$_2$), 14.1 (*C*H$_3$), 10.1 (*C*H$_3$), 10.0 (*C*H$_3$). ^{31}P{^{1}H} NMR (121.49 MHz, 298K, $CDCl_3$): δ = 1.40 (HOleyl*P*O$_4$), 1.27 (H$_3$*P*O$_4$). MS (ESI negative mode): 347.2342 ($[HOleylPO_4]^-$). MS (ESI positive mode): 242.2849 $[(2\text{-}EtC_6H_{12})_2NH_2]^+$).

[(2-EtC$_6$H$_{12}$)$_2$NH$_2$][H(C$_{13}$H$_{27}$)PO$_4$]

Synthesised from bis(2-ethylhexyl)amine (10.0 mL, 33.3 mmol) and $H_2(C_{13}H_{27})PO_4$ (9.34 g, 33.3mmol); 17.1 g of $[(2\text{-}EtC_6H_{12})_2NH_2][H(C_{13}H_{27})PO_4]$ (colourless oil, 98 %). ^{1}H NMR (300.13 MHz, 298K, $CDCl_3$): δ = 8.26 (3H, s, br, N-*H*/O-*H*), 3.87 (2H, m, br, α-C*H*$_2$ of phosphate), 2.84 (4H, m, α-C*H*$_2$ of ammonium), 1.75 (2H, m, br, C*H*), 1.05-1.62 (30H, m, br, overlapping C*H* and C*H*$_2$ peaks), 0.58-0.96 (27H, m, br, overlapping C*H*$_3$ peaks). ^{13}C{^{1}H} NMR (100.61 MHz, 298K, $CDCl_3$): δ = 66.2 (*C*H$_2$), 64.2 (*C*H$_2$), 49.3 (*C*H$_2$), 49.2 (*C*H$_2$), 35.0 (*C*H), 34.9 (*C*H), 30.2 (*C*H$_2$), 30.2 (*C*H$_2$), 28.4 (*C*H$_2$), 28.4 (*C*H$_2$), 23.3 (*C*H$_2$), 23.2 (*C*H$_2$), 22.9 (*C*H$_2$), 14.0 (*C*H$_3$), 10.2 (*C*H$_3$), 10.1 (*C*H$_3$). ^{31}P{^{1}H} NMR (121.49 MHz, 298K, $CDCl_3$): δ = 1.43 (H(C$_{13}$H$_{27}$)*P*O$_4$), 1.38 (H$_2$*P*O$_4$). MS (ESI negative mode): 279.1729 ([H(C$_{13}$H$_{27}$)PO$_4$]$^-$). MS (ESI positive mode): 242.2851 ([(2-EtC$_6$H$_{12}$)$_2$NH$_2$]$^+$).

[(2-EtC$_6$H$_{12}$)$_3$NH][H(C$_{13}$H$_{27}$)PO$_4$]

Synthesised from tris(2-ethylhexyl)amine (20.0 mL, 46.2 mmol) and $H_2(C_{13}H_{27})PO_4$ (12.9 g, 46.2 mmol); 28.9 g of $[(2\text{-}EtC_6H_{12})_3NH][H(C_{13}H_{27})PO_4]$ (colourless oil, 99 %). ^{1}H NMR (300.13 MHz, 298K, $CDCl_3$): δ = 9.56 (2H, s, br, N-*H*/O-*H*), 3.93 (2H, m, br, α-C*H*$_2$ of phosphate), 2.66 (6H, s, br, α-C*H*$_2$ of ammonium), 1.11-1.86 (42H, m, br, overlapping C*H* and C*H*$_2$ peaks), 0.66-0.97 (33H, m, br, overlapping C*H*$_3$ peaks). ^{13}C{^{1}H} NMR (100.61 MHz, 298K, $CDCl_3$): δ = 66.3 (*C*H$_2$), 64.4 (*C*H$_2$), 58.9 (*C*H$_2$), 35.2 (*C*H), 31.2 (*C*H$_2$), 29.4 (*C*H$_2$), 28.5 (*C*H$_2$), 26.7 (*C*H$_2$), 24.2 (*C*H$_2$), 23.0 (*C*H$_2$), 22.9 (*C*H$_2$), 22.9 (*C*H$_2$), 19.3 (*C*H$_3$), 14.4 (*C*H$_3$), 14.1 (*C*H$_3$), 12.2 (*C*H$_3$), 10.4 (*C*H$_3$). ^{31}P{^{1}H} NMR (121.49 MHz, 298K, $CDCl_3$): δ = 1.64 (H(C$_{13}$H$_{27}$)*P*O$_4$), −0.35 (H$_3$*P*O$_4$). MS (ESI negative mode): 279.1727 ([H(C$_{13}$H$_{27}$)PO$_4$]$^-$). MS (ESI positive mode): 354.4133 ([(2-EtC$_6$H$_{12}$)$_3$NH]$^+$).

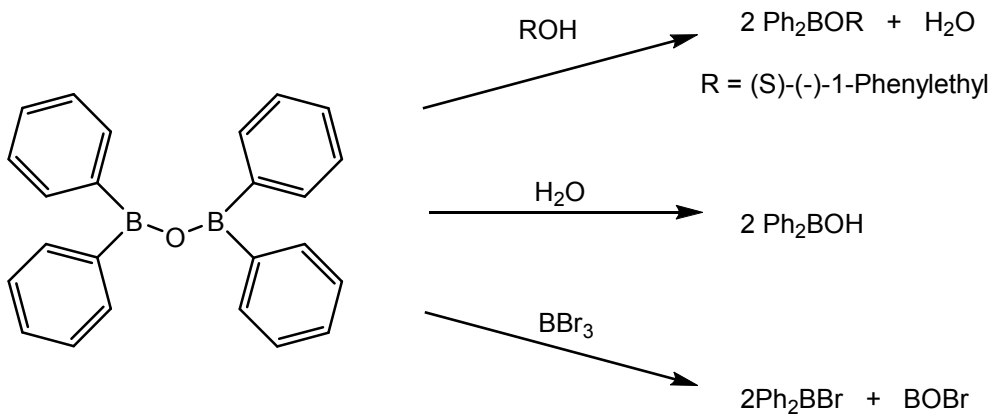
[(2-EtC$_6$H$_{12}$)NH$_3$][H(C$_{13}$H$_{27}$)PO$_4$]

Synthesised from (2-ethylhexyl)amine (10.0 mL, 61.1 mmol) and $H_2(C_{13}H_{27})PO_4$ (17.1 g, 61.1 mmol); 25.0 g of $[(2\text{-}EtC_6H_{12})_3NH][H(C_{13}H_{27})PO_4]$ (colourless oil, quant.). ^{1}H NMR (300.13 MHz, 298K, $CDCl_3$): δ = 8.70 (2H, s, br, O-*H*), 8.06 (3H, s, br, N-*H*), 3.85 (2H, m, br, α-C*H*$_2$ of phosphate), 2.83 (6H, s, br, α-C*H*$_2$ of ammonium), 1.00-1.83 (25H, m, br, overlapping C*H* and C*H*$_2$ peaks), 0.90 (21H, m, br, overlapping C*H*$_3$ peaks). ^{13}C{^{1}H} NMR (100.61 MHz, 298K, $CDCl_3$): δ = 66.2 (*C*H$_2$), 64.1 (*C*H$_2$), 42.4 (*C*H$_2$), 37.4 (*C*H), 30.1 (*C*H$_2$), 29.4 (*C*H$_2$), 28.4 (*C*H$_2$), 26.7 (*C*H$_2$), 23.4 (*C*H$_2$), 23.0 (*C*H$_2$), 22.9 (*C*H$_2$), 19.3 (*C*H$_3$), 14.4 (*C*H$_3$), 14.1 (*C*H$_3$), 12.2 (*C*H$_3$), 10.1 (*C*H$_3$). ^{31}P{^{1}H} NMR (121.49 MHz, 298K, $CDCl_3$): δ = 0.98 (H_3PO_4), 0.23 ($H(C_{13}H_{27})PO_4$). MS (ESI negative mode): 279.1724 ($[H(C_{13}H_{27})PO_4]^-$). MS (ESI positive mode): 130.1600 ($[(2\text{-}EtC_6H_{12})NH_3]^+$).

Chapter III
Pyroborate Compounds

3.1 Introduction

Compounds containing a B-O-B linkage have been known since the 1950s, when the syntheses and characterisation of several diboroxanes, compounds of the form $(R_2B)_2O$, were reported (R = Ph, ^{n}Bu).[128] For instance, Lappert *et al.* reported the use of diphenyldiboroxane in the synthesis of a range of organoboron products (Scheme 3.1), with the reaction with (*S*)-(−)-1-phenylethanol preserving stereochemistry in the product.[128a]



Scheme 3.1 Reactions of diphenyldiboroxane.[128a]

Following these early investigations, diboroxane compounds were generally not studied in their own right, but were instead reported as hydrolysis products.[129] However, Wagner and co-workers utilised this method of formation of diboroxanes, using them as starting materials for the synthesis of 9,10-dihydro-9,10-diboraanthracenes, which exhibited promising luminescence properties for boron-doped π-conjugated systems.[130]

The commercial applications of diboroxanes have been investigated throughout recent decades, with a patent being filed for the use of aryl and alkyl di- and triboroxanes as promoters in the hydrocyanation of olefins.[131] Furthermore, diboroxanes were used

as starting materials in the syntheses of a range of ammonium cyclic borate compounds which have been found to act as fungicides.[132]

Pyroborate compounds, based on the structure of pyroboric acid (Figure 3.1a), have been researched since the 1950s to a greater extent, due to their apparent commercial applications, particularly in the automotive industry. For example, several patents for the use of alkyl pyroborates as fuel additives were filed during the late 1950s and early 1960s,[133] such an example is that of alkenyl, pyroborate which was found to be effective in minimising the formation of deposits in carburettors (Figure 3.1b).[133f] Similarly, Irish filed a patent in 1960 describing the use of alkenyl and alkyl pyroborate compounds as stabilisers for lubricating oils.[134]

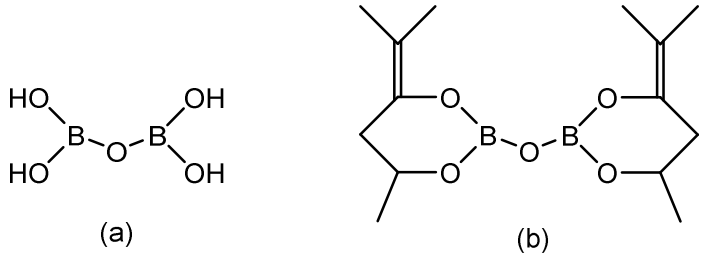


Figure 3.1 (a) The structure of pyroboric acid and (b) alkenyl pyroborate compound used as a fuel additive to lower carburettor deposits.[133f]

The use of pyroborates in lubricating oils is an area of particular interest, and the incorporation of carbonyl moieties into the structure of these compounds has allowed for even more effective compositions. For instance, pyroborate compounds containing amides incorporating long alkyl chains have been found to be effective additives in motor fuel and lubricants, an example of which is shown in Figure 3.2.[133d, 135] Moreover, ester groups have been incorporated in a similar fashion to provide pyroborate compounds which efficiently act as fuel and lubricant additives.[136]

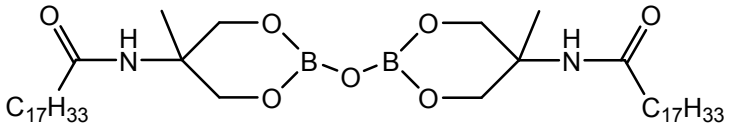


Figure 3.2 Example of an amido pyroborate used as a fuel/lubricant additive.[135a]

Sulfur-containing lubricant additives are well known through the widespread use of ZDDPs previously discussed, and this idea has been utilised with pyroborate compounds, with the use of pyroborate sulfide compounds as friction-reducing additives being reported.[137]

A limiting factor in the use of pyroborate compounds is their susceptibility to hydrolysis, owing to the empty p_z orbital present on both boron centres (Figure 3.3). This is the case for the majority of three-coordinate borate compounds, and attack of the boron atoms by a Lewis basic compound is a key mode of reactivity of such compounds.

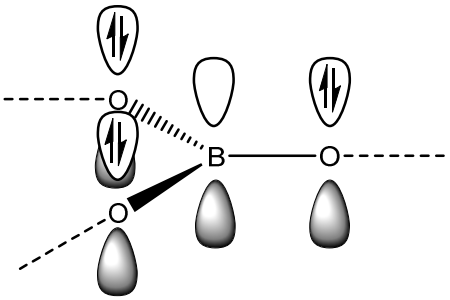


Figure 3.3 Bonding model for three-coordinate borate compounds.

This has been circumvented by E. L. Kay, who took advantage of this reactivity by synthesising ammonium salts of pyroborate compounds, involving the donation of a lone pair of electrons from an aryloxy substituent into the empty p_z orbital on boron (Figure 3.4).[138] This gave a range of pyroborate compounds which were not only hydrolytically stable, but also stable thermally and to oxidation.

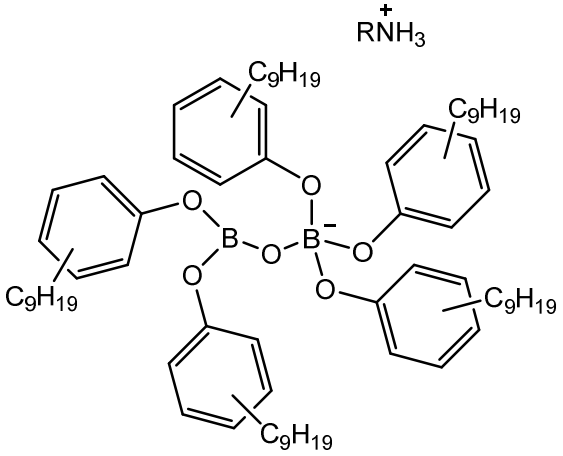


Figure 3.4 Hydrolytically stable ammonium pyroborate lubricant additive.[138]

Pyroborate compounds have shown interesting reactivity, and so have been of high academic interest in recent years. $(catB)_2O$ (cat = $O_2C_6H_4$-1,2) has been shown to react with phenolic polymers to give novel resins with good flame-retardant properties.[139] The presence of boron in the polymer was also shown to limit degradation of the resin. The tetra-acetyl pyroborate $[(AcO)_2B]_2O$ has been utilised in the synthesis of (trifluoromethyl)trialkoxyborates as CF_3 sources in copper-mediated trifluoromethylation reactions.[140] These trialkyoxyborates proved to be stable, non-volatile, easy to store and handle solids capable of achieving high yields under mild and neutral conditions, rendering them superior to the previously employed methods, which required the use of a low-boiling liquid reagent and basic additives. Recently, it was reported that $(pinB)_2O$ (pin = $O_2C_2Me_4$) reacts with various hydrosilanes in the presence of molybdenum catalysts in an unprecedented selective formation of boryl silyl ethers, which could have future use in functional inorganic materials (Figure 3.5).[141] This pyroborate had previously been found to react with tri-*tert*-butylphosphine imide to give an unexpected triborate compound containing three- and four-coordinate boron centres.[142]

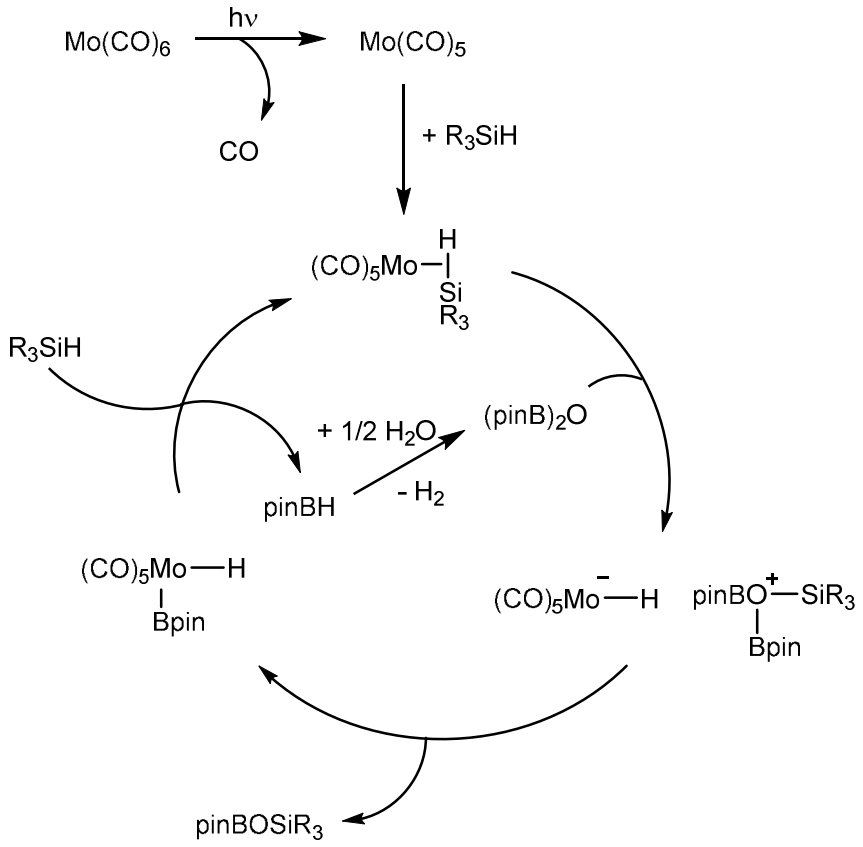
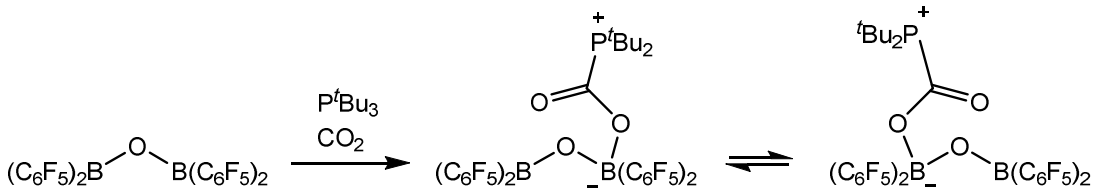


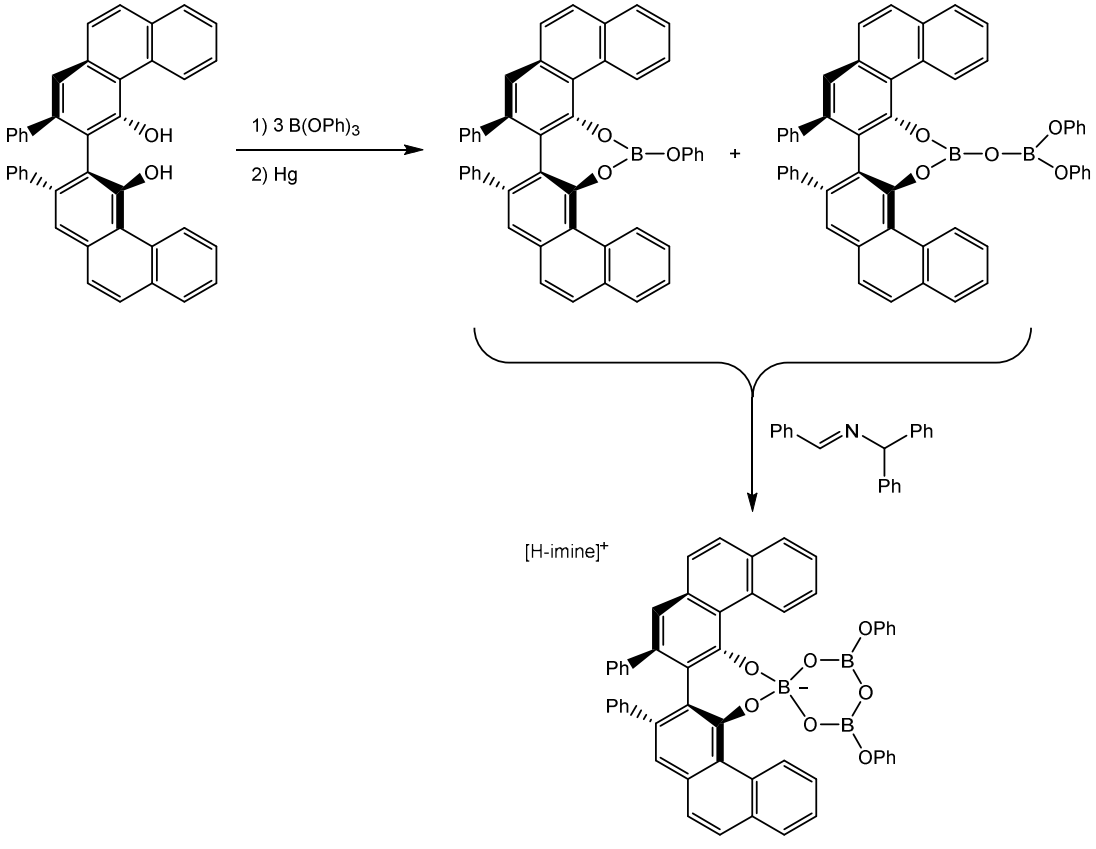
Figure 3.5 Catalytic cycle for the formation of boryl silyl ethers in the reaction of $(pinB)_2O$ and hydrosilanes.[141]

The empty p_z orbitals present in diboroxane and pyroborate compounds are also responsible for the Lewis acidity of these species, which has been utilised in various studies. For instance, Stephan *et al.* reported the use of a $[(C_6F_5)_2B]_2O$-containing frustrated Lewis pair (FLP) in the activation of CO_2 (Scheme 3.2).[143] X-ray diffraction and NMR experiments indicated that the CO_2 molecule does not bridge the two boron centres, but is instead interchanged between them in a monodentate fashion. Furthermore, Pringle and co-workers further took advantage of the Lewis acidic nature of diboroxane compounds, using diphenyldiboroxane as a Lewis acid promoter in the catalysis of the hydrocyanation of 3-pentenenitrile, with high selectivity towards the linear product.[144]



Scheme 3.2 Diboroxane-containing FLP in activation of CO_2.[143]

There has been some research activity into the Lewis acidity of pyroborate compounds, particularly focusing on their involvement in aziridination reactions. For instance, it has been proposed that a pyroborate ester formed from the chiral VAPOL or VANOL ligands acts as a Lewis acidic catalyst to form enantionmerically pure aziridines.[145] However, it was later postulated that these pyroborates were



Scheme 3.3 Formation of VAPOL BOROX catalyst from a pyroborate precatalyst.[146]

precatalysts to cyclic BOROX catalysts, containing three- and four-coordinate boron centres (Scheme 3.3).[146]

The pyroborate derivative of similar binaphthol ligands has been utilised in the preparation of enantiomerically pure analogues from the racemic ligand mixtures, using the Lewis adduct with (*S*)-proline to impart *R* or *S* stereochemistry on the binaphthol ligands.[147]

$(catB)_2O$ has been shown to be a competing Lewis acid by-product in the deoxygenation of sulfoxides *via* catecholborane, which can significantly hinder the reaction rate.[148] This was counteracted by using the borane in excess to form a more reactive Lewis acid-base adduct, greatly increasing the reaction rate. $(catB)_2O$ has also been briefly investigated for its use as a chelating Lewis acid for the binding of bidentate anions by Aldridge and co-workers,[149] which is discussed in greater detail in Chapter V. Although some progress has been made in understanding the Lewis acidity of pyroborate compounds, this is still a severely underdeveloped area of research and so there is much scope for further study into this field.

3.2 Experimental

3.2.1 General Procedure for the Synthesis of PIB Catechols

Under a nitrogen atmosphere, catechol (330 g, 3.00 mol) was mechanically stirred at 200 rpm in toluene (690 mL) for 20 min. $BF_3 \cdot Et_2O$ (55.6 g, 0.39 mol) was added over 2 min and the reaction mixture stirred at 400 rpm for 20 min. To this mixture was added polyisobutylene in toluene (1.04 L) over 2.5 h, taking care to keep the reaction mixture below 25 °C. During this time the mixture became red in colour. The reaction mixture was then stirred at 400 rpm at room temperature for 16 h. The mixture was quenched with ammonium hydroxide (160 g) over 1 h, taking care to keep the reaction mixture below 25 °C, during which time the mixture became off-white. The mixture was filtered through FAX-5 filter aid over several days, during which time the mixture became black. The resulting solution was distilled *in vacuo* at 180 °C to remove residual water, toluene and catechol to give the products as highly viscous black oils.

4-PIB$_{550}$catechol

Synthesised from 550 M_w polyisobutylene (1100 g, 2.00 mol); 1200 g of PIB_{550} catechol (black viscous oil, 92 %). ^{1}H NMR (400.13 MHz, 298 K, $CDCl_3$): δ = 6.91 (1H, s, br, Ar-*H*), 6.80 (1H, s, br, Ar-*H*), 5.23 (2H, s, br, O-*H*), 1.78 (2H, s, br, C*H*$_2$), 1.25-1.48 (22H, m, br, overlapping C*H*$_2$ peaks), 1.22 (3H, s, br, C*H*$_3$), 0.91-1.17 (54H, m, br, overlapping C*H*$_3$ peaks), 0.83 (6H, s, br, overlapping C*H*$_3$ peaks). ^{13}C{^{1}H} NMR (100.61 MHz, 298 K, $CDCl_3$): δ = 144.1 (Ar-q*C*), 142.9 (Ar-q*C*), 140.7 (Ar-q*C*), 118.7 (Ar-*C*H), 114.8 (Ar-*C*H), 59.5 (*C*H$_2$), 59.4 (*C*H$_2$), 59.1 (*C*H$_2$), 59.0 (*C*H$_2$), 58.8 (*C*H$_2$), 58.4 (*C*H$_2$), 58.3 (*C*H$_2$), 58.2 (*C*H$_2$), 38.3 (q*C*), 38.2 (q*C*), 38.1 (q*C*), 38.0 (q*C*), 37.8 (q*C*), 37.7 (q*C*), 32.6 (*C*H$_3$), 32.5 (*C*H$_3$), 32.2 (*C*H$_3$), 31.8 (*C*H$_3$), 31.5 (*C*H$_3$), 31.3 (*C*H$_3$), 31.2 (*C*H$_3$), 31.2 (*C*H$_3$), 31.1 (*C*H$_3$), 30.8 (*C*H$_3$), 30.6 (*C*H$_3$). (ESI

negative mode) Expected: 672.2 Found 950.8 (M+5^{i}Bu^{-}). Fragment ions: 894.8 (M+4^{i}Bu^{-}), 838.8 (M+3^{i}Bu^{-}), 782.6 (M+2^{i}Bu^{-}), 725.6 (M+^{i}Bu^{-}), 669.6 (M^{-}), 613.5 (M−^{i}Bu^{-}), 557.6 (M−2^{i}Bu^{-}), 501.4 (M−3^{i}Bu^{-}), 445.4 (M−4^{i}Bu^{-}), 389.4 (M−5^{i}Bu^{-}), 389.4 (M−6^{i}Bu^{-}), 333.4 (M−7^{i}Bu^{-}).

4-PIB$_{1000}$catechol

Synthesised from 1000 M_w polyisobutylene (2000 g, 2.00 mol); 2200 g of PIB_{1000} catechol (black viscous oil, 98 %). ^{1}H NMR (400.13 MHz, 298 K, $CDCl_3$): δ = 6.90 (1H, s, br, Ar-*H*), 6.79 (2H, s, br, Ar-*H*), 5.10 (2H, s, br, O-*H*), 1.78 (2H, s, br, CH_2), 1.25-1.49 (34H, m, br, overlapping CH_2 peaks), 1.21 (3H, s, br, CH_3), 0.91-1.18 (90H, m, br, overlapping CH_3 peaks), 0.83 (6H, s, br, overlapping CH_3 peaks). ^{13}C{^{1}H} NMR (125.77 MHz, 298 K, $CDCl_3$): δ = 143.1 (Ar-q*C*), 141.9 (Ar-q*C*), 139.7 (Ar-q*C*), 117.7 (Ar-*C*H), 114.5 (Ar-*C*H), 112.8 (Ar-*C*H), 58.5 (*C*H$_2$), 58.4 (*C*H$_2$), 58.1 (*C*H$_2$), 57.8 (*C*H$_2$), 57.4 (*C*H$_2$), 57.2 (*C*H$_2$), 37.2 (q*C*), 37.2 (q*C*), 37.1 (q*C*), 36.9 (q*C*), 36.8 (q*C*), 31.6 (*C*H$_3$), 31.4 (*C*H$_3$), 31.2 (*C*H$_3$), 31.1 (*C*H$_3$), 30.5 (*C*H$_3$), 30.2 (*C*H$_3$), 30.1 (*C*H$_3$), 30.1 (*C*H$_3$), 29.8 (*C*H$_3$), 29.6 (*C*H$_3$). MS (ESI negative mode) Expected: 1121.1 Found 1063.8 (M−^{i}Bu^{-}). Fragment ions: 1008.8 (M−2^{i}Bu^{-}), 951.6 (M−3^{i}Bu^{-}), 895.6 (M−4^{i}Bu^{-}), 839.6 (M−5^{i}Bu^{-}), 783.6 (M−6^{i}Bu^{-}), 727.4 (M−7^{i}Bu^{-}), 671.4 (M−8^{i}Bu^{-}), 615.4 (M−9^{i}Bu^{-}), 559.4 (M−10^{i}Bu^{-}), 501.4 (M−11^{i}Bu^{-}), 445.4 (M−12^{i}Bu^{-}), 389.4 (M−13^{i}Bu^{-}), 333.4 (M−14^{i}Bu^{-}), 277.4 (M−15^{i}Bu^{-}), 221.2 (M−16^{i}Bu^{-}), 165.2 (M−17^{i}Bu^{-}), 109.2 (catechol).

3.2.2 General Procedure for the Synthesis of Straight-chain Alkyl Catechols

Under an argon atmosphere, catechol (78.8 g, 716 mmol), xylenes (120 mL) and amberlyst-15 (5.05 g) were mechanically stirred at 400 rpm. An alpha-olefin was added and the resulting mixture was heated at 140 °C for 16 h. The heating was

stopped and, once the temperature fell below 85 °C, hexane (200 mL) was added. The mixture solidified, which was counteracted by the addition of water (200 mL) and stirring at 400 rpm for 30 min. The mixture was filtered and the organic phase separated, washed with water (2 × 100 mL) and dried over magnesium sulfate. Volatiles were removed *in vacuo* and the resulting residue was distilled *in vacuo* at 150 °C to remove residual xylenes and catechol, giving the products as dark red oils.

4-dodecylcatechol

Synthesised from 1-dodecene (48.2 g, 286 mmol); 56.8 g of 4-dodecylcatechol and residual disubstituted species, as evidenced by additional $^{13}C\{^{1}H\}$ peaks (red/purple oil, 72 %). ^{1}H NMR (400.13 MHz, 298 K, $CDCl_3$): δ = 6.43-6.88 (3H, m, Ar-*H*), 5.15 (2H, s, br, O-*H*), 1.35-1.88 (4H, m, br, overlapping C*H*$_2$ peaks), 0.99-1.33 (18H, m, br, overlapping C*H*$_2$ peaks), 0.66-0.98 (5H, m, br, overlapping C*H*$_3$ peaks). $^{13}C\{^{1}H\}$ NMR (100.61 MHz, 298 K, $CDCl_3$): δ = 143.3 (Ar-q*C*), 142.8 (Ar-q*C*), 141.5 (Ar-q*C*), 141.2 (Ar-q*C*), 134.3 (Ar-q*C*), 120.2 (Ar-*C*H), 119.8 (Ar-*C*H), 119.5 (Ar-*C*H), 119.2 (Ar-*C*H), 115.2 (Ar-*C*H), 114.5 (Ar-*C*H), 114.0 (Ar-*C*H), 112.5 (Ar-*C*H), 47.3 (*C*H$_2$), 35.6 (*C*H$_2$), 34.1 (*C*H$_2$), 31.9 (*C*H$_2$), 29.8 (*C*H$_2$), 29.7 (*C*H$_2$), 29.6 (*C*H$_2$), 29.3 (*C*H$_2$), 27.7 (*C*H$_2$), 27.6 (*C*H$_2$), 22.7 (*C*H$_2$), 20.9 (*C*H$_2$), 14.1 (*C*H$_3$). MS (ESI negative mode) Expected: 277.2173 Found 277.2180 ($M-H^-$).

4-(C_{16}-C_{18})catechol

Synthesised from a mixture of C_{16}-C_{18} alpha-olefins (68.4 g, 287 mmol); 69.5 g of 4-(C_{16}-C_{18})catechol (red/purple oil, 69 %). ^{1}H NMR (400.13 MHz, 298 K, $CDCl_3$): δ = 6.53-6.85 (3H, m, Ar-*H*), 4.96-5.28 (2H, m, br, O-*H*), 1.39-1.89 (4H, m, br, overlapping C*H*$_2$ peaks), 1.02-1.37 (30H, m, br, overlapping C*H*$_2$ peaks), 0.71-0.95 (6H, m, br, overlapping C*H*$_3$ peaks). $^{13}C\{^{1}H\}$ NMR (100.61 MHz, 298 K, $CDCl_3$): δ

= 143.3 (Ar-q*C*), 142.8 (Ar-q*C*), 142.2 (Ar-q*C*), 141.5 (Ar-q*C*), 141.1 (Ar-q*C*), 140.0 (Ar-q*C*), 139.6 (Ar-q*C*), 134.3 (Ar-q*C*), 132.7 (Ar-q*C*), 132.4 (Ar-q*C*), 120.4 (Ar-*C*H), 120.3 (Ar-*C*H), 120.2 (Ar-*C*H), 119.8 (Ar-*C*H), 119.5 (Ar-*C*H), 119.2 (Ar-*C*H), 115.2 (Ar-*C*H), 114.5 (Ar-*C*H), 114.5 (Ar-*C*H), 114.0 (Ar-*C*H), 112.5 (Ar-*C*H), 112.3 (Ar-*C*H), 40.1 (*C*H_2), 39.4 (*C*H_2), 38.6 (*C*H_2), 37.1 (*C*H_2), 36.7 (*C*H_2), 35.9 (*C*H_2), 35.4 (*C*H_2), 32.5 (*C*H_2), 31.9 (*C*H_2), 29.7 (*C*H_2), 29.4 (*C*H_2), 27.7 (*C*H_2), 27.6 (*C*H_2), 22.7 (*C*H_2), 22.5 (*C*H_2), 21.0 (*C*H_2), 14.1 (*C*H_3), 12.2 (*C*H_3), 12.1 (*C*H_3). MS (ESI negative mode): 333.2789 ($C_{22}H_{37}O_2^-$), 361.3104 ($C_{24}H_{41}O_2^-$).

3.2.3 General Procedure for the Synthesis of Pyroborate Esters

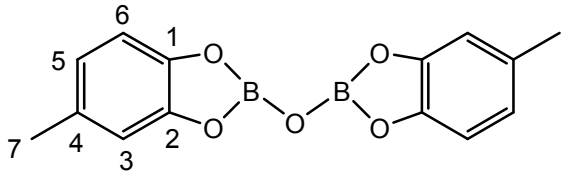
To a stirred suspension of the relevant diol in toluene (75-150 mL) was added boric acid. The reaction mixture was heated at reflux for 72 h with the azeotropic removal of water, with the exception of **[5]** which was heated for 16 h. Upon cooling to room temperature, the reaction mixture was filtered. The resulting solid was dried to give the final products as off-white powders. Solutions of **[4]**, **[6]** and **[8]** had to be cooled to –30 °C to induce precipitation of the product before filtration was carried out. Compounds **[13]-[17]** were isolated *via* the removal of volatiles *in vacuo* from the filtrate to give the final products as oils.

(catB)$_2$O [1]

Synthesised from catechol (5.93 g, 53.9 mmol) and boric acid (3.33 g, 53.5 mmol) in 75 mL toluene. Yield: 5.77 g (85 %). Data was consistent with that reported in the literature.[149] ^{1}H NMR (400.13 MHz, 298 K, $CDCl_3$): δ = 7.23 (4H, m, Ar-*H*), 7.11 (4H, m, Ar-*H*). ^{13}C{^{1}H} NMR (100.61 MHz, 298 K, $CDCl_3$): δ = 147. 5 (Ar-q*C*), 123.0 (Ar-*C*H), 112.6 (Ar-*C*H). ^{11}B{^{1}H} NMR (128.38 MHz, 298 K, $CDCl_3$): δ = 22.4.

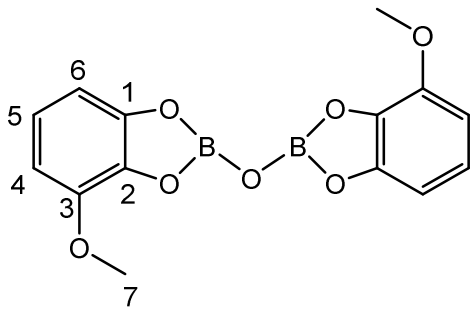
MS (EI) Expected: 254.0562 Found: 254.0564 (M^+). Anal. Calcd for $C_{12}H_8B_2O_5$: C, 56.79, H, 3.18. Found: C, 56.68, H, 3.25 %.

(4-MecatB)$_2$O [2]



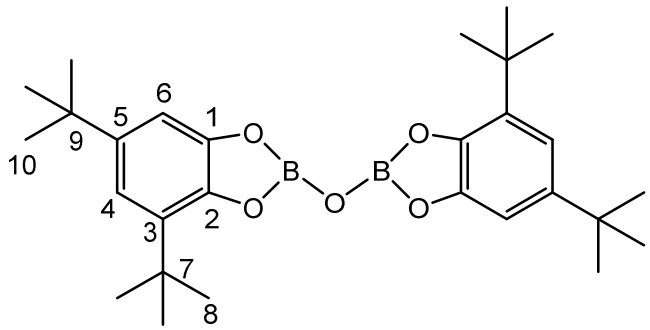
Synthesised from 4-methylcatechol (6.00 g, 48.3 mmol) and boric acid (2.97 g, 48.0 mmol) in 75 mL toluene. Extraction into dichloromethane was required to remove residual toluene from the product. Yield: 6.22 g (92 %). ^{1}H NMR (400.13 MHz, 298 K, $CDCl_3$): δ = 7.09 (2H, d, ^3J = 8 Hz, H6), 7.04 (2H, s, H3), 6.88 (2H, d, ^3J = 8 Hz, H5), 2.38 (6H, s, H7). ^{13}C{^{1}H} NMR (100.61 MHz, 298 K, $CDCl_3$): δ = 147.5 (C1), 145.4 (C2), 132.9 (C4), 123.1 (C5), 113.2 (C3), 111.9 (C6), 21.4 (C7). ^{11}B{^{1}H} NMR (128.38 MHz, 298 K, $CDCl_3$): δ = 22.5. MS (EI) Expected: 282.0871 Found: 282.0860 (M^+). Fragment ions: 281.0806 ($M-H^+$), 175.0364 ($C_7H_5B_2O_4^+$), 149.0407 ($C_7H_6BO_3^+$), 105.0335 ($C_7H_5O^+$), 91.0543 ($C_7H_5^+$), 77.0387 ($C_6H_5^+$). Anal. Calcd for $C_{14}H_{12}B_2O_5$: C, 59.66, H, 4.29. Found: C, 59.70, H, 4.26 %.

(3-MeOcatB)$_2$O [3]



Synthesised from 3-methoxycatechol (5.01 g, 35.8 mmol) and boric acid (2.26 g, 36.5 mmol) in 75 mL toluene. Yield: 2.60 g (46 %). ^{1}H NMR (300.13 MHz, 298 K, $CDCl_3$): δ = 7.03 (2H, t, ^{3}J = 8 Hz, H5), 6.88 (2H, dd, ^{3}J = 9 Hz, ^{4}J = 1 Hz, H6), 6.73 (2H, dd, ^{3}J = 9 Hz, ^{4}J = 1 Hz, H4), 3.98 (6H, s, H7). ^{13}C{^{1}H} NMR (75.47 MHz, 298 K, $CDCl_3$): δ = 148.7 (C1), 145.6 (C3), 135.8 (C2), 122.9 (C5), 107.8 (C4), 105.6 (C6), 56.5 (C7). ^{11}B{^{1}H} NMR (96.29 MHz, 298 K, $CDCl_3$): δ (ppm) = 22.2. MS (EI) Expected: 315.08 Found 314.08 (M^+). Fragment ions: 166.06 ($C_7H_6BO_4^+$), 151.04 ($C_6H_3BO_4^+$). Anal. Calcd for $C_{14}H_{12}B_2O_7$: C, 53.58, H, 3.85. Found: C, 53.47, H, 3.73 %.

(3,5-^{t}Bu$_2$catB)$_2$O [4]



Synthesised from 3,5-di-*tert*-butylcatechol (5.00 g, 22.5 mmol) and boric acid (1.38 g, 22.3 mmol) in 75 mL toluene. Yield: 2.81 g (53 %). ^{1}H NMR (300.13 MHz, 298 K, $CDCl_3$): δ = 7.16 (2H, s, H6), 7.07 (2H, s, H4), 1.46 (18H, s, H8), 1.35 (18H, s, H10). ^{13}C{^{1}H} NMR (75.47 MHz, 298 K, $CDCl_3$): δ = 147.5 (C1), 145.7 (C5), 143.1 (C2), 134.9 (C3), 116.5 (C4), 107.7 (C6), 35.0 (C7), 34.4 (C9), 31.7 (C10), 29.7 (C8). ^{11}B{^{1}H} NMR (96.29 MHz, 298 K, $CDCl_3$): δ (ppm) = 22.6. MS (EI): Expected: 476.3129 Found: 476.3123 (M^+). Fragment ions: 463.4 ($M-Me^+$), 447.4 ($M-2Me^+$), 435.4 ($M-3Me^+$), 248.2 ($C_{14}H_{20}BO_3^+$), 233.2 ($C_{14}H_{20}BO_2^+$), 233.2 ($C_{14}H_{22}O_2^+$), 205.1 ($C_{13}H_{17}O_2^+$), 175.0 ($C_{11}H_{11}O_2^+$), 149.0 ($C_9H_9O_2^+$). 109.0 ($C_6H_3O_2^+$). Anal. Calcd for $C_{28}H_{40}B_2O_5$: C, 70.32, H, 8.43. Found: C, 70.19, H, 8.34 %.

(Br$_4$catB)$_2$O [5]

Synthesised from tetrabromocatechol (10.0 g, 23.5 mmol) and boric acid (1.44 g, 23.3 mmol) in 150 mL toluene. Yield: 4.12 g (40 %). $^{11}B\{^1H\}$ NMR (96.29 MHz, 298 K, $CDCl_3$): δ (ppm) = 22.9. MS (APCI): Expected: 886.3397 ($M+H^+$) Found: 886.3385 ($M+H^+$). Fragment ions: 805.4213 ($M-Br^+$), 644.1027 ($M-3Br^+$), 563.5755 ($M-4Br^+$), 479.4815 ($M-5Br^+$), 452.6777 ($C_6BBr_4O_3^+$), 424.6658 ($C_6Br_4O_2^+$), 371.7616 ($C_6BBr_3O_3^+$), 257.2471 ($C_6B_2BrO_5^+$), 129.0655 ($C_6BO_3^+$), 109.1007 ($C_6H_5O_2^+$). Anal. Calcd for $C_{12}Br_8B_2O_5$: C, 16.29. Found: C, 16.27 %.

(4-PIB$_{550}$catB)$_2$O [6]

Synthesised from 4-PIB$_{550}$catechol (10.5 g 15.9 mmol) and boric acid (976 mg, 15.8 mmol) in 150 mL toluene. Yield: 10.1 g (95 %). ^1H NMR (400.13 MHz, 298 K, $CDCl_3$): δ = 6.91 (2H, s, br, Ar-*H*), 6.79 (4H, m, br, Ar-*H*), 1.78 (3H, s, br, C*H*$_3$), 1.26-1.47 (46H, m, br, overlapping C*H*$_2$ peaks), 1.22 (6H, s, br, C*H*$_3$), 0.91-1.19 (117H, m, br, overlapping C*H*$_3$ peaks), 0.77-0.90 (12H, m, br, overlapping C*H*$_3$ peaks). $^{13}C\{^1H\}$ NMR (100.61 MHz, 298 K, $CDCl_3$): δ = 137.9 (Ar-q*C*), 129.1 (Ar-*C*), 128.3 (Ar-C), 125.0 (Ar-*C*), 59.6 (*C*H$_2$), 59.4 (*C*H$_2$), 59.2 (*C*H$_2$), 58.9 (*C*H$_2$), 58.2 (*C*H$_2$), 38.3 (q*C*), 38.2 (q*C*), 38.1 (q*C*), 38.0 (q*C*), 37.8 (q*C*), 32.6 (*C*H$_3$), 32.5 (*C*H$_3$), 32.2 (*C*H$_3$), 31.3 (*C*H$_3$), 31.2 (*C*H$_3$), 31.1 (*C*H$_3$), 30.8 (*C*H$_3$), 30.6 (*C*H$_3$), 21.5 (*C*H$_3$). $^{11}B\{^1H\}$ NMR (128 MHz; $CDCl_3$): δ = 23.7. MS (MALDI TOF): 1349 (M^-), 1292 ($M-{}^iBu^-$).

(4-PIB$_{1000}$catB)$_2$O [7]

Synthesised from 4-PIB$_{1000}$catechol (10.8 g, 10.8 mmol) and boric acid (666 mg, 10.7 mmol) in 150 mL toluene. Yield: 10.7 g (99 %). ^{1}H NMR (400.13 MHz, 298 K, $CDCl_3$): δ = 7.02 (2H, m, br, Ar-*H*), 6.84-6.94 (2H, m, br, Ar-*H*), 6.79 (2H, m, br, Ar-*H*), 1.26-1.51 (74H, m, br, overlapping C*H*$_2$ peaks), 1.73-1.84 (3H, m, br, C*H*$_3$), 1.44-1.35 (72H, m, br, C*H*$_2$), 1.22 (6H, s, br, C*H*$_3$), 0.92-1.17 (192H, m, br, overlapping C*H*$_3$ peaks), 0.78-0.89 (12H, m, br, overlapping C*H*$_3$ peaks). ^{13}C{^{1}H} NMR (100.61 MHz, 298 K, $CDCl_3$): δ = 119.9 (Ar-q*C*), 118.8 (Ar-*C*H), 114.8 (Ar-*C*H), 113.8 (Ar-*C*H), 110.8 (Ar-q*C*), 110.3 (Ar-q*C*), 77.2 (q*C*), 59.6 (*C*H$_2$), 59.4 (*C*H$_2$), 58.9 (*C*H$_2$), 58.5 (*C*H$_2$), 58.2 (*C*H$_2$), 38.2 (q*C*), 32.5 (*C*H$_3$), 31.2 (*C*H$_3$), 31.1 (*C*H$_3$), 31.1 (*C*H$_3$), 30.8 (*C*H$_3$), 30.6 (*C*H$_3$). ^{11}B{^{1}H} NMR (128.38 MHz, 298 K, $CDCl_3$): δ = 23.8.

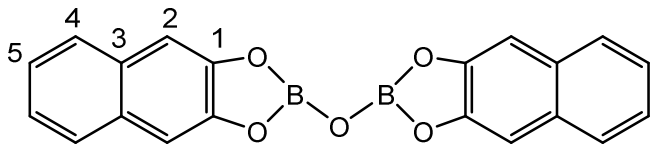
(4-dodecylcatB)$_2$O [8]

Synthesised from 4-dodecylcatechol (35.3 g, 127 mmol) and boric acid (7.77 g, 126 mmol) in 350 mL toluene. Yield: 37.1 g (99 %). %). ^{1}H NMR (400.13 MHz, 298 K, $CDCl_3$): δ = 6.74-7.18 (3H, m, br, Ar-*H*), 2.10-3.18 (2H, m, br, C*H*$_2$), 1.40-1.78 (4H, m, br, C*H*$_2$), 0.99-1.78 (18H, m, br, C*H*$_2$), 0.71-0.95 (5H, m, br, C*H*$_3$). ^{13}C{^{1}H} NMR (100.61 MHz, 298 K, $CDCl_3$): δ = 147.9 (Ar-q*C*), 145.8 (Ar-q*C*). 131.0 (Ar-q*C*), 122.2 (Ar-*C*H), 122.1 (Ar-*C*H), 120.8 (Ar-*C*H), 111.4 (Ar-*C*H), 110.9 (Ar-*C*H), 109.8 (Ar-*C*H), 109.4 (Ar-*C*H), 47.9 (*C*H$_2$), 46.1 (*C*H$_2$), 41.7 (*C*H$_2$), 40.0 (*C*H$_2$), 39.5 (*C*H$_2$), 38.7 (*C*H$_2$), 37.9 (*C*H$_2$), 37.3 (*C*H$_2$), 36.9 (*C*H$_2$), 35.5(*C*H$_2$), 35.1 (*C*H$_2$), 34.0 (*C*H$_2$), 31.9 (*C*H$_2$), 29.7 (*C*H$_2$), 29.7 (*C*H$_2$), 29.6 (*C*H$_2$), 29.6 (*C*H$_2$), 29.4 (*C*H$_2$), 29.3 (*C*H$_2$), 28.3 (*C*H$_2$), 27.7 (*C*H$_2$), 27.6 (*C*H$_2$), 27.3 (*C*H$_2$), 27.2 (*C*H$_2$), 22.7 (*C*H$_2$), 20.8 (*C*H$_2$), 14.1 (*C*H$_3$), 12.2 (*C*H$_3$). ^{11}B{^{1}H} NMR (128.38 MHz, 298 K, $CDCl_3$): δ = 23.6. MS (MALDI TOF) Expected: 590.431 Found: 590.405 (M^-).

(4-(C_{16}-C_{18})catB)$_2$O [9]

Synthesised from 4-(C_{16}-C_{18})catechol (50.0 g, 144 mmol) and boric acid (8.81 g, 143 mmol) in 500 mL toluene. Yield: 51.2 g (98 %). ^{1}H NMR (400.13 MHz, 298 K, $CDCl_3$): δ = 6.53-7.21 (6H. m, br, Ar-*H*), 1.41-1.79 (6H, m, br, C*H*$_2$), 1.00-1.40 (52H, m, br, C*H*$_2$), 0.62-0.97 (9H, m, br, C*H*$_3$). ^{13}C{^{1}H} NMR (100.61 MHz, 298 K, $CDCl_3$): δ = 132.4 (Ar-q*C*), 130.9 (Ar-q*C*), 129.0 (Ar-q*C*), 129.0 (Ar-q*C*), 128.2 (Ar-q*C*), 122.1 (Ar-*C*H), 122.0 (Ar-*C*H), 121.5 (Ar-*C*H), 120.8 (Ar-*C*H), 111.4 (Ar-*C*H), 110.9 (Ar-*C*H), 109.8 (Ar-*C*H), 109.4 (Ar-*C*H), 109.2 (Ar-*C*H), 38.7 (*C*H$_2$), 37.3 (*C*H$_2$), 36.9 (*C*H$_2$), 36.8 (*C*H$_2$), 35.5 (*C*H$_2$), 35.1 (*C*H$_2$), 31.9 (*C*H$_2$), 29.7 (*C*H$_2$), 29.7 (*C*H$_2$), 29.6 (*C*H$_2$), 29.4 (*C*H$_2$), 28.3 (*C*H$_2$), 27.7 (*C*H$_2$), 27.6 (*C*H$_2$), 22.7 (*C*H$_2$), 20.7 (*C*H$_3$), 14.1 (*C*H$_3$), 12.2 (*C*H$_3$). ^{11}B{^{1}H} NMR (128.38 MHz, 298 K, $CDCl_3$): δ = 23.8. MS (MALDI TOF): 703.518 ($C_{44}H_{73}B_2O_5^-$), 731.552 ($C_{47}H_{77}B_2O_5^-$), 759.578 ($C_{48}H_{81}B_2O_5^-$).

(Naph-1,2-O$_2$B)$_2$O [10]



Synthesised from 1,2-dihydroxynaphthalene (10.0 g, 62.4 mmol) and boric acid (3.83g, 61.9 mmol) in 150 mL toluene. Yield: 8.80 g (81 %). ^{1}H NMR (300.13 MHz, 298 K, $CDCl_3$): δ = 7.85 (2H, q, ^{3}J = 3 Hz, H4), 7.61 (2H, s, H2), 7.47 (2H, q, ^{3}J = 3 Hz, H5). ^{13}C{^{1}H} NMR (75.47 MHz, 298 K, $CDCl_3$): δ = 146.1 (C1), 129.4 (C3), 126.7 (C4), 124.1 (C5), 107.8 (C2). ^{11}B{^{1}H} NMR (96.29 MHz, 298 K, $CDCl_3$): δ (ppm) = 22.7. MS (EI) Expected: 354.0878 Found: 354.0893 (M^+).

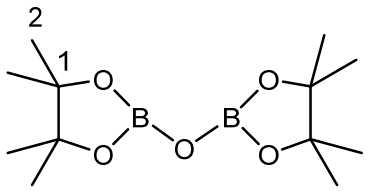
(Ph{NH}$_2$B)$_2$O [11]

Synthesised from *o*-phenylenediamine (5.00 g, 46.2 mmol) and boric acid (2.84 g, 46.0 mmol) in 75 mL toluene. Yield: 3.84 g (67 %). ^{1}H NMR (400.13 MHz, 298 K, $CDCl_3$): δ = 6.89–7.00 (8H, m, Ar-*H*), 5.79 (4H, s, br, N-*H*). $^{13}C\{^{1}H\}$ NMR (100.61 MHz, 298 K, $CDCl_3$): δ = 134.6 (Ar-q*C*), 119.2 (Ar-*C*H), 110.6 (Ar-*C*H). $^{11}B\{^{1}H\}$ NMR (128.38 MHz, 298 K, $CDCl_3$): δ = 23.4. MS (EI) Expected: 250.1197 Found: 250.1205 (M^+). Anal. Calcd for $C_{12}H_{12}B_2N_4O$: C, 57.68, H, 4.84, N, 22.42. Found: C, 57.53, H, 4.78, N, 22.38 %.

(Bn-1,3-O$_2$B)$_2$O [12]

Synthesised from 2-hydroxybenzyl alcohol (5.00 g, 40.3 mmol) and boric acid (2.48 g, 40.0 mmol) in 75 mL toluene. Yield: 2.20 g (39 %). ^{1}H NMR (300.13 MHz, 298 K, $CDCl_3$): δ = 7.22 (2H, m, Ar-*H*), 7.04 (2H, td, ^{3}J = 8 Hz, ^{4}J = 1 Hz, Ar-*H*), 7.00 (4H, m, br, Ar-*H*), 5.23 (4H, s, CH_2). $^{13}C\{^{1}H\}$ NMR (75.47 MHz, 298 K, $CDCl_3$): δ = 150.0 (Ar-q*C*), 128.7 (Ar-*C*H), 124.5 (Ar-*C*H), 123.0 (Ar-*C*H), 121.7 (Ar-q*C*), 118.0 (Ar-*C*H), 64.6 (*C*H_2). $^{11}B\{^{1}H\}$ NMR (96.29 MHz, 298 K, $CDCl_3$): δ (ppm) = 17.4. MS (EI) Expected: 282.0871 Found: 282.0880 (M^+). Fragment ions: 281.0816 ($M-H^+$), 175.0368 ($M-Ph(C=O)H^+$), 77.0385 ($C_6H_5^+$). Anal. Calcd for $C_{14}H_{12}B_2O_5$: C, 59.66, H, 4.29. Found: C, 59.65, H, 4.35 %.

(pinB)$_2$O [13]



Synthesised from pinacol (5.00 g, 42.3 mmol) and boric acid (2.60 g, 42.0 mmol) in 75 mL toluene. Yield: 5.01 g (88 %). Data was consistent with that reported in the literature.[142] ^{1}H NMR (400.13 MHz, 298 K, $CDCl_3$): δ = 1.27 (12H, s, H2). $^{13}C\{^1H\}$ NMR (100.61 MHz, 298 K, $CDCl_3$): δ = 83.1 (C2), 24.5 (C1). $^{11}B\{^1H\}$ NMR (128.38 MHz, 298 K, $CDCl_3$): δ = 21.1. MS (EI) Expected: 270.1810 Found: 270.1815 (M^+). Fragment ions: 255.1485 ($C_{11}H_{21}B_2O_5^+$). Anal. Calcd for $C_{12}H_{24}B_2O_5$: C, 53.39, H, 8.96. Found: C, 53.26, H, 8.87 %.

(CH$_3$(CH$_2$)$_{11}$-1,2-O$_2$B)$_2$O[14]

Synthesised from 1,2-tetradecanediol (5.00 g, 21.7 mmol) and boric acid (1.66 g, 21.6 mmol) in 75 mL toluene. Yield: 5.21 g (98 %). ^{1}H NMR (400.13 MHz, 298 K, $CDCl_3$): δ = 4.10-4.55 (4H, m, C*H*$_2$), 3.64-3.95 (2H, m, C*H*), 1.07-1.76 (44H, m, overlapping C*H*$_2$ peaks), 0.89 (6H, t, ^3J = 7 Hz, C*H*$_3$). $^{13}C\{^1H\}$ NMR (100.61 MHz, 298 K, $CDCl_3$): δ = 76.5 (*C*H), 70.4 (*C*H$_2$), 35.9 (*C*H$_2$), 31.9 (*C*H$_2$), 29.6 (*C*H$_2$), 29.6 (*C*H$_2$), 29.5 (*C*H$_2$), 29.5 (*C*H$_2$), 29.4 (*C*H$_2$), 29.3 (*C*H$_2$), 24.8 (*C*H$_2$), 24.6 (*C*H$_2$), 22.7 (*C*H$_2$), 14.1 (*C*H$_3$). $^{11}B\{^1H\}$ NMR (128 MHz; $CDCl_3$): δ = 22.9. MS (EI) Expected: 494.4314 Found: 494.4363 (M^+). Fragment ions: 479.4079 ($M-Me^+$), 464.6005 ($M-2Me^+$), 452.3997 ($M-Pr^+$), 436.4084 ($M-2Et^+$), 436.4084 ($M-Bu^+$), 423.3843 ($M-C_5H_{11}^+$), 409.3472 ($M-2Pr^+$), 395.3222 ($M-C_7H_{15}^+$). Anal. Calcd for $C_{28}H_{56}B_2O_5$: C, 68.03, H, 11.42. Found: C, 68.03, H, 11.54 %.

(CH$_3$(CH$_2$)$_{13}$-1,2-O$_2$B)$_2$O[15]

Synthesised from 1,2-hexadecanediol (10.0 g, 38.7 mmol) and boric acid (2.38 g, 38.4 mmol) in 150 mL toluene. Yield: 10.3 g (99 %). ^{1}H NMR (400.13 MHz, 298 K, $CDCl_3$): δ = 4.81-4.00 (4H, m, C*H*$_2$), 3.91-3.18 (2H, m, C*H*), 1.83-1.05 (52H, m, overlapping C*H*$_2$ peaks), 0.89 (6H, t, ^3J = 8 Hz, C*H*$_3$). ^{13}C{^{1}H} NMR (100.61 MHz, 298 K, $CDCl_3$): δ = 76.5 (*C*H), 70.4 (*C*H$_2$), 36.0 (*C*H$_2$), 32.0 (*C*H$_2$), 29.7 (*C*H$_2$), 29.7 (*C*H$_2$), 29.6 (*C*H$_2$), 29.5 (*C*H$_2$), 29.5 (*C*H$_2$), 29.4 (*C*H$_2$), 24.8 (*C*H$_2$), 22.7 (*C*H$_2$), 14.1 (*C*H$_3$). ^{11}B{^{1}H} NMR (128 MHz; $CDCl_3$): δ = 22.7. MS (EI) Expected: 550.5 Found: 550.5 (M^+). Fragment ions: 493.5 ($M-2Et^+$), 283.3 ($C_{13}H_{24}B_2O_5^+$). 223.2 ($C_9H_{13}B_2O_5^+$), 194.2 ($C_7H_8B_2O_5^+$), 187.2 ($C_6H_6B_2O_5^+$). 156.2 ($C_4H_6B_2O_5^+$). Anal. Calcd for $C_{32}H_{64}B_2O_5$: C, 69.82, H, 11.72. Found: C, 69.75, H, 11.82 %.

(CH$_3$(CH$_2$)$_{15}$-1,2-O$_2$B)$_2$O[16]

Synthesised from 1,2-octadecanediol (10.0 g, 34.9 mmol) and boric acid (2.14 g, 34.6 mmol) in 150 mL toluene. Yield: 10.1 g (96 %). ^{1}H NMR (400.13 MHz, 298 K, $CDCl_3$): δ = 5.13-3.92 (4H, m, C*H*$_2$), 3.93-3.21 (2H, m, C*H*), 2.34-0.98 (58H, m, overlapping C*H*$_2$ peaks), 0.89 (6H, t, ^3J = 8 Hz, C*H*$_3$). ^{13}C{^{1}H} NMR (100.61 MHz, 298 K, $CDCl_3$): δ = 76.5 (*C*H), 70.5 (*C*H$_2$), 36.0 (*C*H$_2$), 31.9 (*C*H$_2$), 29.7 (*C*H$_2$), 29.7 (*C*H$_2$), 29.6 (*C*H$_2$), 29.6 (*C*H$_2$), 29.6 (*C*H$_2$), 29.5 (*C*H$_2$), 29.5 (*C*H$_2$), 29.4 (*C*H$_2$), 24.8 (*C*H$_2$), 24.7 (*C*H$_2$), 22.7 (*C*H$_2$), 14.1 (*C*H$_2$). ^{11}B{^{1}H} NMR (128.38 MHz, 298 K, $CDCl_3$): δ = 22.9. MS (EI) Expected: 606.6 Found: 606.6 (M^+). Fragment ions: 548.6 ($M-2Et^+$), 394.4 ($C_{21}H_{40}B_2O_5^+$), 380.4 ($C_{20}H_{38}B_2O_5^+$), 310.3 ($C_{15}H_{28}B_2O_5^+$), 296.3 ($C_{14}H_{26}B_2O_5^+$), 281.0 ($C_{13}H_{24}B_2O_5^+$), 251.3 ($C_{11}H_{17}B_2O_5^+$). Anal. Calcd for $C_{36}H_{72}B_2O_5$: C, 71.28, H, 11.96. Found: C, 71.13, H, 11.87 %.

(GMO-B)$_2$O [17]

Synthesised from glycerol mono-oleate (5.76 g, 16.2 mmol) and boric acid (1.00 g, 16.1 mmol) in 150 mL toluene. Yield: 5.88 g (98 %). ^{1}H NMR (400.13 MHz, 298 K, $CDCl_3$): δ = 5.35 (4H, m, C*H*), 4.44-4.14 (4H, m, br, CH_2), 4.10 (2H, m, C*H*), 2.35 (4H, m, CH_2), 2.02 (6H, m, CH_2), 1.63 (4H, s, br, CH_3), 1.31 (38H, m, CH_2), 0.89 (6H, t, ^{3}J = 4 Hz, CH_3). ^{13}C{^{1}H} NMR (100.61 MHz, 298 K, $CDCl_3$): δ = 173.9 (*C*=O), 128.2 (*C*H), 73.8 (*C*H), 67.2 (*C*H), 65.3 (*C*H_2), 65.0 (*C*H_2), 64.8 (*C*H_2), 34.3 (*C*H_2), 34.1 (*C*H_2), 32.6 (*C*H_2), 31.9 (*C*H_2), 29.8 (*C*H_2), 29.7 (*C*H_2), 29.5 (*C*H_2), 29.3 (*C*H_2), 29.1 (*C*H_2), 27.2 (*C*H_2), 27.2 (*C*H_2), 24.9 (*C*H_2), 22.7 (*C*H_2), 14.1 (*C*H_3). ^{11}B{^{1}H} NMR (128.38 MHz, 298 K, $CDCl_3$): δ = 23.2, 18.2 ($B(OH)_3$).

3.2.4 Lewis Acidity Determination

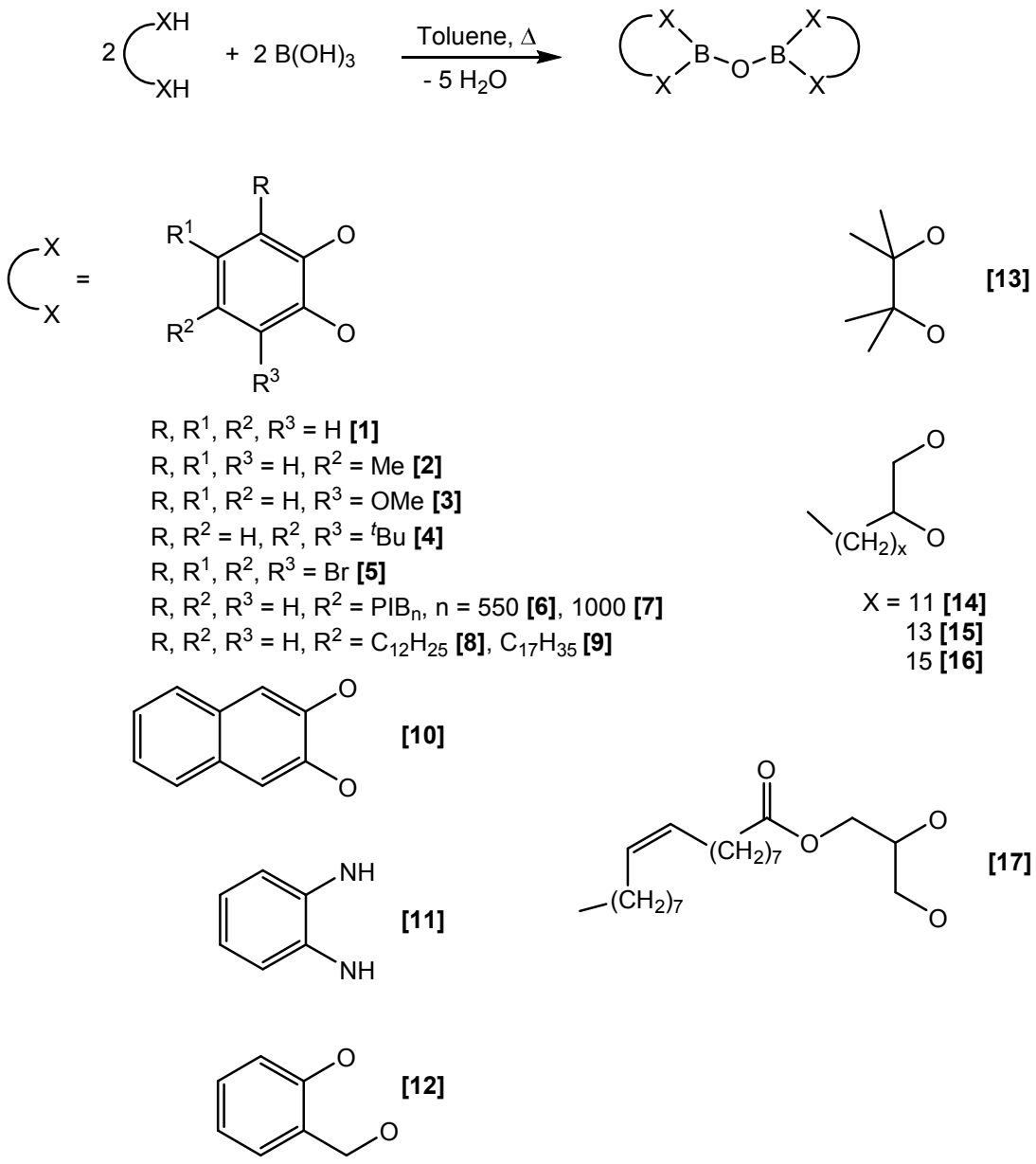
Lewis acidity determination *via* the Gutmann-Beckett method used a procedure similar to that described by Britovsek *et al*.[150] Here, the Lewis acid and triethylphosphine oxide were placed together in a 1:2 ratio in a glass vial and dissolved in a minimum of dry $CDCl_3$. The solution was transferred to an NMR tube, and the ^{31}P{^{1}H} NMR chemical shift recorded at 298 K.

3.3 Results and Discussion

3.3.1 Synthesis of Pyroborate Compounds

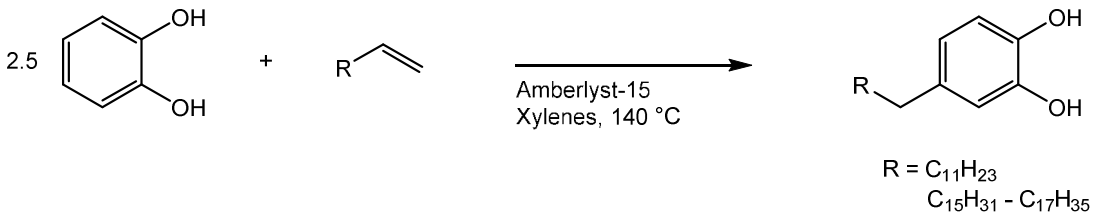
A series of pyroborate esters was synthesised *via* a methodology modified from that reported by Nöth and co-workers.[151] Condensation of a range of diols with boric acid in refluxing toluene with the azeotropic removal of water resulted in the formation of pyroborates **[1]-[17]** in acceptable to excellent yields (39-99 %) (Scheme 3.4). Compounds were analysed by NMR spectroscopy and mass spectrometry, with their bulk purity being affirmed *via* the use of CHN elemental analysis. The reactions could be conveniently monitored *via* the amount of water collected in the Dean-Stark trap, and were typically run for 72 hours to ensure full conversion to the pyroborate species. The only exception to this was the perbrominated pyroborate **[5]** which was synthesised in 16 hours, as longer reaction times led to decomposition of the product, liberating HBr gas and yielding a mixture of differently substituted brominated pyroborate species.

Many of the pyroborates synthesised contain a catechol moiety, with substituents being varied in the 3, 4, 5 and 6-positions of the aromatic ring. Compounds **[1]-[5]** could be conveniently synthesised from commercially available catechol-containing precursors, whereas the relevant catechol species to form **[6]-[9]** were synthesised *via* Friedel-Crafts alkylation reactions. PIB_{550} and PIB_{1000} catechols were synthesised using $BF_3{\cdot}Et_2O$ as a reaction catalyst, and the temperature of the reaction was kept below 25 °C to prevent decomposition of the polyisobutylene chains into smaller fragments. As both molecular weight polyisobutylenes were of a broad polydispersity, ^1H and ^{13}C NMR spectra for both PIB catechols and resulting



Scheme 3.4 Synthesis of pyroborate esters.

pyroborates **[6]** and **[7]** were broad, of a low-resolution and contained many peaks. Furthermore, the ESI-MS spectra of these catechols show peaks for the molecular ions, and fragments with varying lengths of polyisobutylene chains. For the shorter, more reactive straight chain alkyl catechols, Amberlyst-15 was used as a solid acid catalyst which could be conveniently separated *via* filtration after the reaction (Scheme 3.5). A 2.5-fold excess of catechol was necessary for these reactions as the



Scheme 3.5 Synthesis of alkyl catechols.

shorter chain lengths involved increased the likelihood of disubstitution occurring, due to the lack of steric hindrance on the phenyl ring. Despite only the mono-substituted catechols being present in the ESI-MS spectra of both dodecylcatechol and the mixture of C_{16}-C_{18} catechol, there is evidence of some disubstitution occurring due to an increased number of resonances in the ^{1}H and $^{13}C\{^{1}H\}$ NMR spectra of the products. Moreover, since the mixture of C_{16}-C_{18} catechols was synthesised from a mixture of starting alpha olefins, a range of products is to be expected. However, for industrial applications (*e.g.* for use in lubricating oils) using technical, rather than analytical grade starting materials, such discrepancy in purity is acceptable, and so these compounds and their subsequent pyroborate compounds **[8]** and **[9]** may be used in such a manner.

Electron-withdrawing or donating groups were incorporated into the pyroborate compounds in order to probe the effect this had on the Lewis acidity of the resulting species, and long alkyl chains were utilised with the aim of imparting these compounds with oil-solubility when used in anion-binding reactions and subsequent testing (see Chapters V and VI). Both inductive and resonance electron-donating groups were incorporated into the catechol moiety to give compounds **[2]**, **[3]** and **[4]**. Crystals of **[3]** suitable for analysis by X-ray diffraction were obtained *via*

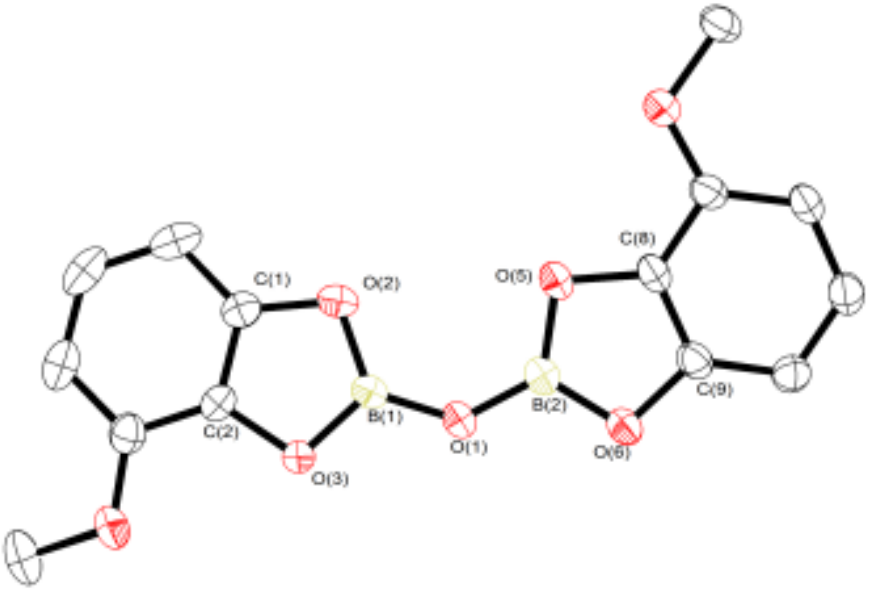


Figure 3.6 The molecular structure of [3]. Thermal ellipsoids are set at the 50% probability level. Hydrogen atoms omitted for clarity.

Table 3.1 Selected bond lengths (Å) and angles (°) for [3].

O(1)–B(1)	1.352(3)
O(1)−B(2)	1.347(3)
O(2)−B(1)	1.381(3)
O(2)−C(1)	1.392(3)
O(3)−B(1)	1.381(3)
O(3) −C(2)	1.391(2)
O(5) −B(2)	1.383(3)
O(5) −C(8)	1.398(3)
O(6) −B(2)	1.385(3)
O(6) −C(9)	1.380(2)
B(1) −O(1) −B(2)	134.52(19)
O(1) −B(1) −O(2)	126.72(19)
O(1) −B(1) −O(3)	120.29(19)
O(2) −B(1) −O(3)	113.0(2)
O(1) −B(2) −O(5)	126.6(2)
O(1) −B(2) −O(6)	120.4(2)
O(5) −B(2) −O(6)	112.96(19)

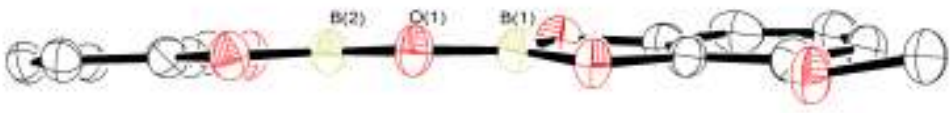


Figure 3.7 Side-on view of the molecular structure of [3], illustrating the deviation from planarity of 8.36(12)°. Thermal ellipsoids are set at the 50% probability level. Hydrogen atoms omitted for clarity.

storage of a concentrated solution in toluene at −30 °C. It can be seen from the crystal structure that the molecule adopts an *anti*-configuration (Figure 3.6; relevant bond lengths and angles are given in Table 3.1). Each boron centre is in a distorted trigonal planar environment due to the rigidity of the catechol moieties restricting the O–B–O angles in proximity to the phenyl rings to 113.0(2)° and 112.96(19)°, significantly lower than the ideal 120° for trigonal planar geometries. This is compensated for by wide O–B–O angles in proximity to the B–O–B bridge of 126.72(19)° and 126.6(2)° and is similar to the solid-state structure of **[1]** previously reported,[151] which exhibits O–B–O angles of 113.2(1)° and 125.6(1)°, indicating the same effect of the rigidity of the diol on the resulting angles around the boron centres. It would appear that this effect is not purely due to the rigid aromatic diols present in **[1]** and **[3]**, and may partially be a consequence of the 1,2 configuration, as pinacol-derived pyroborate **[13]** exhibits angles of 114.2(3)° and 125.7(3)°, which are less distorted than those of **[1]** and **[3]**, but still deviate significantly from ideal trigonal planar geometry.[152] The molecular structure of **[3]** features a B–O–B angle of 134.52(19)°, which is intermediate between the values exhibited by **[1]** and **[13]** [135.9(2)° and 132.6(3)° respectively].

The B–O bond lengths of **[3]** are within the range reported for **[1]** and **[13]** [**[1]**: 1.346(17)-1.376(16) Å; **[3]**: 1.347(3)-1.381(3) Å; **[13]**: 1.359(4)-1.363(4) Å], and those reported for typical triaryloxy borate esters.[153] **[3]** contains the longest B(1)–O(2)/B(1)–O(3) bond lengths of the three pyroborate species, suggesting possible destabilisation of the pyroborate and lengthening of the B–O bonds *via* delocalisation of the methoxy group into the phenyl rings. Indeed, the opposite effect is observed for triaryloxy borate esters containing electron-withdrawing fluorinated groups, which exhibit shorter B–O bond lengths of 1.346(9)-1.371(1) Å,[150, 154] with the highly electron deficient $B[O\text{-}3,5\text{-}(CF_3)_2C_6H_3]_3$ exhibiting B–O bond lengths no greater than 1.363(3) Å.

The molecular structure of **[3]** is almost planar, with the two five-membered boron heterocycles of the molecule deviating from planarity by only 8.36(12)° (Figure 3.7). Similarly, pinacolato pyroborate **[13]** deviates from planarity by only 11.0(3)°. This is in stark contrast with that of **[1]**, which has a much more bent structure, containing boron heterocycles at an angle of 66.38(9)° to one another.

The catecholato motif was expanded further through the use 1,2-dihydroxynaphthalene to give the previously reported naphthyl-derivative **[10]**,[155] which contains another aromatic ring for a greater electron-withdrawing effect, and imparts further rigidity into the compound. Furthermore, *o*-phenylenediamine was utilised to provide a pyroborate compound containing N-donor, rather than O-donor atoms **[11]**, to probe the effect this has on the resulting Lewis acidity and reactivity of the compound, and to provide a further area of substitution, *via* possible deprotonation and alkylation pathways. 2-Hydroxybenzyl alcohol was utilised to synthesise a benzyl derivative of the aromatic pyroborates, **[12]**. This was of interest both to probe the

effect of having both an aryl and alkyl donor oxygen atoms and to investigate whether this synthetic methodology could be extended to 1,3- rather than 1,2-diols.

Confirmation that the reactions were successful was indicated by the presence of a single resonance in the $^{11}B\{^{1}H\}$ NMR spectra of the products, which was found between 21.1 and 23.2 ppm. These are in the expected range for three-coordinate pyroborate compounds,[156] which is downfield of typical trialkoxy and triaryloxy borates,[157] indicating the deshielding effect of having the two borate centres in close proximity to one another. Typically, the presence of more electron-withdrawing groups on the diol gave rise to slight downfield shifts in the resulting $^{11}B\{^{1}H\}$ NMR spectra, as the boron centre became more deshielded. Compound **[17]**, synthesised from glycerol mono-oleate (GMO), exhibited the highest $^{11}B\{^{1}H\}$ chemical shift of 23.2 ppm, which can be attributed to the ester group drawing electrons away from the boron centre, deshielding it to a greater extent than the aromatic diols, regardless of their substitution. The $^{11}B\{^{1}H\}$ NMR spectrum of **[17]** also contained a second peak at 18.2 ppm, suggesting the presence of boric acid, which usually exhibits a $^{11}B\{^{1}H\}$ resonance of *ca.* 19 ppm in $CDCl_3$.[157a, 158] Initially, this was believed to be due to contamination of the sample with boric acid, but it was found that, despite the two components of the mixture having very different properties and solubilities, the boric acid could not be separated through solvent extraction. Furthermore, it was possible that the boric acid persisted as a hydrolysis product, as **[17]** slowly decomposed. However, even when stored under rigorously anhydrous conditions and analysed using only dry $CDCl_3$, the boric acid remained present in all samples, and the peak corresponding to the product did not diminish. It is therefore suggested that the boric acid is in fact somewhat partially bound to **[17]**, possibly due to hydrogen bonding between the hydroxyl protons of the acid and the carbonyl oxygen on the GMO

moiety. Benzyl compound **[12]** exhibited a significantly upfield $^{11}B\{^{1}H\}$ resonance of 17.4 ppm compared to the other pyroborates synthesised, a phenomenon which has been observed previously with four-coordinate benzyl bis-borate species.[159]

Pyroborate $(pinB)_2O$ **[13]** has been synthesised previously by Stephan *et al*. in high yield, but this involved the reaction of pinacol borane, a highly flammable material, with either a phosphine oxide, which had to first be prepared *via* a two-step synthesis, or using trimethylamine oxide.[142] Both of these methodologies require the removal of unwanted volatile, hazardous and malodorous side-products, and the latter involved a reaction under static vacuum, which presents a further hazard. Therefore, the condensation route we have utilised would be the preferred method for the formation of this species.

Compounds **[1]**-**[5]** and **[10]**-**[13]** were synthesised and stored under anhydrous conditions, as the electron-deficient boron centres render these compounds highly susceptible to hydrolysis *via* moisture in the air. However, the addition of long-chain substituents provided sufficient hydrolytic stability to the pyroborate compounds to allow them to be manipulated under standard atmospheric conditions. This phenomenon has been previously reported by Zheng and co-workers, who found long alkyl chains provided hydrolytic stability to nitrogen-containing borate esters.[97] Furthermore, it has been previously reported that hindered phenols are able to impart hydrolytic stability to borate esters.[160] Compound **[8]**, containing a moderately short dodecyl chain, was found to have intermediate hydrolytic stability, and decomposed slowly over several days. Therefore, this pyroborate was stored under an argon atmosphere and reacted on quickly before appreciable decomposition occurred.

Compounds **[14]-[16]** were synthesised in excellent yields of 96-99 %, which may be attributed to their extremely low solubility in toluene, resulting in no loss of product during filtration.

3.3.2 Lewis Acidity of Pyroborate Compounds

The Lewis acidity of each pyroborate compound was measured using the Gutmann-Beckett method, which utilises the Lewis basicity of triethylphosphine oxide and measures the change in $^{31}P\{^{1}H\}$ NMR chemical shift ($\Delta\delta$) between the base and its resulting adduct.[161] This can then give an indication of their affinity towards Lewis bases, and hence their potential as Lewis base binders or Lewis acid catalysts. For this, two equivalents of triethylphosphine oxide and the relevant pyroborate compound were dissolved together in $CDCl_3$, and the resulting $^{31}P\{^{1}H\}$ chemical shift compared to that of unbound triethylphosphine oxide. In order for the Lewis acidities of this series to be compared with other Lewis acidic compounds in the literature, their Acid Numbers (ANs) were also calculated, using the method originally outlined by Gutmann (Table 3.2).[162] Here, the Lewis acidity is standardised using Equation 2, scaled between the $^{31}P\{^{1}H\}$ NMR chemical shift of triethylphosphine oxide in the Lewis inert solvent hexane (δ = 41.0 ppm, AN = 0) and the $^{31}P\{^{1}H\}$ NMR chemical shift of triethylphosphine oxide in strongly Lewis acidic $SbCl_5$ (δ = 86.1 ppm, AN = 100).

The most Lewis acidic pyroborate was found to be the naphthyl compound **[10]**, which exhibited a $\Delta\delta$ value of 32.1 (AN = 95.5). The two aromatic rings of the naphthyl moiety sufficiently withdraw electrons from the boron centre to give the

Table 3.2 Lewis acidity values of tested pyroborate compounds.

Pyroborate	Δδ	AN
[1]	31.6	94.6
[2]	31.5	94.4
[3]	31.7	94.8
[4]	12.6	52.7
[5]	30.2	88.8
[6]	4.2	34.2
[7]	6.5	39.2
[8]	6.4	38.9
[10]	32.1	95.5
[11]	0.4	25.6
[12]	1.5	28.1
[13]	0.0	24.8
[14]	0.6	26.0
[17]	1.5	28.0

$$(2)\ AN = 2.21 \times (\delta_{sample} - 41.0)$$

Equation 2. Calculation of Acid Number (AN) from $^{31}P\{^{1}H\}$ chemical shift of sample.

most acidic p_z orbital of the series. Somewhat surprisingly, the methoxy-substituted compound **[3]** was the next Lewis acidic pyroborate in the series, exhibiting a Δδ value of 31.7 (AN = 94.8). It may have been expected that the electron-donating methoxy groups would reduce the Lewis acidity of the compound but, as indicated by the crystal structure of **[3]**, the resonance donation of the methoxy groups appear to destabilise the B–O bonds, elongating them and leaving the Lewis acidic boron centre open for attack by a Lewis base. The most Lewis acidic pyroborates in this series, **[1]-[3]** and **[10]**, are stronger Lewis acids than a series of fluorinated frustrated Lewis pairs previously reported by Stephan *et al*, exhibiting ANs of 94.4-95.5 compared to 73.1-85.6.[163]

Inductively-donating alkyl substituents on the aromatic ring cause the Lewis acidity of the resulting pyroborates to be significantly lowered. Indeed, even the 4-methylcatechol-substituted compound **[2]** exhibits a Δδ value of 31.5, 0.1 lower than the unsubstituted catecholato pyroborate **[1]**, indicating the effect of additional electron density being donated into the ring on the Lewis acidity of the boron centre. This is shown to a further extent by the di-*tert*-butyl compound **[4]**, which has a significantly lower Δδ value of 12.6 (AN = 52.7) due to the strong electron-donating ability of the two *tert*-butyl groups. Furthermore, the addition of oil-solubilising PIB_{550}, PIB_{1000} and dodecyl chains greatly reduced the Lewis acidity of the resulting pyroborates **[6]**-**[8]**, with the resulting ANs dropping to 34.2, 39.2 and 38.9 respectively. This effect must be taken into account when these compounds are being considered for applications in oils, as their ability to act as Lewis acids will be compromised if solubility is to be achieved.

The perbrominated pyroborate compound **[5]** was found to be significantly less Lewis acidic than **[1]**, exhibiting a Δδ value of 30.2. This was surprising, as the electron-withdrawing bromine atoms would be expected to draw electron density away from the boron centres, rendering them more Lewis acidic. Indeed, it is well established that *para*-bromide has an inductively withdrawing effect in aromatic systems greater than that of hydrogen or substituents such as fluoride, which are able to donate π electrons into the benzene ring, exhibiting a Hammett parameter of 0.23 *vs* 0.00 and 0.06, respectively.[164] DFT calculations reveal the optimised geometry of the molecule to be significantly twisted (Figure 3.9), most likely due to the steric demands of the eight bromide substituents. This may decouple the π-systems of the two boron centres, reducing their electron-withdrawing effect on each other, and therefore rendering each boron atom less Lewis acidic.

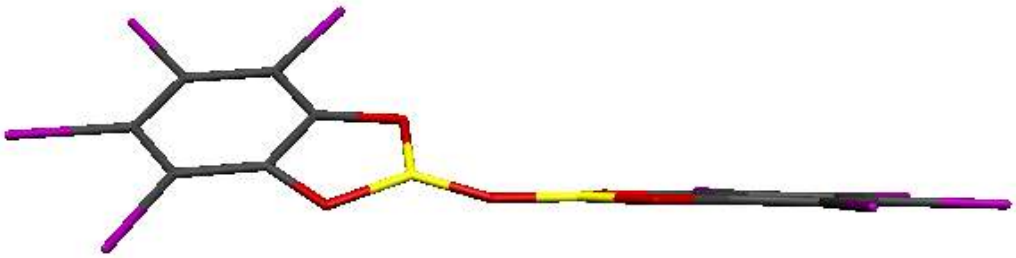


Figure 3.8 DFT Calculated optimised structure of [5], indicating high degree of twist in the molecule.

Amido pyroborate **[11]** was found to exhibit very low Lewis acidity, with a Δδ value of 0.4 being observed (AN = 25.6). This is indicative of a strong B-N π interaction moving electron density into the empty p_z orbital on the boron centre, greatly limiting its ability to accept an electron pair. A similar phenomenon has been observed for $B(NMe_2)_3$, which exhibited an AN of only 9.1.[161]

Replacing one of the phenoxy donor atoms with an alkoxy group had a very pronounced effect on the Lewis acidity. The Δδ value of benzyl compound **[12]** of 1.46 (AN = 28.1) is significantly lower than its catecholato analogues, highlighting the need for electron-withdrawing aromatic groups to give sufficient Lewis acidity to pyroborate compounds. Given this information, it is unsurprising that the fully alkyl-derived pyroborate compounds **[13]**-**[16]** were found to be barely Lewis acidic at all, with the triethylphosphine oxide remaining virtually unchanged upon mixing with the products.

3.3.3 Computational Chemistry

A small selection of the pyroborate compounds were studied computationally using DFT calculations in order to probe the nature of the vacant p_z orbital on each boron centre (see Chapter II for details of computational method used). The LUMO energies

of **[1]**, **[3]**, and **[11]**, the LUMO+2 energy of **[5]** and the LUMO+4 energy of **[10]** were calculated so that a comparison between these and their respective Lewis acidities could be made. These orbitals were calculated as they were representative of the empty p_z orbitals on the boron centres. These particular pyroborate compounds were studied as they represented the broadest differences in Lewis acidity, and so it was anticipated that computational studies would give some insight into the marked differences observed.

Unexpectedly, there does not appear to be a direct correlation between the energy of the empty p_z orbital of a compound and its Lewis acidity (Figure 3.8) with perbrominated pyroborate **[5]** having the lowest energy p_z orbital of the series, despite an intermediate level of Lewis acidity. This suggests that it is not the energy of the empty p_z orbital alone which dictates the Lewis acidity of these species. However, alkyl pyroborate **[13]** has a p_z orbital of considerably higher energy than its aromatic counterparts, perhaps indicating the dramatic effect that changing to

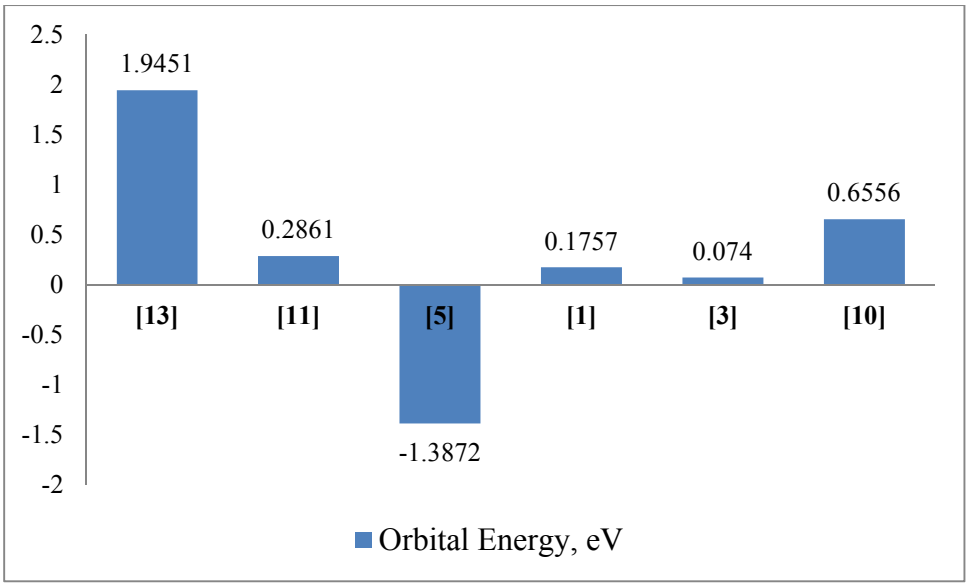
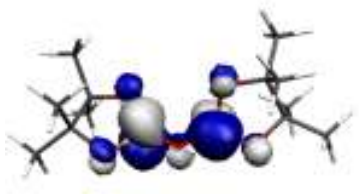
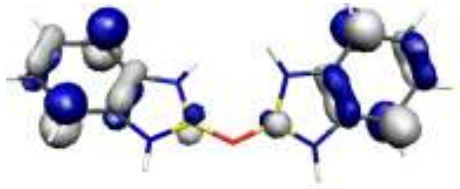
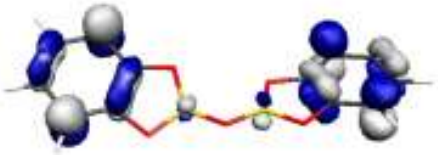
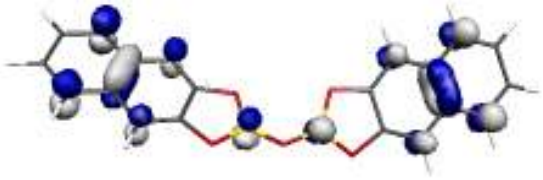
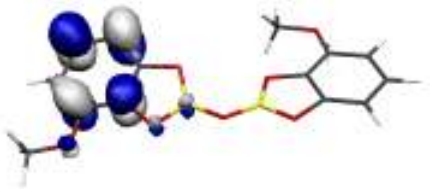
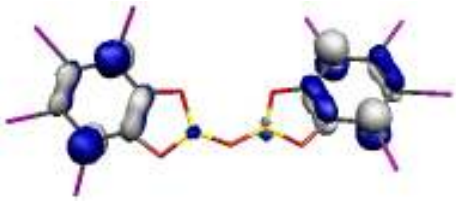


Figure 3.9 DFT Calculated molecular orbital energies for LUMOs ([11], [1] and [3]), LUMO+1 ([13]), LUMO+2 ([5]) and LUMO+4 ([10]).

Table 3.3 DFT Calculated molecular orbital diagrams for LUMOs ([11], [1] and [3]), LUMO+1 ([13]), LUMO+2 ([5]) and LUMO+4 ([10]).

 **[13]**	 **[11]**
 **[1]**	 **[10]**
 **[3]**	 **[5]**

alkoxy donor groups has on the resulting pyroborate compound. This mirrors the Lewis acidity results, as **[13]** has the lowest AN of the series of pyroborate compounds of 24.84, and may suggest that in the case of alkoxy pyroborates, the energy of the empty p_z orbital is a key factor in determining the resulting Lewis acidity of these species.

The empty p_z orbitals of each compound can be visualised in the calculated molecular orbital diagrams for the LUMOs (**[1]**, **[3]** and **[11]**), LUMO+1 (**[13]**), LUMO+2 (**[5]**) and LUMO+4 (**[10]**) (Table 3.3). Once again, alkyl pyroborate **[13]** exhibits significant deviation from the aromatic compounds, affording highly diffuse empty p_z

orbitals on its boron centres. Furthermore, pyroborates **[1]**, **[5]**, **[10]** and **[11]** have considerably larger aromatic contribution to these molecular orbitals, confirming that it may be the electron-withdrawing phenyl rings which impart higher Lewis acidity to these species.

The DFT calculation performed for compound **[3]** allows for a comparison between the optimised calculated geometry and the structural data of the compound obtained through X-ray crystallography to be made (Table 3.4). Experimental bond lengths and angles are in good agreement with calculated values, indicating a good level of accuracy from the calculation methodology used.

Table 3.4 Bond lengths (Å) and angles (°) obtained through X-ray diffraction analysis and DFT calculations.

	X-ray Structure	DFT Calculation	% Difference
O(1)-B(1)	1.352(3)	1.356	+ 0.3
O(1)-B(2)	1.347(3)	1.357	+ 0.7
O(2)-B(1)	1.381(3)	1.391	+ 0.7
O(3)-B(1)	1.381(3)	1.385	+ 0.3
O(5)-B(2)	1.383(3)	1.387	+ 0.3
O(6)-B(2)	1.385(3)	1.384	− 0.1
B(1)-O(1)-B(2)	134.52(19)	131.81	− 2.0
O(1)-B(1)-O(2)	126.72(19)	125.71	− 0.8
O(1)-B(1)-O(3)	120.29(19)	122.08	+ 1.5
O(2)-B(1)-O(3)	113.0(2)	112.21	− 0.7
O(1)-B(2)-O(5)	126.6(2)	125.61	− 0.8
O(1)-B(2)-O(6)	120.4(2)	122.24	+ 1.5
O(5)-B(2)-O(6)	112.96(19)	112.15	− 0.7

3.4 Conclusions

A series of known (**[1]**, **[10]**, **[13]**) and novel pyroborate esters has been synthesised from a variety of aryl and alkyl 1,2- and 1,3-diols, **[1]**-**[17]**, highlighting the wide scope of this synthetic methodology. These species were characterised by ^{1}H, $^{13}C\{^{1}H\}$ and $^{11}B\{^{1}H\}$ spectroscopy, mass spectrometry and CHN elemental analysis. Generally, pyroborates with more electron-withdrawing substituents exhibited more downfield $^{11}B\{^{1}H\}$ resonances. 3-Methoxycatecholato pyroborate **[3]** was further characterised by single crystal X-ray diffraction, which showed the two boron centres to be in distorted trigonal planar environments in the molecule which deviated slightly from planarity.

The Lewis acidity of the pyroborate compounds was investigated *via* the Gutmann-Beckett method, revealing a significant drop in Lewis acidity as alkyl substituents are incorporated into the species. Aromatic moieties were found to be crucial for imparting Lewis acidity. Calculation of the Acid Numbers of the compounds highlighted the high Lewis acidity of compounds **[1]**-**[3]** and **[10]**, suggesting their possible suitability as Lewis acid anion binders or catalysts. DFT calculations suggest that the lower than expected Lewis acidity of perbrominated species **[5]** may be due to twisting of the molecule, which decouples the π-electron network between the two boron centres.

DFT calculations performed on compounds **[1]**, **[3]**, **[5]**, **[10]**, **[11]** and **[13]** indicated that the energy of the empty p_z orbitals of the two boron centres in the pyroborate compounds may directly contribute to their resulting Lewis acidity only for alkoxy-donor species, with the aromatic compounds not offering an obvious correlation between these two parameters. Furthermore, pinacol pyroborate **[13]** contains highly diffuse empty p_z orbitals, which may degrade its Lewis acidity.

3.5 Future Work

Due to the promising scope of the synthetic methodology employed thus far in these studies, the further synthesis of pyroborates derived from a greater range of 1,2- and 1,3-diols would be desirable. This would focus on the use of more electron-withdrawing substituents on catechol rings, in order to attempt to increase the Lewis acidities of the resulting pyroborates even further (Figure 3.9).

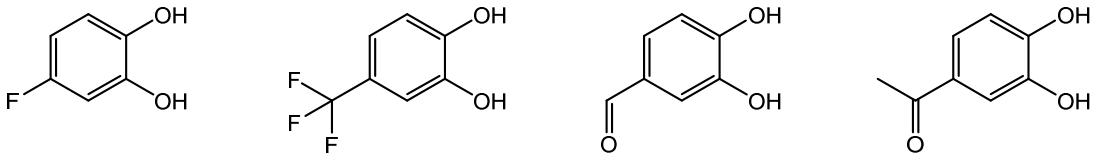
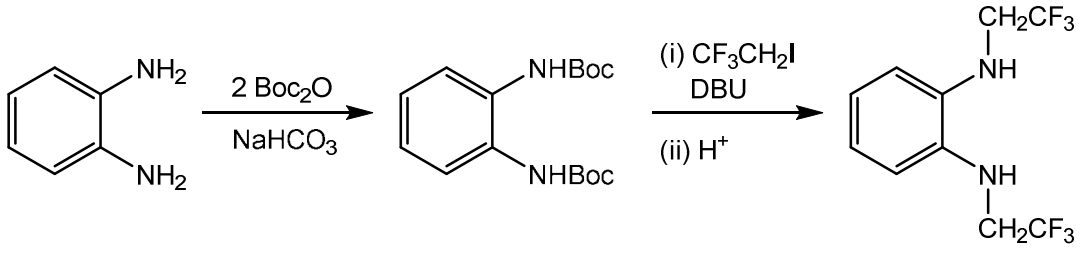


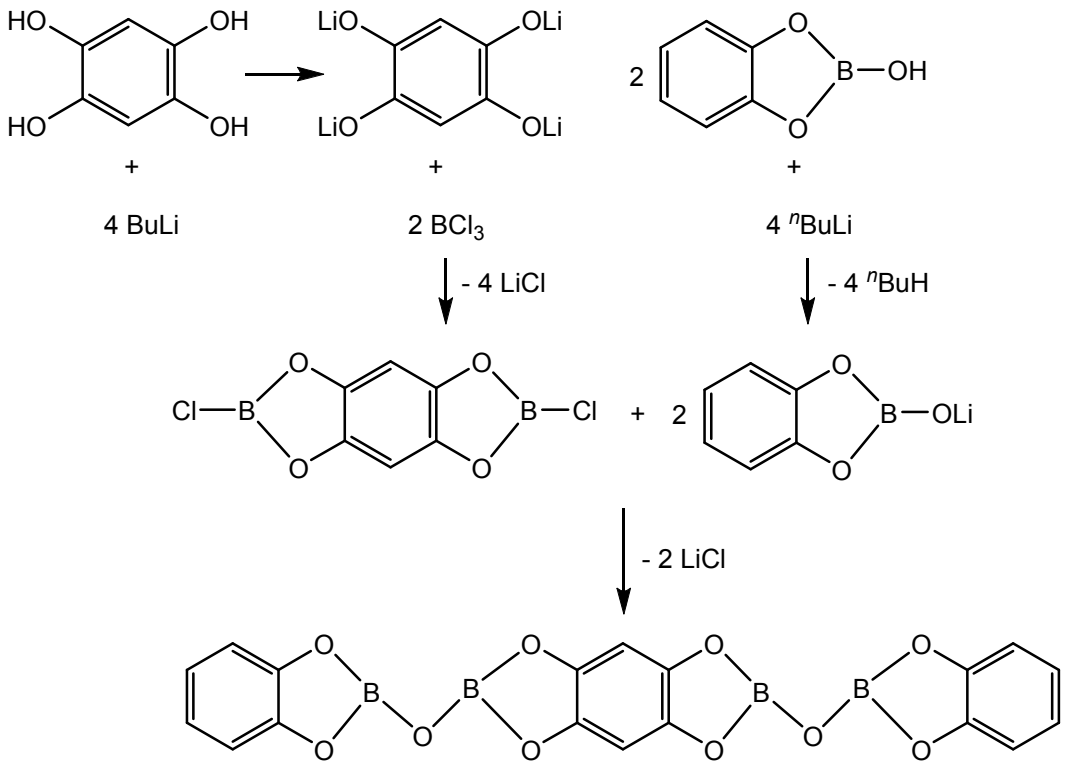
Figure 3.10 Electron-deficient catechol species to be used in future work.

Electron-withdrawing groups would also be incorporated into amino pyroborate **[11]**, to investigate if electron density may be drawn away from the boron centre, allowing this species to act as a stronger Lewis acid. As nitrogen centres allow for another area of substitution, a new avenue of structural variation of these pyroborate compounds may be opened. This may be achieved through substitution of two of the protons of *o*-phenylenediamine with trifluoroethyl groups (Scheme 3.6), before forming the resulting pyroborate through the synthetic methodology described above.



Scheme 3.6 Modification of o-phenylenediamine.

In order to enhance the Lewis acidity of the catecholato pyroborates even further, the synthesis of a dimeric pyroborate may be attempted using 1,2,4,5-tetrahydroxybenzene (Scheme 3.7), the convenient synthesis of which has been reported from commercially available 2,5-dihydroxyquinone.[165] If this were to be successful, a novel range of Lewis acids containing four boron centres would be accessible, which may prove to be of use in anion binding or as Lewis acid catalysts.



Scheme 3.7 Possible synthetic route to dimeric pyroborate species.

Chapter IV Four-coordinate Bis-borate Compounds

4.1 Introduction

There has been significant research interest into the study of four-coordinate bis-borate anions in recent decades, which may in part be due to their inherent stability arising from the full p_z orbital on the boron centre (see Chapter III). Therefore, many applications for such species have been investigated from as early as 1959, when a patent was filed for the use of glycol borates salted with *p*-xylylene diamine as corrosion inhibitors in lubricating oils.[166] Four-coordinate bis-borates were further studied for this purpose in 2012, when borate compounds derived from soybean oils were found to be effective anti-wear additives.[167] These compounds contained both three- and four-coordinate boron centres (Figure 4.1), and were found to perform particularly well when combined with ZDDPs.

Four-coordinate bis-borate compounds have been reported to have uses for enantiomeric induction and separation. For example, sodium borates have been

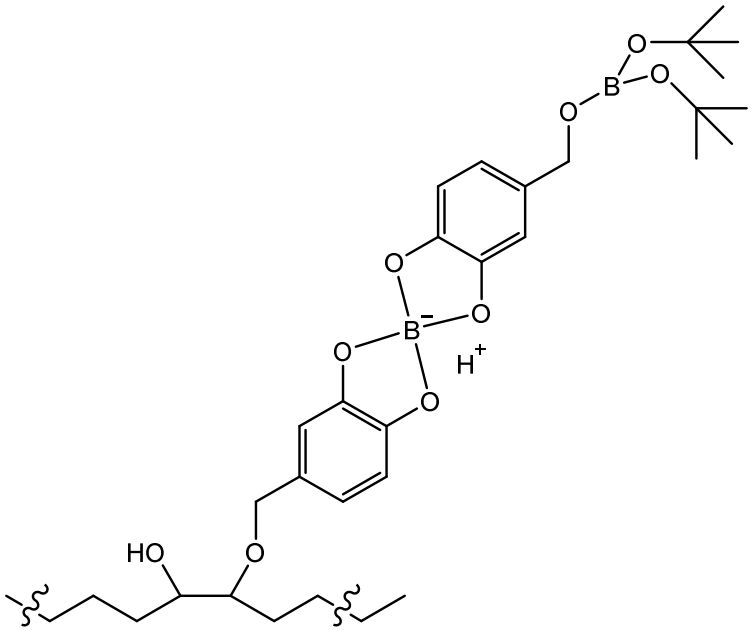


Figure 4.1 Example of a four-coordinate borate-containing anti-wear additive.[167b]

found to be able to separate diastereoisomeric 1,2- and 1,3-diols.[168] Furthermore, a four-coordinate binaphthol borate has been used as a chiral promoter in asymmetric Diels-Alder and Aldol-type reactions.[169] The same anionic borate has been as used as a counterion with $Cu(NCMe)_4^+$ to induce enantioselectivity in olefin aziridination and cyclopropanation.[170] This was achieved through effective ion-pairing in the chiral pocket created by the borate anion, which could be tuned through varying ligands, temperature and solvent.

Four-coordinate bis-borate compounds have been increasingly investigated for their application in electrochemistry, and the first patent for such use was filed in 1968.[171] Here, sodium and ammonium catecholato, naphthalenato and salicylato borates were applied as electrolytes in capacitors, with good electrical stability. This has since been extended to the use of lithium bis-borates to give a series of non-toxic, thermally, chemically and electrochemically stable inexpensive electrolytic compounds, but unfortunately applications in lithium ion batteries were not possible due to the voltage window for such compounds being too small (−500-3000 mV),.[172] Lithium oxalate bis-borates have also been studied for their use as electrolytes, with lithium (malonato oxalate) borate (LiMOB – Figure 4.2a) giving highly conductive solutions, suggesting that such species may be viable for use in lithium-ion batteries if their solubility in organic solvents can be increased.[173] Subsequently, this was achieved by replacement of the malonato moiety with catechol, giving [1,2-benzenediolato(2-)-O,O-oxalato]borate (LBDOB), which formed a highly conductive and stable electrolyte in organic solvents.[174]

Four-coordinate bis-borate motifs have been investigated recently in the area of supramolecular chemistry and covalent organic frameworks, as their tetrahedral

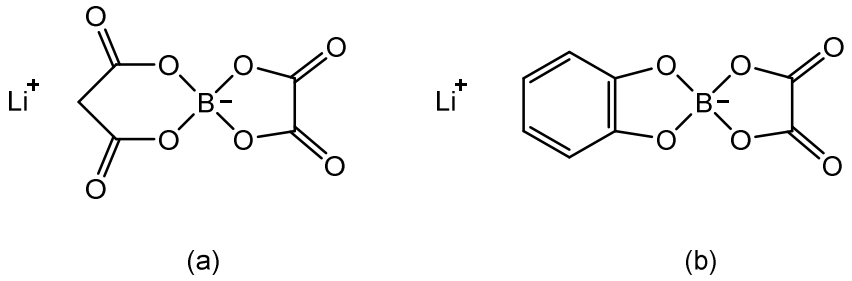


Figure 4.2 The structures of (a) LiMOB[173] and (b) LBDOB.[174]

shape allows for the design of discrete macromolecules containing tetrahedral vertices. Furthermore, the use of boron, rather than metals, with its low atomic weight as a centre in extended frameworks is desirable for cheap, low-density supramolecular materials. A notable example is the use of four-coordinate D_3-symmetric cyclophanes to form "bowls" which are able to stick back-to-back *via* interactions with cationic metal complexes to form chains.[175] It was later found that the addition of different metal cations could extend the chain into a heterobimetallic supramolecular polymer (addition of K^+) or break up the chain into smaller units (addition of Ba^{2+}).[176]

A supramolecular four-coordinate bis-borate complex incorporating anthracene moieties has been synthesised which selectively fluoresces upon binding of chloride through hydrogen bonding interactions.[177] The four-coordinate boron centre allowed the ideal positioning of hydroxy and amide protons on each ligand, leading to efficient binding of two chloride anions (Figure 4.3). The tetrahedral shape formed by four-coordinate bis-borates has been further exploited in the formation of molecular squares linked together by angular spirobisindane ligands.[178] These squares were then able to be "glued" together *via* interactions with cations, forming infinite columns with large central channels which are exceptionally stable to temperature, vacuum and solvent loss. A hexaphenol ligand has been used to form double helicate structures built

around alternating tetrahedral bis-borate centres and sodium cations, further exemplifying the usefulness of these motifs as nodes in supramolecular structures.

In addition to their involvement in the applications described above, catecholato four-coordinate bis-borate compounds have been of particular academic interest, being first reported in 1977 by Pizer *et al*., who discovered that the mechanism of formation of the borate was dominated by a proton transfer reaction.[179] For instance, $[cat_2B]^-$ has been found to coordinate to a range of rhodium complexes,[180] a bis(diphenylphosphino)methane derivative being found to catalyse the diboration

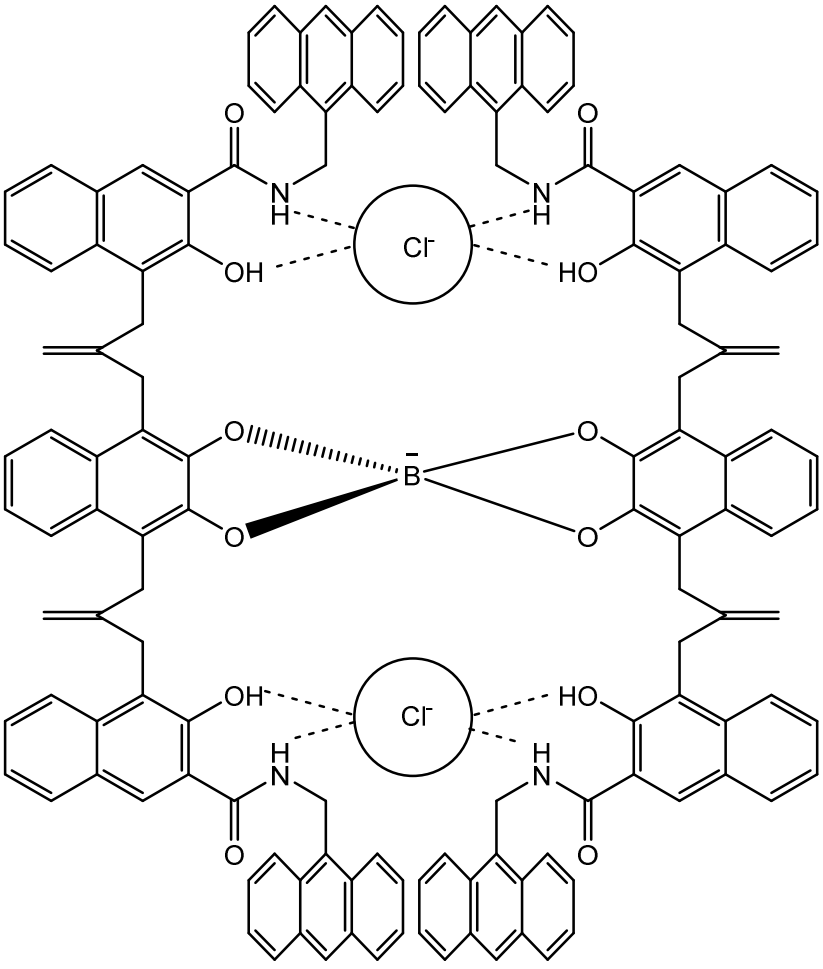


Figure 4.3 Fluorescent four-coordinate bis-borate compound which selectively binds chloride.[177]

of vinylarenes, norbornene, stilbene and β-methylstyrene. Furthermore, four-coordinate bis-borates derived from diphenylphosphinylmethyl-catechols have been utilised as templating chelate ligands in the synthesis of novel silver complexes.[181]

Owing to the diverse range of applications of four-coordinate bis-borates, there is a real need for the further synthesis and study of these species, so that their formation and properties may be better understood.

4.2 Experimental

4.2.1 General Procedure for the Synthesis of Ammonium Bis-borates

The diol was heated with stirring to the point of melting. To this was added the relevant amine and boric acid, and the mixture was heated at 115 °C for 2 h, with the exception of **[27]** and **[28]** which had to be heated at 200 °C due to the high melting point of tetrabromocatechol. Once heating was stopped, the resulting off-white solid was typically pure, with the exception of **[19]** which was purified *via* sublimation *in vacuo* (5 x 10^{-2} mbar) at 115 °C for 16 h.

Variata: [24] and **[25]** were synthesised using two equivalents of triethylamine to ensure full conversion to the final product. Compounds **[21]**, **[27]** and **[34]** were synthesised in toluene (35 mL) with the azeotropic removal of water. Filtration of the reaction mixtures gave **[21]** and **[34]** as off-white solids, and **[27]** as an orange oil.

[HNEt$_3$][cat$_2$B] [18]

Synthesised from catechol (500 mg, 4.53 mmol), triethylamine (0.32 mL, 2.26 mmol) and boric acid (140 mg, 2.26 mmol). Yield: 715 mg (96 %). ^{1}H NMR (300.13 MHz, 298 K, $CDCl_3$): δ = 8.61 (1H, s, br, N-*H*), 6.66 (8H, s, br, Ar-*H*), 3.01 (6H, m, C*H*$_2$), 1.11 (9H, t, ^3J = 7 Hz, C*H*$_3$). ^{13}C{^{1}H} NMR (75.47 MHz, 298 K, $CDCl_3$): δ = 150.5 (Ar-q*C*), 119.0 (Ar-*C*H), 109.1 (Ar-*C*H), 46.4 (*C*H$_2$), 8.39 (*C*H$_3$). ^{11}B{^{1}H} NMR (96.29 MHz, 298 K, $CDCl_3$): δ = 13.9. Anal. Calcd for $C_{18}H_{24}BNO_4$: C, 65.67, H, 7.35, N, 4.25. Found: C, 65.53, H, 7.28, N, 4.29 %.

[HN^{n}Bu$_3$][cat$_2$B] [19]

Synthesised from catechol (500 mg, 4.53 mmol), tri-*n*-butylamine (0.54 mL, 2.26 mmol) and boric acid (140 mg, 2.26 mmol). Yield: 330 mg (35 %). ^{1}H NMR (400.13

MHz, 298 K, $CDCl_3$): δ = 9.07 (1H, s, br, N-*H*), 6.68 (8H, m, Ar-*H*), 2.96 (6H, m, C*H*$_2$), 1.52 (6H, m, C*H*$_2$), 1.23 (6H, m, C*H*$_2$), 0.87 (9H, t, ^3J = 7 Hz, C*H*$_3$). $^{13}C\{^1H\}$ NMR (100.61 MHz, 298 K, $CDCl_3$): δ = 150.6 (Ar-q*C*), 118.8 (Ar-*C*H), 109.1 (Ar-*C*H), 52.4 (*C*H$_2$), 25.1 (*C*H$_2$), 19.8 (*C*H$_2$), 13.5 (*C*H$_3$). $^{11}B\{^1H\}$ NMR (128.38 MHz, 298 K, $CDCl_3$): δ = 14.0. Anal. Calcd for $C_{24}H_{36}BNO_4$: C, 69.74, H, 8.78, N, 3.39. Found: C, 69.62, H, 8.88, N, 3.46 %.

[(2-EtC$_6$H$_{12}$)$_2$NH$_2$][cat$_2$B] [20]

Synthesised from catechol (500 mg, 4.55 mmol), bis(2-ethylhexyl)amine (0.68 mL, 2.27 mmol) and boric acid (140 mg, 2.27 mmol). Yield: 793 mg (97 %). ^1H NMR (400.13 MHz, 298 K, $CDCl_3$): δ = 7.48 (2H, s, br, N-*H*), 6.66 (8H, m, Ar-*H*), 2.66 (4H, s, C*H*$_2$), 1.57 (2H, sept, ^3J = 6 Hz, C*H*), 0.83-1.23 (16H, m, C*H*$_2$), 0.77 (6H, t, ^3J = 7 Hz, C*H*$_3$), 0.57 (6H, t, ^3J = 8 Hz, C*H*$_3$). $^{13}C\{^1H\}$ NMR (100.61 MHz, 298 K, $CDCl_3$): δ = 150.1 (Ar-q*C*), 119.2 (Ar-*C*H), 109.2 (Ar-*C*H), 53.2 (*C*H$_2$), 35.8 (*C*H), 29.8 (*C*H$_2$), 27.8 (*C*H$_2$), 23.0 (*C*H$_2$), 22.7 (*C*H$_2$), 14.0 (*C*H$_3$), 9.8 (*C*H$_3$). $^{11}B\{^1H\}$ NMR (128.38 MHz, 298 K, $CDCl_3$): δ = 13.8. Anal. Calcd for $C_{28}H_{44}BNO_4$: C, 71.64, H, 9.49, N, 2.98. Found: C, 71.57, H, 9.49, N, 3.02 %.

[H$_3$N^{n}Bu][cat$_2$B] [21]

Synthesised from catechol (500 mg, 4.55 mmol), 1-butylamine (0.22 mL, 2.27 mmol) and boric acid (140 mg, 2.27 mmol). Yield: 631 mg (92 %). ^1H NMR (400.13 MHz, 298 K, DMSO-d_6): δ = 7.55 (3H, s, br, N-*H*), 6.48 (8H, m, br, Ar-*H*), 2.77 (2H, t, ^3J = 7 Hz, C*H*$_2$), 1.49 (2H, quin, ^3J = 8 Hz, C*H*$_2$), 1.31 (2H, sext, ^3J = 7 Hz, C*H*$_2$), 0.88 (3H, t, ^3J = 7 Hz, C*H*$_3$). $^{13}C\{^1H\}$ NMR (100.61 MHz, 298 K, DMSO-d_6): δ = 152.0 (Ar-q*C*), 117.8 (Ar-*C*H), 108.1 (Ar-*C*H), 39.1 (*C*H$_2$), 29.6 (*C*H$_2$), 19.5 (*C*H$_2$), 13.9

(*C*H_3). $^{11}B\{^1H\}$ NMR (128.38 MHz, 298 K, $CDCl_3$): δ = 13.7. Anal. Calcd for $C_{16}H_{20}BNO_4$: C, 63.81, H, 6.69, N, 4.65. Found: C, 63.73, H, 6.78, N, 4.72 %.

[HNEt$_3$][4-Mecat$_2$B] [22]

Synthesised from 4-methylcatechol (500 mg, 4.03 mmol), triethylamine (0.28 mL, 2.02 mmol) and boric acid (125 mg, 2.02 mmol). Yield: 705 mg (98 %). ^1H NMR (300.13 MHz, 298K, $CDCl_3$): δ = 8.61 (1H, s, br, N-*H*), 6.48-6.55 (4H, m, br, Ar-*H*), 6.41-6.47 (2H, m, br, Ar-*H*), 2.99 (6H, q, ^3J = 7 Hz, C*H*$_2$), 2.23 (6H, s, Ar-C*H*$_3$), 1.10 (9H, t, ^3J = 7 Hz, C*H*$_3$). $^{13}C\{^1H\}$ NMR (75.47 MHz, 298K, $CDCl_3$): δ = 150.5 (Ar-q*C*), 148.1 (Ar-q*C*), 128.2 (Ar-q*C*), 118.6 (Ar-*C*H), 110.1 (Ar-*C*H), 108.3 (Ar-*C*H), 46.39 (*C*H$_2$), 21.4 (Ar-*C*H$_3$), 8.4 (*C*H$_3$). $^{11}B\{^1H\}$ NMR (96.29 MHz, 298K, $CDCl_3$): δ = 14.0. Anal. Calcd for $C_{20}H_{28}BNO_4$: C, 67.24, H, 7.90, N, 3.92. Found: C, 67.03, H, 7.81, N, 3.85 %.

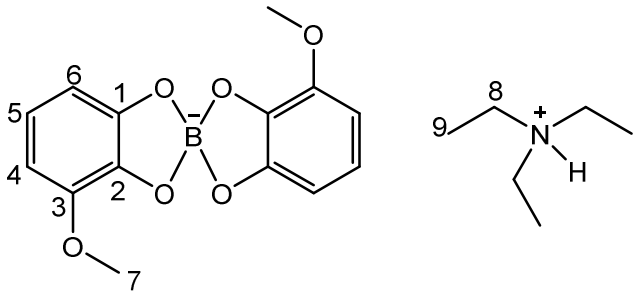
[HN^{n}Bu$_3$][4-Mecat$_2$B] [23]

Synthesised from 4-methylcatechol (500 mg, 4.03 mmol), tri-*n*-butylamine (0.48 mL, 2.02 mmol) and boric acid (125 mg, 2.02 mmol). Yield: 889 mg (99 %). ^1H NMR (300.13 MHz, 298K, $CDCl_3$): δ = 8.72 (1H, s, br, N-*H*), 6.38-6.55 (6H, m, br, Ar-*H*,), 2.91 (6H, m, br, C*H*$_2$), 2.23 (6H, s, Ar-C*H*$_3$), 1.47 (6H, m, br, C*H*$_2$), 1.18 (6H, sext, ^3J = 7 Hz, C*H*$_2$), 0.83 (9H, t, ^3J = 7 Hz, C*H*$_3$). $^{13}C\{^1H\}$ NMR (75.47 MHz, 298K, $CDCl_3$): δ = 150.6 (Ar-q*C*), 148.3 (Ar-q*C*), 128.1 (Ar-*C*H), 118.5 (Ar-*C*H), 110.2 (Ar-*C*H), 108.2 (Ar-*C*H), 52.4 (*C*H$_2$), 25.1 (*C*H$_2$), 21.3 (*C*H$_2$), 19.8 (*C*H$_3$), 13.4 (*C*H$_3$). $^{11}B\{^1H\}$ NMR (96.29 MHz, 298K, $CDCl_3$): δ = 14.0. Anal. Calcd for $C_{26}H_{40}BNO_6$: C, 70.75, H, 9.13, N, 3.17. Found: C, 70.68, H, 9.21, N, 3.25 %.

[(2-EtC$_6$H$_{12}$)$_2$NH$_2$][4-Mecat$_2$B] [24]

Synthesised from 4-methylcatechol (500 mg, 4.03 mmol), bis(2-ethylhexyl)amine (0.61 mL, 2.01 mmol) and boric acid (125 mg, 2.01 mmol). Yield: 982 mg (98 %). ^{1}H NMR (400.13 MHz, 298K, $CDCl_3$): δ = 6.37-6.59 (6H, m, Ar-*H*), 2.66 (4H, d, ^{3}J = 8 Hz, C*H*$_2$), 2.22 (6H, s, C*H*$_2$), 1.54 (2H, sept, ^{3}J = 8 Hz, C*H*), 1.85-2.04 (16H, m, br, C*H*$_2$), 0.79 (6H, t, ^{3}J = 8 Hz, C*H*$_3$), 0.63 (6H, t, ^{3}J = 8 Hz, C*H*$_3$). ^{13}C{^{1}H} NMR (100.6 MHz, 298K, $CDCl_3$): δ = 150.1 (Ar-*C*), 147.9 (Ar-*C*), 128.3 (Ar-*C*), 119.0 (Ar-*C*H), 110.3 (Ar-*C*H), 108.6 (Ar-*C*H), 52.8 (*C*H$_2$), 35.9 (*C*H), 29.9 (*C*H$_2$), 28.0 (*C*H$_2$), 23.1 (*C*H$_2$), 22.9 (*C*H$_2$), 21.2 (Ph-*C*H$_3$), 14.0 (*C*H$_3$), 9.8 (*C*H$_3$). ^{11}B{^{1}H} NMR (128.38 MHz, 298K, $CDCl_3$): δ = 13.9. Anal. Calcd for $C_{30}H_{48}BNO_4$: C, 72.42, H, 9.72, N, 2.82. Found: C, 72.39, H, 9.70, N, 2.86 %.

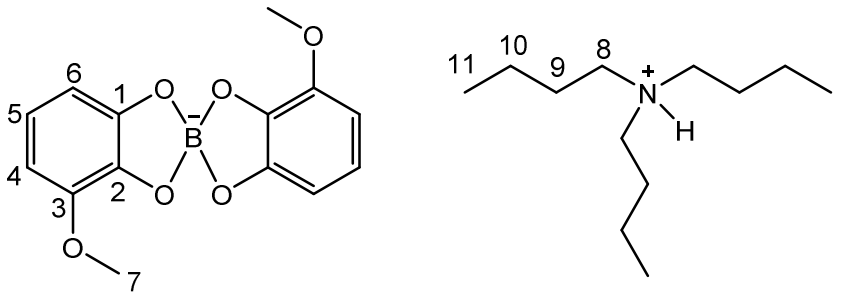
[HNEt$_3$][3-MeOcat$_2$B] [25]



Synthesised from 3-methoxycatechol (500 mg, 3.57 mmol), triethylamine (0.50 mL, 3.57 mmol) and boric acid (110 mg, 1.78 mmol). Yield: 621 mg (87 %). ^{1}H NMR (300.13 MHz, 298K, $CDCl_3$): δ = 8.85 (1H, s, br, N-*H*), 6.61 (2H, t, ^{3}J = 8 Hz, H5), 6.44 (2H, dd, ^{3}J = 8 Hz, ^{4}J = 1 Hz, H6), 6.38 (2H, dd, ^{3}J = 9 Hz, ^{4}J = 1 Hz, H4), 3.81 (6H, s, H7), 3.04 (6H, q, ^{3}J = 7 Hz, H8), 1.11 (9H, t, ^{3}J = 7 Hz, H9). ^{13}C{^{1}H} NMR (75.47 MHz, 298K, $CDCl_3$): δ = 152.0 (C1), 143.7 (C3), 138.2 (C2), 118.5 (C5), 104.4 (C4), 103.9 (C6), 56.3 (C7), 45.9 (C8), 8.3 (C9). ^{11}B{^{1}H} NMR (96.29 MHz, 298K,

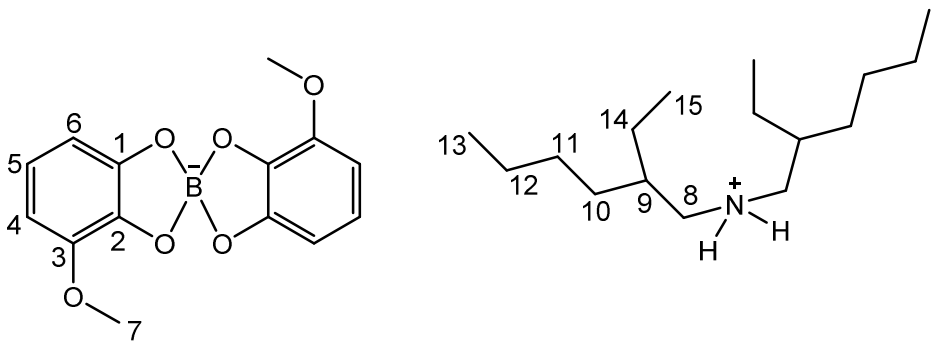
$CDCl_3$): δ = 14.2. Anal. Calcd for $C_{20}H_{28}BNO_4$: C, 61.71, H, 7.25, N, 3.60. Found: C, 61.82, H, 7.25, N, 3.69 %.

[HN^{n}Bu$_3$][3-MeOcat$_2$B] [26]



Synthesised from 3-methoxycatechol (500 mg, 3.57 mmol), tri-*n*-butylamine (0.42 mL, 1.78 mmol) and boric acid (110 mg, 1.78 mmol). Yield: 842 mg (99 %). ^{1}H NMR (300.13 MHz, 298K, $CDCl_3$): δ = 6.61 (2H, t, ^3J = 8 Hz, H5), 6.46 (2H, dd, ^3J = 8 Hz, ^4J = 1 Hz, H6), 6.38 (2H, dd, ^3J = 8 Hz, ^4J = 1 Hz, H4), 3.83 (6 Hz, s, H7), 2.94 (6H, m, br, H8), 1.48 (6H, m, br, H9), 1.20 (6H, sext, ^3J = 7 Hz, H10), 0.84 (9H, t, ^3J = 7 Hz, H11). ^{13}C{^{1}H} NMR (75.47 MHz, 298K, $CDCl_3$): δ = 152.2 (C1), 143.7 (C3), 138.3 (C2), 118.4 (C5), 104.4 (C4), 104.1 (C6), 56.3 (C7), 51.7 (C8), 24.9 (C9), 19.8 (C10), 13.5 (C11). ^{11}B{^{1}H} NMR (96.29 MHz, 298K, $CDCl_3$): δ = 14.2. Anal. Calcd for $C_{26}H_{40}BNO_4$: C, 65.96, H, 8.59, N, 2.96. Found: C, 65.59, H, 8.59, N, 2.99 %.

[(2-EtC$_6$H$_{12}$)$_2$NH$_2$][3-MeOcat$_2$B] [27]



Synthesised from 3-methoxycatechol (500 mg, 3.57 mmol), bis(2-ethylhexyl)amine (0.54 mL, 1.78 mmol) and boric acid (110 mg, 1.78 mmol). Yield: 905 mg (96 %). ^{1}H NMR (400.13 MHz, 298K, $CDCl_3$): δ = 6.58 (2H, t, ^{3}J = 8 Hz, H5), 6.41 (2H, dd, ^{3}J = 8 Hz, ^{4}J = 1 Hz, H6), 6.35 (2H, dd, ^{3}J = 8 Hz, ^{4}J = 1 Hz, H4), 3.77 (6H, s, H7), 2.70 (4H, d, ^{3}J = 7 Hz, H8), 1.57 (2H, sept, ^{3}J = 6 Hz, H9), 0.88-1.31 (16H, m, br, H10-12, H14), 0.79 (6H, t, ^{3}J = 6 Hz, H13/15), 0.64 t, ^{3}J = 7 Hz, H13/15). ^{13}C{^{1}H} NMR (100.6 MHz, 298K, $CDCl_3$): δ = 151.5 (C1), 143.8 (C3), 138.2 (C2), 118.4 (C5), 104.3 (C4), 103.9 (C6), 56.0 (C7), 52.6 (C8), 36.2 (C9), 30.1 (*C*H_2), 28.0 (*C*H_2), 23.2 (*C*H_2), 22.8 (*C*H_2), 14.0 (C13/C15), 9.9 (C13/C15). ^{11}B{^{1}H} NMR (128.38 MHz, 298K, $CDCl_3$): δ = 14.1. Anal. Calcd for $C_{30}H_{48}BNO_6$: C, 68.05, H, 9.14, N, 2.65. Found: C, 68.13, H, 9.25, N, 2.70 %.

[HNEt$_3$][Br$_4$cat$_2$B] [28]

Synthesised from tetrabromocatechol (2.00 g, 4.70 mmol), triethylamine (0.33 mL, 2.35 mmol) and boric acid (145 mg, 2.35 mmol). Yield : 1.69 g (75 %). ^{1}H NMR (300.13 MHz, 298K, $CDCl_3$): δ = 8.67 (1H, s, br, N-*H*), 3.11 (6H, m, C*H*$_2$), 1.30 (9H, t, ^{3}J = 7 Hz, C*H*$_3$). ^{13}C{^{1}H} NMR (75.47 MHz, 298K, $CDCl_3$): δ = 148.9 (Ar-q*C*), 129.0 (Ar-q*C*), 128.2 (Ar-q*C*), 125.3 (Ar-q*C*), 115.9 (Ar-q*C*), 104.6 (Ar-q*C*), 46.8 (*C*H_2), 8.8 (*C*H_3). ^{11}B{^{1}H} NMR (96.29 MHz, 298K, $CDCl_3$): δ = 13.5.

[HN^{n}Bu$_3$][Br$_4$cat$_2$B] [29]

Synthesised from tetrabromocatechol (500 mg, 1.18 mmol), tri-*n*-butylamine (0.15 mL, 0.588 mmol) and boric acid (36.0 mg, 0.588 mmol). Yield: 393 mg (64 %). ^{1}H NMR (300.13 MHz, 298K, $CDCl_3$): δ = 9.43 (1H, s, br, N-*H*), 3.03 (6H, m, br, C*H*$_2$), 1.69 (6H, m, br, C*H*$_2$), 1.35 (6H, sext, ^{3}J = 7 Hz, C*H*$_2$), 0.95 (9H, t, ^{3}J = 7 Hz, C*H*$_3$). ^{11}B{^{1}H} NMR (128.38 MHz, 298K, $CDCl_3$): δ = 13.6.

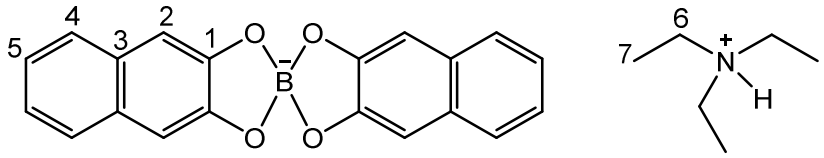
[(2-EtC$_6$H$_{12}$)$_2$NH$_2$][4-PIB$_{550}$cat$_2$B] [30]

Synthesised from 4-PIB$_{550}$catechol (20.0 g, 30.4 mmol), bis(2-ethylhexyl)amine (4.6 mL, 15.2 mmol) and boric acid (9.39 g, 15.2 mmol). Yield: 24.4 g (99 %). ^{11}B{^{1}H} NMR (128.38 MHz, 298K, $CDCl_3$): δ = 13.9. ICP-OES: Calculated percentage: B: 0.81 %; found: B: 0.54 %.

[(2-EtC$_6$H$_{12}$)$_2$NH$_2$][4-PIB$_{1000}$cat$_2$B] [31]

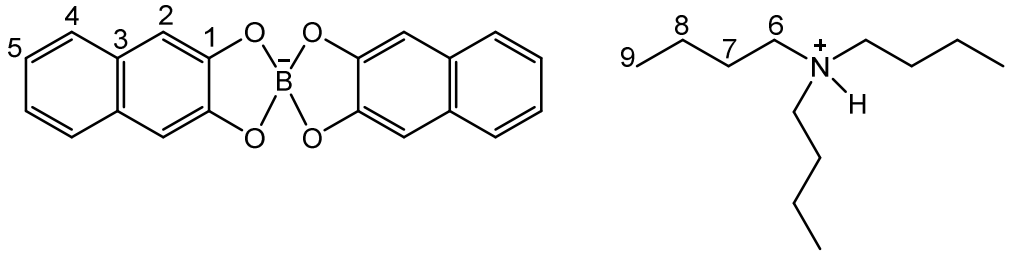
Synthesised from 4-PIB$_{1000}$catechol (20.2 g, 20.2 mmol), bis(2-ethylhexyl)amine (3.0 mL, 10.1 mmol) and boric acid (624 mg, 10.1 mmol). Yield: 22.3 g (98 %). ^{11}B{^{1}H} NMR (128.4 MHz; 298K; $CDCl_3$): δ = 14.0. ICP-OES: Calculated percentage: B: 0.43 %, N: 0.56 %; found: B: 0.36 %, N: 0.81 %.

[HNEt$_3$][(Naph-1,2-O$_2$)$_2$B] [32]



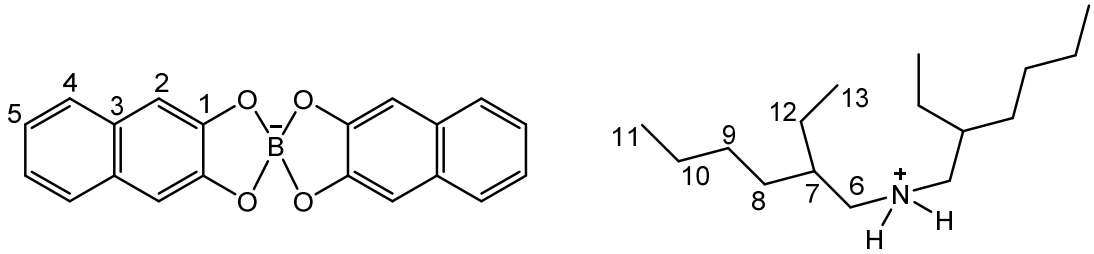
Synthesised from 1,2-dihydroxynaphthalene (500 mg, 3.12 mmol), triethylamine (0.22 mL, 1.56 mmol) and boric acid (97.0 mg, 1.56 mmol). Yield: 668 mg (99 %). ^{1}H NMR (300.13 MHz, 298K, $CDCl_3$): δ = 8.59 (1H, s, br, N-*H*), 7.62 (4H, q, ^3J = 3 Hz, H4), 7.25 (4H, q, ^3J = 3 Hz, H5), 7.01 (4H, s, H2), 3.02 (6H, m, H6), 1.12 (9H, t, ^3J = 7 Hz, H7). ^{13}C{^{1}H} NMR (75.47 MHz, 298K, $CDCl_3$): δ = 151.3 (C1), 129.9 (C3), 126.5 (C4), 122.8 (C5), 103.9 (C2), 46.5 (C6), 8.4 (C7). ^{11}B{^{1}H} NMR (96.29 MHz, 298K, $CDCl_3$): δ = 14.1.

[HN^{n}Bu$_3$][(Naph-1,2-O$_2$)$_2$B] [33]



Synthesised from 1,2-dihydroxynaphthalene (500 mg, 3.12 mmol), tri-*n*-butylamine (0.37 mL, 1.56 mmol) and boric acid (97.0 mg, 1.56 mmol). Yield : 548 mg (69 %). ^{1}H NMR (300.13 MHz, 298K, $CDCl_3$): δ = 8.63 (1H, s, br, N-*H*), 7.61 (4H, t, ^{3}J = 3 Hz, H4), 7.23 (4H, ^{3}J = 3 Hz, H5), 6.99 (4H, s, H2), 2.93 (6H, m, br, H6), 1.49 (6H, m, br, H7), 1.16 (6H, sext, ^{3}J = 7 Hz, H8), 0.78 (9H, t, ^{3}J = 7 Hz, H9). ^{13}C{^{1}H} NMR (75.47 MHz, 298K, $CDCl_3$): δ = 151.5 (C1), 129.9 (C3), 126.4 (C4), 122.7 (C5), 103.9 (C2), 52.6 (C6), 25.1 (C7), 19.8 (C8), 13.3 (C9). ^{11}B{^{1}H} NMR (96.29 MHz, 298K, $CDCl_3$): δ = 14.2.

[(2-EtC$_6$H$_{12}$)$_2$NH$_2$][(Naph-1,2-O$_2$)$_2$B] [34]



Synthesised from 1,2-dihydroxynaphthalene (500 mg, 3.12 mmol), bis(2-ethylhexyl)amine (0.47 mL, 1.56 mmol) and boric acid (97.0 mg, 1.56 mmol). Yield: 825 mg (93 %). ^{1}H NMR (400.13 MHz, 298K, $CDCl_3$): δ = 7.34 (4H, q, ^{3}J = 3 Hz, H4), 7.21 (4H, q, ^{3}J = 3 Hz, H5), 6.76 (4H, s, H2), 2.84 (4H, d, ^{3}J = 7 Hz, H6), 1.53 (2H, sept, ^{3}J = 6 Hz, H7), 0.70-1.25 (16H, m, br, H8-10, H12), 0.65 (6H, td, ^{3}J = 8 Hz, ^{4}J = 3 Hz, H13/H15), 0.56 (6H, m, H13/H15). ^{13}C{^{1}H} NMR (100.6 MHz, 298K,

$CDCl_3$): δ = 150.9 (C1), 129.9 (C3), 126.5 (C4), 123.0 (C5), 104.4 (C2), 52.1 (C6), 35.4 (C7), 29.7 (*C*H_2), 27.9 (*C*H_2), 22.8 (*C*H_2), 22.7 (*C*H_2), 13.8 (C13/C15), 9.6 (C13/C15). $^{11}B\{^1H\}$ NMR (128.38 MHz, 298K, $CDCl_3$): δ = 14.1.

[HNEt$_3$][(Bn-1,3-O$_2$)$_2$B] [35]

Synthesised from 2-hydroxybenzylalcohol (500 mg, 4.03 mmol), triethylamine (0.28 mL, 2.02 mmol) and boric acid (125 mg, 2.02 mmol). Yield: 603 mg (83 %). ^1H NMR (300.13 MHz, 298K, $CDCl_3$): δ = 10.32 (1H, s, v.br, N-*H*), 7.03 (2H, t, ^3J = 8 Hz, Ar-*H*), 6.89 (2H, d, ^3J = 7 Hz, Ar-*H*), 6.73 (2H, d, ^3J = 8 Hz, Ar-*H*), 6.68 (2H, t, ^3J = 7 Hz, Ar-*H*), 4.83 (4H, s, CH_2), 2.92 (6H, q, ^3J = 7 Hz, CH_2), 1.1 (9H, t, ^3J = 7 Hz, CH_3). $^{13}C\{^1H\}$ NMR (75.47 MHz, 298K, $CDCl_3$): δ = 156.4 (Ar-q*C*), 129.0 (Ar-q*C*), 128.2 (Ar-*C*H), 127.5 (Ar-*C*H), 124.6 (Ar-*C*H), 117.4 (Ar-*C*H), 62.2 (Ar-*C*H_2), 45.1 (*C*H_2), 8.2 (*C*H_3). $^{11}B\{^1H\}$ NMR (128.38 MHz, 298K, $CDCl_3$): δ = 2.2. Anal. Calcd for $C_{20}H_{28}BNO_4$: C, 67.24, H, 7.90, N, 3.92. Found: C, 67.13, H, 7.79, N, 3.86 %.

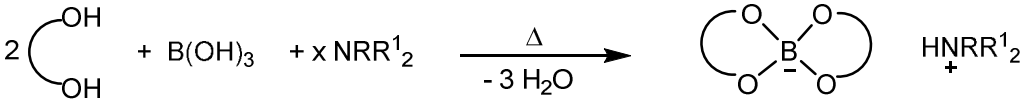
[HN^{n}Bu$_3$][(Bn-1,3-O$_2$)$_2$B] [36]

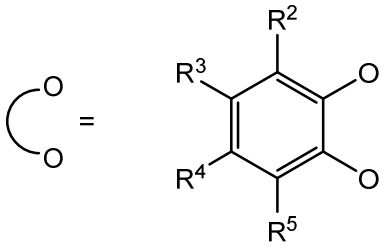
Synthesised from 2-hydroxybenzylalcohol (500 mg, 4.03 mmol), tri-*n*-butylamine (0.50 mL, 2.02 mmol) and boric acid (125 mg, 2.02 mmol). Yield: 886 mg (99 %). ^1H NMR (400.13 MHz, 298K, $CDCl_3$): δ = 10.70 (1H, s, br, N-*H*), 7.05 (2H, t, ^3J = 7 Hz, Ar-*H*), 6.90 (2H, d, ^3J = 8 Hz, Ar-*H*), 6.77 (2H, d, ^3J = 8 Hz, Ar-*H*), 6.69 (2H, ^3J = 7 Hz, Ar-*H*), 4.84 (4H, s, CH_2), 2.88 (6H, m, br, CH_2), 1.50 (6H, m, br, CH_2), 1.21 (6H, sext, ^3J = 7 Hz, CH_2), 0.85 (9H, t, ^3J = 7 Hz, CH_3). $^{13}C\{^1H\}$ NMR (100.6 MHz, 298K, $CDCl_3$): δ = 156.5 (Ar-q*C*), 127.4 (Ar-q*C*), 125.7 (Ar-*C*H), 124.5 (Ar-*C*H), 117.6 (Ar-*C*H), 117.3 (Ar-*C*H), 62.3 (*C*H_2), 51.8 (*C*H_2), 24.9 (*C*H_2), 20.0 (*C*H_2), 13.5 (*C*H_3). $^{11}B\{^1H\}4$ NMR (128.38 MHz, 298K, $CDCl_3$): δ = 2.2. Anal. Calcd for $C_{26}H_{40}BNO_4$: C, 70.75, H, 9.13, N, 3.17. Found: C, 70.68, H, 9.16, N, 3.27 %.

4.3 Results and Discussion

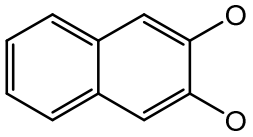
4.3.1 Synthesis of Four-coordinate Bis-borate Compounds

A series of four-coordinate bis-borate species was synthesised from a range of diols and amines, primarily *via* the solvent-free synthesis outlined in Scheme 4.1. This is an extremely straightforward and efficient synthetic methodology, as no additional reagents or solvents are required, and the resulting products are generally formed with high purity, thus requiring no further purification. An exception to this was compound **[19]**, which was purified *via* sublimation at 115 °C and 5 x 10^{-2} mbar overnight. This method is particularly effective as the high reaction temperature

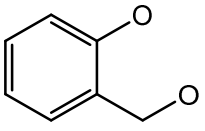




R, R^1 = Et, R^2, R^3, R^4, R^5 = H, x = 1 **[18]**
R, R^1 = ^{n}Bu, R^2, R^3, R^4, R^5 = H, x = 1 **[19]**
R = H, R^1 = 2-EtC_6H_{12}, R^2, R^3, R^4, R^5 = H, x = 1 **[20]**
R = ^{n}Bu, R^1 = H, R^3, R^4, R^5 = H, x = 1 **[21]**
R, R^1 = Et, R^2, R^3, R^5 = H, R^4 = Me, x = 1 **[22]**
R, R^1 = ^{n}Bu, R^2, R^3, R^5 = H, R^4 = Me, x = 1 **[23]**
R = H, R^1 = 2-EtC_6H_{12}, R^2, R^3, R^5 = H, R^4 = Me, x = 1 **[24]**
R, R^1 = Et, R^2, R^3, R^4 = H, R^5 = OMe, x = 2 **[25]**
R, R^1 = ^{n}Bu, R^2, R^3, R^4 = H, R^5 = OMe, x = 1 **[26]**
R = H, R^1 = 2-EtC_6H_{12}, R^3, R^3, R^4 = H, R^5 = OMe, x = 1 **[27]**
R, R^1 = Et, R^2, R^3, R^4, R^5 = Br, x = 1 **[28]**
R, R^1 = ^{n}Bu, R^2, R^3, R^4, R^5 = Br, x = 1 **[29]**
R, R^2, R^3 = H, R^2 = PIB_n, n = 550, x = 1 **[30]**, 1000, x = 1 **[31]**



R, R^1 = Et, x = 1 **[32]**
R, R^1 = ^{n}Bu, x = 1 **[33]**
R = H, R^1 = 2-EtC_6H_{12}, x = 1 **[34]**



R, R^1 = Et, x = 1 **[35]**
R, R^1 = ^{n}Bu, x = 1 **[36]**

Scheme 4.1 Synthesis of bis-borate compounds.

employed causes the water which is driven off from the reaction to evaporate, leaving the desired product behind. This is a simpler method than those reported for similar ammonium bis-borates, which use aqueous conditions, requiring purification with organic solvents.[182] Triethylamine, tri-*n*-butylamine and bis(2-ethylhexyl)amine were utilised in order to probe the effect this variation would have on the $^{11}B\{^{1}H\}$ chemical shifts and solid state structures of the resulting compounds.

The conditions for some of the reactions involving triethylamine were altered to account for its high volatility. For example, the reactions to form **[21]** and **[25]** required two equivalents of triethylamine to ensure full conversion took place. Due to the reaction temperature of 115 °C, the remaining unreacted triethylamine boiled off, leaving the pure reaction product behind. This method proved unsuccessful for compounds **[22]**, **[27]** and **[35]**, however, and a synthetic route involving the azeotropic removal of water in toluene was utilised. This methodology proved more successful, leading to the isolation of **[22]**, **[27]** and **[35]** following filtration of the reaction mixtures.

Confirmation of the formation of the catechol-derived compounds **[18]**-**[34]** is firstly evident from a single peak in the $^{11}B\{^{1}H\}$ NMR spectra between 13.6 and 14.2 ppm. Although δ_B values of *ca.* 14 ppm are relatively high compared to four-coordinate aryl borates,[153a, 183] previous studies have reported $^{11}B\{^{1}H\}$ NMR chemical shifts in this region for similar 1,2-chelating aromatic bis-borate species.[159b, 184] Surprisingly, bis-borates derived from 1,4-binaphthyl diols exhibit much lower $^{11}B\{^{1}H\}$ chemical shifts of *ca*. 9 ppm.[185] Furthermore, benzyl compounds **[35]** and **[36]** exhibited even lower δ_B values of 2.2 ppm, in line with what has been reported for similar tetra-*n*-

butylammonium derivatives,[159a] indicating that deviation from 1,2-chelation of four-coordinate bis-borate species leads to a significant drop in $^{11}B\{^1H\}$ chemical shift. ^1H and $^{13}C\{^1H\}$ NMR spectroscopy further confirmed successful formation of the desired compounds, and elemental analyses agree well with predicted values, indicating the purity of each material.

In order to assess their viability as possible lubricant additives, two bis-catecholato borates incorporating long polyisobutylene chains were synthesised, **[30]** and **[31]** (Scheme 4.1). The longer-chain bis(2-ethylhexyl)ammonium counterion was used with the intention of imparting good oil solubility in the final products. Confirmation of the successful formation of the products is indicated by the presence of a single peak in their $^{11}B\{^1H\}$ NMR spectra at 13.9 and 14.0 ppm respectively. Furthermore, ICP-OES analyses agree well with the structures of the compounds. Unfortunately, neither compound was found to be sufficiently oil-soluble for anti-wear testing to be performed, therefore this application was not pursued further.

There is some deviation in $^{11}B\{^1H\}$ chemical shift between 1,2-chelating bis-borates [**18**]-[**34**] with changing substituents on the aromatic rings. For instance, upon the introduction of methoxy groups in the 3-position of the phenyl rings in compounds **[25]**-**[27]**, the δ_B values increase by 0.2-0.3 ppm when compared to unsubstituted catechol analogues **[18]**-**[20]**. Although these differences are extremely small, they are above the range of error reported in ^{11}B and ^{10}B NMR studies,[186] and so may be significant. It may have been expected that the methoxy groups would shield the boron centre, but it was found in Chapter III that the resonance donation from these substituents may in fact weaken the B-O bonds in pyroborate **[3]**, rendering the boron centre more Lewis acidic. A similar phenomenon may be occurring in bis-borates **[25]**-**[27]**, deshielding the boron centres and causing a downfield shift in the resulting

$^{11}B\{^{1}H\}$ spectra. Similarly, the introduction of a second electron-withdrawing phenyl ring in naphthyl bis-borates **[32]**-**[34]** deshields the boron centres, resulting in downfield shifts of 0.2-0.3 ppm. Conversely, upfield shifts of 0.4 ppm are observed in perbrominated compounds **[28]** and **[29]** compared to catecholato species **[18]** and **[19]**. This indicates that the inductively electron-withdrawing effect of the bromine atoms is outweighed by the donation of the lone pairs of each bromine atom into the phenyl rings, shielding the boron centres.

The $^{11}B\{^{1}H\}$ chemical shifts of these species also appear to be affected by the choice of ammonium counterion used. There appears to be a consistent upfield shift upon changing from tertiary amines to a secondary amine, with δ_B values dropping by 0.1-0.2 ppm. This effect is also observed when changing from a secondary to a primary amine, as shown by the upfield shift of 0.1 ppm observed between compounds [**20]** and **[21]**. Although these differences in chemical shift are relatively small, they may indicate interactions between amine protons on the counterion with the oxygen atoms on the borate species, lowering the electron-withdrawing effect of an oxygen donor atom, thus leaving more electron density on the boron centre.

4.3.2. Crystallographic Analysis

Crystals of **[18]**, **[21]**, **[26]**, **[32]** and **[33]** suitable for X-ray diffraction were grown from concentrated solutions in dichloromethane at room temperature. The crystal structures of **[21]** and **[32]** contain three and two molecules of dichloromethane in the asymmetric unit, respectively. Crystals of **[19]** and **[28]** suitable for X-ray diffraction were grown from concentrated solutions in toluene, and the crystal structure of **[28]** contains a disordered molecule of toluene in its asymmetric unit. With the exception of **[21]**, the solid-state structure of each compound consists of a single four-coordinate

bis-borate anion connected to an ammonium counterion by a hydrogen bond *via* the O4 oxygen atom. The boron atom in each case is in a distorted tetrahedral environment, with O–B–O angles ranging between 103.1(13)° and 114.9(15)°. These are within the range reported for similar aromatic bis-borate species.[181, 184b, 184c, 185, 187] In each case, there are two O-B-O angles which are much

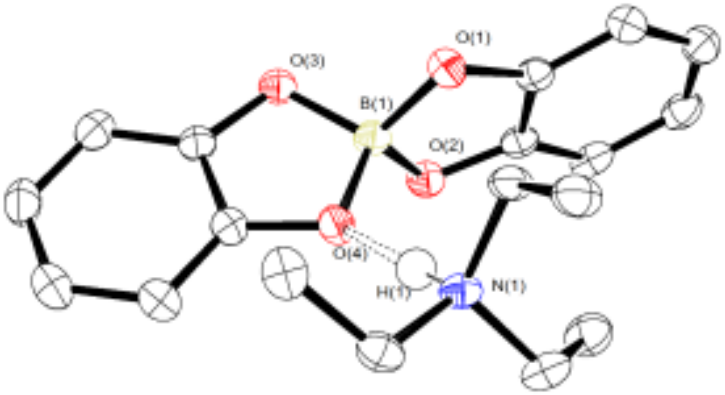


Figure 4.4 The molecular structure of [18]. Thermal ellipsoids are set at the 50% probability level. Hydrogen atoms (except for N-H) omitted for clarity.

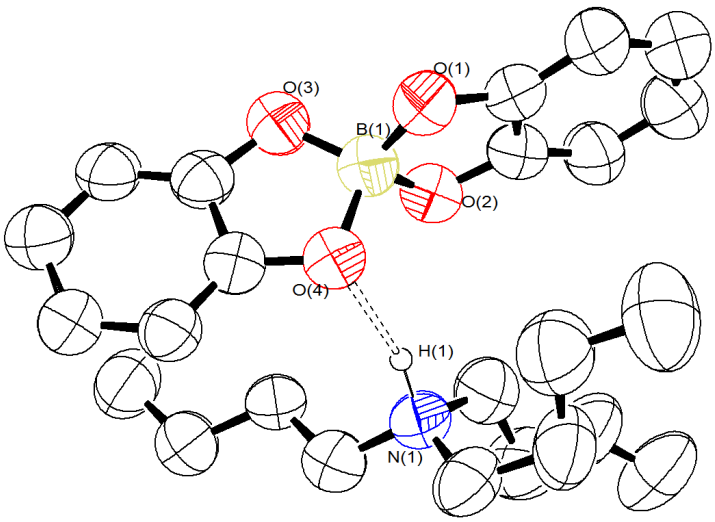


Figure 4.5 The molecular structure of [19]. Thermal ellipsoids are set at the 50% probability level. Hydrogen atoms (except for N-H) and disordered carbon atoms on butyl chain omitted for clarity.

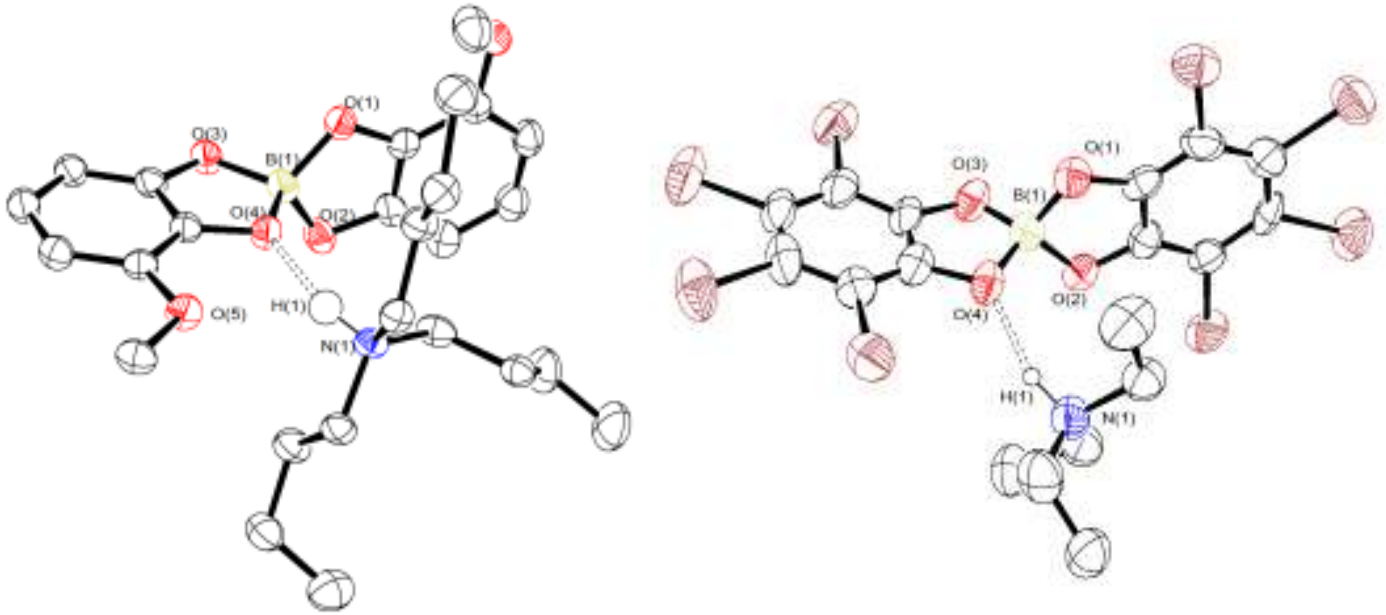


Figure 4.6 The molecular structure of [HN^{n}Bu$_3$][3-MeOcat$_2$B] [26] (left) and [HNEt$_3$][Br$_4$cat$_2$B] [28] (right). Thermal ellipsoids are set at the 50% probability level. Hydrogen atoms (except for N-H), disordered carbon atoms on butyl chain ([26]) and disordered toluene molecule ([28]) omitted for clarity.

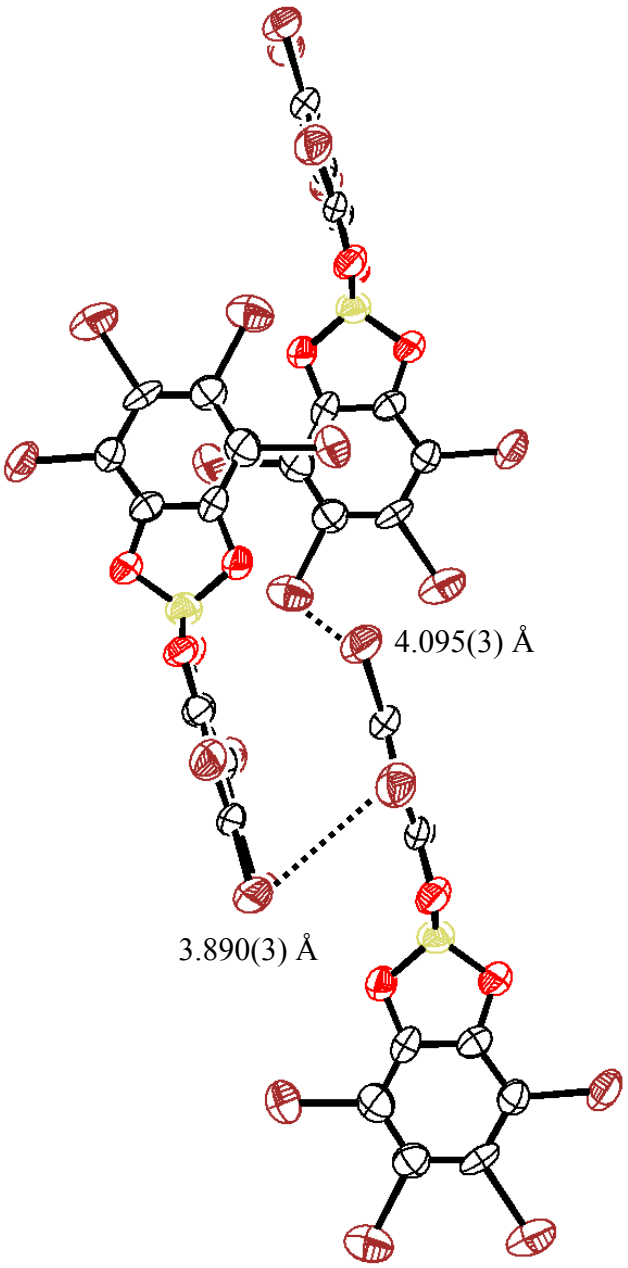


Figure 4.7 Packing of anionic portion of [28], showing possible Br···Br contacts.

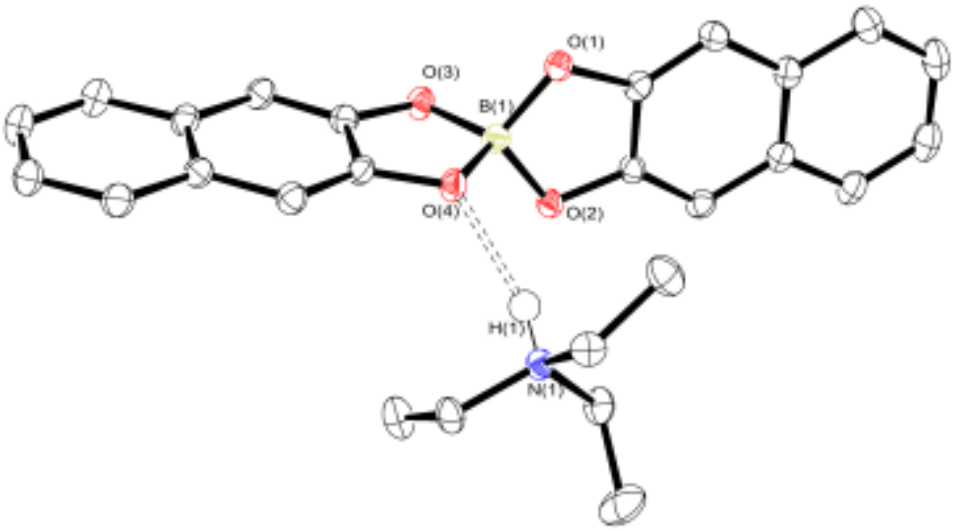


Figure 4.8 The molecular structure of [32]. Thermal ellipsoids are set at the 50% probability level. Hydrogen atoms (except for N-H) and two dichloromethane molecules omitted for clarity.

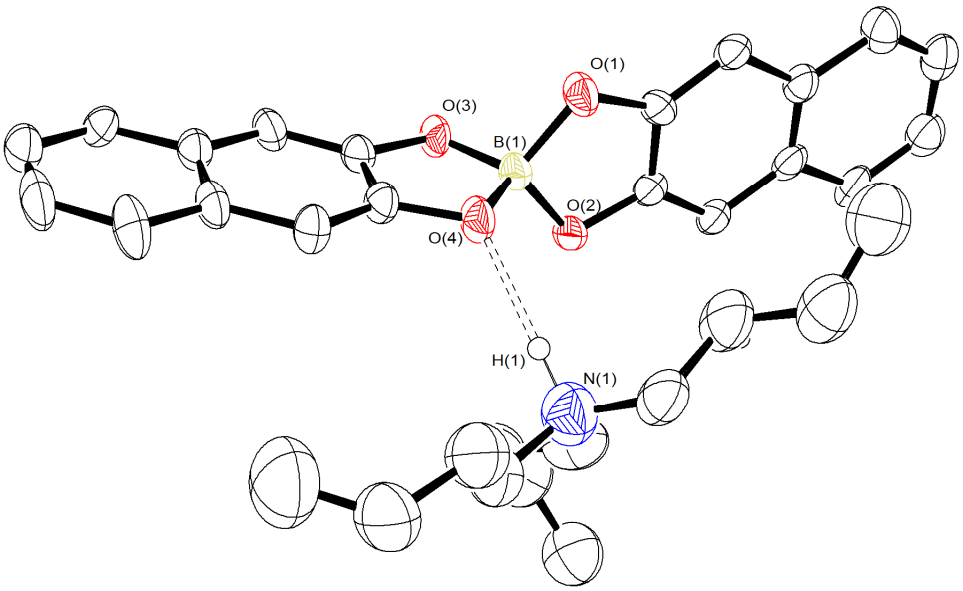


Figure 4.9 The molecular structure of [33]. Thermal ellipsoids are set at the 50% probability level. Hydrogen atoms (except for N-H) and disordered carbon atoms on butyl chain omitted for clarity.

smaller than the other four [103.1(13)-106.9(13)° *vs* 108.6(14)-114.9(15)°], which serves to elongate the anionic units tetragonally, giving them approximate D_{2d} symmetry. This phenomenon is common to many $E(OH)_4^{0/-1}$ or $E(OR)_4^{0/-1}$ motifs, where E = C, Si, or B.[188] However, each borate is found to deviate from approximate D_{2d} symmetry by varying amounts, as one half of the anion bends towards the other (Figure 4.10). This can be viewed quantitatively in Table 4.2, where the difference in the distances between oxygen atoms in the bent portion of each anion and the centre of the least squares plane defined by the orthogonal five-membered ring describes the degree of bending in the anion. Compound **[28]** clearly contains the most bent anion, with a difference between the two oxygen atoms and the orthogonal five-membered ring of 0.109(9) Å being exhibited. This may be due to long-range interactions between bromine atoms on neighbouring borate anions drawing the tetrabromocatechol rings towards one another, bending the overall anion (Figure 4.10). Such interactions have been previously reported by Quayle *et al.* in the rhodium bis-borate *trans*-$[RhBr_{0.26}Cl_{0.74}H(PMe_3)_4][B(1,2\text{-}O_2C_6Br_4)]\cdot CH_2Cl_2$, where the packing of the anion is dominated by Br···Br contacts.[188d] The nearest Br···Br distance in **[28]** is 3.890(3) Å, which is longer than those observed by Quayle *et al.* (3.287-3.656 Å), but is in the region of the sum of the Van der Waals radii for two bromine atoms (3.8-4.2 Å),[189] suggesting a weak interaction. Following this, bis-borate anions of the compounds **[18]**, **[26]** and **[33]** are bent to a similar degree, each exhibiting a difference of *ca*. 0.8 Å. Similar values have been observed in the literature.[181, 187a, 187d] Compound **[32]** exhibits a difference of only 0.035(19) Å, and **[19]** exhibits the least deviation from approximate D_{2d} symmetry with a difference of only 0.008(14) Å being observed. Both these compounds exhibit the longest hydrogen bond distances of this series [**[19]** 2.981(14) Å; **[32]** 3.041(15) Å], and so the greater degree of

linearity of the anions in these species may be due to weaker interactions with their respective cations. A similar effect was observed in 1,10-phenanthrolinium bis-borate [Hphen][cat$_2$B] (phen = $C_{12}H_8N_2$), which exhibited one of the longest hydrogen bond distance in a series of bis-borate species [2.854(2) Å], and the smallest difference in the distances between oxygen atoms in the bent portion of each anion and the centre of the least squares plane defined by the orthogonal five-membered ring of 0.007(2) Å.[187d]

With the exception of **[26]**, the boron-containing five-membered chelate rings of each compound are almost planar, with root mean squared (rms) deviations from the least squares mean plane being between 0.0069 and 0.0581 Å. **[26]** exhibits significant deviation from this, with the rms deviation from the least squares mean plane being 0.4372 and 0.1648 Å for each five membered ring. In each case the chelate rings are found to pucker to a small extent, which is best described by the dihedral angles between the BO_2 and O_2C_2 least square planes (Table 4.2). Dihedral angles of 1.4(14)-13.7(14)° are observed, which are within the range reported for similar ammonium bis-catecholato borates (0.8(2)-13.9(2)°).[187d] These angles follow a similar trend to the bending of the anion described above, suggesting that these two phenomena may be related. Again, perbrominated species **[28]** shows the most deviation from planarity and **[19]** the least, with compounds **[18]**, **[26]** and **[33]** exhibiting intermediate values. With the exception of methoxy bis-borate **[26]**, the five-membered chelate rings are found to be approximately perpendicular to one another (**[18]** 89.83(3)°; **[19]** 89.3(4)°, **[28]** 89.0(4)°; **[32]** 86.90(6)°; **[33]** 89.7(2)°. **[26]** exhibits an angle between the two least squares planes of 80.72(8)°. This is unusual, as similar bis-borate species contain five-membered chelate rings which have been found to be perpendicular to each other within 3°.[187d] It is conceivable that the methoxy oxygen atom O5 is able to participate

in a hydrogen bonding interaction with the N-H proton on the ammonium counterion, twisting the entire chelate towards the counterion, causing a significant deviation from perpendicularity.

The O1–B1–O3 angles are the largest for compounds **[18]** [113.55(10)°], **[19]** [114.9(15)°], **[26]** [113.63(17)°] and **[28]** [114.7(11)°], which may be attributed to the hydrogen bond pulling O4 forward, reducing the O4–B1–O2 bond angle at the front of the molecule and opening up the O1–B1–O3 angle at the back. A similar effect has been reported for the interaction between oxygen atoms in bis-binaphthol borates and sodium atoms, resulting in narrowing of the O–B–O angles involving O···Na interactions.[185] For each bis-borate compound, the O–B–O angles between the two oxygen atoms on the same aryl ring [O1–B1–O2 and O3–B1–O4] are the smallest (**[18]** 105.41(9)° and 104.05(9)°; **[19]** 106.9(13)° and 103.1(13)°; **[26]** 104.20(17)° and 103.84(16)°; **[28]** 103.8(10)° and 105.4(11)°; **[32]** 105.17(13)° and 104.57(13)°; **[33]** 104.4(6)° and 106.0(6)°), indicating the contraction of the O–B–O angles caused by the rigidity of the aryl rings, which has been noted for similar four-coordinate bis-borate species.[187e]

The N1···O4 hydrogen bond distances vary significantly between the bis-borate compounds, with a range of 2.757(2)-3.041(15) Å being observed. These values are at the higher end of the range usually observed for such species,[187a, 187c, 187d, 190] suggesting that these are relatively weak interactions. There appears to be no correlation between whether triethylammonium or tri-*n*-butylammonium counterions are present in the species, as tri-*n*-butylammonium species **[26]** and **[33]** contain the shortest and longest observed hydrogen bond distances respectively [**[26]** 2.757(2) Å; **[33]** 3.041(15) Å]. It is conceivable that the short hydrogen bond exhibited by **[26]** may be due to the electron-withdrawing effect of the methoxy substituents, drawing

electron density away from the borate centre towards the chelating oxygen atoms, making them more potent hydrogen bond acceptors. It is possible that the small deviations in hydrogen bond lengths between **[18]**, **[19]**, **[28]** and **[32]** is due to crystal packing effects.

With the exception of **[33]**, the B1–O4 bond is the longest (**[18]** 1.5049(9) Å; **[19]** 1.524(18) Å; **[26]** 1.506(2) Å; **[28]** 1.511(17) Å; **[32]** 1.491(12) Å), which may be attributed to weakening of the B–O bond due to the participation of the O4 oxygen atom in a hydrogen bonding interaction. This has been previously reported for similar ammonium bis-borate species,[187d] and a similar effect is also reported for B–O bonds containing interactions between oxygen atoms in bis-borate anions and other cations, such as sodium, silver, barium and rhodium.[181, 184b, 184c, 185] This confirms the above hypothesis that hydrogen bonding interactions are occurring between the oxygen atoms on the bis-borate anions, deshielding the boron centres. In the case of **[33]**, it is conceivable that a steric clash occurs between the *n*-butyl chain on the counterion and the naphthyl ring, which is alleviated by the lengthening of the B1–O1 and B1–O2 bonds and concurrent widening of the O4–B1–O2 bond angle. This may also explain why **[33]** exhibits the longest hydrogen bond distance of 3.041(15) Å, as the *n*-butyl chain hinders the approach of the ammonium counterion.

With the exception of **[26]**, the B1–O2 bond is the second longest B–O bond distance (**[18]** 1.4778(15) Å; **[19]** 1.493(19) Å; **[28]** 1.490(18) Å; **[32]** 1.481(2) Å; **[33]** 1.486(11) Å). This may be attributed to the aryl rings moving away from the boron centre in order to prevent steric clash with the ammonium counterion. In the

Table 4.1 Selected bond lengths (Å) and angles (°) for bis-borate compounds.

	[18]	**[19]**	**[26]**	**[28]**	**[32]**	**[33]**
B(1)–O(1)	1.4730(15)	1.439(18)	1.484(3)	1.484(18)	1.472(2)	1.492(11)
B(1)–O(2)	1.4778(15)	1.493(19)	1.480(3)	1.490(18)	1.481(2)	1.486(11)
B(1)−O(3)	1.4755(15)	1.462(18)	1.476(3)	1.422(19)	1.479(2)	1.474(11)
B(1)–O(4)	1.5049(15)	1.524(18)	1.506(2)	1.511(17)	1.491(2)	1.461(11)
O(1)–B1–O(2)	105.41(9)	106.9(13)	104.20(17)	103.8(10)	105.17(13)	104.4(6)
O(1)–B(1)–O(3)	113.55(10)	114.9(15)	113.63(17)	114.7(11)	111.14(14)	110.9(7)
O(3)–B(1)–O(4)	104.05(9)	103.1(13)	103.84(16)	105.4(11)	104.57(13)	106.0(6)
O(4)–B(1)–O(2)	110.83(10)	108.6(14)	110.45(17)	110.7(11)	108.78(14)	112.1(7)
O(1)–B(1)–O(4)	111.34(9)	111.0(14)	111.32(17)	109.9(12)	112.84(14)	112.2(7)
O(3)–B(1)–O(2)	111.81(9)	112.2(14)	113.59(18)	112.4(12)	114.51(14)	111.4(7)
N(1)···O(4)	2.8107(13)	2.981(14)	2.757(2)	2.901(15)	2.8854(19)	3.041(15)

Table 4.2 Approximate deviations of anion from D_{2d} symmetry.

	[18]	**[19]**	**[26]**	**[28]**	**[32]**	**[33]**
Distance between O and centre of plane (Å)	2.3913(9)	4.447(10)	2.3913(9)	2.484(9)	2.4170(14)	2.385(6)
Distance between O and centre of plane (Å)	2.4777(9)	2.439(10)	2.4777(9)	2.375(1)	2.4519(13)	2.468(6)
Difference (Å)	0.087(13)	0.008(14)	0.080(13)	0.109(9)	0.035(19)	0.083(8)
Dihedral angle between BO_2 and O_2C_2 planes (°)	7.99(11)	1.4(14)	6.27(18)	13.7(14)	4.06(16)	8.6(8)

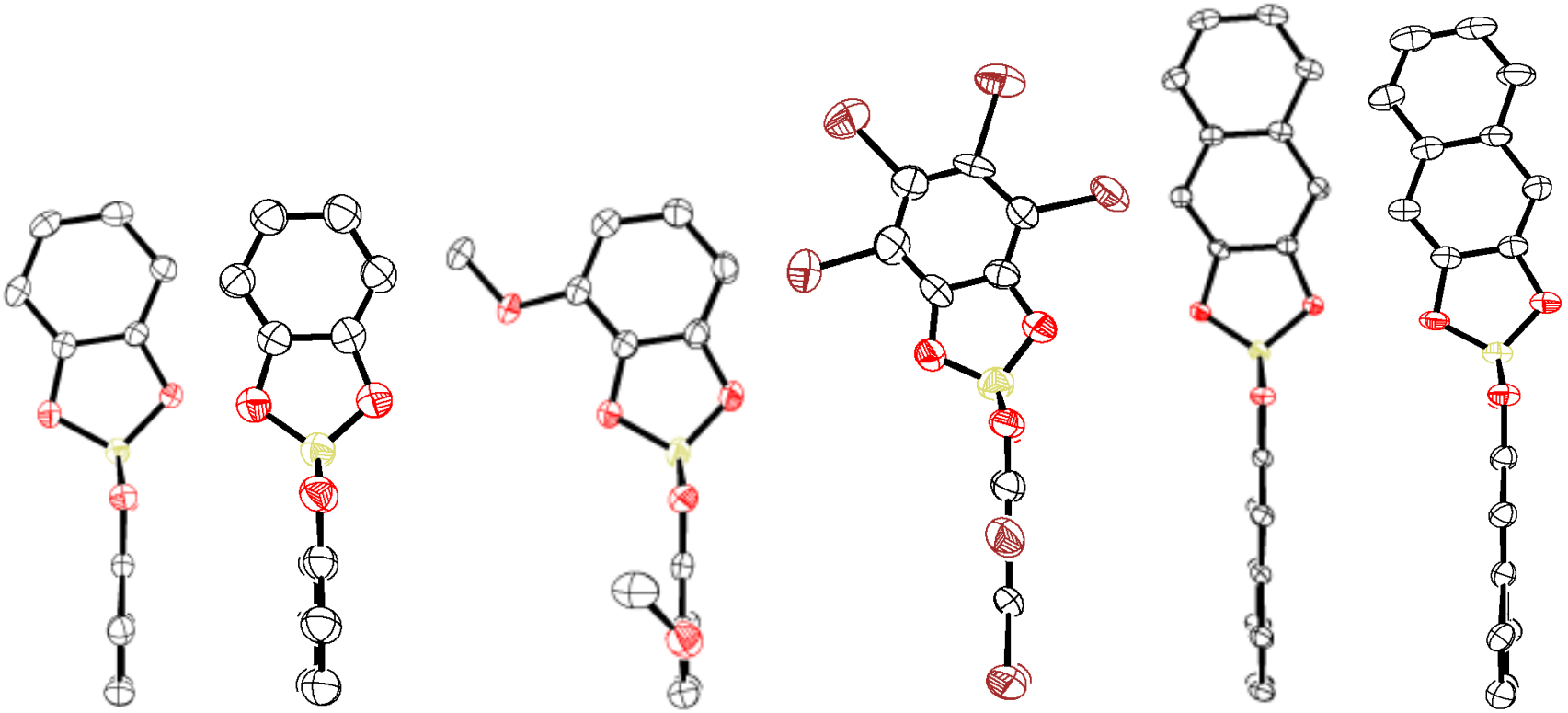


Figure 4.10 Anion components of [18], [19], [26], [32] and [33], showing degree of bending away from approximate D_{2d} symmetry.

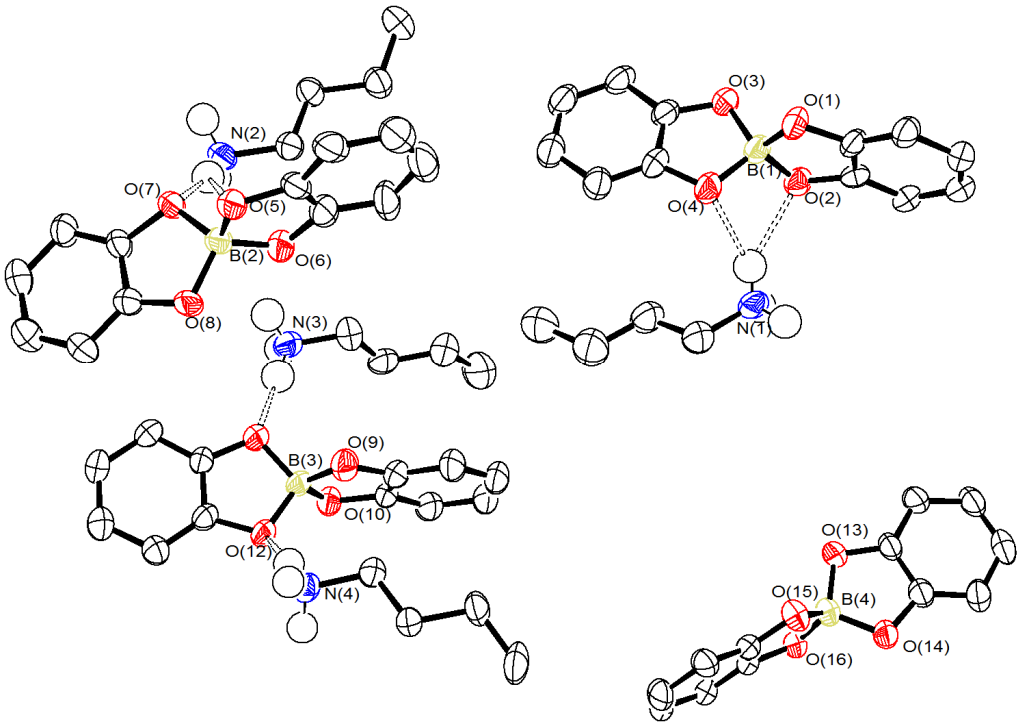


Figure 4.11 The asymmetric unit of the solid-state structure of [21]. Thermal ellipsoids are set at the 50% probability level. Hydrogen atoms (except for N-Hs) and three dichloromethane molecules omitted for clarity.

Table 4.3 Selected bond lengths (Å) and angles (°) for [21].

B(1)−O(1)	1.483(9)	O(1)−B(1)−O(2)	105.6(5)	O(9)−B(3)−O(12)	113.5(6)
B(1)−O(2)	1.459(8)	O(1)−B(1)−O(3)	112.1(5)	O(11)−B(3)−O(10)	109.7(5)
B(1)−O(3)	1.504(8)	O(3)−B(1)−O(4)	104.0(5)	O(13)−B(4)—O(14)	105.1(5)
B(1)−O(4)	1.481(9)	O(4)−B(1)−O(2)	112.6(5)	O(13)−B(4)-O(15)	112.0(5)
B(2)−O(5)	1.485(9)	O(1)−B(1)−O(4)	111.4(6)	O(15)−B(3)−O(16)	104.3(5)
B(2)−O(6)	1.472(8)	O(3)−B(1)−O(2)	111.2(6)	O(16)−B(3)−O(14)	112.3(5)
B(2)−O(7)	1.497(7)	O(5)−B(2)−O(6)	105.3(5)	O(13)−B(4)−O(16)	112.5(6)
B(2)−O(8)	1.469(6)	O(5)−B(2)−O(7)	110.3(5)	O(15)−B(4)−O(14)	110.9(6)
B(3)−O(9)	1.446(9)	O(7)−B(2)−O(8)	104.9(4)		
B(3)−O(10)	1.497(9)	O(8)−B(2)−O(6)	113.3(5)		
B(3)−O(11)	1.491(9)	O(5)−B(2)−O(8)	111.7(6)		
B(3)−O(12)	1.480(8)	O(7)−B(2)−O(6)	111.5(6)		
B(4)−O(13)	1.469(9)	O(9)−B(3)−O(10)	105.2(5)		
B(4)−O(14)	1.477(8)	O(9)−B(3)−O(11)	114.1(5)		
B(4)−O(15)	1.496(9)	O(11)−B(3)−O(12)	104.8(5)		
B(4)−O(16)	1.468(9)	O(12)−B(3)−O(10)	109.6(5)		

case of **[26]**, the B1–O1 bond is the second longest B–O bond distance [1.484(3) Å], which may be attributed to the methoxy group being situated on that side of the anion, and so this bond must elongate to prevent the methoxy substituent from clashing with the *n*-butyl chain of the counterion.

Compound **[21]** was found to have a solid-state structure containing [^{n}BuNH$_3$][cat$_2$B] in four different configurations in its asymmetric unit (Figure 4.11). At first glance, it would appear that the *n*-butylammonium counterions do not bridge bis-borate anions, despite the potential for additional hydrogen bonds *via* the other acidic protons present on each nitrogen atom. Furthermore, it would also appear that the B4-containing bis-borate anion is unconnected to an ammonium counterion and so is not participating in hydrogen bonding at all. However, upon further inspection it can be seen that there are further hydrogen bonding interactions occurring beyond the asymmetric unit into the

crystal lattice, with each *n*-butylammonium counterion bridging two bis-borate anions (Table 4.4). The hydrogen bonding distances span 2.806(7) to 3.108(7) Å, which are at the top of the range previously reported for similar bis-borate compounds.[187a, 187c, 187d, 190] This may indicate weak hydrogen bonding interactions, but it is also possible that the longer distances are necessary to prevent steric clashes between neighbouring ion pairs. Furthermore, the presence of three dichloromethane molecules within the asymmetric unit may force the ammonium bis-borates to be spaced further apart from one another.

Table 4.4 Hydrogen bond distances (Å) for [21].

N(1) –O(4)	3.108(7)
N(1) –O(2)	2.957(7)
N(2) –O(5)	2.869(6)
N(2) –O(7)	2.826(7)
N(3) –O(11)	2.822(8)
N(4) –O(12)	2.877(7)
N(2) –O(15)	2.806(7)
N(3) –O(16)	2.956(6)
N(3) –O(13)	2.879(9)
N(1) –O(8)	2.847(6)
N(4) –O(1)	2.827(7)
N(1) –O(3)	2.861(8)
N(4) –O(10)	2.844(7)

4.3.3 Conductivity Study

As four-coordinate bis-borate species have shown promise as electrolytes for electrochemical applications,[171-174, 191] a preliminary study into the conductivities of a selection of these compounds was carried out. This may give an indication of the

Table 4.5 Conductivity results for bis-borate compounds.

Compound	Conductivity (μScm^{-1})
[26]	0.856
[27]	1.27
[33]	2.64
[34]	1.36
[35]	0.333
[36]	0.357

$$(3)\ \sigma = K/R$$

Equation 3. Calculation of conductivity (σ) from impedence (R) of sample. K = cell constant.

degree of association between the cations and anions in these species, and hence their utility in electrochemical applications. For this, the impedance of a 0.09 M THF solution of each species was measured, which could then be converted to a conductivity *via* Equation 3 (Table 4.5). The cell constant, K, was found from measuring the impedance of a 0.117 M solution of KCl with known conductivity.

A higher concentration solution of *ca.* 0.90 M was desirable, so that the resulting conductivities may be more easily compared with those reported in the literature for lithium bis-borates.[172-174, 191a] However, the poor solubility of these compounds led to a lower concentration being necessary. Consequently, very low conductivities were found for these species, ranging from 0.333 to 2.64 μScm^{-1}. These are at least three orders of magnitude lower than those reported for lithium bis-borates, which were reported to be 0.60-11.07 mScm^{-1}.[172-174, 191a] Furthermore, as the mobility of ions in solution is inversely proportional to their hydrodynamic radii (Equation 4), it is

conceivable that the larger cations present in this study has led to a significant decrease in ion mobility, and so lower conductivities have been observed. Moreover, comparisons between the conductivities observed here are not possible, as atmospheric CO_2 can drastically affect conductivity measurements for electrolytes exhibiting conductivities of < 10 μScm^{-1}, due to dissolution of the gas to give carbonic acid, H_3CO_3, which then dissociates.[192] Modifications must be made to enhance the solubilities of these compounds before their utility as electrolytes may be appreciable, and a comparison between their structural properties and resulting conductivities may be made.

$$(4)\ u = ze/6\pi\eta a$$

Equation 4. Relationship between ion mobility (u) and hydrodynamic radius (a). z = charge of ion, e = elementary charge, η = viscosity of solution.

4.4 Conclusions

A series of four-coordinate bis-borate species **[18]-[33]** has been synthesised from a variety of aromatic 1,2- and 1,3-diols *via* a simple, largely solvent-free methodology. These species were characterised *via* ^{1}H, $^{13}C\{^{1}H\}$ and $^{11}B\{^{1}H\}$ NMR spectroscopies, and their bulk purity affirmed *via* CHN elemental analysis. Two long-chain derivatives **[30]** and **[31]** were further analysed by ICP-OES, but were found to be insufficiently oil-soluble for anti-wear testing to be carried out. The $^{11}B\{^{1}H\}$ NMR chemical shift of the bis-borate species were found to be sensitive to both the substitution on the aromatic rings and choice of ammonium counterion. As also found in Chapter III, the presence of methoxy substituents appeared to remove electron density from the boron centre, deshielding it and leading to a slight shift downfield. Naphthyl bis-borates **[32]** and **[33]** also had an electron-withdrawing effect, increasing the resulting δ_B values, while perbrominated species **[28]** and **[29]** exhibited upfield signals due to the donation of bromine lone pairs into the aromatic systems. The incorporation of additional protons into the ammonium counterion used led to subsequent upfield shifts in the resulting $^{11}B\{^{1}H\}$ NMR spectra, mostly likely due to increased numbers of hydrogen bonding interactions between the counterion and the borate.

Compounds **[18]**, **[19]**, **[21]**, **[26]**, **[32]** and **[33]** were further analysed by X-ray crystallography. In each case, the boron centre was in a distorted tetrahedral environment, with anionic structures which deviated from approximate D_{2d} symmetry by varying amounts, highlighting how intermolecular and hydrogen bonding interactions can affect the resulting solid-state structures of these bis-borate species. Hydrogen bond distances were found to be relatively long compared to related species, indicating weak hydrogen bonding interactions. However, these hydrogen bonds did affect the structure of the resulting bis-borate species, altering both B–O bond lengths

and O–B–O angles. The additional hydrogen bonding interactions offered by the primary-ammonium counterion in **[21]** led to ion pairs which were bridged by both anions and cations, leading to several different configurations of the same bis-borate species in the solid state.

Preliminary conductivity investigations were carried out for compounds **[26]**, **[27]**, **[33]**, **[34]**, **[35]** and **[36]**. These species were found to exhibit lower conductivities than similar lithium bis-borates in the literature, which may be attributed to their lack of solubility and large ionic radii. Therefore, in their current form, these compounds are unsuitable for electrochemical applications.

4.5 Future Work

Future work would initially consist of further variation in both the bis-borate anion and ammonium counterion to give a wider range of compounds for study. This may include electron-withdrawing or sterically demanding groups in the catechol moiety to probe how this affects the chemical and structural properties of the resulting compounds (Figure 4.12). It may also be advantageous to use dopamine as the chelate, as this may provide a zwitterionic bis-borate species which may exhibit interesting structural and chemical properties.

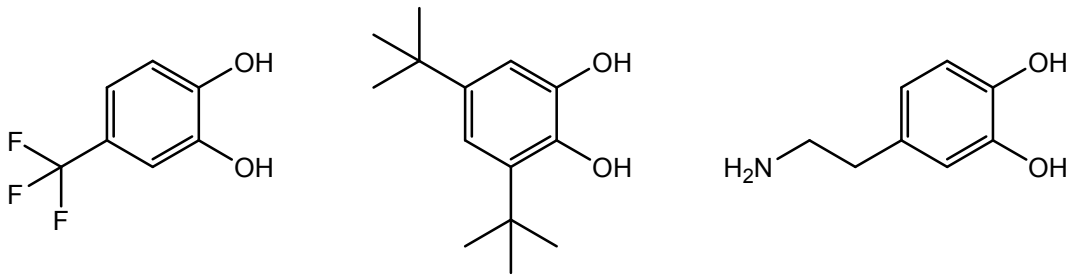


Figure 4.12 Possible further variation in catechol species.

Following this, further variation in the ammonium counterion can be performed to probe the effect this has on the resulting compounds (Figure 4.13). This may include diethylamine and di-*n*-butylamine, to ascertain as to what the effect of secondary ammonium counterions have on the resulting solid-state structure of the bis-borate species. Furthermore, electron-deficient and electron-rich amines may be utilised to probe the effect this has on the resulting compounds. Moreover, diamines such as ethylenediamine may be used in an attempt to synthesise species where bis-borate anions are bridged by a common cation.

In order to further probe the utility of these bis-borate species as electrolytes, analogous lithium bis-borates may be synthesised, which may prove useful as

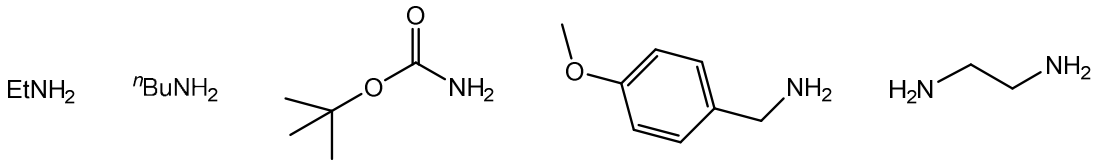
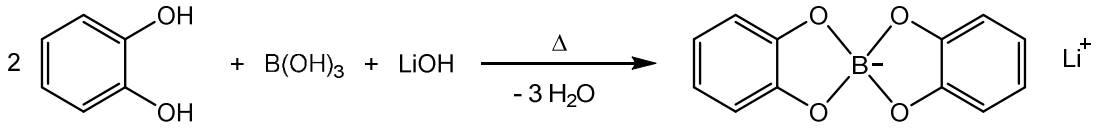


Figure 4.13 Possible further variation in amine.

electrolytes in lithium ion battery applications. These compounds should be accessible *via* a similar methodology to that described above, employing lithium hydroxide in place of an amine (Scheme 4.2). Similar species have been synthesised using lithium and barium hydroxides in water, and so an aqueous solvent mixture may be required for these reactions to be successful.[184b, 191a] The smaller ionic radius of the Li^+ cations may increase the ionic mobility of these species, and so improve their conductivity. Furthermore, these compounds would be readily solvated by THF, allowing more concentrated solutions to be accessed, and increasing the resulting conductivity.



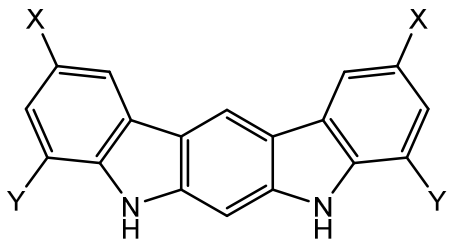
Scheme 4.2 Potential synthesis of lithium bis-borate species.

Chapter V
Anion-Binding Studies

5.1 Introduction

The study of anion binding, including the binding of bidentate anions, has attracted significant research interest throughout recent years, due to the ubiquity of these anions throughout nature and in commercial products.[193] For example, organic and inorganic phosphates are key components of many biochemical reactions and make up biological molecules such as DNA and RNA.[194] Furthermore, the pollution of phosphate compounds found in fertilisers into natural water sources has contributed significantly to eutrophication and the damage of ecological systems.[195] Similarly, the nitrate anion has been found to be extremely damaging to natural ecosystems,[196] and is increasingly studied because of its complex effects on health and the human body.[197] Carboxylate anions are also of significant interest, with the acetate anion being a key component in the "acetate switch", a vital biological process carried out by cells.[198] Moreover, sodium benzoate is a commonly used food additive and must be monitored both for quality control purposes and because its presence has been connected with medical complications such as urticaria.[199] Consequently, intensive investigations have been made into sensing anions electrochemically,[200] optically[201] and colorimetrically.[202]

By far the dominating method of binding these anions in molecular systems throughout recent years has been the use of hydrogen bonding interactions. An example of such a system is the indolocarbazole family of sensors reported by Beer and co-workers in 2005 (Figure 5.1), which utilised two N-H hydrogen bond donors, exhibiting binding constants of *ca.* 10^5 M^{-1} for the $H_2PO_4^-$ and $PhCO_2^-$ anions in acetone.[203] This motif was further developed by Jeong *et al*., who extended the molecule to incorporate pyridyl functionalities.[204] These imparted hydrogen bond acceptor components into the molecule, which complemented the N-H donor



X = H, Me
Y = H, Br

Figure 5.1 Indolocarbazole compounds which bind anions through hydrogen bonds.[203]

functionalities and allowed for highly selective binding of the $H_2PO_4^-$ anion with a binding constant of 110,000 ± 15,000 M^{-1} in acetonitrile.

Molecular anion receptors have incorporated amide or urea functionalities to provide hydrogen bond donors, such as the bipyridyl diamide bis-ferrocene ruthenium complex reported by Beer and co-workers, which selectively bound the $H_2PO_4^-$ anion, switching on a new emission in the complex, indicating the potential of this system as an optical sensor.[205] Reinhoudt *et al.* reported the use of both macrocyclic and acyclic receptors containing four urea moieties which bound the $H_2PO_4^-$ anion in 1:1 and 2:1 stoichiometries respectively.[206]

Macrocyclic molecules have been utilised as receptors for a variety of bidentate anions. An early example of this includes a study by Sessler *et al.* published in 1996, outlining the use of protonated sapphyrins for the highly efficient binding of various phosphate compounds, with binding strengths of between 500 and 18,000 M^{-1} in d-methanol reported.[207] Other examples include work by Hamilton *et al*., including a

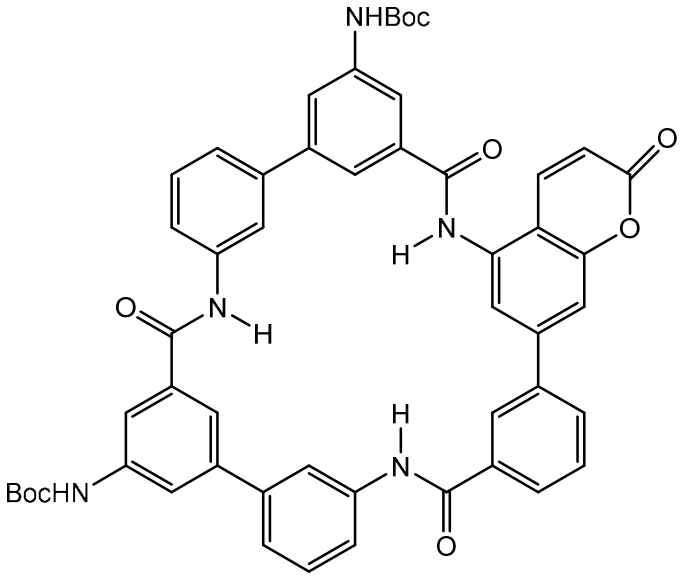


Figure 5.2 A macrocyclic compound which selectively binds $H_2PO_4^-$.[208]

simple macrocycle incorporating three amide functionalities (Figure 5.2), selectively binding the $H_2PO_4^-$ anion with a binding constant in the magnitude of 10^6 M^{-1} in 1:1 DMSO/1,4-dioxane.[208] Similar studies by the same research group reported the use of symmetrical triamide macrocycles which bound dihydrogen phosphate, sulfate and nitrate anions, again showing selectivity towards $H_2PO_4^-$.[209]

Cyclic calix[4]pyrrole compounds have also been found to bind the dihydrogen phosphate anion effectively and selectively through hydrogen-bonding interactions, with anchoring acyl groups in the *meso* positions enhancing the binding ability of the molecule.[210] More recently, the synthesis of a catenane made up of two macrocycles containing amide hydrogen bond donors has been reported and used to bind the nitrate anion selectively over halide, phosphate and carboxylate anions.[211] Beer and co-workers have taken this use of supramolecular chemistry even further *via* the use of rotaxanes containing amide functionalities which selectively bind sulfate,[212] and nitrate[213] anions.

Early examples of molecular anion receptors utilising cationic charges to bind anions *via* electrostatic interactions proved to be rather ineffective, even when zwitterionic species were used to minimise competition with counterions, with very weak binding being observed.[214] However, greater success was achieved when this was combined with hydrogen-bonding interactions, an example of which being a series of molecular receptors synthesised by Beer and co-workers utilising imidazolium substituents in tandem with amide hydrogen bond donors to bind halides and $H_2PO_4^-$.[215] Similarly, a flexible amide-pyridinium receptor reported by Gong *et al*. was found to bind acetate anions extremely selectively and effectively, with a binding constant of $1.1 \pm 0.1 \times 10^5$ M^{-1} reported in acetonitrile.[216]

A less developed area of research for the binding and recognition of bidentate anions is the use of Lewis acidic receptor molecules. An early example of such work is the use of UO_2 salenes reported by Reinhoudt *et al.* which combined a Lewis acidic UO_2 centre with amide hydrogen bond donors to selectively bind $H_2PO_4^-$ with binding strengths in the region of 10^5 M^{-1} in acetonitrile/DMSO (99:1).[217] Significant interest has been paid to the use of Lewis acidic mercury clusters and macrocycles for the binding of predominantly halide anions.[218] This has since been extended to include the coordination of the nitrate anion, with a mercuracarborand containing four mercury centres proving able to complex two nitrate anions within its solid state structure.[219] However, no binding data was collected, so the strength of the coordination is unknown.

Boron-containing compounds are well known for their Lewis acidity, which is being particularly reflected by the growing research interest into frustrated Lewis pairs,[220] and so significant attention has been paid to the anion-binding properties of these

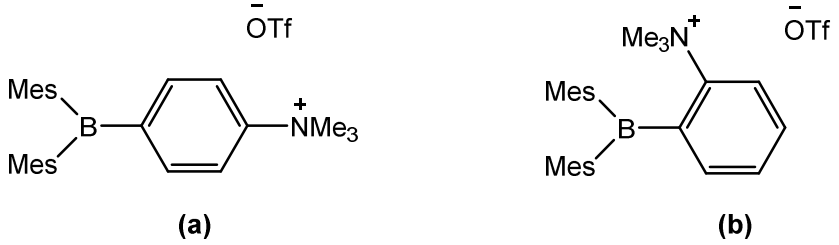


Figure 5.3 Ammonium boranes for used for sensing (a) CN^- and (b) F^-.[221]

species. Much of this work focuses on the recognition and sensing of fluoride or cyanide anions, an example of which is the highly selective complexation of CN^- and F^- by relatively simple ammonium borane cations, reported by Gabbaï *et al.* (Figure 5.3), with complex 5.3(a) exhibiting a binding strength of *ca*. 10^8 M^{-1} for the binding of cyanide H_2O/DMSO (60:40).[221] Aldridge and co-workers have carried out similar work, incorporating a ferrocene-like moiety to give a highly selective colorimetric receptor for cyanide which displays a bright pink colour upon complexation.[222]

There has been much interest in the use of bidentate boron-containing Lewis acid compounds, the earliest report of which being the "hydride sponge", 1,8-naphthalenediylbis(dimethylborane), which complexes H^-, F^-, Cl^- and OH^- anions *via* a chelation effect.[223] Again, this area of research focuses greatly on fluoride binding, and has been utilised with great success for this application. An example includes the use of a 9-thia-10-boraanthracene-containing bidentate diborane as a highly selective and effective colorimetric fluoride sensor exhibiting a binding constant of 5 x 10^9 M^{-1} in THF.[202c] This motif has been altered to include heteronuclear bidentate Lewis acid receptors, an example of which is the highly selective phosphorescent fluoride sensor reported by Gabbaï *et al*., which utilised boron and mercury Lewis acid centres, with a binding strength of greater than 10^8 M^{-1} in THF (Figure 5.4a).[224] Gabbaï further developed this idea through an unusual highly selective bidentate tellurium-containing

Lewis acid receptor for fluoride anions (Figure 5.4b), utilising the high polarizability and electropositivity of the tellurium centre.[225]

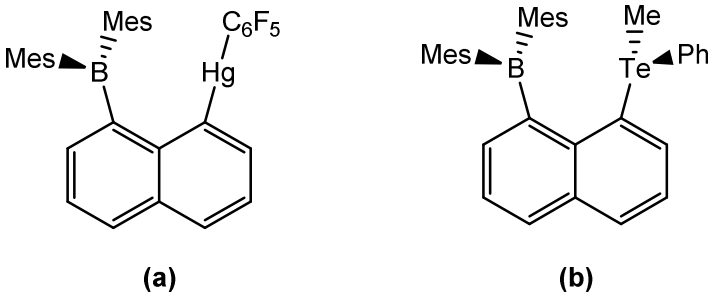


Figure 5.4 Heteronuclear bidentate receptors which effectively bind F^-.[224]

Whilst the area of Lewis acid anion receptors is well-developed, the use of mono- and bidentate Lewis acid molecules to bind bidentate anions has received surprisingly little attention. Some group 13 species have been briefly investigated for their use as Lewis acidic bidentate anion receptors, although in-depth binding studies have not been carried out. An example is the chelation of bis[bis(trimethylsilyl)methyl]digallane by imidotetraphenyldiphosphinate, reported by Uhl *et al.*, where two anions were able to bind to the gallium centres.[226] The same digallane also coordinates carboxylate and dicarboxylate anions, the latter of which allow the formation of macrocyclic compounds containing two Ga−Ga bonds.[227] Similarly, Uhl and co-workers have reported the ability for a methylene-bridged dialuminium compound to complex the nitrate anion, with each Lewis acidic aluminium centre binding to the bidentate anion to form a six-membered metallocycle (Figure 5.5).[228]

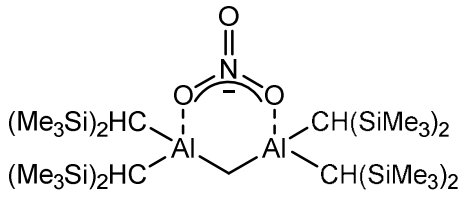


Figure 5.5 Dialuminium compound which is able to complex NO_3^-.[228]

Bidentate Lewis acidic borate species have been investigated to a surprisingly small extent, with Aldridge and co-workers having described the catecholato pyroborate compound **[1]** (see Chapter III), which was used to bind the acetate and dihydrogen phosphate anions (Figure 5.6).[149] However, only the acetate species was investigated for its binding strength, offering a binding constant of 1500 ± 550 M^{-1} in $CDCl_3$. The structure of the dihydrogen phosphate-bound compound was inferred through comparisons with its acetate analogue and a previously reported η^2(O,O) bound $H_2PO_4^-$ species, and so further investigation of this and similar species and their anion-binding chemistry is desirable.

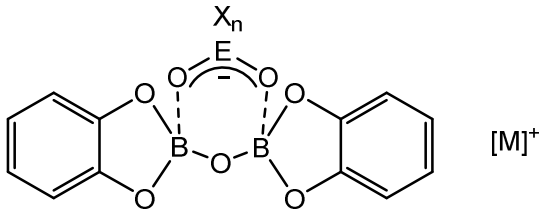


Figure 5.6 Pyroborate anion-bound compounds, where EX_n = CCH_3, $[M]^+$ = $[PPN]^+$ and $P(OH)_2$, $[M]^+$ = $[N^nBu_4]^+$.[149]

5.2 Experimental

5.2.1 Synthesis

Isolation of [N^{n}Bu$_4$][cat$_2$B] [36]

To a stirred suspension of $(catB)_2O$ (300 mg, 1.18 mmol) in dichloromethane (5 mL) was added $[N^nBu_4][H_2PO_4]$ (400 mg, 1.18 mmol) in dichloromethane (5 mL). The reaction mixture was stirred at room temperature for 24 h, before being filtered. The filtrate was concentrated to *ca.* 5 mL and layered with hexane. Storage of the layered solution at 10 °C overnight resulted in the formation of colourless crystals of **[36]**, which were isolated *via* filtration and dried under vacuum. The filtrate was stored at room temperature overnight, resulting in a second crop of **[36]**. Yield: 0.1 g (14 %). ^{1}H NMR (400.13 MHz, 298 K, $CDCl_3$): δ = 6.60 (8H, m, Ar-*H*), 3.02 (8H, m, C*H*$_2$), 1.45 (8H, m, C*H*$_2$), 1.29 (8H, m, C*H*$_2$), 0.94 (12H, t, ^3J = 8 Hz, C*H*$_3$). ^{13}C{^{1}H} NMR (100.61 MHz, 298 K, $CDCl_3$): δ = 151.9 (Ar-*C*), 117.8 (Ar-*C*), 108.6 (Ar-*C*), 58.0 (*C*H$_2$), 23.8 (*C*H$_2$), 19.6 (*C*H$_2$), 13.7 (*C*H$_3$). ^{11}B{^{1}H} NMR (128.38 MHz, 298 K, $CDCl_3$): δ = 14.3. Anal. Calcd for $C_{28}H_{44}BNO_4$: C, 71.64, H, 9.45, N, 2.98. Found: C, 71.56, H, 9.51, N, 2.88 %.

Hydrolysis of (catB)$_2$O

To a stirred suspension of $(catB)_2O$ (100 mg, 0.390 mmol) in dichloromethane (10 mL) was added water (0.10 mL, 5.56 mmol). The reaction mixture was stirred at room temperature for 1.5 h, resulting in the formation of a white precipitate. Filtration led to the isolation of a white solid, which was found to be boric acid: ^{11}B{^{1}H} NMR (128.38 MHz, 298 K, D_2O): δ = 19.4. Removal of volatiles *in vacuo* led to the isolation

of a white solid, which was found to be catechol: ^{1}H NMR (400.13 MHz, 298 K, $CDCl_3$): δ = 6.86 (4H, m, Ar-*H*), 5.26 (2H, s, br, O-*H*).

Reaction of [N^{n}Bu$_4$][H$_2$PO$_4$] with B(OPh)$_3$

[N^{n}Bu$_4$][H$_2$PO$_4$] (10 mg, 0.0295 mmol) was dissolved in $CDCl_3$ and transferred to a J. Young's tap NMR tube. $B(OPh)_3$ (17 mg, 0.0586 mmol) was dissolved in $CDCl_3$ and added to the tube. The solution was mixed and the NMR experiments were performed. ^{1}H NMR (400.13 MHz, 298 K, $CDCl_3$): δ = 6.74-7.42 (35H, m, br, Ar-*H*), 2.80 (8H, t, ^{3}J = 7 Hz, C*H*$_2$), 1.27 (8H, m, br, C*H*$_2$), 1.20 (8H, m, C*H*$_2$), 0.80 (12H, t, ^{3}J = 7 Hz, C*H*$_3$). ^{11}B{^{1}H} NMR (128.38 MHz, 298 K, $CDCl_3$): δ = 16.3, 2.8, 0.3. ^{31}P{^{1}H} NMR (162.49 MHz, 298 K, $CDCl_3$): δ = −17.41.

Reaction of [HN^{n}Bu$_3$][H^{n}BuPO$_4$] with B(OPh)$_3$

[HN^{n}Bu$_3$][H^{n}BuPO$_4$] (10 mg, 0.0295 mmol) was dissolved in $CDCl_3$ and transferred to a J. Young's tap NMR tube. $B(OPh)_3$ (17 mg, 0.0586 mmol) was dissolved in $CDCl_3$ and added to the tube. The solution was mixed and the NMR experiments were performed. ^{1}H NMR (400.13 MHz, 298 K, $CDCl_3$): δ = 10.74 (1H, s, br, N-*H*), 7.31 (5H, s, br, Ar-*H*), 6.61-7.24 (22H, m, br, Ar-*H*), 6.47 (2H, s, br, Ar-*H*), 4.00 (2H, m, br, α-C*H*$_2$ of phosphate), 2.82 (6H, s, br, α-C*H*$_2$ of ammonium), 1.59 (2H, m, br, β-C*H*$_2$ of phosphate), 1.49 (6H, m, β-C*H*$_2$ of ammonium), 1.34 (2H, m, γ-C*H*$_2$ of phosphate), 1.19 (6H, sext, ^{3}J = 7 Hz, γ-C*H*$_2$ of ammonium), 0.88 (3H, m, C*H*$_3$ of phosphate), 0.83 (9H, t, ^{3}J = 7 Hz, C*H*$_3$ of ammonium). ^{11}B{^{1}H} NMR (128.38 MHz, 298 K, $CDCl_3$): δ = 16.1, 0.1, −1.6. ^{31}P{^{1}H} NMR (162.49 MHz, 298 K, $CDCl_3$): δ = −13.14, −14.68, −21.33.

Attempted Synthesis of [HN^{n}Bu$_3$][B(^{n}BuPO$_4$)$_2$]

To a stirred sample of mono-*n*-butylphosphate (500 mg, 3.25 mmol) was added boric acid (100 mg, 1.63 mmol) and tri-*n*-butylamine (0.40 mL, 1.63 mmol) and the resulting mixture heated at 100 °C for 2 h. Heating was stopped and the mixture was allowed to reach room temperature, resulting in the formation of a colourless oil. $^{11}B\{^1H\}$ NMR (96.29 MHz, 298 K, $CDCl_3$): δ = −1.0, −3.4. $^{31}P\{^1H\}$ NMR (162.49 MHz, 298 K, $CDCl_3$): δ = 0.90, −6.13, −12.43.

Attempted Synthesis of [HN^{n}Bu$_3$][B(^{n}BuPO$_4$)(H^{n}BuPO$_4$)$_2$]

To a stirred sample of mono-*n*-butylphosphate (500 mg, 3.25 mmol) was added boric acid (67.0 mg, 1.08 mmol) and tri-*n*-butylamine (0.26 mL, 1.08 mmol) and the resulting mixture heated at 100 °C for 16 h. Heating was stopped and the mixture was allowed to reach room temperature, resulting in the formation of a colourless oil. $^{11}B\{^1H\}$ NMR (96.29 MHz, 298 K, $CDCl_3$): δ = −1.0, −3.4. $^{31}P\{^1H\}$ NMR (162.49 MHz, 298 K, $CDCl_3$): δ = 0.70, −6.26, −12.58.

Attempted Synthesis of [HN^{n}Bu$_3$][B(H^{n}BuPO$_4$)$_4$]

To a stirred sample of mono-*n*-butylphosphate (500 mg, 3.25 mmol) was added boric acid 50.2 mg, 0.812 mmol) and tri-*n*-butylamine (0.20 mL, 0.812 mmol) and the resulting mixture heated at 100 °C for 2 h. Heating was stopped and the mixture was allowed to reach room temperature, resulting in the formation of a colourless oil. $^{11}B\{^1H\}$ NMR (96.29 MHz, 298 K, $CDCl_3$): δ = −3.4. $^{31}P\{^1H\}$ NMR (162.49 MHz, 298 K, $CDCl_3$): δ = 0.82, −6.35, −12.93.

Reaction of $(catB)_2O$ with NMe_4F

NMe_4F (10 mg, 0.118 mmol) was suspended in CD_3CN and transferred to a J. Young's tap NMR tube. $(catB)_2O$ (30 mg, 0.118 mmol) was dissolved in CD_3CN and added to the tube. The solution was sonicated for 5 minutes and the NMR experiments were ran. ^1H NMR (400.13 MHz, 298 K, CD_3CN): δ = 7.00 (3H, s, br, Ar-H), 6.58 (5H, s, br, Ar-H), 3.04 (12H, s, CH_3). $^{11}B\{^1H\}$ NMR (96.29 MHz, 298 K, CD_3CN): δ = 23.5, 21.5, 19.7, 14.2, 7.3, −0.6, −1.2. $^{19}F\{^1H\}$ NMR (282.40 MHz, 298 K, CD_3CN): δ = −141.61 (s, v.br), −146.15 (s, br), −151.32 (s), −151.38 (s).

Attempted reaction of $(catB)_2O$ with N^nBu_4Br

$(catB)_2O$ (200 mg, 0.788 mmol) was suspended in dichloromethane (5 mL) with stirring. N^nBu_4Br (254 mg, 0.788 mmol) was suspended in dichloromethane (5 mL) and added. The reaction mixture was stirred at room temperature for 24 h, filtered and the volatiles removed *in vacuo* to give an off-white residue. NMR experiments revealed no reaction had taken place.

Conversion of $(catB)_2O$ to $[H^nNBu_3][cat_2B]$

$(catB)_2O$ (200 mg, 0.788 mmol) and catechol (173 mg, 1.58 mmol) were dissolved in dichloromethane (10 mL) with stirring. Tri-*n*-butylamine (0.37 mL, 1.58 mmol) was added and the resulting mixture stirred at room temperature for 24 h. The reaction mixture was filtered and the volatiles removed *in vacuo* to give a white solid. NMR data matched that recorded for $[H^nNBu_3][cat_2B]$ **[19]**.

General Procedure for the Synthesis of Anion-bound Borates

To a stirred solution of pyroborate in dichloromethane the anion-containing species of choice in dichloromethane was added. The reaction mixture was stirred at room

temperature for 24 h, filtered and the volatiles subsequently removed *in vacuo*. Trituration with hexane was sometimes necessary to obtain model compounds **[37]-[52]** as off-white powders.

{HN^{n}Bu$_3$}{[(catB)$_2$O][H^{n}BuPO$_4$]} [37]

Synthesised from (catB)$_2$O (1.00 g, 3.94 mmol) and [HN^{n}Bu$_3$][H^{n}BuPO$_4$] (1.34 g, 3.94 mmol) in 20 mL dichloromethane. Yield: 2.14 g (91 %). ^{1}H NMR (400.13 MHz, 298 K, $CDCl_3$): δ = 9.05 (1H, s, N-*H*), 6.68 (8H, s, Ar-*H*), 4.02 (2H, s, α-C*H*$_2$ of phosphate), 2.95 (6H, m, α-C*H*$_2$ of ammonium), 1.53 (8H, q, ^3J = 8 Hz, overlapping C*H*$_2$ peaks), 1.26 (8H, s, ^3J = 8 Hz, overlapping C*H*$_2$ peaks), 0.86 (12H, t, ^3J = 8 Hz, overlapping C*H*$_3$ peaks). ^{13}C NMR (100.61 MHz, 298 K, $CDCl_3$): δ = 150.5 (Ar-*C*), 118.9 (Ar-*C*), 109.2 (Ar-*C*), 52.3 (*C*H$_2$), 25.0 (*C*H$_2$), 19.8 (*C*H$_2$), 13.5 (*C*H$_3$). ^{11}B{^{1}H} NMR (128.38 MHz, 298 K, $CDCl_3$): δ = 14.0. 6.1, −3.7. ^{31}P{^{1}H} NMR (162.49 MHz, 298 K, $CDCl_3$): δ = −16.75. Anal. Calcd for $C_{28}H_{46}B_2NO_9P$: C, 56.69, H, 7.82, N, 2.36. Found: C, 56.56, H, 7.72, N, 2.45 %. ICP-OES: Calculated percentage: B: 3.64 %, P: 5.22 %. Found: B: 3.70 %, P: 5.49 %. UV/vis (CH_2Cl_2) λmax/nm (ε/dm^3 mol^{-1} cm^{-1}): 235 (13440), 283 (40000).

{HNEt$_3$}{[(catB)$_2$O][H^{n}BuPO$_4$]} [38]

Synthesised from (catB)$_2$O (398 mg, 1.57 mmol) and [HNEt$_3$][H^{n}BuPO$_4$] (400 mg, 1.57 mmol) in 20 mL dichloromethane. Yield: 422 mg (53 %). ^{1}H NMR (300.13 MHz, 298 K, $CDCl_3$): δ = 8.71 (1H, s, br, N-*H*), 6.80 (8H, s, br, Ar-*H*), 4.09 (s, br, α-C*H*$_2$ of phosphate), 3.07 (6H, m, α-C*H*$_2$ of ammonium), 1.26-1.85 (4H, m, br, overlapping C*H*$_2$ peaks of phosphate), 1.17 (9H, t, ^3J = 7 Hz, C*H*$_3$ of ammonium), 0.86 (3H, m, br, C*H*$_3$ of phosphate). ^{13}C NMR (76.46 MHz, 298 K, $CDCl_3$): δ = 148.1 (Ar-q*C*), 120.1 (Ar-*C*H), 111.5 (Ar-*C*H), 68.5 (*C*H$_2$), 46.4 (*C*H$_2$), 31.8 (*C*H$_2$), 18.4 (*C*H$_2$), 13.5 (*C*H$_3$),

8.4 (*C*H_3). $^{11}B\{^1H\}$ NMR (96.29 MHz, 298 K, $CDCl_3$): δ = 21.6, 14.7, 5.9, −1.8, −3.7. $^{31}P\{^1H\}$ NMR (121.49 MHz, 298 K, $CDCl_3$): δ = −17.26. Anal. Calcd for $C_{22}H_{34}B_2NO_9P$: C, 51.90, H, 6.73, N, 2.75. Found: C, 51.68, H, 6.58, N, 2.57 %.

{H$_3$N^{n}Bu}{[(catB)$_2$O][H^{n}BuPO$_4$]} [39]

Synthesised from $(catB)_2O$ (1.00 g, 3.94 mmol) and $[H_3N^nBu][H^nBuPO_4]$ (895 mg, 3.94 mmol) in 40 mL dichloromethane. Yield: 993 mg (54 %). ^1H NMR (400.13 MHz, 298 K, $CDCl_3$): δ = 7.65 (3H, s, br, N-H), ^1H NMR (400.13 MHz, 298 K, $CDCl_3$): δ = 7.65 (3H, s, br, N-*H*), 6.49-7.13 (16H, m, br, Ar-*H*), 3.58-4.22 (2H, m, br, C*H*$_2$), 3.16 (2H, s, br, C*H*$_2$), 1.76 (2H, s, br, C*H*$_2$), 1.43 (4H, s, br, C*H*$_2$), 1.22 (2H, s, br, C*H*$_2$), 0.91 (6H, s, br, C*H*$_3$), 0.73 (1.5H, s, br, C*H*$_3$), 0.54 (3H, t, ^3J = 7 Hz, C*H*$_3$). $^{13}C\{^1H\}$ NMR (100.61 MHz, 298 K, $CDCl_3$): δ = 149.5 (Ar-q*C*), 148.8 (Ar-q*C*), 121.6 (Ar-q*C*), 119.7 (Ar-*C*H), 109.6 (Ar-*C*H), 108.9 (Ar-*C*H), 68.6 (*C*H$_2$), 40.2 (*C*H$_2$), 31.4 (*C*H$_2$), 29.9 (*C*H$_2$), 19.7 (*C*H$_2$), 18.1 (*C*H$_2$), 13.5 (*C*H$_3$), 13.2 (*C*H$_3$). $^{11}B\{^1H\}$ NMR (96.29 MHz, 298 K, $CDCl_3$): δ = 20.4, 6.0, −1.0. $^{31}P\{^1H\}$ NMR (121.49 MHz, 298 K, $CDCl_3$): δ = −18.60. Anal. Calcd for $C_{20}H_{30}B_2NO_9P$: C, 49.94, H, 6.29, N, 2.91. Found: C, 49.85, H, 6.18, N, 2.86 %.

{HN^{n}Bu$_3$}{[(4-MecatB)$_2$O][H^{n}BuPO$_4$]} [40]

Synthesised from $(4\text{-MecatB})_2O$ (1.00 g, 3.55 mmol) and $[HN^nBu_3][H^nBuPO_4]$ (1.20 g, 3.55 mmol). Yield: 1.63 g (74 %). ^1H NMR (400.13 MHz, 298 K, $CDCl_3$): δ = 9.19 (1H, s, br, N-*H*), 6.54 (4H, s, br, Ar-*H*), 6.47 (2H, s, br, Ar-*H*), 4.00 (2H, m, br, α-C*H*$_2$ of phosphate), 2.95 (6H, m, br, α-C*H*$_2$ of ammonium), 2.23 (6H, s, C*H*$_3$), 1.53 (8H, m, *J* = 8 Hz, overlapping C*H*$_2$ peaks), 1.25 (8H, sext, ^3J = 8 Hz, overlapping C*H*$_2$ peaks), 0.87 (12H, t, ^3J = 8 Hz, overlapping C*H*$_3$ peaks). $^{13}C\{^1H\}$ NMR (100.61 MHz, 298 K, $CDCl_3$): δ = 150.5 (Ar-q*C*), 148.3 (Ar-q*C*), 128.2 (Ar-q*C*), 118.6 (Ar-*C*H), 110.4 (Ar-

*C*H), 108.3 (Ar-*C*H), 67.4 (*C*H_2), 52.3 (*C*H_2), 32.1 (*C*H_2), 25.0 (*C*H_2), 21.3 (*C*H_3), 19.8 (*C*H_2), 18.6 (*C*H_2), 13.6 (*C*H_3), 13.5 (*C*H_3). $^{11}B\{^1H\}$ NMR (128.38 MHz, 298 K, $CDCl_3$): δ = 14.0, 6.0, −4.0. $^{31}P\{^1H\}$ NMR (121.49 MHz, 298 K, $CDCl_3$): δ = −16.85. Anal. Calcd for $C_{30}H_{50}B_2NO_9P$: C, 57.99, H, 8.11, N, 2.23. Found: C, 57.72, H, 8.25, N, 2.35 %.

{HN^{n}Bu$_3$}{[(3-MeOcatB)$_2$O][H^{n}BuPO$_4$] [41]

Synthesised from (3-MeOcatB)$_2$O (1.00 g, 3.19 mmol) and [HN^{n}Bu$_3$][H^{n}BuPO$_4$] (1.08 g, 3.19 mmol) in 40 mL dichloromethane. Yield: 1.45 g (70 %). ^1H NMR (300.13 MHz, 298 K, $CDCl_3$): δ = 9.16 (1H, br, N-*H*), 6.62 (2H, t, ^3J = 8 Hz, Ar-*H*), 6.48 (2H, d, ^3J = 7 Hz, Ar-*H*), 6.38 (2H, t, ^3J = 8 Hz, Ar-*H*), 4.07 (2H, m, br, α-C*H*$_2$ of phosphate), 3.84 (6H, s, O-C*H*$_3$), 2.98 (6H, m, α-C*H*$_2$ of ammonium), 1.64 (2H, s, v.br, β-C*H*$_2$ of phosphate), 1.51 (6H, m, β-C*H*$_2$ of ammonium), 1.23 (6H, sext, ^3J = 7 Hz, γ-C*H*$_2$ of ammonium), 0.85 (12H, t, ^3J = 7 Hz, overlapping C*H*$_3$ peaks). $^{13}C\{^1H\}$ NMR (100.61 MHz, 298 K, $CDCl_3$): δ = 152.2 (Ar-q*C*), 143.7 (Ar-q*C*), 118.5 (Ar-q*C*), 104.4 (Ar-*C*H), 104.2 (Ar-*C*H), 56.3 (O-*C*H$_3$), 56.1 (*C*H_2), 51.7 (*C*H_2), 32.1 (*C*H_2), 24.8 (*C*H_2), 19.7 (*C*H_2), 18.6 (*C*H_2), 13.6 (*C*H_3), 13.5 (*C*H_3). $^{11}B\{^1H\}$ NMR (96.29 MHz, 298 K, $CDCl_3$): δ = 14.3, 5.6, −3.6. $^{31}P\{^1H\}$ NMR (121.49 MHz, 298 K, $CDCl_3$): δ = −15.17. Anal. Calcd for $C_{30}H_{50}B_2NO_{11}P$: C, 55.15, H, 7.71, N, 2.14. Found: C, 54.90, H, 7.72, N, 2.20 %.

{HN^{n}Bu$_3$}{[(Br$_4$catB)$_2$O][H^{n}BuPO$_4$] [42]

Synthesised from (Br$_4$catB)$_2$O (500 mg, 0.566 mmol) and [HN^{n}Bu$_3$][H^{n}BuPO$_4$] (192 mg, 0.566 mmol) in 20 mL dichloromethane. Yield: 400 mg (58 %). ^1H NMR (400.13 MHz, 298 K, $CDCl_3$): δ = 4.11 (2H, m, br, α-C*H*$_2$ of phosphate), 3.06 (6H, m, br, α-C*H*$_2$ of ammonium), 1.66 (2H, s, br, β-C*H*$_2$ of phosphate), 1.54 (6H, m, β-C*H*$_2$ of

ammonium), 1.41 (2H, m, br, γ-CH_2 of phosphate), 1.28 (6H, sext, ^3J = 7 Hz, γ-CH_2 of ammonium), 0.91 (12H, t, ^3J = 7 Hz, overlapping CH_3 peaks). $^{13}C\{^1H\}$ NMR (75.47 MHz, 298 K, $CDCl_3$): δ = 148.5 (Ar-q*C*), 116.4 (Ar-q*C*), 104.8 (Ar-q*C*), 52.3 (*C*H_2), 25.1 (*C*H_2), 19.6 (*C*H_2), 13.5 (*C*H_3). $^{11}B\{^1H\}$ NMR (128.38 MHz, 298 K, $CDCl_3$): δ = 13.4, 5.5, −2.3. $^{31}P\{^1H\}$ NMR (121.49 MHz, 298 K, $CDCl_3$): δ = −17.71. Anal. Calcd for $C_{28}H_{38}Br_8B_2NO_{11}P$: C, 27.47, H, 3.13, N, 1.14. Found: C, 27.29, H, 3.04, N, 1.17 %.

{HN^{n}Bu$_3$}{[(Naph-1,2-O$_2$B)$_2$O][H^{n}BuPO$_4$] [43]

Synthesised from (naph-1,2-$O_2B)_2O$ (300 mg, 0.848 mmol) and [HN^{n}Bu$_3$][H^{n}BuPO$_4$] (288 mg, 0.848 mmol) and 20 mL dichloromethane. Yield: 510 mg (88 %). ^1H NMR (300.13 MHz, 298 K, $CDCl_3$): δ = 8.63 (1H, s, br, N-*H*), 7.62 (4H, q, ^3J = 3 Hz, Ar-*H*), 7.25 (4H, q, ^3J = 3 Hz, Ar-*H*), 6.99 (4H, s, Ar-*H*), 4.12 (2H, s, br, α-CH_2 of phosphate), 2.94 (6H, m, α-CH_2 of ammonium), 1.50 (8H, m, overlapping CH_2 peaks), 1.18 (8H, m, overlapping CH_2 peaks), 0.79 (12H, t, ^3J = 7 Hz, overlapping CH_3 peaks). $^{13}C\{^1H\}$ NMR (100.61 MHz, 298 K, $CDCl_3$): δ = 151.5 (Ar-q*C*), 129.9 (Ar-q*C*), 126.4 (Ar-*C*H), 122.7 (Ar-*C*H), 103.9 (Ar-*C*H), 52.6 (*C*H_2), 31.9 (br, *C*H_2 of phosphate), 25.1 (*C*H_2), 19.7 (*C*H_2), 18.6 (br, *C*H_2 of phosphate), 13.6 (br, *C*H_3 of phosphate), 13.4 (*C*H_3). $^{11}B\{^1H\}$ NMR (96.29 MHz, 298 K, $CDCl_3$): δ = 14.2, 5.7, −3.8. $^{31}P\{^1H\}$ NMR (121.49 MHz, 298 K, $CDCl_3$): δ = −17.00.

{HN^{n}Bu$_3$}{[(catB)$_2$O][H^{i}BuPO$_4$]} [44]

Synthesised from $(catB)_2O$ (300 mg, 1.18 mmol) and [HN^{n}Bu$_3$][H^{i}BuPO$_4$] (400 mg, 1.18 mmol) in 20 mL dichloromethane. Yield: 424 mg (61 %). ^1H NMR (400.13 MHz, 298 K, $CDCl_3$): δ = 9.08 (1H, s, br, N-*H*), 6.69 (8H, s, br, Ar-*H*), 3.79 (2H, s, br, α-CH_2 of phosphate), 2.97 (6H, m, br, α-CH_2 of ammonium), 1.92 (1H, s, br, CH), 1.53

(6H, m, br, β-CH_2 of ammonium), 1.25 (6H, sext, ^3J = 7 Hz, γ-CH_2 of ammonium), 0.87 (15H, t, ^3J = 7 Hz, CH_3). $^{13}C\{^1H\}$ NMR (100.61 MHz, 298 K, $CDCl_3$): δ = 150.5 (Ar-q*C*), 118.9 (Ar-*C*H), 109.2 (Ar-*C*H), 52.3 (*C*H2), 28.8 (*C*H2), 25.0 (*C*H_2), 22.6 (*C*H), 19.8 (*C*H_2), 18.6 (*C*H_3), 13.5 (*C*H_3). $^{11}B\{^1H\}$ NMR (96.29 MHz, 298 K, $CDCl_3$): δ = 23.6, 14.0, 6.2, −3.2. $^{31}P\{^1H\}$ NMR (121.49 MHz, 298 K, $CDCl_3$): δ = −16.78. Anal. Calcd for $C_{28}H_{46}B_2NO_9P$: C, 56.69, H, 7.82, N, 2.36. Found: C, 56.51, H, 7.86, N, 2.36 %.

{HN^{n}Bu$_3$}{[(catB)$_2$O][^{n}Bu$_2$PO$_4$]} [45]

Synthesised from $(catB)_2O$ (1.00 g, 4.10 mmol) and [HN^{n}Bu$_3$][^{n}Bu$_2$PO$_4$] (1.62 g, 4.10 mmol) in 30 mL dichloromethane. Yield: 2.58 g (97 %). ^1H NMR (400.13 MHz, 298 K, $CDCl_3$): δ = 9.68 (1H, s, br, N-*H*), 6.68 (8H, m, br, Ar-*H*), 4.05 (4H, m, br, α-CH_2 of phosphate), 2.95 (6H, m, α-CH_2 of ammonium), 1.57 (10H, m, overlapping CH_2 peaks), 1.30 (10H, m, overlapping CH_2 peaks), 0.88 (15H, m, overlapping CH_3 peaks). $^{13}C\{^1H\}$ NMR (100.61 MHz, 298 K, $CDCl_3$): δ = 150.6 (Ar-q*C*), 118.8 (Ar-*C*H), 109.2 (Ar-*C*H), 67.7 (br, *C*H_2 of phosphate, 52.0 (*C*H_2), 32.1 (d, $^3J_{CP}$ = 7 Hz, *C*H_2 of phosphate), 25.0 (*C*H_2), 19.9 (*C*H_2), 18.6 (*C*H_2), 13.5 (br, *C*H_3 of phosphate), 13.5 (*C*H_3). $^{11}B\{^1H\}$ NMR (96.29 MHz, 298 K, $CDCl_3$): δ = 13.8, 6.6, −1.0. $^{31}P\{^1H\}$ NMR (121.49 MHz, 298 K, $CDCl_3$): δ = −5.90. Anal. Calcd for $C_{32}H_{54}B_2NO_9P$: C, 59.19, H, 8.38, N, 2.16. Found: C, 59.30, H, 8.29, N, 2.27 %.

{N^{n}Bu$_4$}{[(catB)$_2$O][AcO]} [46]

Synthesised from $(catB)_2O$ (500 mg, 1.97 mmol) and [^{n}NBu$_4$][AcO] (594 mg, 1.97 mmol). Yield: 720 mg (66 %). ^1H NMR (300.13 MHz, 298 K, $CDCl_3$): δ (ppm) = 6.66 (8H, m, br, Ar-*H*), 3.00 (8H, m, br, CH_2), 2.15 (3H, s, CO_2CH_3), 1.31 (16H, m, overlapping CH_2 peaks), 0.89 (12H, t, ^3J = 7 Hz, CH_3). $^{13}C\{^1H\}$ NMR (100.61 MHz,

298 K, $CDCl_3$): δ = 218.6 (*C*=O), 151.3 (Ar-q*C*), 117.8 (Ar-*C*H), 109.4 (Ar-*C*H), 57.8 (*C*H_2), 23.7 (*C*H_2), 19.4 (*C*H_2), 13.6 (*C*H_3). $^{11}B\{^1H\}$ NMR (96.29 MHz, 298 K, $CDCl_3$): δ = 21.8, 14.3, 9.8, 2.4. Anal. Calcd for $C_{30}H_{48}B_2NO_7$: C, 64.77, H, 8.70, N, 2.52. Found: C, 64.71, H, 8.51, N, 2.49 %.

{N^{n}Bu$_4$}{[(3-MeOcatB)$_2$O][AcO]} [47]

Synthesised from (3-MeOcatB)$_2$O (500 mg, 1.59 mmol) and [^{n}NBu$_4$][AcO] (480 mg, 1.59 mmol). Yield: 730 mg (75 %). ^1H NMR (300.13 MHz, 298 K, $CDCl_3$): δ = 6.19-6.67 (6H, m, br, Ar-*H*), 3.80 (6H, m, O-C*H*$_3$), 3.00 (8H, m, br, C*H*$_2$), 2.12 (3H, s, br, CO_2C*H*$_3$), 1.37 (8H, m, br, C*H*$_2$), 1.21 (8H, m, br, C*H*$_2$), 0.85 (12H, m, br, C*H*$_3$). $^{13}C\{^1H\}$ NMR (75.47 MHz, 298 K, $CDCl_3$): δ = 222.5 (*C*=O), 151.4 (Ar-q*C*), 142.2 (Ar-q*C*), 138.4 (Ar-q*C*), 115.7 (Ar-*C*H), 103.3 (Ar-*C*H), 102.0 (Ar-*C*H), 56.4 (*C*H_2), 55.1 (O-*C*H_3), 22.2 (*C*H_2), 18.0 (*C*H_2), 12.2 (*C*H_3). $^{11}B\{^1H\}$ NMR (96.29 MHz, 298 K, $CDCl_3$): δ = 21.9, 14.5, 10.9, 2.3. Anal. Calcd for $C_{32}H_{52}B_2NO_9$: C, 62.36, H, 8.50, N, 2.27. Found: C, 62.23, H, 8.41, N, 2.19 %.

{N^{n}Bu$_4$}{[(catB)$_2$O][C$_6$H$_5$CO$_2$]} [48]

Synthesised from (catB)$_2$O (300 mg, 1.18 mmol) and [^{n}NBu$_4$][$C_6H_5CO_2$] (400 mg, 1.18 mmol). Yield: 260 mg (36 %). ^1H NMR (400.13 MHz, 298 K, $CDCl_3$): δ = 8.12 (2H, s, br, *o*-benzoate), 7.55 (1H, s, br, *p*-benzoate), 7.38 (2H, s, br, *m*-benzoate), 6.80–6.58 (8H, m, Ar-H_{cat}), 3.01 (8H, t, ^3J = 8 Hz, C*H*$_2$), 1.39 (8H, m, C*H*$_2$), 1.27, (8H, m, C*H*$_2$), 0.88 (12H, t, ^3J = 7 Hz, C*H*$_3$). $^{13}C\{^1H\}$ NMR (100.61 MHz, 298 K, $CDCl_3$): δ = 151.9 (*C*=O), 151.8 (Ar-q$C_{benzoate}$), 151.5 (Ar-qC_{cat}), 133.9 (*p*-benzoate), 130.7 (*o*-benzoate), 128.1 (*m*-benzoate), 118.3 (Ar–CH_{cat}), 117.9 (Ar–CH_{cat}), 109.2 (Ar–CH_{cat}), 108.5 (Ar–CH_{cat}), 57.8 (*C*H_2), 23.7 (*C*H_2), 19.4 (*C*H_2), 13.6 (*C*H_3). $^{11}B\{^1H\}$

NMR (128.38 MHz, 298 K, $CDCl_3$): δ = 14.3, 9.4, 2.7. Anal. Calcd for $C_{35}H_{49}B_2NO_7$: C, 68.09, H, 8.00, N, 2.27. Found: C, 67.78, H, 8.12, N, 2.36.

{N^{n}Bu$_4$}{[(3-MeOcatB)$_2$O][C$_6$H$_5$CO$_2$]} [49]

Synthesised from (3-MeOcatB)$_2$O (300 mg, 0.956 mmol) and [^{n}NBu$_4$][$C_6H_5CO_2$] (350 mg, 0.956 mmol). Yield: 63 mg (21 %). %). ^{1}H NMR (400.13 MHz, 298 K, $CDCl_3$): δ = 8.12 (2H, s, br, *o*-benzoate), 7.59 (1H, s, br, *p*-benzoate), 7.44 (2H, s, br, *m*-benzoate), 6.65–6.31 (6H, m, Ar-H_{cat}), 3.84 (6H, m, O-CH_3), 3.02 (8H, t, ^3J = 8 Hz, CH_2), 1.40 (8H, m, CH_2), 1.21, (8H, m, CH_2), 0.86 (12H, t, ^3J = 7 Hz, CH_3). ^{13}C{^{1}H} NMR (100.61 MHz, 298 K, $CDCl_3$): δ = 153.1 (*C*=O), 152.9 (Ar-q$C_{benzoate}$), 143.9 (Ar-qC_{cat}), 143.6 (Ar-qC_{cat}), 139.9 (Ar-qC_{cat}), 133.7 (*p*-benzoate), 130.3 (*o*-benzoate), 128.3 (*m*-benzoate), 117.0 (Ar–CH_{cat}), 104.8 (Ar–CH_{cat}), 103.4 (Ar–CH_{cat}), 57.7 (CH_2), 56.5 (CH_2), 23.6 (CH_2), 19.3 (CH_2), 13.6 (CH_3). ^{11}B{^{1}H} NMR (96.29 MHz, 298 K, $CDCl_3$): δ = 14.5, 9.4. Anal. Calcd for $C_{37}H_{54}B_2NO_9$: C, 65.50, H, 8.02, N, 2.06. Found: C, 65.47, H, 7.63, N, 2.14 %.

{N^{n}Bu$_4$}{[(catB)$_2$O][SO$_3$CH$_3$]} [50]

Synthesised from (catB)$_2$O (310 mg, 1.22 mmol) and [^{n}NBu$_4$][SO_3CH_3] (408 mg, 1.22 mmol). Yield: 184 mg (26 %). ^{1}H NMR (300.13 MHz, 298 K, $CDCl_3$): δ = 6.87 (8H, s, br, Ar-*H*), 3.09 (8H, t, ^3J = 8 Hz, CH_2), 2.98 (3H, s, CH_3), 1.52 (8H, m, CH_2), 1.35 (8H, m, CH_2), 0.95 (12H, t, ^3J = 7 Hz, CH_3). ^{13}C{^{1}H} NMR (100.61 MHz, 298 K, $CDCl_3$): δ = 149.0 (Ar-q*C*), 120.9 (Ar-*C*H), 111.1 (Ar-*C*H), 58.2 (CH_2), 39.3 (CH_3), 23.7 (CH_2), 19.5 (CH_2), 13.6 (CH_3). ^{11}B{^{1}H} NMR (96.29 MHz, 298 K, $CDCl_3$): δ = 17.1, 14.3, 6.95. Anal. Calcd for $C_{29}H_{47}B_2NO_8S$: C, 58.90, H, 8.01, N, 2.37. Found: C, 59.02, H, 7.97, N, 2.37 %.

{N^{n}Bu$_4$}{[(3-MeOcatB)$_2$O][SO$_3$CH$_3$]} [51]

Synthesised from (3-MeOcatB)$_2$O (300 mg, 0.956 mmol) and [^{n}NBu$_4$][SO$_3$CH$_3$] (340 mg, 0.956 mmol). Yield: 52 mg (8 %). ^{1}H NMR (400.13 MHz, 298 K, CDCl$_3$): δ = 6.95–6.52 (6H, m, Ar-*H*), 3.88 (6H, br, O-C*H*$_3$), 3.11 (8H, t, ^3J = 8 Hz, C*H*$_2$), 2.93 (3H, s, C*H*$_3$), 1.53 (8H, m, C*H*$_2$), 1.32 (8H, m, C*H*$_2$), 0.93 (12H, t, ^3J = 7 Hz, C*H*$_3$). ^{13}C{^{1}H} NMR (100.61 MHz, 298 K, CDCl$_3$): δ = 117.2 (Ar-q*C*), 58.2 (*C*H$_2$), 39.3 (*C*H$_3$), 23.7 (*C*H$_2$), 19.5 (*C*H$_2$), 13.6 (*C*H$_3$). ^{11}B{^{1}H} NMR (128.38 MHz, 298 K, CDCl$_3$): δ = 21.0, 14.5, 6.90. Anal. Calcd for C$_{35}$H$_{54}$B$_2$NO$_8$S: C, 57.16, H, 7.89, N, 2.15. Found: C, 57.01, H, 7.69, N, 2.05 %.

{N^{n}Bu$_4$}{[(catB)$_2$O][NO$_3$]} [52]

Synthesised from (catB)$_2$O (310 mg, 1.22 mmol) and [^{n}NBu$_4$][NO$_3$] (408 mg, 1.22 mmol). Yield: 335 mg (51 %). ^{1}H NMR (400.13 MHz, 298 K, CDCl$_3$): δ = 6.58-6.67 (6H, m, br, Ar-*H*), 2.99 (8H, t, ^3J = 8 Hz, C*H*$_2$), 1.44 (8H, m, C*H*$_2$), 1.28 (8H, m, C*H*$_2$), 0.91 (12H, t, ^3J = 7 Hz, C*H*$_3$). ^{13}C{^{1}H} NMR (100.61 MHz, 298 K, CDCl$_3$): δ = 151.1 (Ar-q*C*), 117.9 (Ar-*C*H), 108.5 (Ar-*C*H), 58.1 (*C*H$_2$), 23.7 (*C*H$_2$), 19.5 (*C*H$_2$), 13.6 (*C*H$_3$). ^{11}B{^{1}H} NMR (128.38 MHz, 298 K, CDCl$_3$): δ = 14.2, 6.84. Anal. Calcd for C$_{28}$H$_{46}$B$_2$N$_2$O$_8$: C, 60.02, H, 8.28, N, 5.00. Found: C, 60.39, H, 7.86, N, 4.97.

{HN^{n}Bu$_3$}{[(4-PIB$_{1000}$catB)$_2$O][H^{n}BuPO$_4$]} [53]

Synthesised from (4-PIB$_{1000}$catB)$_2$O (22.0 g, 11.0 mmol) and [(HN^{n}Bu$_3$][H^{n}BuPO$_4$] (3.68 g, 11.0 mmol) in 400 mL dichloromethane. Yield: 26.5 g (91 %). ^{11}B{^{1}H} NMR (128.38 MHz, 298K, CDCl$_3$): δ = 13.8, 5.8, −3.3. ^{31}P{^{1}H} NMR (121.49 MHz, 298K, CDCl$_3$): δ = −10.38. ICP-OES: Calculated percentage: B: 0.83 %, P: 1.18 %; found: B: 0.64 %, P: 1.48 %.

{(2-EtC$_6$H$_{12}$)$_2$NH$_2$}{[(4-PIB$_{1000}$catB)$_2$O][H^{n}BuPO$_4$]} [54]

Synthesised from (4-PIB$_{1000}$catB)$_2$O (22.0 g, 11.0 mmol) and [(HN^{n}Bu$_3$][H(2-EtC$_6$H$_{12}$)PO$_4$] (4.35 g, 10.8 mmol) in 400 mL dichloromethane. Yield: 24 g (86 %). ^{11}B{^{1}H} NMR (128.38 MHz, 298K, CDCl$_3$): δ = 13.9, 5.6, −3.4. ^{31}P{^{1}H} NMR (121.49 MHz, 298K, CDCl$_3$): δ = −0.11, −6.84, −13.54. ICP-OES: Calculated percentage: B: 0.83 %, P: 1.18 %; found: B: 0.64 %, P: 1.48 %.

{HN^{n}Bu$_3$}{[(4-PIB$_{1000}$catB)$_2$O][H(2-EtC$_6$H$_{12}$)PO$_4$]} [55]

Synthesised from (4-PIB$_{1000}$catB)$_2$O (1.00 g, 0.493 mmol) and [(HN^{n}Bu$_3$][H(2-EtC$_6$H$_{12}$)PO$_4$] (195 mg, 0.493 mmol) in 20 mL dichloromethane. Yield: 1.05 g (88 %). ^{11}B{^{1}H} NMR (128.38 MHz, 298K, CDCl$_3$): δ = 14.1, 5.9, −3.4. ^{31}P{^{1}H} NMR (121.49 MHz, 298K, CDCl$_3$): δ = −4.78. ICP-OES: Calculated percentage: B: 0.81 %, P: 1.16 %; found: B: 0.72 %, P: 1.48 %.

{(2-EtC$_6$H$_{12}$)$_2$NH$_2$}{[(4-PIB$_{1000}$catB)$_2$O][H(2-EtC$_6$H$_{12}$)PO$_4$]} [56]

Synthesised from (4-PIB$_{1000}$catB)$_2$O (1.00 g, 0.493 mmol) and [(2-EtC$_6$H$_{12}$)$_2$NH$_2$][H(2-EtC$_6$H$_{12}$)PO$_4$] (222 mg, 0.493 mmol) in 20 mL dichloromethane. Yield: 797 mg (66 %). ^{11}B{^{1}H} NMR (128.38 MHz, 298K, CDCl$_3$): δ = 13.9, 5.8, −3.1. ^{31}P{^{1}H} NMR (121.49 MHz, 298K, CDCl$_3$): δ = −9.82. ICP-OES: Calculated percentage: B: 0.79 %, P: 1.14 %; found: B: 0.46 %, P: 1.36 %.

{(2-EtC$_6$H$_{12}$)NH$_3$}{[(4-PIB$_{1000}$catB)$_2$O][H(2-EtC$_6$H$_{12}$)PO$_4$]} [57]

Synthesised from (4-PIB$_{1000}$catB)$_2$O (46.5 g, 22.9 mmol) and [(2-EtC$_6$H$_{12}$)NH$_3$][H(2-EtC$_6$H$_{12}$)PO$_4$] (7.76 g, 22.9 mmol) in 600 mL dichloromethane. Yield: 55 g (93 %). ^{11}B{^{1}H} NMR (128.38 MHz, 298K, CDCl$_3$): δ = 5.9, −2.9. ^{31}P{^{1}H} NMR (121.49 MHz, 298K, CDCl$_3$): δ = −10.03. ICP-OES: Calculated percentage: B: 0.83 %, P: 1.18 %; found: B: 0.81 %, P: 1.43 %.

{(2-EtC$_6$H$_{12}$)$_3$NH}{[(4-PIB$_{1000}$catB)$_2$O][H(2-EtC$_6$H$_{12}$)PO$_4$]} [58]

Synthesised from (4-PIB$_{1000}$catB)$_2$O (39.1 g, 19.2 mmol) and [(2-EtC$_6$H$_{12}$)$_3$NH][H(2-EtC$_6$H$_{12}$)PO$_4$] (10.8 g, 19.2 mmol) in 600 mL dichloromethane. Yield: 50 g (93 %). ^{11}B{^{1}H} NMR (96.29 MHz, 298 K, CDCl$_3$): δ = 14.2, 5.8, −3.4. ^{31}P{^{1}H} NMR (121.49 MHz, 298K, CDCl$_3$): δ = −6.10. ICP-OES: Calculated percentage: B: 0.76 %, P: 1.09 %; found: B: 0.78 %, P: 1.75 %.

{C$_{12}$H$_{25}$NH$_3$}{[(4-PIB$_{1000}$catB)$_2$O][H(2-EtC$_6$H$_{12}$)PO$_4$]} [59]

Synthesised from (4-PIB$_{1000}$catB)$_2$O (46.3 g, 22.8 mmol) and [C$_{12}$H$_{25}$NH$_3$][H(2-EtC$_6$H$_{12}$)PO$_4$] (9.01 g, 22.8 mmol) in 600 mL dichloromethane. Yield: 52 g (87 %). ^{11}B{^{1}H} NMR (96.29 MHz, 298 K, CDCl$_3$): δ = 5.5, −3.3. ^{31}P{^{1}H} NMR (121.49 MHz, 298K, CDCl$_3$): δ = −6.50. ICP-OES: Calculated percentage: B: 0.81 %, P: 1.16 %; found: B: 0.79 %, P: 1.51 %.

{HN^{n}Bu$_3$}{[(4-PIB$_{1000}$catB)$_2$O][H^{n}OctPO$_4$]} [60]

Synthesised from (4-PIB$_{1000}$catB)$_2$O (1.00 g, 0.493 mmol) and [HNBu$_3$][H^{n}OctPO$_4$] (195 mg, 0.493 mmol) in 20 mL dichloromethane. Yield: 1.12 g (94 %). ^{11}B{^{1}H} NMR (128.38 MHz; 298K; CDCl$_3$): δ = 14.1, 5.8, −3.4. ^{31}P{^{1}H} NMR (121.49 MHz,

298 K, $CDCl_3$): δ = −6.26. ICP-OES: Calculated percentage: B: 0.81 %, P: 1.16 %; found: B: 0.41 %, P: 1.47 %.

{(2-EtC$_6$H$_{12}$)$_2$NH$_2$}{[(4-PIB$_{1000}$catB)$_2$O][H^{n}OctPO$_4$]} [61]

Synthesised from (4-PIB_{1000}catB)$_2$O (1.00 g, 0.493 mmol) and [(2-EtC_6H_{12})$_2$$NH_2$][H^{n}OctPO$_4$] (222 mg, 0.493 mmol) in 20 mL dichloromethane. Yield: 1.20 g (98 %). $^{11}B\{^1H\}$ NMR (128.38 MHz, 298K, $CDCl_3$): δ = 13.9, 5.7, −3.2. $^{31}P\{^1H\}$ NMR (121.49 MHz, 298 K, $CDCl_3$): δ = −10.77. ICP-OES: Calculated percentage: B: 0.79 %, P: 1.14 %; found: B: 0.12 %, P: 1.00 %.

{HN^{n}Bu$_3$}{[(4-PIB$_{1000}$catB)$_2$O][(2-EtC$_6$H$_{12}$)$_2$PO$_4$]} [62]

Synthesised from (4-PIB_{1000}catB)$_2$O (21.0 g, 9.23 mmol) and [(2-EtC_6H_{12})$_2$$NH_2$][(2-$EtC_6H_{12}$)$_2$$PO_4$] (4.70 g, 9.23 mmol) in 150 mL dichloromethane. Yield: 25.6 g (99 %). $^{11}B\{^1H\}$ NMR (128.38 MHz, 298K, $CDCl_3$): δ = 14.0. $^{31}P\{^1H\}$ NMR (121.49 MHz, 298K, $CDCl_3$): δ = 0.23. −0.68. ICP-OES: Calculated percentage: B: 0.78 %, P: 1.11 %; found: B: 0.37 %, P: 1.33 %.

{(2-EtC$_6$H$_{12}$)$_2$NH$_2$}{[(4-PIB$_{1000}$catB)$_2$O][HOleylPO$_4$]} [63]

Synthesised from (4-PIB_{1000}catB)$_2$O (46.9 g, 23.1 mmol) and [(2-EtC_6H_{12})$_2$$NH_2$][HOleylPO$_4$] (13.6 g, 23.1 mmol) in 600 mL dichloromethane. Yield: 52.0 g (79 %). $^{11}B\{^1H\}$ NMR (128.38 MHz, 298K, $CDCl_3$): δ = 14.0, 5.7, −3.3. $^{31}P\{^1H\}$ NMR (121.49 MHz, 298K, $CDCl_3$): δ = −6.50. ICP-OES: Calculated percentage: B: 0.75 %, P: 1.08 %; found: B: 0.78 %, P: 1.84 %.

{(2-EtC$_6$H$_{12}$)$_2$NH$_2$}{[(4-PIB$_{1000}$catB)$_2$O][H(C$_{13}$H$_{27}$)PO$_4$]} [64]

Synthesised from (4-PIB$_{1000}$catB)$_2$O (46.4 g, 22.8 mmol) and [(2-EtC$_6$H$_{12}$)$_2$NH$_2$][H(C$_{13}$H$_{27}$)PO$_4$] (11.9 g, 22.8 mmol) in 600 mL dichloromethane. Yield: 57 g (90 %). ^{11}B{^{1}H} NMR (128.38 MHz, 298K, CDCl$_3$): δ = 13.9, 5.9, −3.3. ^{31}P{^{1}H} NMR (121.49 MHz, 298K, CDCl$_3$): δ = −7.94. ICP-OES: Calculated percentage: B: 0.77 %, P: 1.11 %; found: B: 0.69 %, P: 1.20 %.

{(2-EtC$_6$H$_{12}$)NH$_3$}{[(4-PIB$_{1000}$catB)$_2$O][H(C$_{13}$H$_{27}$)PO$_4$]} [65]

Synthesised from (4-PIB$_{1000}$catB)$_2$O (48.0 g, 23.6 mmol) and [(2-EtC$_6$H$_{12}$)NH$_3$][H(C$_{13}$H$_{27}$)PO$_4$] (9.67 g, 23.6 mmol) in 600 mL dichloromethane. Yield: 56 g (88 %). ^{11}B{^{1}H} NMR (128.38 MHz, 298K, CDCl$_3$): δ = 5.6, −3.2. ^{31}P{^{1}H} NMR (121.49 MHz, 298K, CDCl$_3$): δ = −12.60. ICP-OES: Calculated percentage: B: 0.81 %, P: 1.15 %; found: B: 0.77 %, P: 1.58 %.

{(2-EtC$_6$H$_{12}$)$_3$NH}{[(4-PIB$_{1000}$catB)$_2$O][H(C$_{13}$H$_{27}$)PO$_4$]} [66]

Synthesised from (4-PIB$_{1000}$catB)$_2$O (45.0 g, 22.1 mmol) and [(2-EtC$_6$H$_{12}$)$_3$NH][H(C$_{13}$H$_{27}$)PO$_4$] (14.0 g, 22.1 mmol) in 600 mL dichloromethane. Yield: 59 g (92 %). ^{11}B{^{1}H} NMR (96.29 MHz, 298K, CDCl$_3$): δ = 14.2, 5.8, −3.4. ^{31}P{^{1}H} NMR (121.49 MHz, 298K, CDCl$_3$): δ = −17.49. ICP-OES: Calculated percentage: B: 0.72 %, P: 1.06 %; found: B: 0.71 %, P: 1.23 %.

{HN^{n}Bu$_3$}{(GMO-B)$_2$O][H^{n}BuPO$_4$]} [67]

Synthesised from (GMO-B)$_2$O (14.5 g, 19.4 mmol) and [HN^{n}Bu$_3$][H^{n}BuPO$_4$] (6.57 g, 19.4 mmol) in 200 mL dichloromethane. Yield: 20.8 g (98 %) ^{11}B{^{1}H} NMR (96.29 MHz, 298K, CDCl$_3$): δ = 5.8, −3.2. ^{31}P{^{1}H} NMR (121.49 MHz, 298K, CDCl$_3$): δ =

−11.55. ICP-OES: Calculated percentage: B: 1.99 %, P: 2.85 %; found: B: 1.43 %, P: 3.20 %.

{HN^{n}Bu$_3$}{[(4-PIB$_{550}$catB)$_2$O][H^{n}BuPO$_4$]} [68]

Synthesised from (4-PIB$_{550}$catB)$_2$O (1.00 g, 0.74 mmol) and [HN^{n}Bu$_3$][H^{n}BuPO$_4$] (251 mg, 0.71 mmol) in 30 mL dichloromethane. Yield: 1.18 g (94 %). ^{11}B{^{1}H} NMR (128.38 MHz, 298K, $CDCl_3$): δ = 14.0, 6.0, −3.4. ^{31}P{^{1}H} NMR (121.49 MHz, 298K, $CDCl_3$): δ = −0.06, −6.49, −14.00. ICP-OES: Calculated percentage: B: 1.26 %, P: 1.80 %; found: B: 1.35 %, P: 2.83 %.

{(2-EtC$_6$H$_{12}$)$_2$NH$_2$}{[(4-PIB$_{550}$catB)$_2$O][H(2-EtC$_6$H$_{12}$)PO$_4$]} [69]

Synthesised from (4-PIB$_{550}$catB)$_2$O (1.25 g, 0.74 mmol) and [(2-EtC$_6$H$_{12}$)$_2$NH$_2$][H(2-EtC$_6$H$_{12}$)PO$_4$] (417 mg, 0.74 mmol) in 20 mL dichloromethane. Yield: 1.65 g (99 %). ^{11}B{^{1}H} NMR (128.38 MHz, 298K, $CDCl_3$): δ = 13.7, 5.6, −3.2. ^{31}P{^{1}H} NMR (121.49 MHz, 298K, $CDCl_3$): δ = 1.14, −5.60. ICP-OES: Calculated percentage: B: 1.18 %, P: 1.69 %; found: B: 0.32 %, P: 2.26 %.

{HN^{n}Bu$_3$}{[(4-PIB$_{550}$catB)$_2$O][H(2-EtC$_6$H$_{12}$)PO$_4$]} [70]

Synthesised from (4-PIB$_{550}$catB)$_2$O (1.16 g, 0.86 mmol) and [(HN^{n}Bu$_3$][H(2-EtC$_6$H$_{12}$)PO$_4$] (339 mg, 0.86 mmol) in 20 mL dichloromethane. Yield: 1.37 g (91 %). ^{11}B{^{1}H} NMR (128.38 MHz, 298K, $CDCl_3$): δ = 14.0, 5.5, −3.3. ^{31}P{^{1}H} NMR (121.49 MHz, 298K, $CDCl_3$): δ = 0.93, −6.01. ICP-OES: Calculated percentage: B: 1.22 %, P: 1.75 %; found: B: 0.29 %, P: 2.13 %.

{(2-EtC$_6$H$_{12}$)$_2$NH$_2$}{[(4-(C$_{16}$-C$_{18}$)catB)$_2$O][H(2-EtC$_6$H$_{12}$)PO$_4$]} [71]

Synthesised from (4-(C$_{16}$-C$_{18}$)catB)$_2$O (51.2 g, 70.1 mmol) and [(2-EtC$_6$H$_{12}$)$_2$NH$_2$][H(2-EtC$_6$H$_{12}$)PO$_4$] (31.6 g, 70.1 mmol) in 700 mL dichloromethane. Yield: 67 g (82 %). ^{11}B{^{1}H} NMR (128.38 MHz, 298K, CDCl$_3$): δ = 13.8, 5.9, −3.0. ^{31}P{^{1}H} NMR (121.49 MHz, 298K, CDCl$_3$): δ = −10.23. ICP-OES: Calculated percentage: B: 1.83 %, P: 2.62 %; found: B: 1.75 %, P: 3.30 %.

{(2-EtC$_6$H$_{12}$)$_2$NH$_2$}{[(4-dodecylcatB)$_2$O][H(2-EtC$_6$H$_{12}$)PO$_4$]} [72]

Synthesised from (4-dodecylcatB)$_2$O (40.9 g, 69.3 mmol) and [(2-EtC$_6$H$_{12}$)$_2$NH$_2$][H(2-EtC$_6$H$_{12}$)PO$_4$] (31.3 g, 69.3 mmol) in 600 mL dichloromethane. Yield: 66 g (92 %). ^{11}B{^{1}H} NMR (128.38 MHz, 298K, CDCl$_3$): δ = 13.9, 5.9, −3.1. ^{31}P{^{1}H} NMR (121.49 MHz, 298K, CDCl$_3$): δ = −9.66. ICP-OES: Calculated percentage: B: 2.07 %, P: 2.97 %; found: B: 1.79 %, P: 3.34 %.

{(2-EtC$_6$H$_{12}$)$_2$NH$_2$}{[(4-dodecylcatB)$_2$O][HOleylPO$_4$]} [73]

Synthesised from (4-dodecylcatB)$_2$O (37.1 g, 62.8 mmol) and [(2-EtC$_6$H$_{12}$)$_2$NH$_2$][HOleylPO$_4$] (37.1 g, 62.8 mmol) in 600 mL dichloromethane. Yield: 55.0 g (74 %). ^{11}B{^{1}H} NMR (128.38 MHz, 298K, CDCl$_3$): δ = 14.0, 5.9, −3.2. ^{31}P{^{1}H} NMR (121.49 MHz, 298K, CDCl$_3$): δ = −10.54. ICP-OES: Calculated percentage: B: 1.83 %, P: 2.62 %; found: B: 1.55 %, P: 3.10 %.

{(2-EtC$_6$H$_{12}$)$_3$NH}{[(4-dodecylcatB)$_2$O][H^{n}BuPO$_4$]} [74]

Synthesised from (4-dodecylcatB)$_2$O (32.0 g, 54.2 mmol) and [(2-EtC$_6$H$_{12}$)$_3$NH][H^{n}BuPO$_4$] (27.5 g, 54.2 mmol) in 600 mL dichloromethane. Yield: 55.0 g (74 %). ^{11}B{^{1}H} NMR (128.38 MHz, 298K, CDCl$_3$): δ = 14.1, 5.6, −3.4.

$^{31}P\{^{1}H\}$ NMR (121.49 MHz, 298K, $CDCl_3$): δ = −7.22. ICP-OES: Calculated percentage: B: 1.97 %, P: 2.82 %; found: B: 1.35 %, P: 2.97 %.

{(2-EtC$_6$H$_{12}$)$_3$NH}{[(catB)$_2$O][H(C$_{13}$H$_{27}$)PO$_4$]} [75]

Synthesised from $(catB)_2O$ (500 mg, 1.97 mmol) and [(2-$EtC_6H_{12})_3NH][H(C_{13}H_{27})PO_4$] (1.25 g, 1.97 mmol) in 20 mL dichloromethane. Yield: 1.62 g (93 %). $^{11}B\{^{1}H\}$ NMR (128.38 MHz, 298K, $CDCl_3$): δ = 14.1, 6.4, −3.3. $^{31}P\{^{1}H\}$ NMR (121.49 MHz, 298K, $CDCl_3$): δ = −17.59. ICP-OES: Calculated percentage: B: 2.44 %, P: 3.49 %; found: B: 2.31 %, P: 4.55 %.

5.2.2 NMR Binding Investigation

Binding stoichiometries were investigated using the method of continuous variation and the plotting of Job plots for each pyroborate-anion pair in dry $CDCl_3$ at 298 K.[229] Ratios of pyroborate to anion were varied so that an overall concentration of 50 mM, was maintained, with the exception of **[10]** (naph-1,2-$O_2B)_2O$ which was maintained at 5 mM due to poor solubility, and the resulting ^{1}H NMR spectra monitored. ^{1}H signals monitored were the α-C*H*$_2$ proton for phosphate anions (β-C*H*$_2$ protons also monitored for *iso*-butylphosphate), the O=C-C*H*$_3$ proton for acetate, the para-C*H* for benzoate and the S-C*H*$_3$ proton for methanesulfonate.

For NMR titrations, a sample of the anion compound was dissolved in $CDCl_3$ (concentrations of 0.005 – 0.2 mM), 0.5 mL of which was used as the host NMR sample. The remainder was used to dissolve a sample of the pyroborate, so that the anion concentration remained constant throughout. Successive aliquots of the pyroborate solution were added to the host NMR sample (typically 0.10-0.33 equivalents), with ^{1}H NMR spectra being recorded after each addition. The changes

in chemical shift of the ^{1}H NMR signals (monitoring the same protons as in the Job plot analyses) were recorded, and the binding constants calculated using WinEQNMR2.[230] Job plot and titration data can be found in Appendix II.

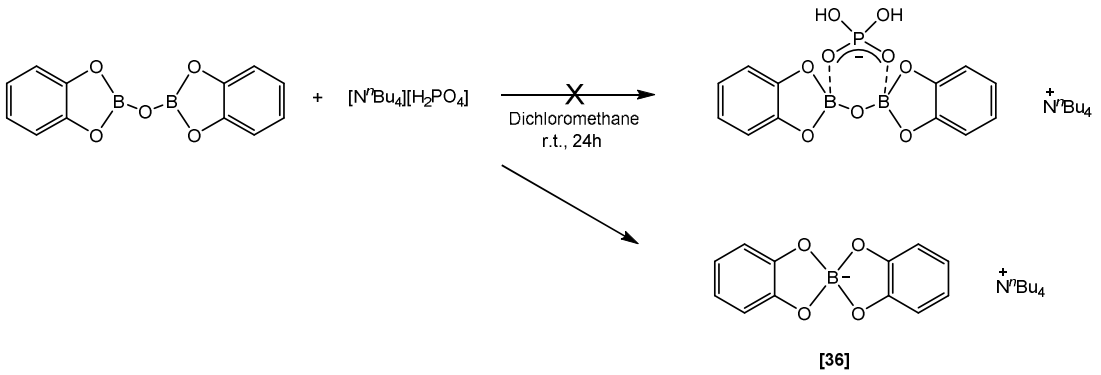
5.3 Results and Discussion

5.3.1 Short-chain Model Anion-bound Borate Compounds

As part of the key aim of this project, which is the synthesis of compounds to be tested for their viability as lubricant additives, it is crucial that the chemistry of these compounds was investigated so that their properties may be better understood. As part of this investigation, a study of the anion-binding ability of the pyroborates in solution was performed. This was achieved through the use of short-chain, model compounds, as they are more straightforward to isolate and purify, and exhibit simpler spectra for characterisation. Moreover, the starting materials required for these syntheses are generally of higher purity, leading to more well-defined products.

5.3.1.1 Studies into Dihydrogen Phosphate Model Compound

Owing to the large amount of interest into phosphorus-containing compounds for lubricant additives (see Chapter I), the main focus of this study was the synthesis and analysis of phosphate-bound borate compounds. This began with the attempted synthesis of the previously reported dihydrogen phosphate-bound catecholato borate, outlined in Scheme 5.1.[149]



Scheme 5.1 Attempted synthesis of dihydrogen phosphate-bound compound.

Despite repeated attempts, the desired compound was not formed, and instead the four-coordinate bis-catecholato compound **[36]** was isolated. This was evident in the $^{11}B\{^{1}H\}$NMR spectrum of the product, which showed a single peak at 14.3 ppm, corresponding to a four-coordinate bis-aryl borate,[159b, 181, 184b, 184c] and within the range of those reported in Chapter IV. The ^{1}H and $^{13}C\{^{1}H\}$ NMR spectra of the product confirm this proposed formulation, as they exhibit well-defined peaks in the aliphatic region corresponding to the *n*-butyl chains of the cation and a multiplet integrating in the correct ratio in the aromatic region, corresponding to the $[cat_2B]^-$ anion. Furthermore, there was no evidence of phosphorus in the final product, as evidenced by the $^{31}P\{^{1}H\}$ NMR spectrum of the product. The reaction was repeated on an NMR scale in a sealed J. Young's tap NMR tube in order to probe whether the phosphate component was being lost during isolation of the product, but again no $^{31}P\{^{1}H\}$ signal was observed. This was surprising, as any unreacted starting material or expected degradation products such as phosphoric acid would exhibit clear peaks in a $^{31}P\{^{1}H\}$ NMR spectrum. It was also established that this phenomenon was not due to bulk hydrolysis of the pyroborate compound **[1]**, as a deliberate hydrolysis reaction of **[1]** *via* addition of excess deionised water led to the formation of boric acid and catechol, which was confirmed by ^{1}H and $^{11}B\{^{1}H\}$ NMR spectroscopic measurements. However, the hygroscopic $[N^{n}Bu_4][H_2PO_4]$ starting material may have contained residual water, despite being dried at *in vacuo* at 60 °C, so partial hydrolysis must be considered. The formation of four-coordinate bis-borate **[36]** was further confirmed by the growth of crystals suitable for X-ray diffraction analysis (Figure 5.7).

In **[36]** the boron centre is in a distorted tetrahedral environment, with O−B−O angles ranging from 104.4(9) to 113.0(9)°, which are within the range of similar bis-borate species reported in Chapter IV and the literature.[181, 184c, 185, 187e] As found in Chapter

IV for similar species, two O−B−O angles are much smaller than the remaining six [104.4(9) and 104.7(9)° *vs* 111.3(8)-113.0(9)°], which elongates the anion tetragonally, affording it approximate D_{2d} symmetry.

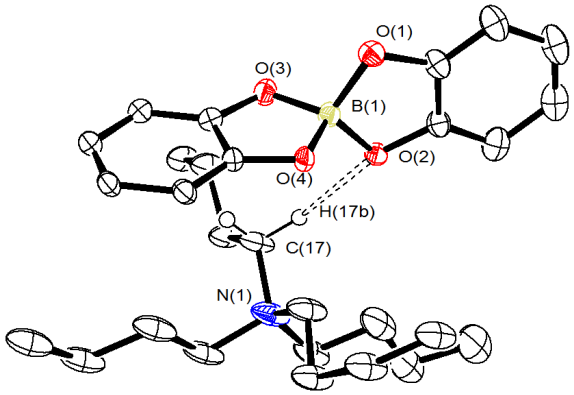


Figure 5.7 Molecular structure of [36]. Thermal ellipsoids are set at the 50% probability level. Hydrogen and disordered carbon atoms from n-butyl chain omitted for clarity.

Table 5.1 Selected bond lengths (Å) and angles (°) for [36].

B(1)−O(1)	1.480(14)
B(1)−O(2)	1.509(14)
B(1)−O(3)	1.489(14)
B(1)−O(4)	1.470(13)
O(1)−B(1)−O(2)	104.4(9)
O(1)−B(1)−O(3)	111.8(9)
O(3)−B(1)−O(4)	104.7(9)
O(4)−B(1)−O(2)	111.3(8)
O(1)−B(1)−O(4)	113.0(9)
O(3)−B(1)−O(2)	111.7(9)
C(17)−O(2)	3.319(13)

The five-membered boron-containing chelate rings of the anion are almost planar, with root mean square deviations from the least squares plane being 0.0148 and 0.0316 Å,

within the range described in Chapter IV. The two chelate rings are found to be approximately perpendicular to one another, exhibiting an angle between the planes of 89.9(3)°. This is very typical of such species, as has been described in Chapter IV and in similar bis-borate compounds reported in the literature.[187d] The solid-state structure of **[36]** contains B−O bonds ranging in length from 1.470(13) to 1.509(14) Å, which are within the range reported in the literature for similar bis-borate species.[181, 184b, 184c, 185, 187a, 187d, 187e]

In order to further understand the transformation of $(catB)_2O$ **[1]** into bis-borate **[36]**, a series of NMR-scale experiments was carried out. This initially involved varying the equivalents of both $(catB)_2O$ and $[N^nBu_4][H_2PO_4]$ and recording the resulting $^{11}B\{^1H\}$ and $^{31}P\{^1H\}$ NMR spectra in an attempt to gain insight into the chemistry taking place between these two species. Experiments were performed which contained increasing partial equivalents of $(catB)_2O$ to $[N^nBu_4][H_2PO_4]$ in $CDCl_3$ to ascertain the ratio of pyroborate required to effect full conversion to the four-coordinate bis-borate species, and when the signal in the $^{31}P\{^1H\}$ NMR spectrum is fully attenuated. The $^{11}B\{^1H\}$ NMR spectra (Figure 5.8) show the initial formation of several boron-containing species, with simultaneous immediate formation of the four-coordinate bis-borate species **[36]**, as evident by the sharp peak at *ca*. 14 ppm. The $^{31}P\{^1H\}$ NMR spectra (Figure 5.9) similarly show the presence of several phosphorus-containing species, with chemical shifts ranging from 2.10 ppm (corresponding to unreacted $[N^nBu_4][H_2PO_4]$) to −11.53 ppm. It is conceivable that peaks in the $^{11}B\{^1H\}$ and $^{31}P\{^1H\}$ NMR spectra at *ca.* −1 and −6 ppm, respectively, may correspond to inorganic borate-phosphate species, as similar chemical shifts for both nuclei are reported for $Na_5B_2P_3O_{13}$.[231] The remaining peaks at *ca.* 6 and −11 ppm in the $^{11}B\{^1H\}$ and $^{31}P\{^1H\}$ NMR spectra respectively may therefore correspond to a phosphate-bound

pyroborate species, which breaks down upon the addition of further equivalents of $(catB)_2O$. The requirement of 0.4 equivalents of $(catB)_2O$ for this process to take place is evident, as full conversion to the four-coordinate bis-borate is observed and the signal in the $^{31}P\{^1H\}$ NMR spectrum is lost completely at this point.

To further probe this phenomenon, the order of addition was reversed, with aliquots of $[N^nBu_4][H_2PO_4]$ being added to $(catB)_2O$. The $^{11}B\{^1H\}$ NMR spectra (Figure 5.10) again show several boron-containing species being present initially, with an excess of the pyroborate being observed at *ca.* 22 ppm. The formation of bis-borate **[36]** is not evident until 0.3 equivalents of $[N^nBu_4][H_2PO_4]$ has been added, with a

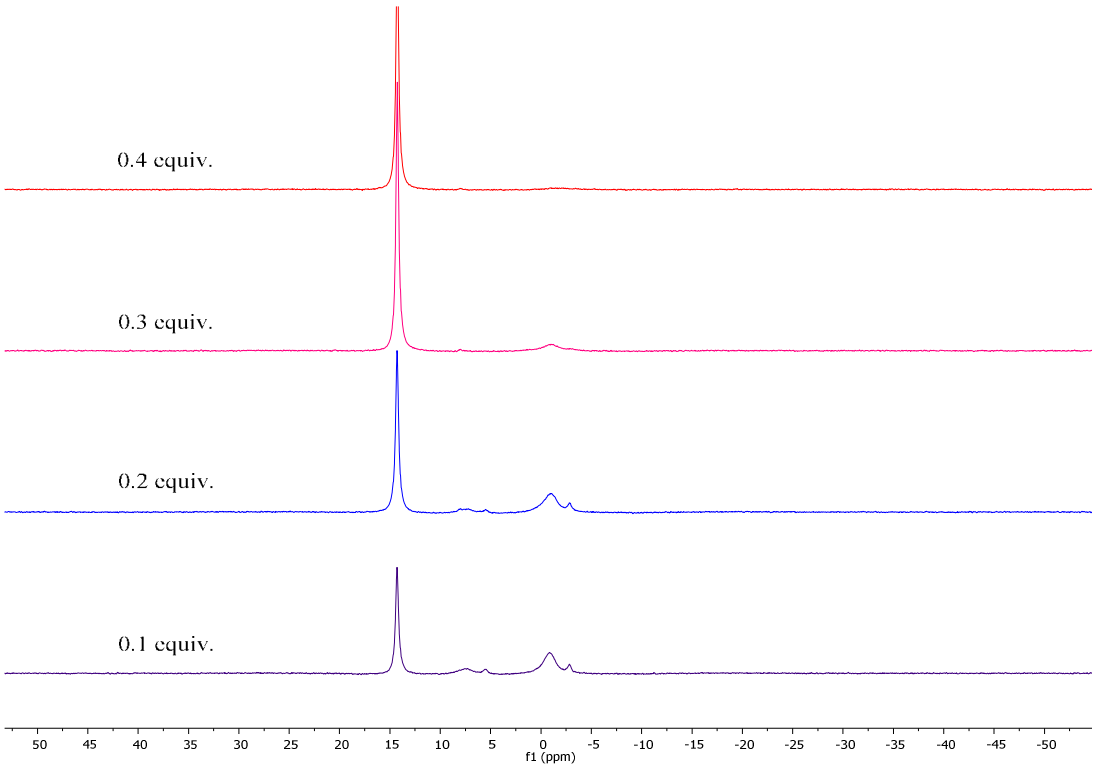


Figure 5.8 $^{11}B\{^1H\}$ NMR spectra resulting from gradual addition of $(catB)_2O$ to $[N^nBu_4][H_2PO_4]$.

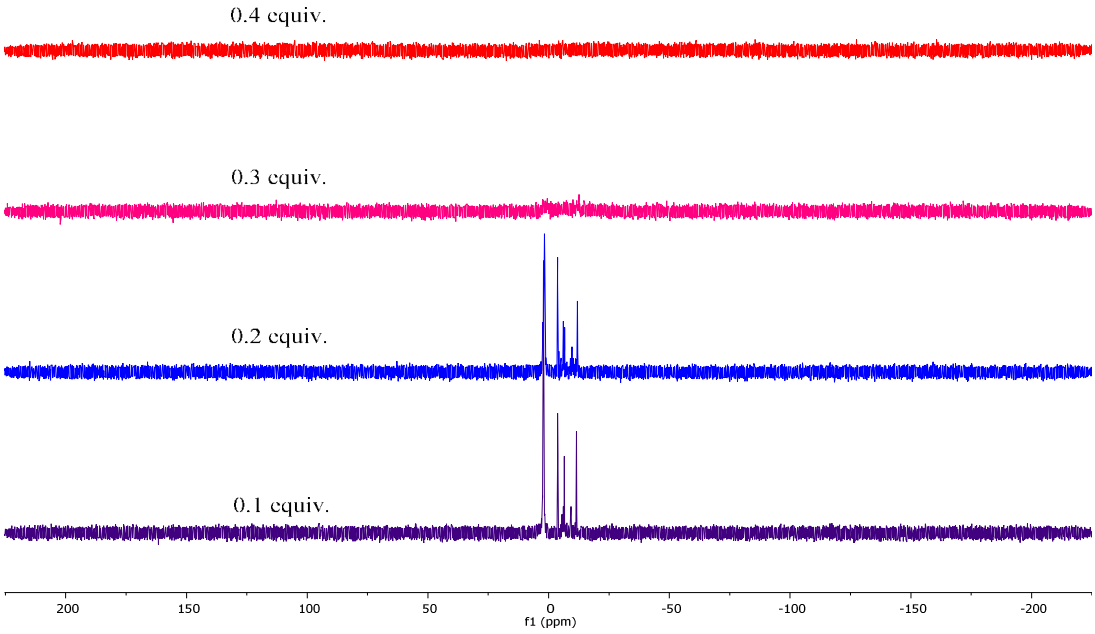


Figure 5.9 $^{31}P\{^{1}H\}$ NMR spectra resulting from gradual addition of $(catB)_2O$ to $[N^nBu_4][H_2PO_4]$.

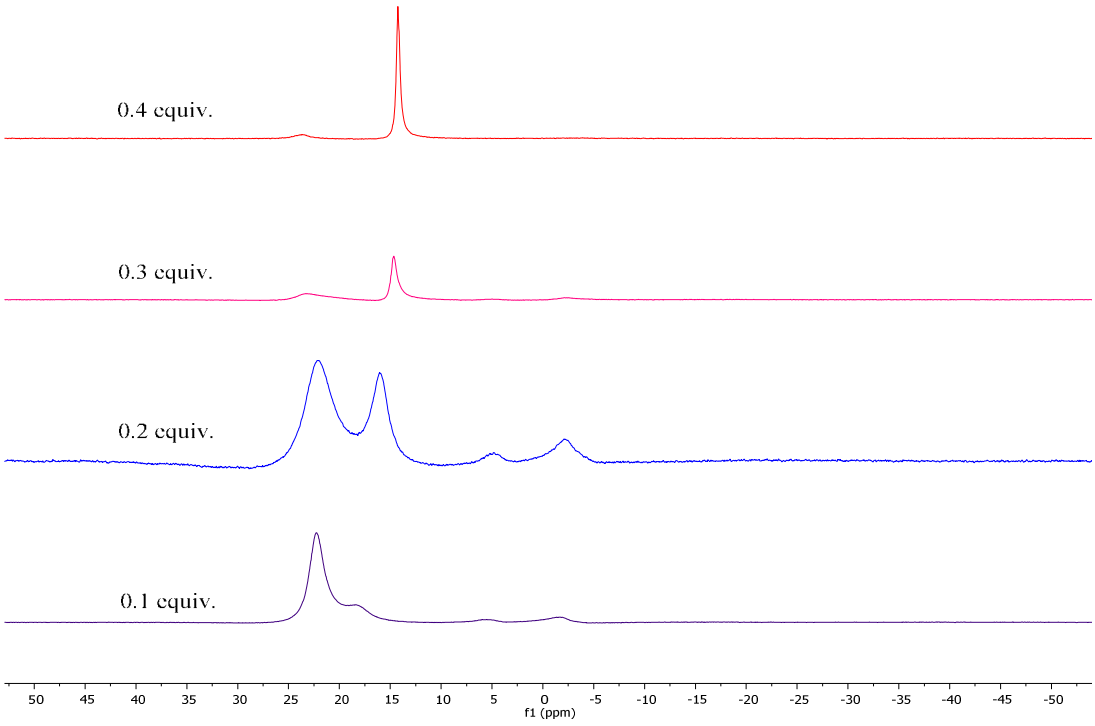


Figure 5.10 $^{11}B\{^{1}H\}$ NMR spectra resulting from gradual addition of $[N^nBu_4][H_2PO_4]$ to $(catB)_2O$.

transient boron-containing species (displaying a resonance at *ca.* 19 ppm) being present beforehand. As this is the expected chemical shift of boric acid in $CDCl_3$,[157a, 158] there may be a similar inorganic boron-containing compound present at this stage. Upon the addition of 0.4 equivalents of $[N^nBu_4][H_2PO_4]$, there is full conversion to the four-coordinate bis-borate species, **[36]**.

The $^{31}P\{^1H\}$ NMR spectra (Figure 5.11) show instantaneous loss of the $^{31}P\{^1H\}$ NMR signal, with only residual noise being observed, suggesting that an excess of pyroborate is essential for this process to occur. The $^{31}P\{^1H\}$ NMR spectra at 0.1 and 0.2 equivalents possibly show very broad peaks at *ca.* −20 ppm, which may correspond to some binding of the phosphate to the pyroborate. The broadness of the signals may be attributed to the presence of ^{10}B and ^{11}B nuclei which possess large quadrupole moments. Moreover, binding of the phosphate may be a dynamic and fluxional process, which may further broaden the peaks in both spectra. This binding is also supported by the peaks at *ca.* 4 and −3 ppm in the $^{11}B\{^1H\}$ NMR spectra (Figure 5.10), which disappear concomitantly with these signals in the $^{31}P\{^1H\}$ NMR spectra.

Following these results, aliquots of $[N^nBu_4][H_2PO_4]$ beyond one equivalent were added to ascertain whether the $^{31}P\{^1H\}$ NMR signal may be reformed. It can be seen in both the $^{11}B\{^1H\}$ and $^{31}P\{^1H\}$ NMR spectra (Figures 5.12 and 5.13) that there is no change until two equivalents of $[N^nBu_4][H_2PO_4]$ are added, whereupon new signals in both spectra begin to appear. These signals continue to increase in intensity until four equivalents are reached, after which little difference is observed upon the addition of further equivalent of $[N^nBu_4][H_2PO_4]$. The spectra appear to be similar to those described above for the gradual addition of 0.1-0.3 equivalents of $(catB)_2O$ to $[N^nBu_4][H_2PO_4]$, suggesting that similar species are being formed.

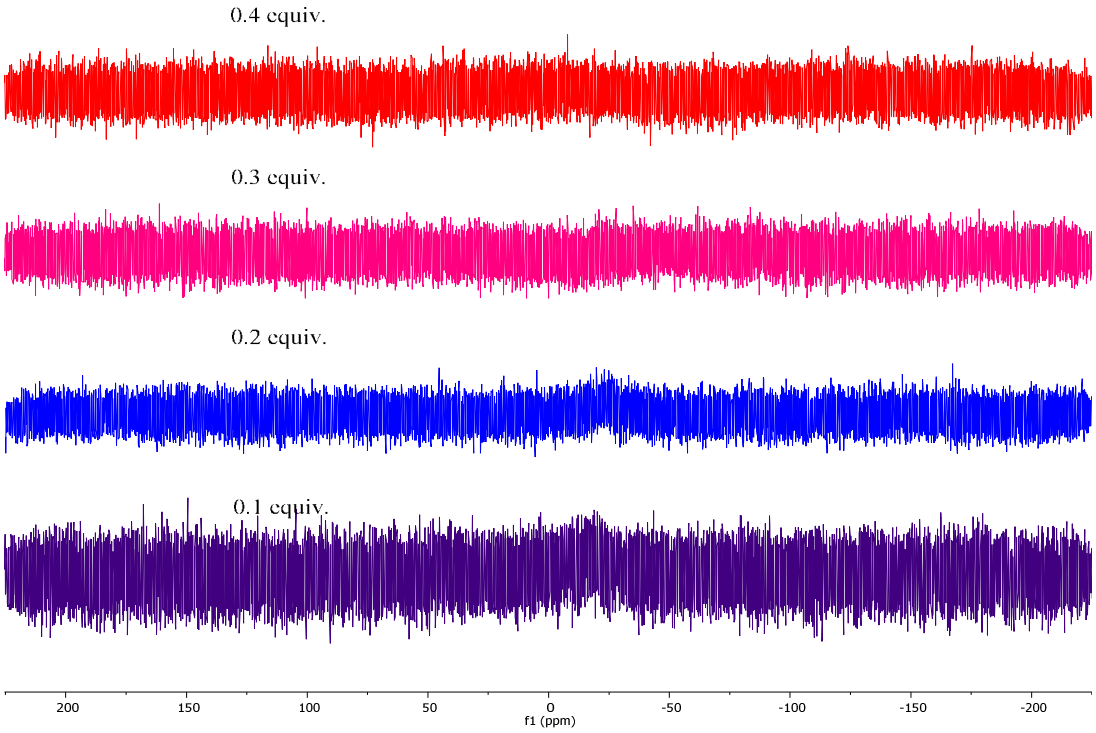


Figure 5.11 $^{31}P\{^{1}H\}$ NMR spectra resulting from gradual addition of $[N^{n}Bu_4][H_2PO_4]$ to $(catB)_2O$.

However, new peaks are present only at −1 ppm in the $^{11}B\{^{1}H\}$ NMR spectrum, suggesting that binding of the phosphate species is not taking place, and only an inorganic borate-phosphate species is being formed. It is possible that the pyroborate species has been completely broken down by the time two equivalents of $[N^{n}Bu_4][H_2PO_4]$ is reached, and so no new binding event takes place.

In order to probe as to whether these phenomena are unique to pyroborate species, an NMR-scale reaction between $[N^{n}Bu_4][H_2PO_4]$ and two equivalents of triethyl borate was attempted. This reaction did not proceed, even when heat was applied to the mixture, as indicated by the presence of signals corresponding to the starting materials being observed in the resulting NMR spectra of the reaction mixture. As aryl pyroborate compounds had proven to be more reactive than alkyl analogues

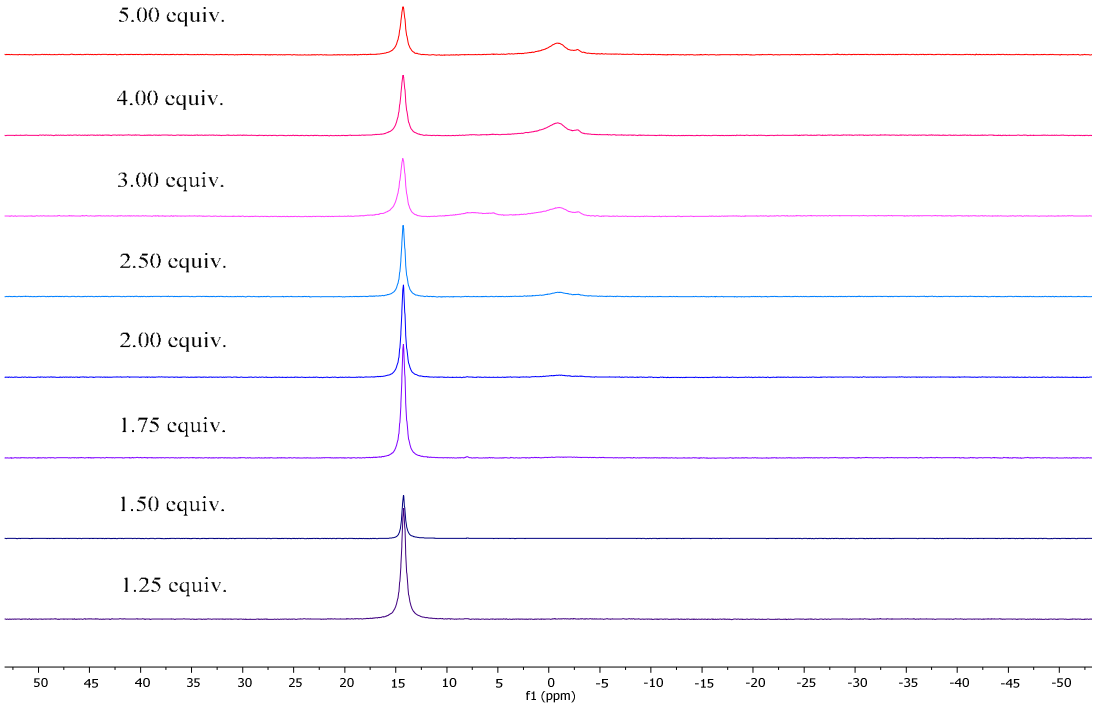


Figure 5.12 $^{11}B\{^1H\}$ NMR spectra resulting from gradual addition of $[N^nBu_4][H_2PO_4]$ to $(catB)_2O$ – above 1 equivalents.

(see Chapter III), a reaction between triphenyl borate and $[N^nBu_4][H_2PO_4]$ was attempted (Scheme 5.2). In this case, a reaction took place, resulting in the appearance of several peaks in the resulting $^{11}B\{^1H\}$ and $^{31}P\{^1H\}$ NMR spectra. Peaks at 2.8 and −0.3 ppm in the $^{11}B\{^1H\}$ NMR spectrum may correspond to the expected phosphate-bound borate product and an inorganic phosphate-borate compound, as described above. It is conceivable that formation of the inorganic phosphate-borate is dynamic and reversible, as evidenced by the very broad signal observed ($\nu_{1/2}$ = 632 Hz). The $^{31}P\{^1H\}$ NMR spectrum of the product is dominated by a large, broad peak at −17.41 ppm, which is a significant upfield shift of *ca.* 19 ppm from the $[N^nBu_4][H_2PO_4]$ starting material. Similar large $^{31}P\{^1H\}$ NMR upfield shifts of 10-16 ppm have previously been reported for protonated sapphyrin compounds binding various phosphate species,[207] suggesting a similar

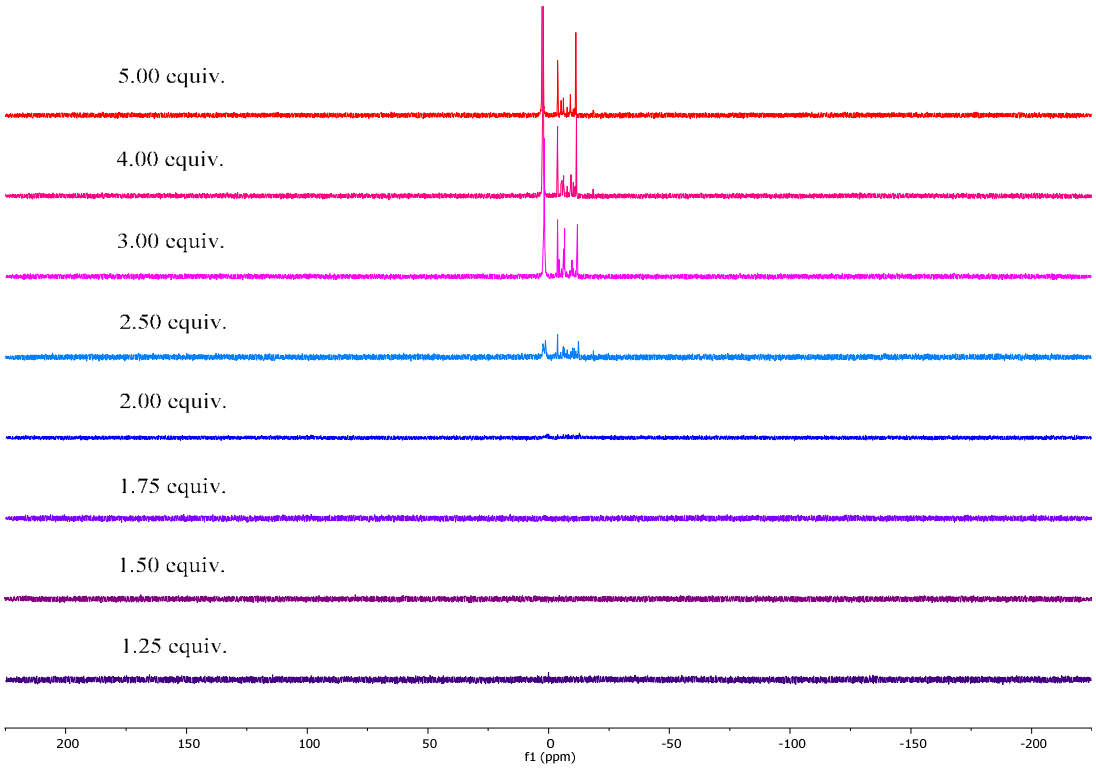
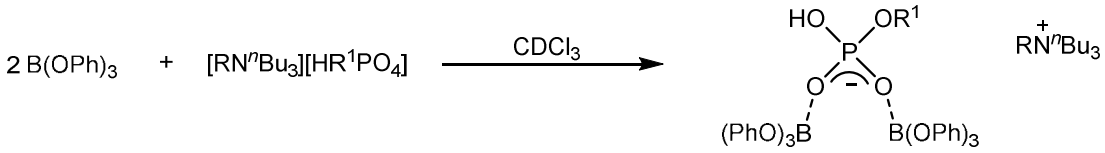


Figure 5.13 $^{31}P\{^{1}H\}$ NMR spectra resulting from gradual addition of $[N^{n}Bu_4][H_2PO_4]$ to $(catB)_2O$ – above 1 equivalents.

complexation is taking place with $B(OPh)_3$. Furthermore, each peak corresponding to the *n*-butylammonium chains on the counterion are significantly shifted from the $[N^{n}Bu_4][H_2PO_4]$ starting material in the ^{1}H NMR spectrum of the product. This suggests binding of the borate species to the phosphate, indicating that the unexpected loss of the $^{31}P\{^{1}H\}$ signal and concurrent formation of a four-coordinate bis-borate is indeed an exclusive result of the use of a pyroborate compound. It is therefore conceivable that the close proximity of two borate centres is key to this reaction proceeding. In order to probe the scope of the reaction with triphenylborate, a reaction with $[HN^{n}Bu_3][H^{n}BuPO_4]$ was performed (Scheme 5.2). This resulted in a similar outcome, with several peaks being observed in both the resulting $^{11}B\{^{1}H\}$ and $^{31}P\{^{1}H\}$ NMR spectra. Although absolute identification of the products of these reactions has not been possible, this does indicate a possible future pathway to



Scheme 5.2 Reactions of triphenylborate and suggested reaction products.

R = N^{n}Bu, H, R^1 = H, ^{n}Bu

phosphate-bound borate species, where variations of the arylborate used may give rise to a novel series of compounds.

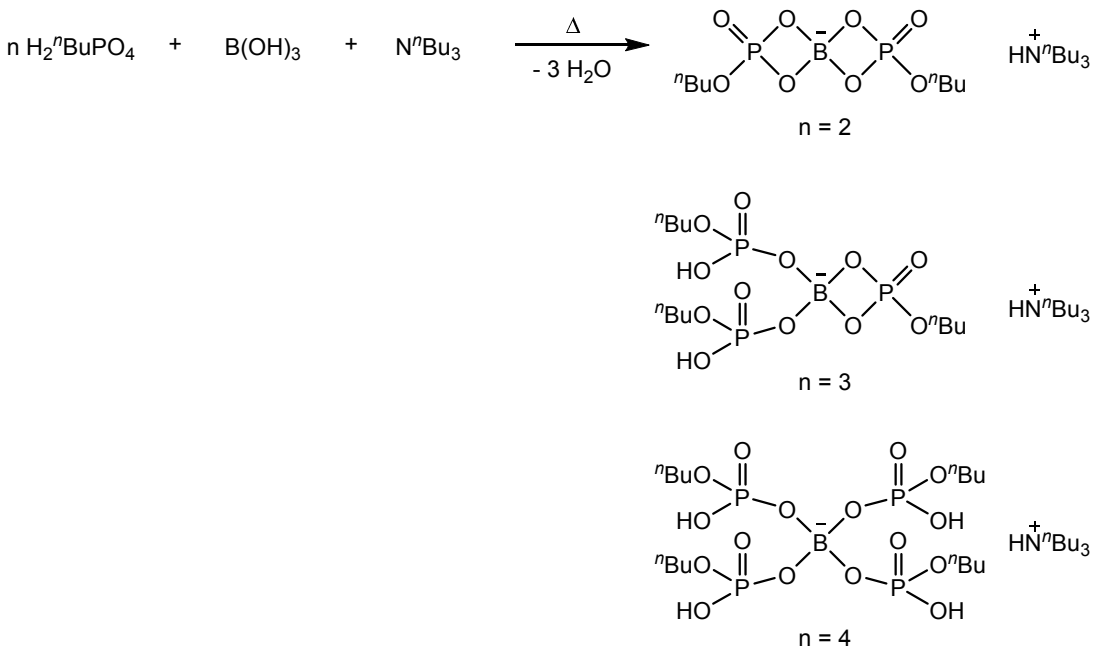
5.3.1.2 Synthesis and Studies into n-Butylphosphate-bound Model Compound

As reactions with the dihydrogen phosphate anion did not yield the expected product, a reaction with alkylphosphate [HN^{n}Bu$_3$][H^{n}BuPO$_4$] was undertaken with the expectation that the presence of an alkyl chain in the phosphate moiety would prevent breakdown and rearrangement of the phosphate-bound species (Scheme 5.4). Confirmation that binding had taken place was evident in the ^{1}H NMR spectrum of the product, where a peak corresponding to the α-CH$_2$ group on the *n*-butyl phosphate chain is present at 4.02 ppm. This is unusually broad for an aliphatic proton signal ($\nu_{1/2}$ = 140 Hz), which may be attributed to broadening of the signal by the ^{11}B nucleus and/or rapid binding and unbinding of the *n*-butylphosphate anion. Moreover, the peak was somewhat attenuated, integrating to only 1.05, suggesting a dynamic process is indeed taking place in solution. Furthermore, peaks in the ^{11}B{^{1}H} NMR spectrum at 14.0, 6.1 and −3.7 ppm suggest simultaneous formation of bis-borate species **[19]**, binding of the *n*-butylphosphate anion to give *n*-butylphosphate-bound compound **[37]** and formation of a catechol-free borate-phosphate species respectively. The peak at 14 ppm is broader than that observed for **[19]**, exhibiting a $\nu_{1/2}$ of 50.1 Hz *vs* 27.0 Hz.

This broadening further suggests a dynamic process is taking place, where **[19]** may be rearranging in solution, possibly converting to **[37]** *in situ.*

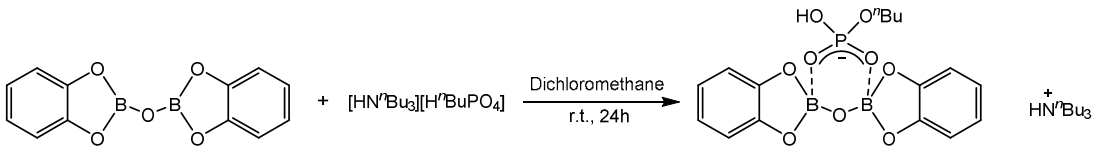
In order to test the hypothesis that one or more catechol-free borate-phosphate compounds are being formed in this reaction, the independent syntheses of such species were attempted. Mono-*n*-butyl phosphate was reacted with boric acid and tri-*n*-butylamine in varying molar ratios, in the hope of forming borate compounds containing two, three and four *n*-butyl phosphate moieties (Scheme 5.3). Inspection of the $^{11}B\{^{1}H\}$ NMR spectra of these species reveals the presence of peaks at −3.4 ppm in each case, with an additional small peak at −1.0 ppm for di- and tri-*n*-butyl phosphate compounds. These match the peaks present in the $^{11}B\{^{1}H\}$ NMR spectrum of **[37]**, suggesting that it is indeed catechol-free borate-phosphate species such as these which are present in solution.

A very broad peak in the $^{31}P\{^{1}H\}$ NMR spectrum ($\nu_{1/2}$ = 7888 Hz) of **[37]** at −16.75 ppm further indicates binding of the *n*-butylphosphate is taking place,[207] with broadening most likely due to a combination of enhanced relaxation through coupling to the quadrupolar ^{11}B nucleus, and rapid exchange of the *n*-butylphosphate. This aligns well with the multiple peaks in the $^{11}B\{^{1}H\}$ NMR spectrum, suggesting that interchange between the three boron-containing species is taking place. Furthermore, $^{31}P\{^{1}H\}$ NMR spectra of the catechol-free borate-phosphates species mentioned above contain broad resonances at *ca*. 0, −5 and −12 ppm, and it is conceivable that interchange between these species and **[37]** in solution gives rise to the very broad $^{31}P\{^{1}H\}$ NMR signal observed for this compound.



Scheme 5.3 Attempted syntheses of proposed catechol-free borate-phosphates.

In order to further probe these dynamic processes, variable temperature NMR experiments were carried out on a sample of **[37]** in CD_2Cl_2 (low temperature) and $CDCl_3$ (high temperature). Firstly, low-temperature NMR experiments were carried out, with ^{1}H, $^{11}B\{^{1}H\}$ and $^{31}P\{^{1}H\}$ NMR spectra being recorded at intervals between 25 °C and −70 °C, with the aim of freezing out the exchanges taking place in solution. The ^{1}H NMR spectra of **[37]** remained mostly unchanged as the temperature was lowered, with the only observed difference being a slight sharpening of the broad peak at 6.71 ppm, affording it a degree of improved resolution (Figure 5.14). Furthermore, the N-H signal at 8.86 ppm has been split into two separate resonances at 8.55 and 8.07 ppm. This suggests that there are two



Scheme 5.4 Synthesis of model compound [37].

different *n*-butylammonium species present in solution, which we may assign to four-coordinate bis-borate **[19]** and phosphate-bound species **[37]**.

The $^{31}P\{^{1}H\}$ NMR spectra of **[37]** did not alter dramatically during cooling, with only a sharpening and increasing in intensity of the peak at *ca.* −17 ppm being observed (Figure 5.15). It is conceivable that there are actually two signals present: the broader signal at −17.2 ppm, corresponding to the phosphate-bound pyroborate **[37]**, and the sharp peak at −18.2 ppm, possibly corresponding to a catechol-free borate-phosphate species, such as those highlighted above. If this is the case, the latter must be frozen out to some degree by the lowered temperature, as its resonance sharpens, whereas the broader peak remains largely unchanged. The most significant changes observed upon lowering the temperature were in the $^{11}B\{^{1}H\}$ NMR spectra of **[37]** (Figure 5.16). As the temperature is lowered, a small, broad resonance at *ca.*

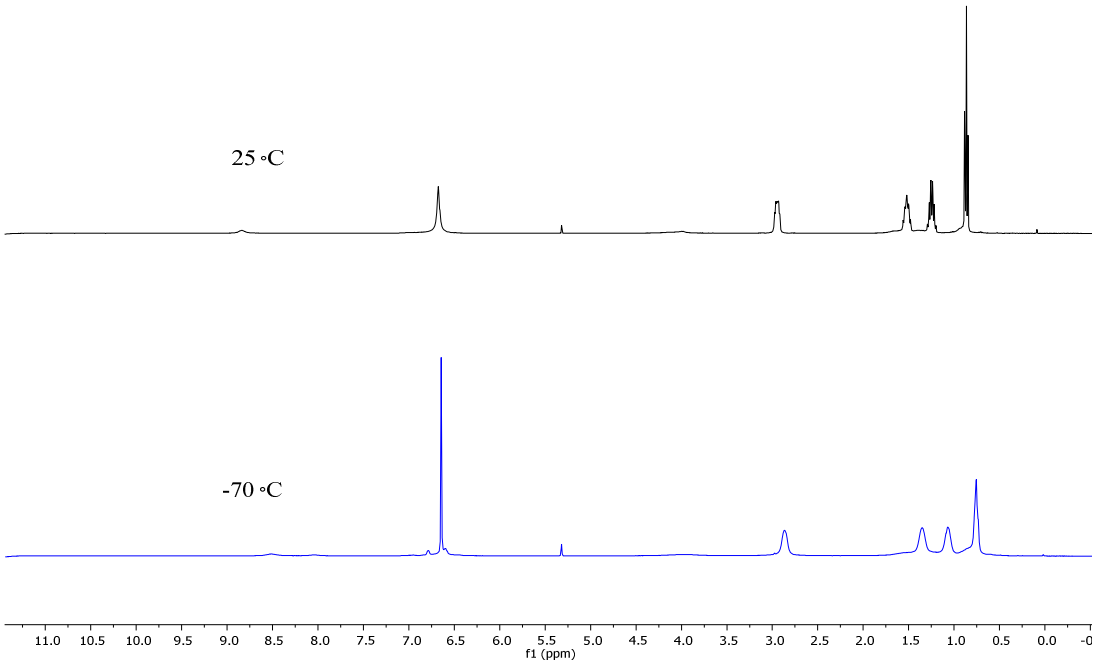


Figure 5.14 ^{1}H NMR spectra of [37] at 25 °C and −70 °C.

22 ppm lowers in intensity, becoming completely attenuated when −30 °C is reached. This may have been attributed to unreacted pyroborate starting material at room temperature. However, this experiment indicates that this peak is most likely due to one of the pyroborate centres remaining unbound as the *n*-butylphosphate anion interchanges between each boron centre, binding in a monodentate fashion. At −30 °C, it would appear that there is not sufficient energy available for this exchange to take place, and so permanent binding to both boron centres takes place. This occurs concomitantly with an increase in intensity of the resonance at *ca.* 6 ppm, further indicating that this peak corresponds to the phosphate-bound species **[37]**. A similar effect was reported by Stephan *et al.* where a fluorinated diboroxane was found to bind carboxylate anions through one boron centre, and exchanged between the two.[143] However, the carboxylate exchange was not frozen out at low temperature, unlike that observed for **[37]**, suggesting stronger binding of the anion in this case.

The broad peak at −3.7 ppm in the $^{11}B\{^{1}H\}$ NMR spectrum is also affected by the reduction in temperature, sharpening into a doublet at −3.3 ppm. If these peaks are indeed due to the catechol-free borate-phosphate species mentioned above, this experiment suggests that there is an increase in the concentration of $[HN^{n}Bu_3][B(^{n}BuPO_4)_2]$ ($\delta_B = -1, -3$ ppm). It is also conceivable that exchange of the *n*-butylphosphate anion between bidentate and monodentate binding to the boron centre: *i.e.* between $[HN^{n}Bu_3][B(^{n}BuPO_4)_2]$ and $[HN^{n}Bu_3][B(^{n}BuPO_4)_3]$/ $[HN^{n}Bu_3][B(^{n}BuPO_4)_4]$ is being frozen out at low-temperature, leading to the

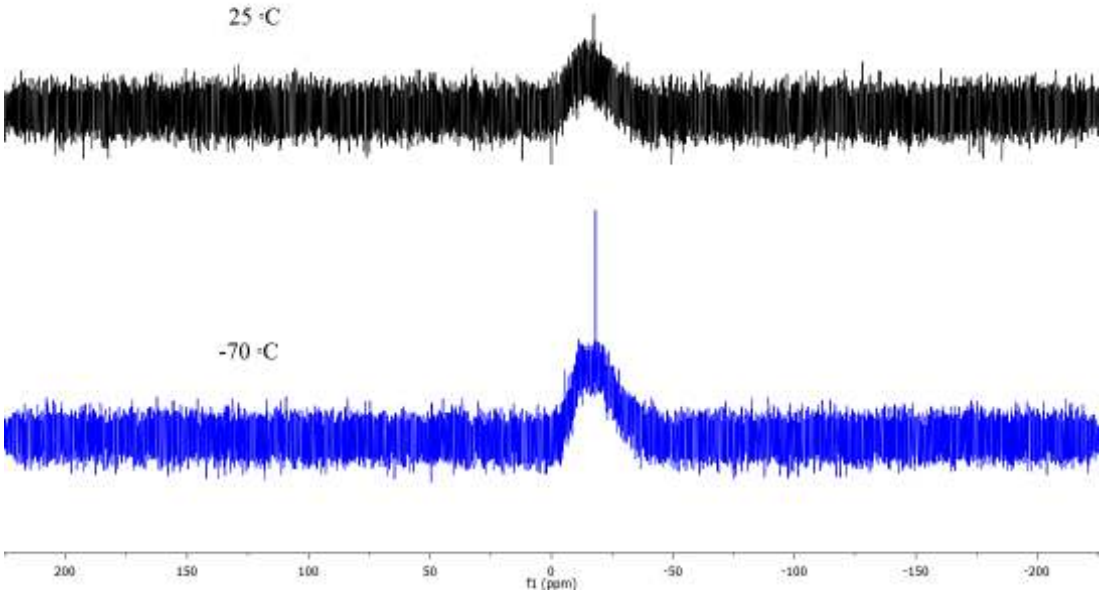


Figure 5.15 $^{31}P\{^{1}H\}$ NMR spectra of [37] at 25 °C and −70 °C.

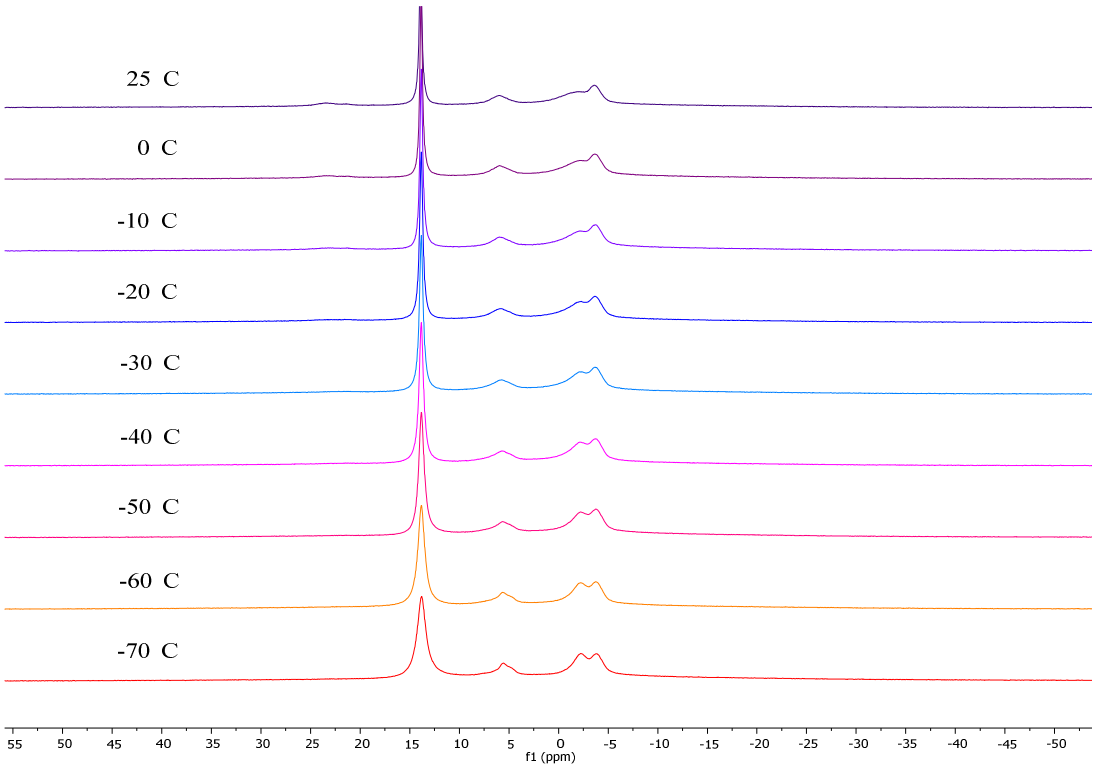


Figure 5.16 $^{11}B\{^{1}H\}$ NMR spectra of [37] between 25 °C and −70 °C.

sharpening of this resonance. To ascertain as to whether these changes are indicative of a dynamic process, or if permanent alterations to the species present have taken place, the temperature was raised back to 25 °C and the $^{11}B\{^{1}H\}$ NMR spectrum rerun. The resonances were identical to those first observed, indicating that these processes are reversible, and so likely to be dynamic exchanges occurring in solution.

Following these investigations, high temperature $^{11}B\{^{1}H\}$ NMR experiments were carried out to probe how elevated temperatures may affect the dynamic processes taking place. $^{11}B\{^{1}H\}$ NMR spectra of **[37]** were recorded at 25 and 50 °C (Figure 5.17). As may be expected, the peak at *ca.* 22 ppm increased in intensity at 50 °C, due to an increased level of dissociation of the *n*-butylphosphate from one of the boron centres, indicating exchange between the two boron atoms occurs more rapidly at elevated temperatures. Furthermore, the resonance at *ca.* 6 ppm is slightly reduced, further suggesting dissociation of the bound *n*-butylphosphate. The peak at −3.7 ppm appears to be unaffected, suggesting exchange between catechol-free borate-phosphate species is unchanged upon the rise in temperature. Once again, the $^{11}B\{^{1}H\}$ NMR spectrum of **[37]** was recorded upon returning to 25 °C, which was identical to that originally recorded, indicating that these processes are also reversible.

In order to investigate the solid-state composition of **[37]**, CHN elemental analysis was carried out, which agreed very well with predicted values for the *n*-butylphosphate-bound product. Furthermore, as this species is a model for later synthesised oil-soluble compounds (vide infra), ICP-OES analysis was undertaken, as this is the elemental analysis method by which oil-soluble compounds are studied by the Lubrizol Corporation. This also agreed well with predicted values, suggesting

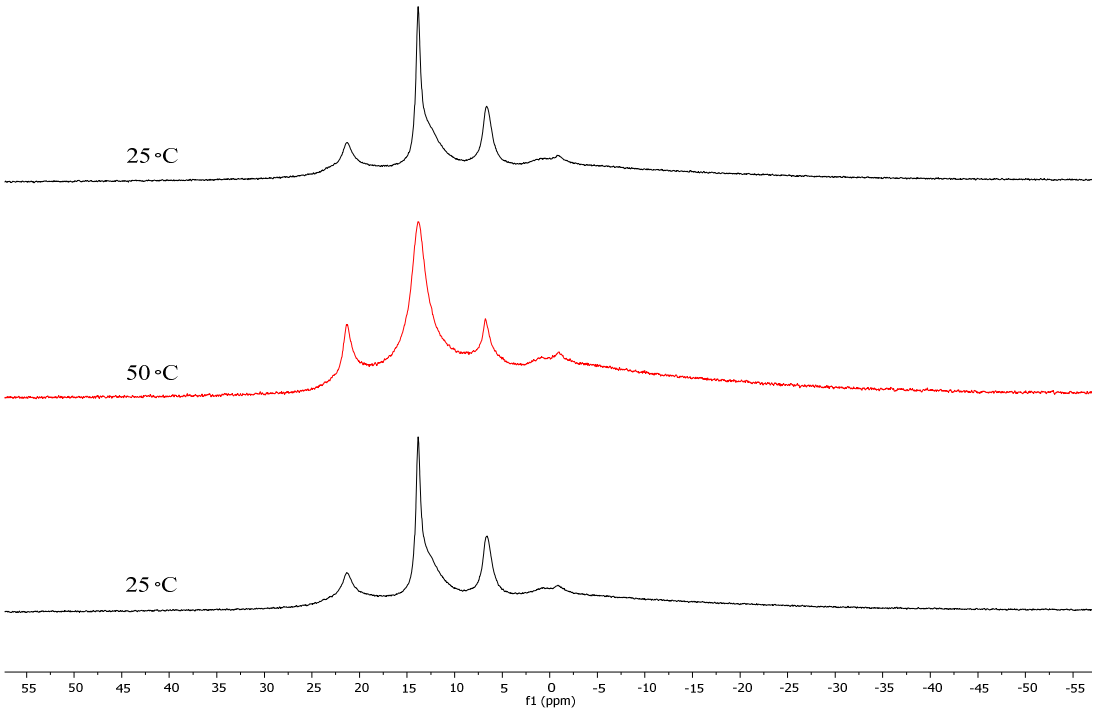


Figure 5.17 $^{11}B\{^1H\}$ NMR spectra of [37] at 25 °C and 50 °C.

[37] indeed has the expected composition in the solid-state. In an attempt to probe this further, a solid-state $^{11}B\{^1H\}$ NMR experiment was carried out on **[37]**. Interestingly, the solution-state $^{11}B\{^1H\}$ NMR was replicated almost perfectly by the solid-state NMR experiment (Figure 5.18), which is highly unusual, as the anisotropy of solid-state samples usually leads to significant line broadening.[232] It is possible that the extremely fast spinning of the sample induced melting of the compound, allowing the molecules to tumble in the molten state, therefore producing a solution-like spectrum. Indeed, replication of solution-state NMR spectra upon melting of samples has been previously reported in the ^{13}C and ^1H solid-state NMR studies of polymers.[233]

An NMR-scale reaction of $(catB)_2O$ with trimethylammonium fluoride (TMAF) was carried out, in order to investigate whether halide anions reacted in a similar way to

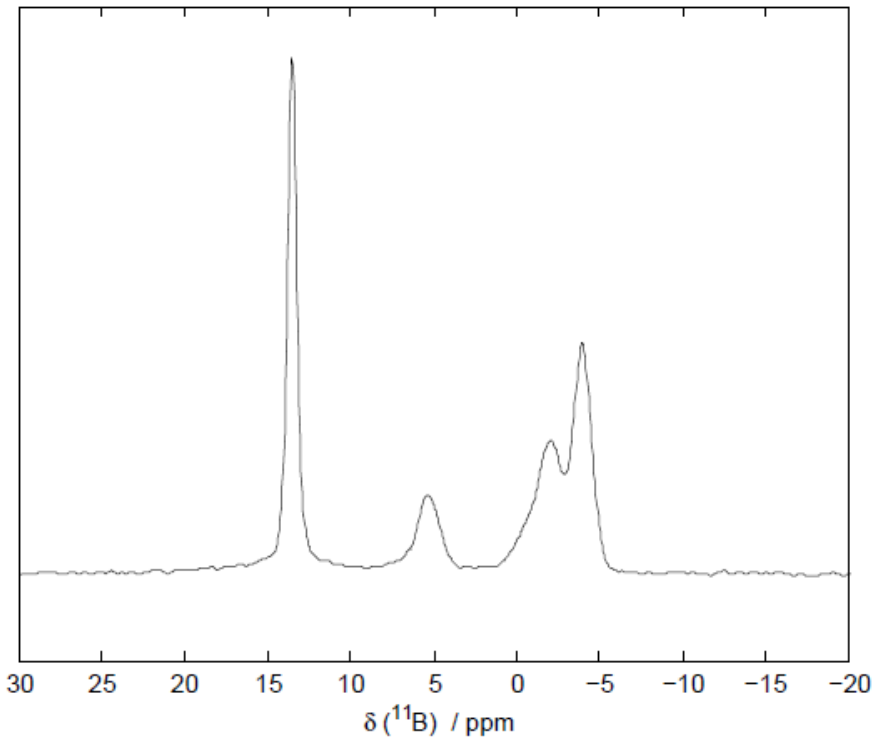


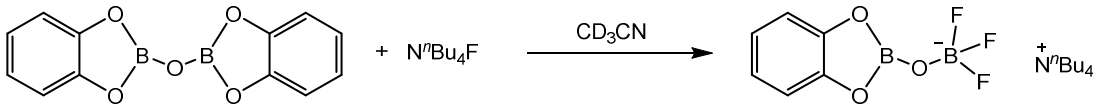
Figure 5.18 Solid-state NMR spectrum of [37].

form a fluoride-bound compound analogous to **[37]**, and to provide another NMR handle for understanding the processes taking place in these reactions. Tetra-*n*-butylammonium fluoride (TBAF) could not be used, as it is known to undergo E2 elimination reactions when attempts are made to dry the product, forming 1-butene,[234] and so TBAF could not be made suitably anhydrous for this reaction. This reaction was originally attempted in $CDCl_3$, for closer comparison with NMR experiments carried out previously, but the insolubility of TMAF in this solvent led to no reaction taking place. Thus, $(catB)_2O$ and TMAF were mixed in a 1:1 ratio in an NMR tube in CD_3CN and the resulting ^{1}H, $^{11}B\{^{1}H\}$ and $^{19}F\{^{1}H\}$ NMR spectra recorded. Evidence that binding had taken place is present in the $^{11}B\{^{1}H\}$ NMR spectrum, where several different resonances are observed. Three peaks are present in the three-coordinate region of the spectrum, at 23.5, 21.5 and 19.7 ppm, which are most likely due to the fact that only one fluoride anion is present, and so at least one

three-coordinate boron centre is unbound at any one time. A peak at 14.2 ppm is present, corresponding to the *in situ* formation of a four-coordinate bis-borate species, most likely of the form $[NMe_4][cat_2B]$. A peak at −1.2 ppm matches that reported for $[NMe_4][BF_4]$,[235] indicating that exchange of the ligands on the boron centre is occurring in solution, mirroring the borate-phosphate compounds postulated above. A broad peak present at 7.1 ppm may correspond to the expected fluoride-bound pyroborate species, which aligns well with the phosphate analogue **[37]**.

The $^{19}F\{^1H\}$ NMR spectrum also contains evidence for the formation of $[NMe_4][BF_4]$, as peaks are present at −151.32 and −151.38 ppm, both of which are similar to data previously reported for this species.[235] These resonances are relatively broad, however, and are not split into the quartet which would be expected from coupling to the spin 3/2 ^{11}B nuclei. This may be due to interconversion between different species taking place faster than the NMR timescale. A similar effect was observed by Reddy and co-workers, who reported that fluoride anions exchanging between different boron centres led to unresolved $^{19}F\{^1H\}$ resonances.[191c] Broad peaks in the $^{19}F\{^1H\}$ NMR spectrum of the reaction between $(catB)_2O$ and TMAF are also present at −141.58 and −146.17 ppm, which may correspond to fluoride-bound pyroborate species, as these are within the range previously reported for fluoride anions bound to boron receptor molecules.[225, 236] This would also correlate well with the $^{11}B\{^1H\}$ peak at 7.1 ppm, indicative of a fluoride-bound analogue of **[37]**. However, it is also possible that the fluoride anions are breaking up one or more of the B-O bonds of the pyroborate compound and forming B-F bonds, resulting in a $[X\text{-}BF_3]^-$ borate species (Scheme 5.5), which has been previously reported by Aldridge and co-workers for ferrocene-derived boronic esters.[237] Therefore, one of these resonances may correspond to such a species. Indeed, the $MeOBF_3^-$ anion has been reported to exhibit a δ_F of −148.8 ppm.

Furthermore, an unassigned peak at −0.6 ppm in the $^{11}B\{^1H\}$ spectrum may correspond to a $[X\text{-}BF_3]^-$ species, as it is similar to the chemical shift of $BF_3{\cdot}OEt_2$ used as the zero in the acquisition of $^{11}B\{^1H\}$ NMR spectra.



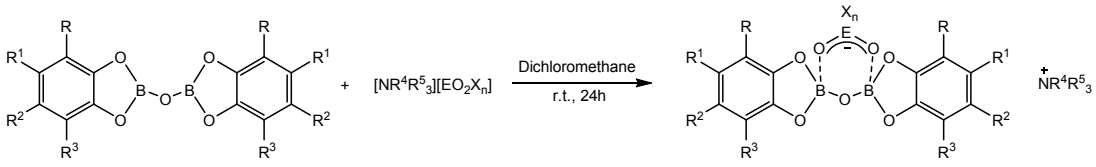
Scheme 5.5 Possible formation of fluorinated compound upon reaction with TMAF.

In order to further probe the effect of different anions, $(catB)_2O$ was also reacted with tetra-*n*-butylammonium bromide. However, unlike that observed for the reaction with TMAF, no reaction took place between these species, with the NMR spectra of the resulting white residue remaining unchanged from that of the starting materials. This suggests that the bromide anion is less reactive than the dihydrogen phosphate, *n*-butylphosphate and fluoride anions, and that the nature of the anion is key to the outcome of these reactions.

Following the synthesis of model compound **[37]**, a series of short-chain anion-bound borate compounds were synthesised utilising this methodology **[38]**-**[52]** (Scheme 5.6). This involved mixing the borate compound of interest with an ammonium salt of the desired anion in dichloromethane for 24 hours. Filtration and evaporation led to isolation of the desired product in most cases, although trituration with hexane was sometimes required.

A variety of pyroborate compounds and anions were utilised to probe the scope of this reaction (Table 5.2), and to investigate the effect of changing the pyroborate, ammonium and anion components on the resulting compounds. Pyroborate

compounds which were found to exhibit very low Lewis acidity (see Chapter III) proved to be entirely unreactive in anion-binding reactions, indicating that it is indeed the Lewis acidity of the boron centres which drive these reactions forward. Attempts were made to bind anions to the benzyl pyroborate **[12]**, as it did exhibit some Lewis acidity, but these reactions did not to go to completion, and so were not investigated further. Following this, pyroborates were only reacted with anions if they were deemed to be sufficiently Lewis acidic according to the Gutmann-Beckett method.



Scheme 5.6 Synthesis of model anion-bound borate compounds.

Table 5.2 Model anion-bound borate compounds.

	EO_2X_n	R	R^1	R^2	R^3	R^4	R^5	R^6	R^7	R^8
[37]	$R^6R^7PO_4$	H	H	H	H	H	^{n}Bu	H	^{n}Bu	-
[38]	$R^6R^7PO_4$	H	H	H	H	H	Et	H	^{n}Bu	-
[39]	$R^6R^7PO_4$	H	H	H	H	^{n}Bu	H	H	^{n}Bu	-
[40]	$R^6R^7PO_4$	H	H	Me	H	H	^{n}Bu	H	^{n}Bu	-
[41]	$R^6R^7PO_4$	H	H	H	OMe	H	^{n}Bu	H	^{n}Bu	-
[42]	$R^6R^7PO_4$	Br	Br	Br	Br	H	^{n}Bu	H	^{n}Bu	-
[43]	$R^6R^7PO_4$	H	Naph	Naph	H	H	^{n}Bu	H	^{n}Bu	-
[44]	$R^6R^7PO_4$	H	H	H	H	H	^{n}Bu	H	^{i}Bu	-
[45]	$R^6R^7PO_4$	H	H	H	H	H	^{n}Bu	^{n}Bu	^{n}Bu	-
[46]	CO_2R^8	H	H	H	H	^{n}Bu	^{n}Bu	-	-	Me
[47]	CO_2R^8	H	H	H	OMe	^{n}Bu	^{n}Bu	-	-	Me
[48]	CO_2R^8	H	H	H	H	^{n}Bu	^{n}Bu	-	-	Ph
[49]	CO_2R^8	H	H	H	OMe	^{n}Bu	^{n}Bu	-	-	Ph
[50]	SO_4Me	H	H	H	H	^{n}Bu	^{n}Bu	-	-	-
[51]	SO_4Me	H	H	H	OMe	^{n}Bu	^{n}Bu	-	-	-
[52]	NO_3	H	H	H	H	^{n}Bu	^{n}Bu	-	-	-

5.3.1.3 Synthesis of Alkylphosphate-bound Model Compounds

As the main focus of this study was the synthesis and analysis of phosphate-bound borate compounds, a series of alkylphosphate-bound compounds **[37]-[45]** were synthesised *via* variation of the pyroborate, alkylphosphate and ammonium counterion components. As changes to the substituents of the pyroborate species were found to dramatically affect their resulting Lewis acidity (see Chapter III), modification of this component was of particular interest. Therefore, analogues of **[37]** were synthesised initially which varied only the pyroborate component: **[40]-[43]**.

The $^{11}B\{^{1}H\}$ NMR spectra of these compounds are very similar to that of **[37]**, with peaks at *ca.* 14, 6, −2 and −4 ppm being observed in each case. With the exception of **[42]**, the peaks at *ca.* 14 ppm are broader than those observed for the analogous four-coordinate bis-borate species (see Chapter IV), suggesting interconversion between these compounds in solution and their corresponding anion-bound species (Table 5.3). **[42]** is derived from the least Lewis acidic pyroborate in this series of anion-bound compounds (*vide supra*), and so it is possible that **[42]** is less favourably formed than the corresponding four-coordinate species **[29]**. Therefore, less interconversion between these compounds takes place in solution, resulting in the lower $\nu_{1/2}$ of 43.6 Hz.

Similar to **[37]**, compounds **[40]-[43]** contain very broad peaks in their $^{31}P\{^{1}H\}$ NMR spectra at −15.17-17.71 ppm, indicative of binding of the *n*-butylphosphate anion.[207] The $^{31}P\{^{1}H\}$ NMR spectra of **[40]** and **[43]** exhibit a sharp peak in the centre of the broad resonances observed, which may correspond to catechol-free

Table 5.3 Comparison of line widths at half height $\nu_{1/2}$ (Hz) of $^{11}B\{^{1}H\}$ signals of different borate species ($\delta B \approx 14$ ppm).

Diol	***n*-**Butylphosphate-bound species	Four-coordinate bis-borate
Catechol	66.8	36.6
4-Methylcatechol	36.6	30.8
3-Methoxycatechol	32.7	28.9
Tetrabromocatechol	43.6	69.3
1,2-Dihydroxynaphthalene	65.5	48.1

borate-phosphate species, which is supported by the peaks at −1.5-3.8 ppm in the $^{11}B(^{1}H)$ NMR spectra of these compounds, and follows that observed for **[37]**.

As the ^{1}H NMR spectrum of **[37]** contains overlapping peaks for the *n*-butylammonium and *n*-butylphosphate components of the compound, alternative ammonium counterions were utilised to see if these could be resolved. Indeed, when triethylammonium mono-*n*-butylphosphate was used to prepare **[38]**, separate ^{1}H NMR resonances for the ammonium and phosphate components were observed. This further indicates that the *n*-butylphosphate-bound species is present, as there is clear evidence of the phosphate protons. As for **[37]**, peaks are observed in the $^{11}B\{^{1}H\}$ NMR spectrum of **[38]** at 14.7, 6.1, −1.8 and −3.6 ppm, with a large peak at 21.7 ppm suggesting a higher proportion of unbound pyroborate in solution. This was investigated further *via* a low temperature NMR experiment, where the $^{11}B\{^{1}H\}$ NMR spectrum of **[38]** in CD_2Cl_2 was run at room temperature and −70 °C (Figure 5.19). At −70 °C, the peak at 21.7 ppm is almost entirely attenuated, confirming that this

corresponds to unbound pyroborate during loss of the *n*-butylphosphate at room temperature, which is frozen out at this lower temperature. Upon returning to room temperature, the spectrum returns to its original state, indicating that this process is reversible. As with the majority of phosphate-bound compounds discussed above, the peak at 14.7 ppm is broader than that exhibited by the analogous four-coordinate bis-borate **[18]**, exhibiting a $\nu_{1/2}$ of 191.6 *vs* 31.8 Hz. This indicates that there is a significant amount of fluxionality in solution, as the *n*-butylphosphate-bound compound interchanges with other species, which aligns well with the large proportion of unbound pyroborate at room temperature. Further confirmation that binding has taken place is present in the $^{31}P\{^{1}H\}$ NMR spectrum of **[38]**, where a peak is present at −17.26 ppm, indicative of a phosphate-bound species.[207]

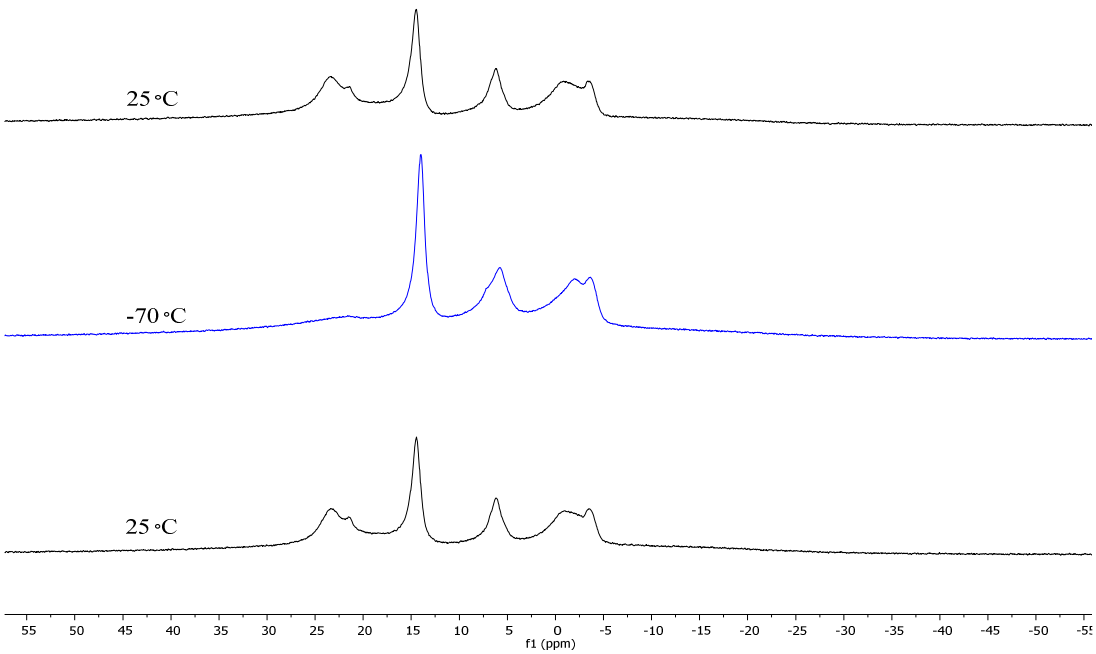


Figure 5.19 $^{11}B\{^{1}H\}$ NMR spectra of [38] at 25 °C and −70 °C.

Moreover, the CHN elemental analysis of **[38]** agrees very well with the predicted values for the proposed formulation.

Following this, a model compound incorporating a primary ammonium counterion derived from 1-butylamine was synthesised, **[39]**, in order to investigate what affect this had on the resulting product composition. Notably, the $^{11}B\{^{1}H\}$ NMR spectrum of **[39]** does not contain a peak at *ca.* 14 ppm, which would correspond to the analogous four-coordinate bis-borate. Instead, peaks are present at 20.4, 6.0 and −1.0 ppm, most likely corresponding to unbound pyroborate, *n*-butylphosphate-bound species **[39]** and a catechol-free bis-borate such as $[H_3N^nBu][B(^nBuPO_4)_2]$, respectively. This is surprising, as the corresponding four-coordinate bis-borate **[21]** is readily accessible (see Chapter IV). Furthermore, the resonance at 6.0 ppm is by far the dominant peak in the spectrum, suggesting a higher ratio of this species in solution, although it must be noted that $^{11}B\{^{1}H\}$ NMR is not strictly quantitative. Surprisingly, given that the four-coordinate bis-borate is not present in solution, the ^{1}H NMR spectrum of **[39]** is very poorly resolved, and shows the presence of several species, as there are twice as many aromatic protons as would be expected and three peaks corresponding to CH_3 groups. These may be attributed to the presence of the catechol-free bis-borate postulated above, which may be obscured in the ^{1}H NMR spectra of other species which contain the four-coordinate bis-borates. The lack of resolution in the peaks may arise from fast conversion between this species and **[39]**.

Finally, different phosphate moieties were incorporated into these model compounds. Firstly, *n*-butylphosphate was replaced with *i*so-butylphosphate in order to probe the effect this had on the resulting compound **[44]**, with the particular aim of providing an improved NMR handle for binding studies of this species (*vide infra*). Indeed, the ^{1}H NMR spectrum of **[44]** shows clear separation of the *i*so-butylphosphate peaks from

the *n*-butylammonium peaks, with the exception of the methyl resonances. Not only does this provide a clearer set of peaks for following in NMR titration experiments (*vide infra*), it indicates that the desired anion-bound species has been formed, as the *i*so-butylphosphate peaks are clearly present. Furthermore, the methylene and methine resonances are partially attenuated, integrating to 1.3 and 0.4 protons respectively, presumably a consequence of coupling to the quadrupolar ^{11}B nucleus. The $^{11}B\{^1H\}$ NMR spectrum of **[44]** is very similar to those described above, containing peaks at 14.0, 6.2, −1.7 and −3.2 ppm, most likely corresponding to four-coordinate bis-borate **[18]**, the *i*so-butylphosphate-bound species **[44]** and two catechol-free borate-phosphate species (*vide supra*). Again, the peak at 14 ppm is broader than that observed for four-coordinate bis-borate **[18]**, affording a $\nu_{1/2}$ of 44.9 *vs* 36.6 Hz, suggesting interconversion between boron-containing species in solution. A broad peak at −16.78 ppm in the $^{31}P\{^1H\}$ NMR spectrum of **[44]** further suggests binding of the *i*so-butylphosphate anion.[207] Moreover, CHN elemental analysis agrees very well with predicted values, indicating the desired composition of **[44]** in the solid-state.

Following this, di-*n*-butylphosphate was investigated as an anion for binding to $(catB)_2O$ in order to probe what affect, if any, two alkyl substituents may have on the resulting anion-bound compound **[45]**. The $^{11}B\{^1H\}$ NMR spectrum of **[45]** is very similar to those described above, containing peaks at 13.8, 6.6, 0.7 and −1.0 ppm, which may correspond to four-coordinate bis-borate **[18]**, the di-*n*-butylphosphate-bound species **[45]** and two catechol-free borate-phosphate species (*vide supra*). Again, the peak at *ca.* 14 ppm is broader than that observed for four-coordinate bis-borate **[18]**, affording a $\nu_{1/2}$ of 96.3 *vs* 36.6 Hz, and suggesting interconversion between boron-containing species in solution. The dynamics of this system were investigated using high temperature NMR spectroscopy. $^{11}B\{^1H\}$ NMR spectra of **[45]** were

recorded at 25 and 50 °C (Figure 5.20). This species was found to behave in a similar manner to the mono-*n*-butylphosphate analogue **[37]**, as the small peak at *ca.* 21 ppm increased in intensity at 50 °C, due to an increased level of dissociation of the di-*n*-butylphosphate anion from one of the boron centres, indicating exchange between the two boron atoms occurs more rapidly at elevated temperatures. Furthermore, the resonance at 6.6 ppm is slightly reduced, further suggesting dissociation of the bound di-*n*-butylphophate.

Notably, the peak at in the $^{31}P\{^{1}H\}$ NMR spectrum of **[45]** is narrower than those discussed above ($\nu_{1/2}$ = 130 Hz) and is significantly downfield of those previously described, being observed at −5.90 ppm. This may be indicative of weaker binding of the anion, which would result less shielding of the phosphorus centre by the

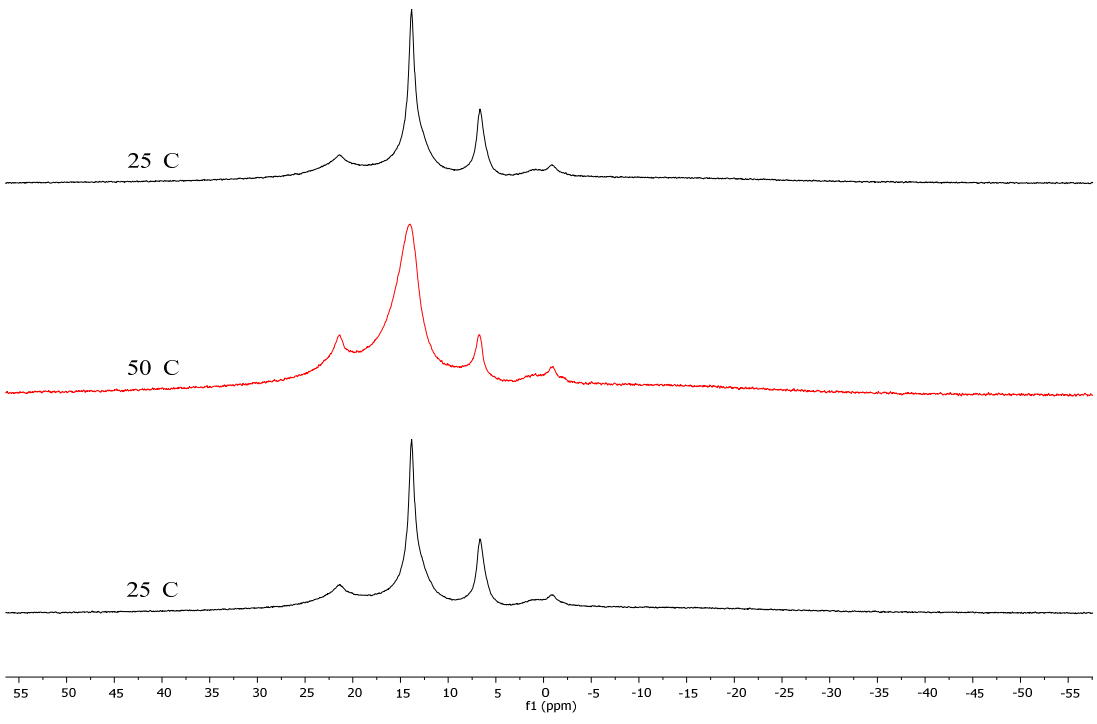


Figure 5.20 $^{11}B\{^{1}H\}$ NMR spectra of [45] at 25 °C and 50 °C.

delocalization of electrons around the anion, and less coupling to the quadrupolar ^{11}B nucleus. CHN elemental analysis agrees very well with predicted values, indicating the desired composition of **[45]** in the solid-state.

5.3.1.4 Synthesis of Other Anion-bound Model Compounds

In order to explore the scope of pyroborate compounds as anion receptor molecules, reactions were carried out to bind carboxylate, sulfonate and nitrate anions with **[1]** and **[3]** to give **[46]**-**[52]**. Although these reactions cannot be monitored by $^{31}P\{^1H\}$ NMR spectroscopy, the binding of carboxylate and sulfonate anions may be monitored by ^1H and $^{13}C\{^1H\}$ NMR spectroscopy, due to the presence of methyl or phenyl substituents on the anions. As the nitrate anion contains no additional NMR handle, the composition of reaction product **[52]** must be inferred through monitoring of the $^{11}B\{^1H\}$ NMR spectrum, inspection of the cation resonances in the ^1H and $^{13}C\{^1H\}$ NMR spectra and CHN elemental analysis. As $(catB)_2O$ has previously been shown to react with [PPN][AcO] to give an acetate-bound product,[149] a reaction between this pyroborate and $[N^nBu_4][AcO]$ was carried out. This would provide the analogous alkylammonium acetate species **[46]** to the phosphate compounds previously discussed. Evidence of successful binding of the acetate anion is present in the ^1H NMR spectrum of **[46]**, where the peak corresponding to the methyl group of the acetate anion is shifted downfield from 1.98 to 2.15 ppm, with significant broadening being observed ($\nu_{1/2}$ 18 *vs* 0.9 Hz). A similar shift was observed in the reaction of $(catB)_2O$ with [PPN][AcO].[149] Furthermore, the peak in the $^{13}C\{^1H\}$ NMR spectrum of **[46]** corresponding to the quaternary carbonyl substituent is shifted significantly downfield from 175.9 to 218.6 ppm, indicating binding of the acetate anion.[149]

The $^{11}B\{^{1}H\}$ spectrum of **[46]** contains peaks at 21.8, 14.3 and 9.8 ppm, which may correspond to unbound pyroborate, four-coordinate bis-borate **[36]** and acetate-bound species **[46]** in solution. There is also a peak at 2.4 ppm which, like the phosphate analogues described above, may be attributed to a catechol-free borate-acetate species, as this chemical shift is similar to those described for tetrakis(haloacyloxy)borates.[238] Again, the peak at 14 ppm is broader than that observed for four-coordinate bis-borate **[36]** ($\nu_{1/2}$ 42.4 *vs* 36.6 Hz), indicating conversion between this species and other boron-containing compounds in solution. CHN elemental analysis agrees very well with predicted values, indicating the desired composition of **[46]** in the solid-state.

The effect of using a more Lewis acidic pyroborate for this reaction was probed *via* a reaction between $(3\text{-MeOcatB})_2O$ and $[N^nBu_4][AcO]$ to give **[47]**. Evidence of successful binding of the acetate anion is present in the ^{1}H NMR spectrum of **[47]**, where the peak corresponding to the methyl group of the acetate anion is shifted downfield from 1.98 to 2.13 ppm, with significant broadening again being observed ($\nu_{1/2}$ 18 *vs* 0.9 Hz). Furthermore, the peak in the $^{13}C\{^{1}H\}$ NMR spectrum of **[46]** corresponding to the quaternary carbonyl substituent is shifted further downfield than that observed for **[46]**, from 175.9 to 222.5 ppm, indicating a greater withdrawal of electrons from these more Lewis acidic boron centres.

The $^{11}B\{^{1}H\}$ spectrum of **[47]** contains peaks at 21.9, 14.5, 10.9 and 2.3 ppm, which may correspond to unbound pyroborate, a four-coordinate bis-borate, acetate-bound species **[47]** and a catechol-free borate-acetate species, as above. Again, the peak at 14 ppm is broader than that observed for four-coordinate bis-borate **[26]** ($\nu_{1/2}$ 66 *vs* 29 Hz), indicating conversion between this species and other boron-containing compounds in solution. CHN elemental analysis agrees very well with predicted values, indicating the desired composition of **[47]** in the solid-state.

In order to investigate whether this methodology could be extended to other carboxylate anions of interest, reactions were carried out between these pyroborates and [^{n}NBu$_4$][$C_6H_5CO_2$] to give **[48]** and **[49]**. Evidence of the binding of the benzoate anion is present in the ^{1}H NMR spectrum of **[48]**, where the peaks corresponding to the benzyl protons of the anion are split and shifted downfield from two multiplets at 8.03 and 7.20 ppm to three broad, unresolved singlets at 8.12, 7.59 and 7.44 ppm, corresponding to the ortho-, para- and meta-protons respectively. The degree of broadening of these resonances is significant ($\nu_{1/2}$ 12 and 6 Hz *vs* 24, 20 and 24 Hz), and may indicate coupling to the quadrupolar ^{11}B nucleus, and fluxionality in solution. Similarly, the peaks corresponding to the CH substituents on the benzoate anion in the ^{13}C{^{1}H} NMR spectrum of **[48]** are shifted downfield from 129.5, 128.3 and 127.7 ppm to 133.8, 130.4 and 128.2 ppm. These resonances are also significantly broadened, exhibiting $\nu_{1/2}$ values of 21, 31 and 12 Hz *vs* 2 Hz for the corresponding tetra-*n*-butylammonium benzoate starting material resonances.

The ^{11}B{^{1}H} spectrum of **[48]** contains peaks at 14.3, 9.4 and 2.7 ppm, which may correspond to four-coordinate bis-borate **[36]**, benzoate-bound species **[48]** and a catechol-free borate-benzoate species, as detailed above. The ^{11}B{^{1}H} spectrum of **[49]** contains only two peaks at 14.5 and 9.4 ppm, suggesting that no conversion to a borate-benzoate occurs in solution, with only interconversion between the anion-bound species **[49]** and a four-coordinate bis-borate taking place.

The binding properties of sulfonate anions have received little attention, despite being known to form genotoxic esters,[239] and so the binding of methylsulfonate was investigated. (catB)$_2$O **[1]** and (3-MeOcatB)$_2$O **[3]** were reacted with [N^{n}Bu$_4$][SO_3CH_3] to give methanesulfonate-bound species **[50]** and **[51]**. Evidence of successful binding of the methansulfonate anion is present in the ^{1}H NMR spectrum

of **[50]**, where the peak corresponding to the methyl group of the anion is shifted downfield from 2.70 to 2.98 ppm, with broadening of the signal observed ($\nu_{1/2}$ 0.8 *vs* 4 Hz). Similarly, in the ^{1}H NMR spectrum of **[51]**, evidence of successful binding of the methansulfonate anion is present as the peak corresponding to the methyl group of the anion is shifted downfield from 2.70 to 2.99 ppm, and broadening of the signal is observed ($\nu_{1/2}$ 0.8 *vs* 3 Hz).

The ^{11}B{^{1}H} spectrum of **[50]** contains peaks at 17.1, 14.3, and 7.0, which may correspond to unbound pyroborate, four-coordinate bis-borate **[36]** and methanesulfonate-bound species **[50]**. Similarly, the ^{11}B{^{1}H} spectrum of **[51]** contains peaks at 18.2, 14.3, and 6.9, which may correspond to unbound pyroborate, four-coordinate bis-borate **[36]** and methanesulfonate-bound species **[51]**. The peak at 14.3 ppm is significantly broader than that observed for four-coordinate bis-borate **[36]** ($\nu_{1/2}$ 87 *vs* 36.6 Hz), indicating conversion between this species and other boron-containing compounds in solution. Unfortunately, an accurate $\nu_{1/2}$ for the analogous resonance could not be calculated for **[50]**, as it overlaps with the peak at 17.1 ppm. Unlike the other anions studied thus far, binding of the methanesulfonate anion appears to affect the electronics of the pyroborate moieties to a great extent, as the peaks corresponding to unbound pyroborate centres in the ^{11}B{^{1}H} spectra at 17.1 and 18.2 for **[50]** and **[51]** respectively, are shifted downfield by 5.3 and 4.0 ppm of the parent pyroborate compounds **[1]** and **[3]** respectively. This may be related to the binding affinity for this anion, which is discussed further below. CHN elemental analyses agree very well with predicted values, indicating the desired compositions of **[50]** and **[51]** in the solid-state.

The nitrate anion was investigated for its binding to pyroborate compounds *via* a reaction between [N^{n}Bu$_4$][NO$_3$] with (catB)$_2$O to give **[52]**. As there is no additional

NMR handle on this anion, explicit binding studies could not be carried out, but characterisation of the resulting compound can indicate the composition of the species. The ^{1}H NMR spectrum of **[52]** does give some indication of binding, as the peaks corresponding to starting pyroborate $(catB)_2O$ **[1]** have been shifted upfield from 7.23 and 7.11 ppm to a broad resonance at 6.58-6.67 ppm. Furthermore, the peaks corresponding to the tetra-*n*-butylammonium cation have been shifted upfield by 0.28, 0.18, 0.11 and 0.05 ppm, and resolution of the multiplets has been lost. The $^{11}B\{^{1}H\}$ NMR spectrum of **[52]** contains peaks at 14.2, and 6.8 ppm, which may correspond to four-coordinate bis-borate **[36]** and nitrate-bound species **[52]**. It is possible that there are in fact two sets of species present in solution, as there is a small shoulder observed at 14.7 ppm, and another small peak at 8.0 ppm. This is not observed for any of the other anions considered in this study, and may indicate that the nitrate anion interacts with the pyroborate compound in a different way to those previously described. CHN elemental analysis agrees very well with predicted values, indicating the desired composition of **[52]** in the solid-state.

5.3.2 Anion Binding Studies of Model Compounds

The binding of a selection of these model compounds was investigated further *via* ^{1}H NMR spectroscopy. As it would appear that fast exchange is occurring on the NMR timescale in these systems, the spectra observed are time-averaged resonances of the pyroborate, anion and anion-bound complexes. Therefore, the observed ^{1}H chemical

$$(5)\ K = [Complex]/[Receptor][Anion]$$

Equation 5. Relation of binding constant (K) to concentrations of the complex, receptor and anion in the mixture.

shift (δ_{obs}) is the mole fraction weighted average of the shifts observed in the free and complexed species ($\delta_{complex}$). Furthermore, the value of the binding constant for these associations depends on the equilibrium concentrations of all species present in the solution (Equation 5). As the identity of $\delta_{complex}$ and [Complex] are unknown, they may be calculated through a series of measurements at different concentrations of starting species, and the data fitted *via* a curve-fitting procedure.[229a]

5.3.2.1 Binding Stoichiometry

Before the binding strengths of pyroborate-anion pairs were calculated, their binding stoichiometries were first investigated *via* the method of continuous variation (*i.e.* the construction of Job plots).[229] A representative example of such a plot is shown in Figure 5.20, indicating where the maxima may be located for differing binding stoichiometries. These data can be found in Appendix II.

5.3.2.1.1 Binding Stoichiometry of Alkylphosphates

The Job plot of $(catB)_2O$ **[1]** with $[HN^nBu_3][H^nBuPO_4]$ contains two maxima at *ca.* 0.4 and 0.7 mole fraction of **[1]**, suggesting the presence of complexes containing 2:1 and 1:2 ratios of *n*-butylphosphate to pyroborate respectively.[229b] This correlates with the NMR data discussed above, indicating the presence of a complex mixture of species in solution and suggesting a combination of 1:1 and 2:1 binding modes may be taking place in the association of $H^nBuPO_4^-$ to **[1]**.

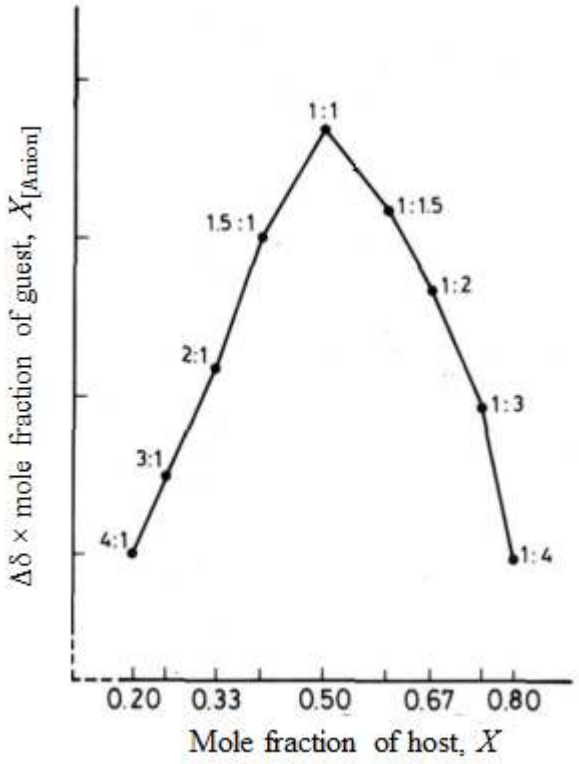


Figure 5.21 Representative Job plot, indicating the location of maxima for a variety of binding stoichiometries.

Although 1:1 binding of dihydrogen phosphate and pyrophosphate anions has been previously reported,[210, 240] there is literature precedent for 2:1 binding of $H_2PO_4^-$ and similar anions, and complex mixtures of the two modes. Indeed, 2:1 binding appears to be particularly prevalent for $H_2PO_4^-$, as this binding mode has been reported for this anion in receptor molecules which bind other anions in the expected 1:1 mode.[241] Beer and co-workers reported the 2:1 binding of $H_2PO_4^-$ to a ruthenium(II) bipyridyl-bis(ferrocene) receptor, which was attributed to the dimerization of the anion in solution.[205] Such dimerization is known for $H_2PO_4^-$, and has been reported previously.[206, 217] Furthermore, the formation of 2:1 guest-to-host complexes has previously been reported for the binding of organic phosphodiesters to polyaza-receptors due to significant dimerization of the phosphodiester guest species.[242] This

was found to be exacerbated *via* hydrogen bonding of the phosphate hydroxyl groups to pyridyl moieties in the receptor, and so it is conceivable that hydrogen bonding interactions between $H^nBuPO_4^-$ and the tri-*n*-butylammonium counterion is increasing the extent of dimerization of the anion, contributing to the degree of 2:1 binding present in solution. It is conceivable, therefore, that the 2:1 binding mode is due to binding of a dimer of $H^nBuPO_4^-$ to **[1].** However, it is also possible that the formation of a catechol-free borate-phosphate species postulated in the above discussion is contributing to this behaviour.

1:2 guest-to-host complexes of $H_2PO_4^-$ and similar anions have also been previously reported. Hamilton and co-workers described the complex formation of a sandwich involving two macrocycles binding through hydrogen bonding interactions to dihydrogen phosphate, hydrogen sulfate, nitrate and halide anions.[209a] It was postulated that the even charge distribution in these anions is responsible for their ability to bind to more than one receptor. Furthermore, Kubo *et al.* attributed the formation of a 1:2 guest-to-host complex between an isothiouronium host species and HPO_4^{2-} to the tetrahedral shape of the anion, as this was not observed for the planar acetate anion.[243] Beer *et al.* have reported the binding of $H_2PO_4^-$ to osmium(II) bipyridyl rotaxanes to be so complex that binding studies could not be carried out for this anion.[244] It is unsurprising, then, considering this literature precedence, that both 1:2 and 2:1 guest-to-host binding modes appear to be present in the binding of $[HN^nBu_3][H^nBuPO_4]$ by **[1]**.

Similar binding modes are observed for the binding of the *iso*-butylphosphate anion by **[1]**, as Job plots for this interaction contain two maxima at *ca.* 0.3 and 0.6, suggesting both 2:1 and 1:2 guest-to-host binding modes are taking place in solution respectively. These were carried out using both the α- and β-CH_2 groups on the *iso*-

butyl substituent to determine whether moving further away from the quadrupolar boron nuclei gave sharper ^{1}H NMR signals and therefore more a resolved Job plot. Slightly sharper maxima were given in the latter case, but they provided the same conclusions as did monitoring the α-protons.

The Job plot of the binding of **[1]** with $^{n}Bu_2PO_4^-$ differs slightly, as two maxima are observed at 0.5 and 0.7, suggesting the presence of 1:1 and 1:2 guest-to-host complexes. This may be attributed to the lack of hydrogen bond donors on the di-*n*-butylphosphate anion, preventing dimerization and formation of a 2:1 guest-to-host complex. This suggests that the presence of 1:2 guest-to-host complexes is indeed due to dimerization of the *n*-butylphosphate anions, as found for dihydrogen phosphate the literature.[205, 242] Furthermore, it would then appear that the desired 1:1 complex is accessible when dimerization of the anion is not taking place. A similar mixture of 1:1 and 2:1 binding modes was reported for the binding of dibenzylphosphate to a bisguanidine receptor, and it was found that addition of D_2O to the mixture led to only 1:1 binding taking place, due to increased solvation of the anion.[245]

A combination of all three of these binding modes appears to be present in the binding of $[HN^{n}Bu_3][H^{n}BuPO_4]$ to $(3\text{-MeOcatB})_2O$ **[3]**, as three maxima are present at 0.3, 0.5 and 0.8. This suggests that increasing the Lewis acidity of the pyroborate increases the complexity of the binding take place. The shift in the second maximum to 0.8 may indicate that up to four pyroborate receptors are interacting with one *n*-butylphosphate anion. Similarly, the more Lewis acidic $(\text{Naph-1,2-}O_2B)_2O$ **[10]** gives a Job plot containing one sharp maximum at 0.8 and another broad maximum between 0.3 and 0.5, suggesting a combination of 2:1, 1:1, 1:2 and 1:4 guest-to-host complexes are present in solution.

Complex binding modes such as these may be better resolved using UV/vis spectroscopy titrations, as much lower concentrations are required. However, these systems are currently unsuitable for this analysis as, lacking UV/vis reporter substituents, these pyroborates do not exhibit transitions which are easily monitored within the operational window of wavelengths of UV/vis spectroscopy.

5.3.2.1.2 Binding Stoichiometry of Other Anions

The binding of AcO^- to both **[1]** and **[3]** gives Job plots containing single sharp peaks at *ca*. 0.4, which may indicate the presence of a 2:1 guest-to-host complex in solution. Although the binding of acetate anions is generally less complex than that of dihydrogen phosphate, with 1:1 binding being reported in most cases,[240c, 246] there is some literature precedence for the formation of 2:1 species. Huang *et al.* report the binding of two acetate anions to one phosphonium anthracene receptor, due to the presence of two phosphonium centres in the species and the complementary shape of the anion over other oxoanions.[247] Moreover, the dicationic isothiouronium receptor which was found to bind $H_2PO_4^-$ in a 2:1 fashion was found to bind AcO^- in a 1:2 guest-to-host mode, which is explained through the different shapes of the anions. It is therefore unsurprising that pyroborates **[1]** and **[3]** demonstrate somewhat different binding behaviour with acetate over dihydrogen phosphate. Furthermore, there are examples of reported 1:1 binding of acetate which present Job plots which lean towards 0.4,[240a, 248] suggesting that 2:1 binding may be also occurring to some extent in these systems. It is conceivable the Job plot in the binding of AcO^- to **[1]** and **[3]** is skewed towards 0.4 due to the presence of a small concentration of the catechol-free borate-acetate implicated by the $^{11}B\{^1H\}$ NMR spectra of **[46]** and **[47]**.

The binding of benzoate appears to be more straightforward, as Job plots for the binding of this anion to **[1]** and **[2]** both show maxima at 0.5, indicative of 1:1 binding. There are no examples of the construction of Job plots to establish binding stoichiometry of benzoate in the literature, but 1:1 binding models have been successfully used to fit titration data in benzoate binding experiments, suggesting this binding mode is typical for this anion.[249] The different binding modes of these two carboxylate anions may be related to their corresponding binding affinities to **[1]** and **[3]** with this anion *versus* those with acetate, which is discussed below.

Similarly, the binding of SO_3Me^- to pyroborate **[1]** appears to follow a 1:1 binding stoichiometry, as the Job plot of this interaction contains a peak at 0.5. No Job plots of the binding of SO_3Me^- have been published, but the binding of this anion with macrocyclic azole amides has been studied assuming 1:1 stoichiometry.[248] Furthermore, studies of the binding of hydrogen sulfate, HSO_4^-, have reported 1:1 binding stoichiometries, although no Job plots have been published.[200b, 250] Moreover, binding of the similar *p*-tosylate anion by rigid macrocyclic amide receptors resulted in 1:1 binding, as confirmed by Job plot.[209b] Notably, there is seemingly no catechol-free borate-methanesulfonate species present in this system, implicated by the $^{11}B\{^1H\}$ NMR spectrum of **[50]** discussed above, which may explain the lack of any 2:1 binding between **[1]** and the methanesulfonate anion in solution.

5.3.2.2 NMR Titrations

The binding of pyroborates **[1]** and **[3]** with various anions was investigated using NMR titration studies. The resulting data was put through the WinEQNMR2 program in order to generate titration curves and binding constants for these interactions (Table 5.4).[230] Titration curves for these data can be found in Appendix II. As the

intereactions of pyroborates with phosphate-containing anions proved to involve a complex array of binding modes, NMR studies of these were not taken further, as the resulting data would have been unreliable.

The binding constants for the interactions between pyroborates **[1]** and **[3]** with acetate are of the same order of magnitude as those presented by several molecular receptors reported in the literature.[215, 240a, 248-249, 251] However, several hydrogen bonding receptors have exhibited binding constants of greater than 10^4 M^{-1},[241a, 246a, 246b, 246d] perhaps indicating that Lewis acid-base interactions are less efficient at binding acetate than hydrogen bonding receptors. The two binding constants are equal within error, suggesting the small difference in Lewis acidity between **[1]** and **[3]** is insufficient to effectively alter the binding affinity of these species for acetate. Although Job plot analyses suggested some 2:1 guest-to-host binding present in these systems, the titration curves for both **[1]** and **[3]** binding to acetate closely resemble a 1:1 system (see Appendix II), suggesting that the 1:1 binding mode is dominant.

Table 5.4 Binding constants (M^{-1}) for the binding of various anions to pyroborates [1] and [3].

Pyroborate	AcO^-	$PhCO_2^-$	SO_3Me^-
[1]	1945 ± 442	995 ± 14	2783 ± 123
[3]	1932 ± 447	1192 ± 29	-

There is a lower binding affinity of the benzoate anion to pyroborates **[1]** and **[3]**, as shown by the lower binding constants of 995 ± 14 M^{-1} and 1192 ± 29 M^{-1} respectively. This may be attributed to the lower basicity of the benzoate anion when compared to

acetate, as the binding strength of these anions may depend on hydrogen bonding interactions with the pyroborate receptor. These binding constants are consistent with many reported in the literature for the binding of benzoate.[249a, 250-251, 252] The only significantly stronger binder of benzoate is a family of simple hydrogen bonding indolocarbazoles reported by Beer and co-workers,[203] which highlight the dramatic effect preorganization of the receptor can have on the resulting binding affinity.

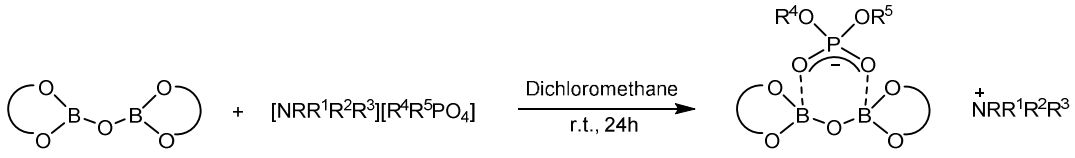
The difference in Lewis acidity between **[1]** and **[3]** appears to have the most marked effect on the binding of benzoate. Although there is no direct comparison in the literature, it has been found that the addition of electron-withdrawing substituents on naphthalene urea derivatives strengthens the binding of benzoate significantly,[249b] and so it may be inferred that the addition of the electron-withdrawing methoxy substituents achieve the same result here.

Pyroborate **[1]** appears to display a strong affinity for methanesulfonate above the other two anions, with this interaction giving the largest binding constant of 2783 ± 123 M^{-1}. This is significantly larger than the binding constants reported for the same anion by macrocyclic azole amides in 95:5 d-DMSO/$CDCl_3$ (13-150 M^{-1}),[248] suggesting that a Lewis acid receptor such as **[1]** is a more efficient binder for this anion. Furthermore, this value is higher than many molecules reported for the binding of the related hydrogen sulfate anion which display higher affinity to other anions,[204, 210, 246a, 246b, 249a, 251a] possibly suggesting that binding of these anions occurs *via* a different mode to similar oxoanions. Indeed, receptors that bind the hydrogen sulfate anion very strongly (>10^6) are highly selective to HSO_4^- and SO_4^{2-},[253] indicating that there may be a difference in binding mode between these and other oxoanions with similar geometries, such as $H_2PO_4^-$.

5.3.3 Synthesis of Long-chain Anion-bound Compounds

In order to extend this methodology for the application of lubricant additives, long-chain alkyl substituents were incorporated into the phosphate, pyroborate and ammonium components of these species (Table 5.5). Phosphate-bound compounds were the primary focus, as phosphorus-containing compounds are of significant interest as lubricant additives (see Chapter I).

Various long-chain substituents were employed, so as to study the effect these had on the resulting lubricating performance of the compounds. For maximum oil solubility initially, (4-PIB$_{1000}$cat)B$_2$O **[7]** was utilised in combination with a range of ammonium alkylphosphates to give compounds **[53]-[66]**. As a starting point, **[7]** was reacted with [HN^{n}Bu$_3$][H^{n}BuPO$_4$] to provide an analogous long-chain analogue



Scheme 5.7 Synthesis of long-chain phosphate-bound borate compounds.

Table 5.5 Long-chain phosphate-bound borate compounds.

		**R**	**R^1**	**R^2**	**R^3**	**R^4**	**R^5**
[53]	PIB_{1000}cat	H	^{n}Bu	^{n}Bu	^{n}Bu	H	^{n}Bu
[54]	PIB_{1000}cat	H	H	2-EtC_6H_{12}	2-EtC_6H_{12}	H	^{n}Bu
[55]	PIB_{1000}cat	H	^{n}Bu	^{n}Bu	^{n}Bu	H	2-EtC_6H_{12}
[56]	PIB_{1000}cat	H	H	2-EtC_6H_{12}	2-EtC_6H_{12}	H	2-EtC_6H_{12}
[57]	PIB_{1000}cat	H	H	H	2-EtC_6H_{12}	H	2-EtC_6H_{12}
[58]	PIB_{1000}cat	H	2-EtC_6H_{12}	2-EtC_6H_{12}	2-EtC_6H_{12}	H	2-EtC_6H_{12}
[59]	PIB_{1000}cat	H	H	H	$C_{12}H_{25}$	H	2-EtC_6H_{12}
[60]	PIB_{1000}cat	H	^{n}Bu	^{n}Bu	^{n}Bu	H	^{n}Oct
[61]	PIB_{1000}cat	H	H	2-EtC_6H_{12}	2-EtC_6H_{12}	H	^{n}Oct
[62]	PIB_{1000}cat	H	^{n}Bu	^{n}Bu	^{n}Bu	2-EtC_6H_{12}	2-EtC_6H_{12}
[63]	PIB_{1000}cat	H	H	2-EtC_6H_{12}	2-EtC_6H_{12}	H	Oleyl
[64]	PIB_{1000}cat	H	H	2-EtC_6H_{12}	2-EtC_6H_{12}	H	$C_{13}H_{27}$
[65]	PIB_{1000}cat	H	H	H	2-EtC_6H_{12}	H	$C_{13}H_{27}$
[66]	PIB_{1000}cat	H	2-EtC_6H_{12}	2-EtC_6H_{12}	2-EtC_6H_{12}	H	$C_{13}H_{27}$
[67]	GMO	H	H	2-EtC_6H_{12}	2-EtC_6H_{12}	H	^{n}Bu

[68]	$PIB_{550}cat$	H	^{n}Bu	^{n}Bu	^{n}Bu	H	^{n}Bu
[69]	$PIB_{550}cat$	H	H	$2\text{-}EtC_6H_{12}$	$2\text{-}EtC_6H_{12}$	H	$2\text{-}EtC_6H_{12}$
[70]	$PIB_{550}cat$	H	^{n}Bu	^{n}Bu	^{n}Bu	H	$2\text{-}EtC_6H_{12}$
[71]	$(C_{16}\text{-}C_{18})cat$	H	H	$2\text{-}EtC_6H_{12}$	$2\text{-}EtC_6H_{12}$	H	$2\text{-}EtC_6H_{12}$
[72]	$C_{12}H_{25}cat$	H	H	$2\text{-}EtC_6H_{12}$	$2\text{-}EtC_6H_{12}$	H	$2\text{-}EtC_6H_{12}$
[73]	$C_{12}H_{25}cat$	H	H	$2\text{-}EtC_6H_{12}$	$2\text{-}EtC_6H_{12}$	H	Oleyl
[74]	$C_{12}H_{25}cat$	H	$2\text{-}EtC_6H_{12}$	$2\text{-}EtC_6H_{12}$	$2\text{-}EtC_6H_{12}$	H	^{n}Bu
[75]	cat	H	$2\text{-}EtC_6H_{12}$	$2\text{-}EtC_6H_{12}$	$2\text{-}EtC_6H_{12}$	H	$C_{13}H_{27}$

of model compound **[37]**, **[53]**. Following this, the length of the alkyl chain on the pyroborate component was continually shortened and combined with a selection of different ammonium alkylphosphate species to give a range of compounds for testing, **[68]**-**[75]** (see Chapter VI for testing parameters, results and discussion).

With the exception of **[75]**, the syntheses of these longer-chain compounds were carried out under normal atmospheric conditions, with no exclusion of air and moisture necessary, as the starting pyroborates **[6]**-**[9]** and **[17]** are air-stable. This allowed for quicker and more convenient isolation of these compounds. However, it must be noted that the high viscosity of these species presents some difficulty in their handling. As most of these species were prepared from starting materials of varying composition which contain a large number of aliphatic protons and carbons, particularly the broadly polydisperse PIB derivatives, ^{1}H and $^{13}C\{^{1}H\}$ NMR spectroscopies were not useful in

the characterisation of these species. Therefore, analysis was focused on $^{11}B\{^{1}H\}$ and $^{31}P\{^{1}H\}$ NMR spectroscopies and ICP-OES elemental analysis.

For the majority of these compounds, their $^{11}B\{^{1}H\}$ NMR spectra are similar to those of the model compounds discussed above, with three resonances being observed at 13.7-14.2, 5.6-6.4 and −3.0-3.4 ppm. As observed for compound **[39]** discussed above, compounds incorporating primary ammonium counterions (**[57]**, **[59]** and **[65]**) do not contain a peak in their $^{11}B\{^{1}H\}$ NMR spectra at *ca.* 14 ppm, which would correspond to a four-coordinate bis-borate species. Conversely, bis-(2-ethylhexyl)phosphate-containing compound **[62]** only exhibits a $^{11}B\{^{1}H\}$ signal at 14.0 ppm, suggesting that a four-coordinate bis-borate is the most stable boron-containing species in solution for this sample. This may be due to the two sterically-encumbered 2-ethylhexyl chains on the phosphate moiety preventing strong binding of the phosphate from taking place, leading to a high rate of dissociation in solution.

Typically, compounds exhibited single broad resonances in their $^{31}P\{^{1}H\}$ NMR spectra between −4.78 and −17.59 ppm, indicative of binding of the alkylphosphate component.[207] Many of these peaks were shifted less upfield than the model examples discussed above, suggesting that the addition of long alkyl chains to the pyroboborate substituents may weaken the binding strength of the boron centres, leading to weaker interaction with the alkylphosphate anions. This is corroborated by the lower ANs observed for long-chain pyroborates **[6]**-**[8]** discussed in Chapter III, indicating reduced Lewis acidity in these species. Compounds **[54]**, **[62]**, **[68]**, **[69]** and **[70]** exhibit additional resonances in their $^{31}P\{^{1}H\}$ NMR spectra at −0.11-1.14 ppm, suggesting the presence of the alkylphosphate starting material. It is possible that the long alkyl chains in these species hinder the binding of the alkylphosphate, so that

conversion between bound and unbound species is slower than that observed for the model species above, leading to the presence of unbound alkylphosphate in solution.

Furthermore, the $^{31}P\{^{1}H\}$ NMR spectra of compounds **[54]** and **[68]** contain a third peak which is shifted upfield to a lesser extent at −6.84 and −6.49 ppm respectively, indicating that there are additional alkylphosphate-bound species in solution. These resonances may be attributed to the monodentate binding of the alkylphosphate anion, as has been observed for carboxylate anions binding to similar bidentate boron Lewis acids.[143] This would involve a lower degree of delocalisation of the negative charge of the anion onto the phosphorus, resulting in less deshielding and a smaller upfield shift of the resonance. Furthermore, it is conceivable that conversion between different borate-phosphate species is slower in solution for these long-chain compounds than the analogous model compounds discussed above, and that these signals are broadened into one resonance for shorter-chain analogues.

In order to confirm the elemental composition of these species before testing was carried out, ICP-OES analysis was carried out on each sample. Generally, these were in good agreement with predicted values (± 0.5 %). When this was not the case, compounds tended to contain slightly elevated levels of phosphorus (+ 0.4-1.1 %) and lower levels of boron (− 0.1-0.9 %), suggesting the presence of a 2:1 complexed species. This corresponds well with the Job plot analyses of the model alkylphosphate-bound species discussed above. However, even with these discrepancies the levels of boron and phosphorus were well within the range of ± 10 % deemed acceptable by the Lubrizol Corporation, and were therefore taken forward for testing for lubricant performance (see Chapter VI).

As further levels of anti-friction and anti-wear testing require greater quantities of material, the scalability of these compounds was investigated. Initially, reactions were carried out on a 1 g scale, to ensure they were successful before more material was expended. It was then found that the scale of reactions could be increased firstly to 20 g, followed by 50 g with no change in the resulting NMR spectra and elemental composition. Furthermore, several reactions were carried out on 150 g scale successfully. Indeed, the only limit found in these investigations was the amount of starting material, and a scale at which these reactions fail is yet to be found. This indicates the viability of these species as commercial additives, as they can be readily produced at large scale.

5.4 Conclusions

Short-chain anion-bound pyroborate species of the general formula $\{[RO_2B)_2O][EO_2X_n]\}\{NR_4\}$ were investigated as models for the longer-chain species to be tested as lubricant additives. Focus was on phosphorus-containing species, owing to the high interest in phosphorus-based additives. Attempts to synthesise a dihydrogen-phosphate bound complex were unsuccessful, with four-coordinate bis-borate $[cat_2B][N^nBu_4]$ **[36]** being isolated. This complex was crystallographically characterised. The formation of **[36]** was investigated using NMR spectroscopy, which revealed that borate-phosphate species may be formed, broken down and reformed, depending on the ratio of each starting material in solution. Furthermore, this process appears to be unique to pyroborate species, as binding occurred successfully between $[N^nBu_4][H_2PO_4]$ and $B(OPh)_3$, which may open a new avenue of research into the synthesis of borate-phosphate species.

Investigations using alkylphosphate-bound species were more successful, with CHN and ICP elemental analysis suggesting the formation of the desired *n*-butylphosphate-bound species **[37]** in the solid state. Investigations *via* NMR spectroscopy indicated highly dynamic behaviour of this compound in solution, with interchange between **[37]**, four-coordinate bis-borate **[19]** and catechol-free borate-phosphate species taking place. Variable temperature NMR experiments indicated that the *n*-butylphosphate interchanged between boron centres at higher temperatures, and this process could be frozen out at −70 °C.

A series of other model compounds was then synthesised, **[38]**-**[52]**, with variation in the bound anion, pyroborate and ammonium counterion being carried out. Like **[37]**, they exhibited dynamic behaviour in solution, but the desired composition was found

in CHN elemental analysis. Sufficient Lewis acidity of the starting pyroborate was vital for the reactions to proceed. It was also found that primary ammonium counterions led to mixtures which do not contain a four-coordinate bis-borate species, despite this compound being synthetically accessible through other routes.

The anion-binding behaviour of a selection of these species was investigated *via* ^{1}H NMR spectroscopy. Job plot analyses suggest a high degree of complexity in the binding of alkylphosphate species, with 1:2 and 2:1 guest-to-host binding modes observed, most likely due to dimerization of the alkylphosphate anions. Shifting to a disubtituted alkylphosphate changes the binding mode to 1:1 and 1:2, as dimerization of the alkylphosphate *via* hydrogen bonding is no longer possible. Increasing the Lewis acidity of the pyroborate receptor appears to lead to a greater complexity in the binding of anions. The binding stoichiometry of other oxoanions appears to be more straightforward, with acetate binding taking place with a mixture of 1:1 and 2:1 guest-to-host binding, and benzoate and methanesulfonate binding in exclusively 1:1 stoichiometries.

The binding strengths of pyroborates **[1]** and **[3]** with various anions were determined using NMR titrations. Binding of acetate and benzoate is modest, and Lewis acidity of the pyroborate receptor has some effect on the resulting binding strength with benzoate. **[1]** shows high affinity to methanesulfonate, which is unusual as receptors specific to anions such as this are rare and usually highly selective. It is possible that methanesulfonate binds in a different mode to the other oxoanions studied, resulting in much stronger binding.

This methodology was easily adapted to the synthesis of long-chain alkylphosphate-bound compounds, and a series of these species was synthesised, **[53]-[75]**. Long

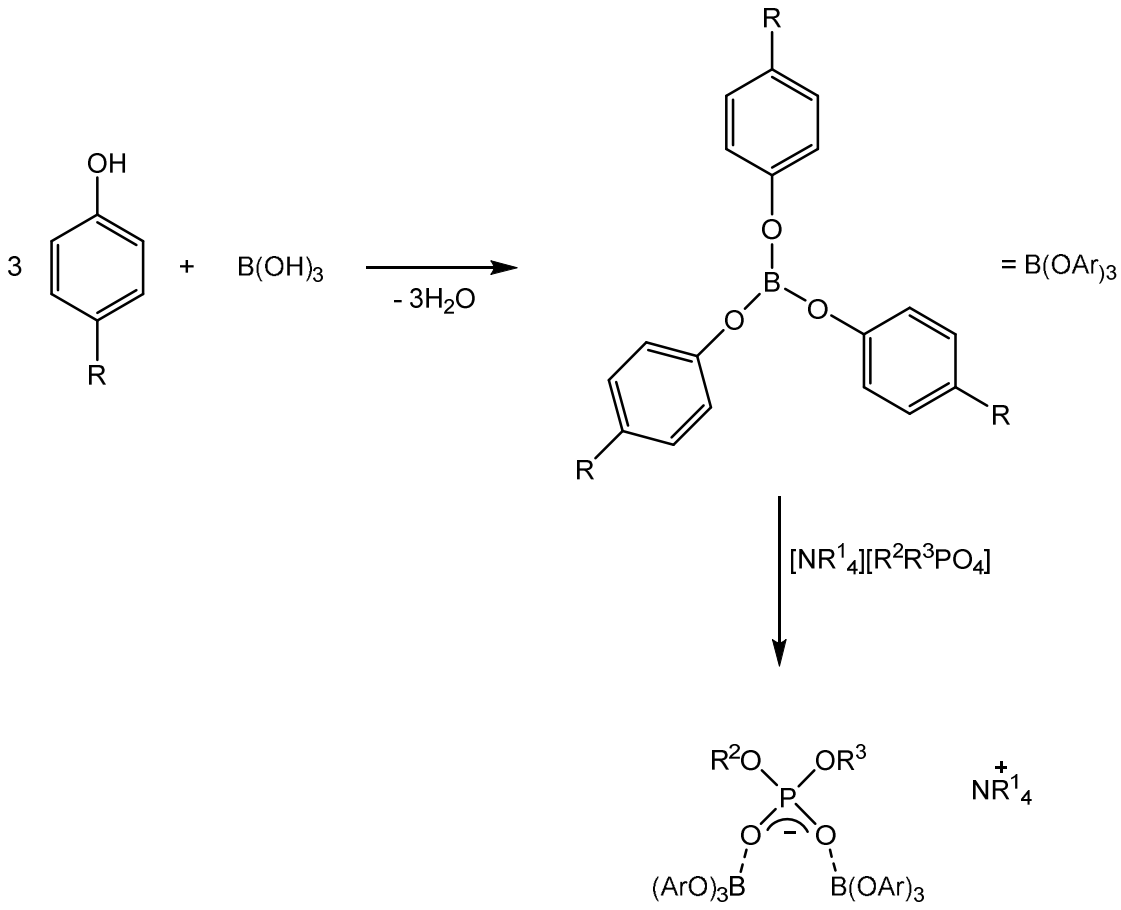
alkyl-chain substituents imparted sufficient hydrolytic stability for these reactions to be carried out under normal atmospheric conditions. Their NMR spectra matched the corresponding short-chain analogues, suggesting these are useful models for longer-chain derivatives. ICP elemental analysis sufficiently matched predicted values, indicating that these species may be tested for their additive performance. The synthesis of longer-chain analogues proved to be easily scaled up, indicating their viability to be commercially produced.

5.5 Future Work

Although considerable effort has been made to understand the chemistry at play in the model compounds discussed in this study, future work would build on this foundation. Firstly, Job plot and NMR titration analyses would be carried out on a greater range of pyroborate-anion pairs, in order to further probe the binding affinity to each anion, and the effect the Lewis acidity of the starting pyroborate has on the resulting species. As complex behaviour was demonstrated by alkylphosphate anion-binding processes, this would be investigated to a greater extent. The parameters of Job plots and NMR titrations may be systemically altered by varying concentrations, number of data points, *etc.* in order to discover the optimum conditions for these experiments and confirm the nature of the species being formed. Furthermore, fitting of the resulting binding curves would be attempted using a variety of software packages in order to try and better model the complex behaviour exhibited. DFT calculations may be carried out on the various solution-phase species postulated in this study, so that a greater understanding of their relative stabilities and propensity to form may be obtained.

How the incorporation of long-chain oil-solubilising substituents affects the resulting anion binding behaviour of the species produced would be investigated. This may be achieved by carrying out Job plot and NMR titration analyses of a selection of the long-chain compounds synthesised in this study. Furthermore, NMR studies of these species dissolved in mineral oil may be carried out, in order to probe the effect this media has on the solution-phase behaviour of these species. It is conceivable that conversion between species in solution may be slowed, allowing for a more thorough investigation into their identity and behaviour to be undertaken.

As a new area of interest, the study of the products formed from reacting triphenyl borate with $[HN^{n}Bu_3][H^{n}BuPO_4]$ and other ammonium alkylphosphates would be carried out, in order to better understand this process. If this is successful, a new family of long-chain borate-phosphates may be synthesised through the use of long-chain phenols (Scheme 5.8), which may be accessed *via* a similar Friedel-Crafts route as used to synthesise PIBcatechols (see Chapter III). These compounds may then be tested for their viability as lubricant additives.



Scheme 5.8 Possible synthesis of a family of novel borate-phosphate species, where R, R^1, R^2 and R^3 are long-chain alkyl substituents.

Chapter VI
Anti-wear Testing of Additives

6.1 Introduction

Lubricant additives are vital for ensuring good lubricant performance and to maintain the longevity and efficiency of automotive machinery. In order for the performance of wear- and friction-reducing additives to be compared and for suitable lubricant packages to be prepared for particular applications, standard testing methods of these fluids have had to be established. This has presented difficulties, as different manufacturers use a wide range of engines and hardware, and full, real-time engine tests are extremely time-consuming and expensive. Therefore, bench-top laboratory tests often using 'accelerated' operating conditions are utilised to give an initial indication of a lubricant's performance.[5] These have been standardised by various organisations, giving testing procedures considered to be practical, relevant and reproducible. For the evaluation of anti-wear performance, these include pin-on-disc,[254] four-ball[255] and HFRR (high frequency reciprocating rig) tests, which all involve metal-on-metal contacts aiming to mimic the conditions found within operating systems.

The HFRR test typically involves a steel ball being rubbed against a steel disc immersed in a fluid containing the test compound(s) (Figure 6.1). Different loads are applied in order to give testing conditions of varying severity. The force of the interaction between the two surfaces is then measured by a force transducer, which may be converted to a friction coefficient (Equation 6). A heating block allows the temperature of the system to be carefully controlled, which may be kept constant or ramped up at intervals throughout the test.

$$(6)\ \mu = F/P$$

Equation 6. Conversion of friction force, F (N) to friction coefficient, μ. P = applied load (N).

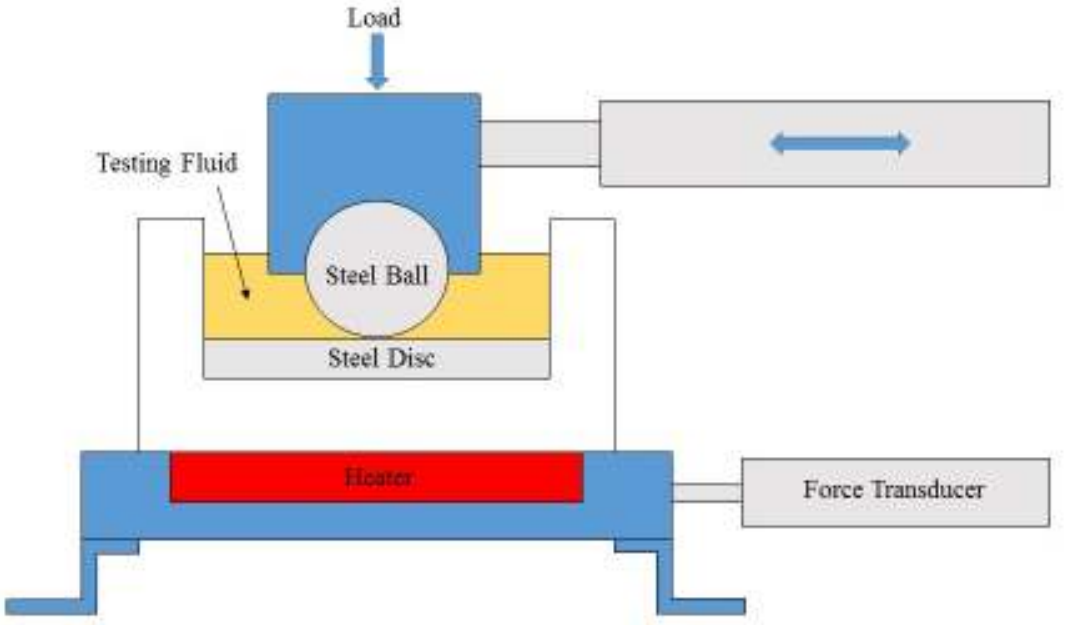


Figure 6.1 Simplified diagram of HFRR setup.

In order to measure the extent of film formation between the two surfaces, a bias voltage is applied across the system, so that the resistance of any film being formed between the two metal surfaces could be measured. The percentage drop in potential measured during the test is reported as the contact potential. Figure 6.2 shows example HFRR traces for "bad", "marginal" and "good" diesel fuels, which highlight the requirement of low friction coefficients and high contact potentials (i.e. good film formation). Furthermore, it is desirable that these parameters remain constant throughout the test, indicating film stability and reliable performance.

The level of wear caused throughout the HFRR test is evaluated by measurement of the wear scar diameter formed on the steel ball, although some studies have found

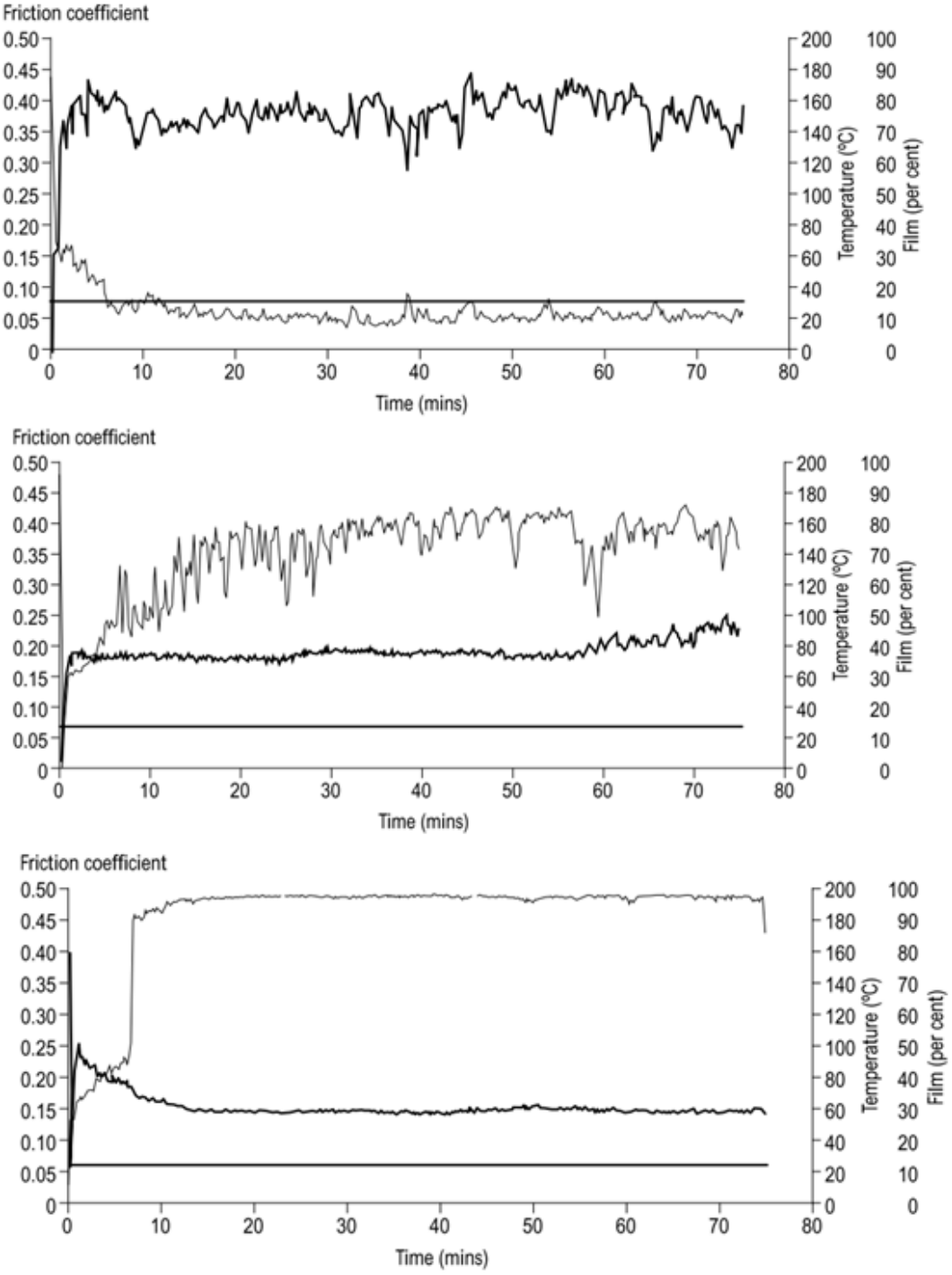


Figure 6.2 Typical "bad" (top), "marginal" (middle) and "good" (bottom) fuels tested by HFRR.[256]

disc measurements to be useful and easier to measure.[257] Either measurement can be made optically with the aid of a metallurgical microscope.

The HFRR test replicates boundary lubrication regimes, and is particularly useful as it can provide tests for both adhesive and fretting wear regimes, depending on the chosen stroke length.[256] It has been found that HFRR testing correlates well with many real fuel/hardware combinations and provides adequate predictions of lubrication performance, and so the International Organization for Standardization (ISO) and ASTM International have specified this as a standard method for assessing lubricity.[258]

6.2 Experimental

Samples were tested for their anti-wear and friction lowering performance on HFRR by Z. Hussain (driveline) and J. Durham (engine oils) of the Lubrizol Corporation at Hazelwood, Derbyshire. The parameters for the tests can be found below (Table 6.1). For single-component tests, all phosphorus-containing compounds were blended to a level of 400 ppm phosphorus in a mixture of Yubase 4, Yubase 6 and PAO100. A bias voltage of 15 mV was applied for contact potential measurements. All HFRR measurements were taken against baseline measurements of existing Lubrizol anti-wear additives.

Table 6.1 Parameters for anti-wear testing of compounds.

	Driveline	**Engine Oils**
Load	100 g and 300 g	200 g and 500 g
Duration	60 min	75 min
Frequency	20 Hz	20 Hz
Temp	Isothermal at 100 °C	15 min. at 40 °C then ramp to 160 °C at 2 °C/min
Metallurgy	Steel on steel	Steel on steel
Measured Parameters	Ave. wear scar	Ave. wear scar
	Ave. friction	Ave. friction
	Ave. contact potential	Ave. contact potential

6.3 Results and Discussion

6.3.1 Screening of Compounds for Lubricant Suitability

The phosphate-bound borates **[53]**-**[75]** were screened for their suitability as lubricant additives. The most crucial properties required of these compounds were solubility in the base oil to be used during performance testing, and stability to atmospheric air and moisture. The latter could conveniently be tested by exposure of the sample to the atmosphere for 24 hours and subsequently 7 days, before ^{11}B and ^{31}P NMR spectroscopies revealed if the compound had remained intact. Oil solubility was tested visually by sonication of typically 5 wt % of the sample in the testing base oil. The temperature was raised until all of the sample was seen to dissolve. The results from these screening tests can be found in Table 6.2.

Whilst the short-chain model compounds discussed in the previous chapter are hydrolytically unstable, and decompose upon exposure to atmospheric air and moisture, hydrolytic stability could be imparted on analogous compounds *via* the use of components containing long alkyl chains. Initially, very long PIB_{1000} chains were incorporated in the pyroborate component of the compounds, which imparted both hydrolytic stability and oil solubility on compounds **[53]**-**[66]**. Indeed, compound **[53]**, a direct PIB_{1000} analogue of model compound **[37]**, was found to be both hydrolytically stable and oil soluble, highlighting that alteration of solely the pyroborate component is able to achieve this result. Compounds **[53]**-**[66]**, all containing the PIB_{1000} motif, were found to be hydrolytically stable and oil-soluble in laboratory tests, although compound **[55]** was found to be insoluble when being blended for testing, and so could not be analysed further. Even so, the range of PIB_{1000} compounds tested contained

sufficient variation in structural components to allow for comparisons to be made of their testing results.

Despite the desirable properties exhibited by the PIB_{1000}-containing compounds, the high molecular weight of this component meant that high quantities of the compounds were needed in order to reach the desired levels of phosphorus in the lubricant mixtures. Therefore, attempts to reduce the molecular weight of the anion-bound borates whilst maintaining hydrolytic stability and oil solubility were made. This was initially carried out *via* the use of shorter PIB_{550} chains, with a direct analogue of model compound **[68]** being tested initially. Unfortunately, despite being hydrolytically stable, this compound was found to be insoluble in oil, and so could not be tested. However, it was found that altering the alkylphosphate and ammonium components to include longer 2-ethylhexyl chains imparted sufficient oil solubility on compounds **[69]** and **[70]** that they could be tested for anti-wear properties.

Encouraged by this success, further attempts at reducing the molecular weight of the compounds were made. Utilising the same catecholato motif, C_{16}-C_{18} and dodecyl chains were incorporated in the pyroborate component in compounds **[71]**, **[72]**, **[73]** and **[74]**. By combining these shorter-chain borates with longer-chain ammonium alkylphosphate components, both good oil solubility and hydrolytic stability were achieved. However, the limit on oil solubility appeared to be reached with compound **[74]**, as the tris(2-ethylhexyl)ammonium counterion was necessary to solubilise the dodecyl-borate and short *n*-butyl phosphate components. This highlights how minor changes to one component of anion-bound borate compounds can drastically alter their properties and so their viability as lubricant additives.

Table 6.2 Screening of suitability of compounds as lubricant additives.

Compound	Borate	Phosphate	Ammonium	Stability	Solubility
[53]	PIB_{1000}cat	Mono-*n*-butyl	Tri-*n*-butyl	Stable	Oil soluble at 5 wt %
[54]	PIB_{1000}cat	Mono-*n*-butyl	Bis(2-ethylhexyl)	Stable	Oil soluble at 5 wt %
[55]	PIB_{1000}cat	Mono(2-ethylhexyl)	Tri-*n*-butyl	Stable	Not oil soluble at LZ
[56]	PIB_{1000}cat	Mono(2-ethylhexyl)	Bis(2-ethylhexyl)	Stable	Oil soluble at 5 wt %
[57]	PIB_{1000}cat	Mono(2-ethylhexyl)	2-Ethylhexyl	Stable	Oil soluble at 5 wt %
[58]	PIB_{1000}cat	Mono(2-ethylhexyl)	Tris(2-ethylhexyl)	Stable	Oil soluble at 5 wt %
[59]	PIB_{1000}cat	Mono(2-ethylhexyl)	Dodecyl	Stable	Oil soluble at 5 wt %
[60]	PIB_{1000}cat	Mono-*n*-octyl	Tri^{n}butyl	Stable	Oil soluble at 5 wt %
[61]	PIB_{1000}cat	Mono-*n*-octyl	Bis(2-ethylhexyl)	Stable	Oil soluble at 5 wt %
[62]	PIB_{1000}cat	Bis(2-ethylhexyl)	Bis(2-ethylhexyl)	Stable	Oil soluble at 5 wt %
[63]	PIB_{1000}cat	Mono-oleyl	Bis(2-ethylhexyl)	Stable	Oil soluble at 5 wt %
[64]	PIB_{1000}cat	Mono$C_{13}H_{27}$	Bis(2-ethylhexyl)	Stable	Oil soluble at 5 wt %
[65]	PIB_{1000}cat	Mono$C_{13}H_{27}$	2-Ethylhexyl	Stable	Oil soluble at 5 wt %
[66]	PIB_{1000}cat	Mono$C_{13}H_{27}$	Tris(2-ethylhexyl)	Stable	Oil soluble at 5 wt %
[67]	GMO	Mono-*n*-butyl	Tri-*n*-butyl	Stable	Oil soluble at 5 wt %
[68]	PIB_{550}cat	Mono-*n*-butyl	Tri-*n*-butyl	Stable	Not oil soluble
[69]	PIB_{550}cat	Mono(2-ethylhexyl)	Tri-*n*-butyl	Stable	Oil soluble at 5 wt %
[70]	PIB_{550}cat	Mono(2-ethylhexyl)	Bis(2-ethylhexyl)	Stable	Oil soluble at 5 wt %
[71]	(C_{16}-C_{18})cat	Mono(2-ethylhexyl)	Bis(2-ethylhexyl)	Stable	Oil soluble at 5 wt %

[72]	Dodecylcat	Mono(2-ethylhexyl)	Bis(2-ethylhexyl)	Stable	Oil soluble at 5 wt %
[73]	Dodecylcat	Mono-oleyl	Bis(2-ethylhexyl)	Stable	Oil soluble at 5 wt %
[74]	Dodecylcat	Mono^{n}butyl	Tris(2-ethylhexyl)	Stable	Oil soluble at 5 wt %
[75]	Cat	Mono$C_{13}H_{27}$	Bis(2-ethylhexyl)	Stable	Not oil soluble

An attempt to synthesise a compound with the lowest possible molecular weight was made when the catechol-derived pyroborate **[1]** was combined with the longest-chain ammonium alkylphosphate available, tris(2-ethylhexyl)ammonium $C_{13}H_{27}$-phosphate, to give compound **[75]**. This compound was found to be hydrolytically stable, but the lack of solubilising chains on the pyroborate meant that the compound was not sufficiently oil soluble to be tested.

As glycerol mono-oleate is already known as a friction-modifier,[259] it was incorporated into compound **[67]** with the aim of adding this property to the proposed anti-wear activity of these phosphate-bound borate species. **[67]** was initially found to be both hydrolytically stable and oil-soluble, but unfortunately decomposed to slowly over time and could not be tested.

6.3.2 Single Component HFRR Testing

Initially, compounds were tested as single components so that any anti-wear performance could be attributed to this single species only, and not arise as a consequence of other additives in the formulation. 4-PIB_{1000}catechol, 4-PIB_{550}catechol and their pyroborate derivatives $(4\text{-}PIB_{550}catB)_2O$ **[6]** and $(4\text{-}PIB_{1000}catB)_2O$ **[7]** were also tested, to provide controls against the alkylphosphate-bound compounds containing these motifs. Furthermore, in order to carry out a structure-performance

analysis of these additives, single changes were carried out for each structural component – pyroborate, ammonium counterion, alkylphosphate – with {(2-$EtC_6H_{12})_2NH_2$}{[(4-PIB_{1000}catB)$_2$O][H(2-EtC_6H_{12})PO_4]} **[56]** chosen as the starting point (Figure 6.3). Data for these tests are tabulated in Appendix III.

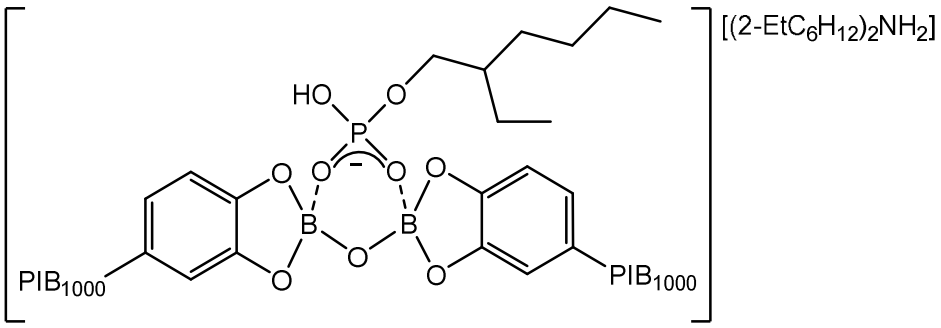


Figure 6.3 Structure of control compound [56].

6.3.2.1 Engine Oil Single Component Testing

6.3.2.1.1 Wear

At 200 g load, two thirds of the compounds tested exhibited equal or lower levels of wear than the baseline additive (202 μm), indicative of general superior additive performance (Figure 6.4). 4-PIB_{1000}catechol presented the lowest level of wear, exhibiting a wear scar diameter of 125 μm. This might suggest that the origin of the anti-wear activity of these compounds is due to the presence of this motif, but (4-PIB_{1000}catB)$_2$O **[7]** exhibited the highest level of wear (312 μm), indicating that the entire complex must contribute to the anti-wear performance. Indeed, PIB_{1000}-containing phosphate-bound compounds **[53]-[66]** exhibit a range of wear scar diameters (144-243 μm), suggesting that small changes in the structure of these additives greatly affects their resulting performance. Of the PIB_{1000}-containing compounds, **[53]** and **[63]** provided the best anti-wear performance, exhibiting wear scar diameters of 144 and 151 μm respectively.

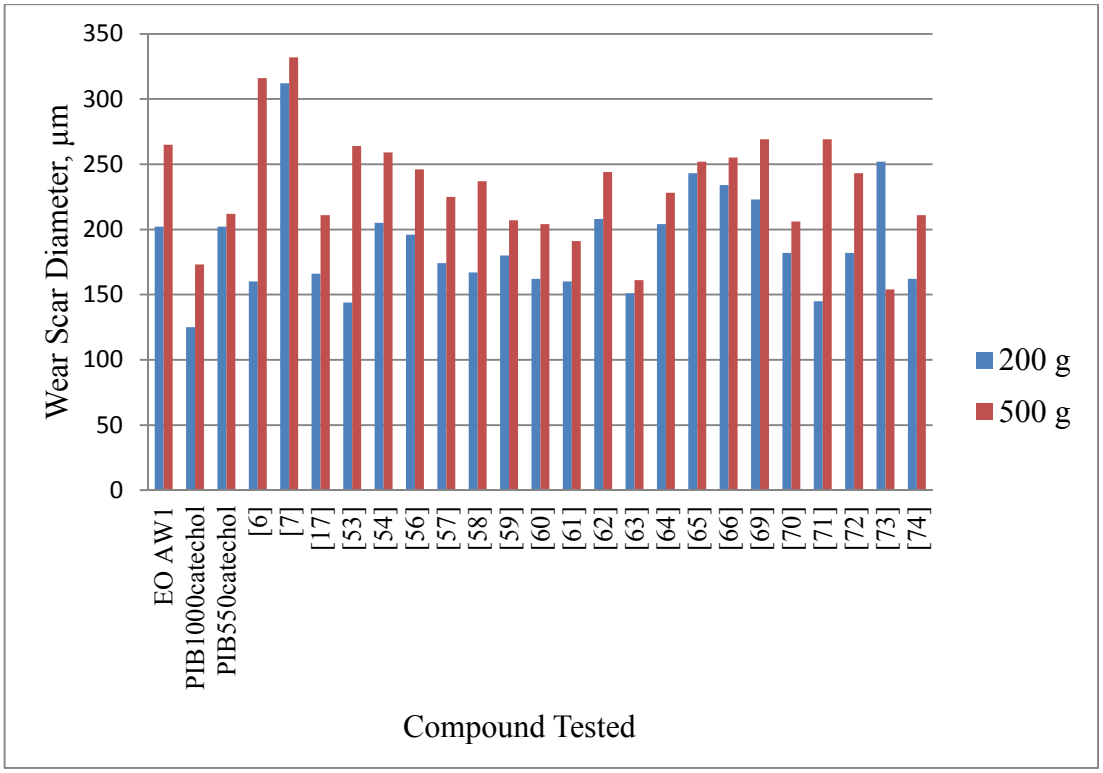


Figure 6.4 Average engine oil wear scar diameter (µm) of tested compounds.

Changing the ammonium counterion of the compounds had a marked effect on the resulting wear scar diameter, reducing it from 196 µm for starting bis(2-ethylhexyl)ammonium-containing compound **[56]** to 174, 167 and 180 µm for compounds containing 2-ethylhexylammonium **[57]**, tris(2-ethylhexyl)ammonium **[58]** and dodecylammonium **[59]** respectively, indicating the pronounced effect changing this component can have on the resulting performance of the additive.

Lengthening the alkyl chain on the alkylphosphate component appears to be beneficial for anti-wear performance, as wear scars of 160 and 151 µm are exhibited on changing from 2-ethylhexylphosphate to *n*-octyl- and oleylphosphate respectively. The use of the highly branched $C_{13}H_{27}$-phosphate has a detrimental effect, increasing the wear scar diameter to 204 µm, higher than the baseline measurement. Indeed, all of the compounds incorporating the $C_{13}H_{27}$-phosphate motif exhibit higher levels of wear

than the baseline, indicating that highly branched alkylphosphates such as this are not useful components for anti-wear performance. Shortening the alkyl chain to an *n*-butyl moiety also appears to impede the anti-wear performance, as **[54]** exhibits a wear scar diameter of 205 μm. This would suggest that the film being formed on the metal surface is not purely inorganic in nature, as the nature of the alkyl chain on the phosphate component affects the resulting performance, in contrast to additives which work *via* the formation of thick iron phosphate films.[57]

Reducing the alkyl chain length of the pyroborate component has an equally marked effect on the resulting anti-wear performance of the compounds at 200 g, but there appears to be no direct correlation between chain length and reduction in wear scar diameter. For instance, reducing the PIB chain from 1000 molecular weight to 550 has a detrimental effect, as compound **[69]** exhibits a wear scar diameter of 223 μm. However, continuing to reduce the chain length of the pyroborate moiety results in a reduction in wear, as C_{16}-C_{18}- and dodecylcatechol-containing species **[71]** and **[72]** exhibit wear scar diameters of 145 and 182 μm respectively. This may be attributed to the higher levels of boron present in these species, as their reduced molecular weights leads to higher relative proportions of boron. This suggests that the boron components are significant in the anti-wear performance of these additives. Indeed, it has been reported that boron may exhibit a partial negative charge under pressure, allowing borate species to be easily absorbed onto positively charged metal surfaces undergoing sliding contacts, resulting in effective formation of lubricating films.[115]

With the exception of **[73]**, the level of wear increased at the higher load of 500 g, due to the increased pressure imparted on the sliding steel surfaces under this harsher test condition. Compound **[73]** exhibited a significant reduction in wear scar diameter of 98 μm, which would not be expected, as even the baseline additive (EO AW1) gives

an increase of 63 μm to 265 μm. This suggests that, despite underperforming at 200 g, **[73]** may find use as an EP additive for use under harsher conditions. Twenty out of the twenty two phosphate-bound species tested exhibited lower levels of wear then the baseline at 500 g, with the two underperforming species **[69]** and **[71]** presenting wear scars of only 4 μm larger than the baseline. This indicates that these species are excellent candidates for anti-wear additives under harsh engine oil conditions, where other additives (such as the baseline in this case) may fail. Pyroborates **[6]** and **[7]** again did not perform well, exhibiting the highest wear scar diameters of 316 and 332 μm respectively, confirming that it is not the pyroborate component alone which imparts anti-wear activity to these species.

6.3.2.1.2 Friction

At 200 g load, two thirds of the compounds tested exhibited lower average coefficients of friction than the baseline additive (0.166), again indicating generally superior additive performance (Figure 6.5). Compounds **[58]** and **[71]** were the most effective, both exhibiting friction coefficients of 0.140. Both of these species contain the mono(2-ethylhexyl)phosphate component, possibly suggesting that this is responsible for the enhanced friction-reducing properties. This is supported by the next best performing species **[72]** also containing this alkylphosphate moiety, which exhibits a friction coefficient of 0.143. Again, the highly branched $C_{13}H_{27}$-phosphate has a detrimental effect, with compounds **[64]**, **[65]** and **[66]** exhibiting high coefficients of friction of 0.173, 0.175 and 0.171 respectively, confirming that this component should be avoided in the design of these additives.

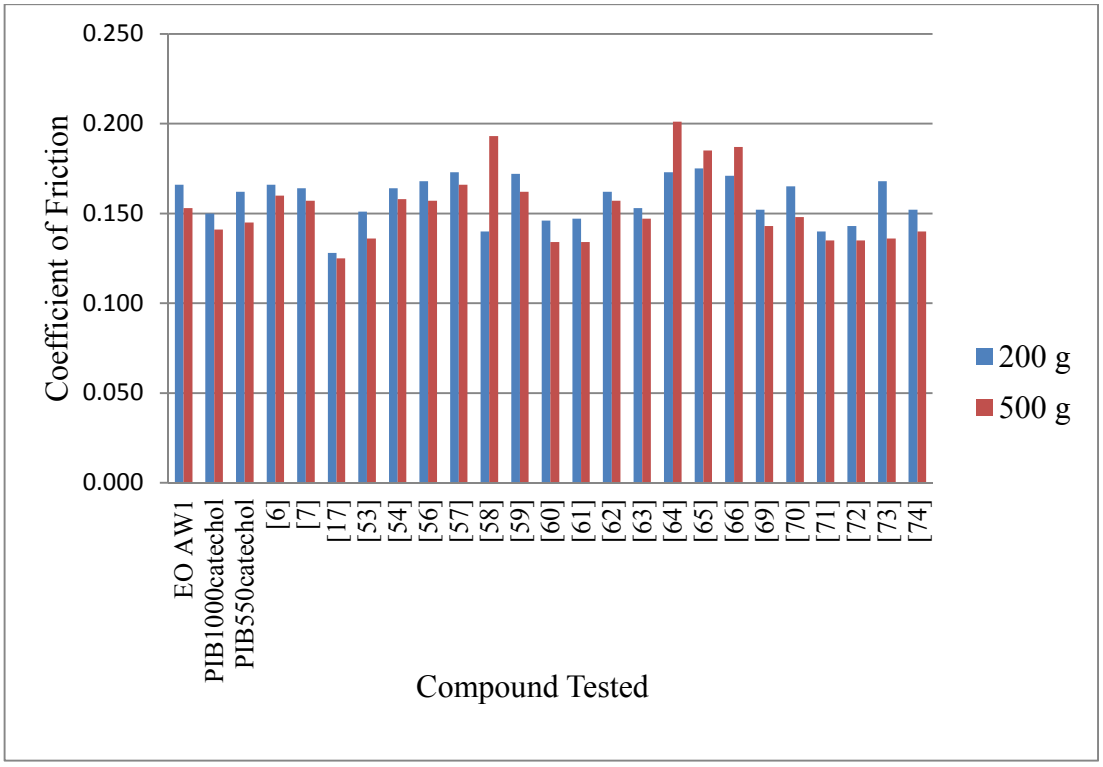


Figure 6.5 Average engine oil coefficient of friction of tested compounds.

Notably, three out of the four compounds which exhibited the highest coefficients of friction ([**57**] 0.173; **[59]** 0.172; **[65]** 0.175) all contain primary ammonium counterions, indicating that this motif must be avoided for efficient reduction of friction. As compounds containing primary ammonium counterions were found not to dissociate to their four-coordinate bis-borate analogues in solution (see Chapter V), it is possible that the lack of this species dissolved within the oil may be detrimental to the performance of these species.

Unlike the wear diameter results, lowering the chain length of the pyroborate moiety directly leads to a lowering in friction, with compounds **[69]**, **[71]** and **[72]** all exhibiting lower friction coefficients than control compound **[56]** (0.168) and the baseline (**[69]** 0.152; **[71]** 0.140; **[72]** 0.143). This may suggest that wear and friction

may not be directly proportional in this system, and wear mechanisms unrelated to friction are taking place between the two steel surfaces.

Upon inspection of the HFRR traces (see Appendix III), it is noteworthy that the majority of these compounds continue to keep friction levels low even when the highest testing temperatures are reached, whereas the baseline additive displays a sharp increase in friction at temperatures of *ca.* 110 °C. Indeed, the levels of friction appear to be continuing to decline for compounds **[53]**, **[54]**, **[56]**, **[57]**, **[59]**, **[60]**, **[61]**, **[62]**, **[69]**, **[72]** and **[73]**, suggesting that these species may continue to perform at even higher temperatures beyond the scope of this test.

At the higher load of 500 g, twenty out of the twenty four compounds tested exhibit lower friction coefficients than at 200 g. This was expected, as the baseline additive also presented a lower friction coefficient of 0.153 at 500 g: a reduction of 0.013. The three $C_{13}H_{27}$-phosphate-containing compounds **[64]**-**[66]** all exhibited higher coefficients of friction at the higher load (**[64]** 0.201; **[65]** 0.185; **[66]** 0.187), and were again amongst the poorest performing species tested. Notably, compound **[58]** contains the tris(2-ethylhexyl)ammonium counterion, which is also present in **[66]**, the second worst performing species at 500 g, exhibiting a coefficient of friction of 0.193. This may suggest that this ammonium species is unsuitable for use under harsher conditions. The two *n*-octylphosphate-containing compounds **[60]** and **[61]** performed the best under this higher load, exhibiting friction coefficients of 0.134, again indicating that longer alkyl chains on the alkylphosphate component are beneficial for the performance of these additives. This is supported by oleylphosphate-containing **[63]**, which presented a good friction coefficient of 0.147.

Shorter chain pyroborate components appear to also lead to an enhancement of friction-reducing properties at the higher load, with dodecyl-and (C_{16}-C_{18})catechol-containing species **[71]**-**[74]** all exhibiting low friction coefficients at 500 g (**[71]** 0.135; **[72]** 0.135; **[73]** 0.136; **[74]** 0.140). This supports the wear scar diameter result that compound **[73]** may find use as an EP additive.

6.3.2.1.3 Contact Potential

The contact potential between the two steel surfaces provides a measure of the film formation on the surfaces, with 100 % representing a perfect film between the two contacts. Two thirds of the samples measured exhibited higher contact potentials than the baseline additive at 200 g (83 %), indicating good film formation between the two surfaces. Furthermore, inspection of the HFRR traces (see Appendix III) show that these are relatively unchanging throughout the test for many compounds, indicating film stability.

For several compounds, there is a drop in contact potential with a concomitant rise in friction coefficient as the temperature is raised, which then stabilises. This may be due to decomposition of the compound to a new species, which must reform a film before continuing to exhibit performance. These compounds all contain PIB_{1000} or PIB_{550} substituents, which may indicate that decomposition of the PIB chain may be occurring during testing, as PIB is known to decompose to lower molecular weight fragments at elevated temperatures.[260] However, pyroborates **[6]** and **[7]** do not undergo this transition, suggesting that incorporation of the pyroborate motif provides sufficient thermal stability to the compounds to prevent decomposition. Furthermore, upon examination of the temperatures at which this film breakdown occurs (Table 6.3), the alkylphosphate-bound species appear to decompose at much

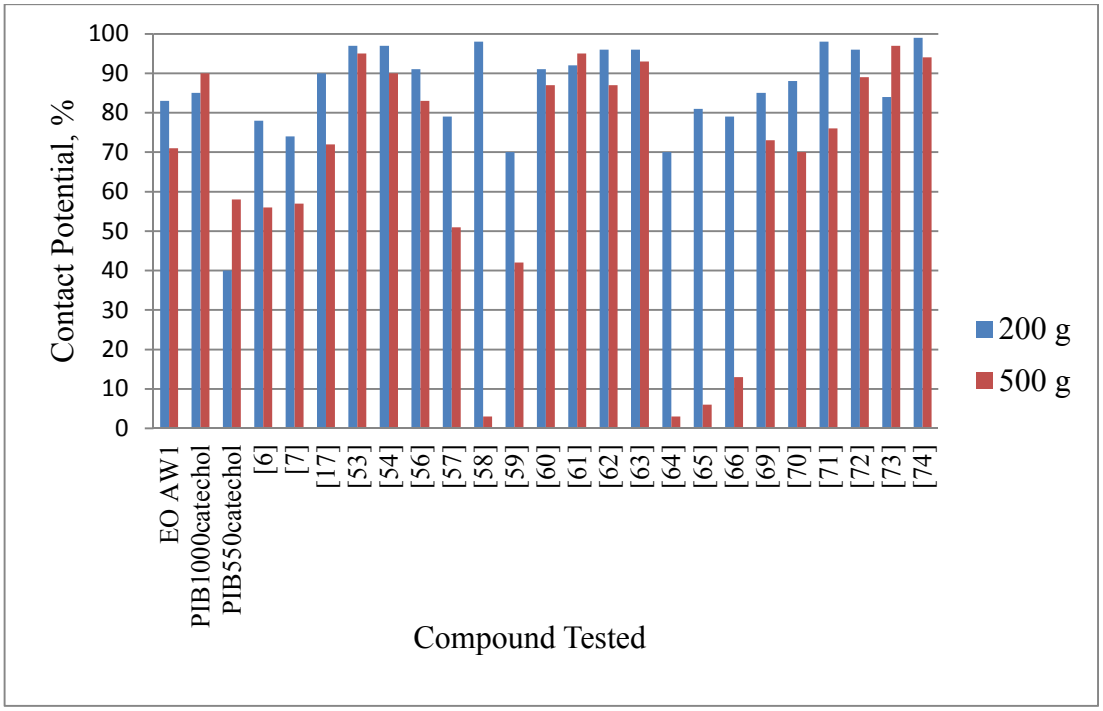


Figure 6.6 Average engine oil contact potential (%) of tested compounds.

higher temperatures than the PIBcatechols from which they are derived, suggesting that some degree of thermal stability is imparted by incorporation of an ammonium alkylphosphate motif. It may then be postulated that the binding of alkylphosphates destabilise the pyroborate component to some extent, but nevertheless still allows the species to remain intact to a significant degree. The decomposition is seemingly not detrimental to the performance of these additives, as friction is either lowered further or kept relatively constant following this transition. This provides an advantage over the baseline additive, which exhibits a sharp rise in friction towards the end of the test.

Notably, both PIBcatechols and pyroborates **[6]** and **[7]** exhibited lower contact potentials than the majority of compounds tested (PIB_{1000}catechol 85 %; PIB_{550}catechol 40 %; **[6]** 78 %; **[7]** 74 %), suggesting that the ammonium alkylphosphate component is essential for forming an effective film between the two

Table 6.3 Temperature at which film breakdown occurs at 200 g load.

Compound	Temperature (°C)
PIB_{1000}catechol	40
PIB_{550}catechol	40
[53]	100
[57]	80
[58]	90
[59]	120
[60]	120
[63]	130
[64]	100
[70]	90

surfaces. Furthermore, this indicates that the dissociation of the alkylphosphate observed for model compounds at elevated temperatures (see Chapter V) does not fully separate the two species, as the presence of the ammonium alkylphosphate affects the resulting film formation.

Compound **[74]** presented the highest contact potential (99 %), and the corresponding HFRR trace shows that the film formed was extremely stable throughout the test. Indeed, the compounds containing lower molecular weight pyroborate chains (**[71]-[74]**) all exhibited particularly stable HFRR traces, possibly due to increased thermal stability through the lack of long PIB substituents. Furthermore, it is possible that the increased levels of boron in these species provides more boron-rich films, which may improve their performance.[85]

The incorporation of primary ammonium counterions appears to lead to a reduction in contact potential, as compounds **[57]**, **[59]** and **[65]** all exhibited low contact potentials (**[57]** 79 %; **[59]** 70 %; **[65]** 81 %), mirroring the higher friction coefficients recorded for these species. Furthermore, the highly branched $C_{13}H_{27}$-phosphate again resulted in a detrimental effect on performance, with compounds **[64]**, **[65]** and **[66]** exhibiting low contact potentials of 70, 81 and 79 % respectively, reinforcing the notion that these components are detrimental for these additives under the conditions for engine oils. Moreover, species containing primary ammonium counterions and $C_{13}H_{27}$-phosphate suffered significant film breakdown at the higher load of 500 g, exhibiting very low contact potentials (**[57]** 51 %; **[59]** 42 %; **[64]** 3 %; **[65]** 6 %; **[66]** 13 %) and demonstrating their unsuitability as engine oil additives under harsher conditions. This suggests that the poor performance of these components may be due to poor film formation.

Generally, compounds formed less efficient films at the higher load, including the baseline additive, which dropped 12 % to a contact potential of 71 %. Fourteen of the compounds outperformed the baseline, exhibiting contact potentials of 72-97 %, indicating superior performance. Compound **[73]** again showed enhanced performance at 500 g, exhibiting a raised contact potential from 84 to 97 %, and offering the best film formation out of all of the species tested at this higher load.

6.3.2.2 Driveline Single Component Testing

6.3.2.2.1 Wear

At the 100 g load, eleven out of the twenty four compounds tested exhibited lower levels of wear than the two baseline additives, DL AW1 (168 μm) and DL AW2 (178 μm) (Figure 6.7). In a similar result to that observed for engine oils, both PIBcatechols

exhibited the lowest levels of wear (PIB_{1000}catecol 103 μm; PIB_{550}catechol 135 μm), suggesting these components may be the origin of the anti-wear properties of these additives under driveline conditions. However, pyroborates **[6]** and **[7]** again exhibited high levels of wear, indicating that the PIBcatechol motifs are not entirely responsible for the anti-wear properties of these species.

Altering the ammonium counterion appears to have a detrimental effect on the anti-wear performance of these species, as changing from bis(2-ethylhexyl)ammonium-containing control compound **[56]** (170 μm) to primary ammonium counterions 2-ethylhexylammonium (**[57]** 217 μm) and dodecylammonium (**[59]** 218 μm) increases the resulting wear diameter. Changing to a tertiary ammonium counterion also increases the level of wear, but to a lesser extent, as tris(2-ethylhexyl)ammonium-containing **[58]** exhibits a wear diameter of 183 μm, suggesting that bis(2-ethylhexyl)ammonium is the optimum counterion for these species under driveline conditions.

As in the engine oils tests, lengthening the alkylphosphate component appears to improve the anti-wear performance of the compounds, as wear scars of 162 and 164 μm are exhibited on changing from 2-ethylhexylphosphate to *n*-octyl- and oleylphosphate respectively. The highly branched $C_{13}H_{27}$-phosphate again increases the wear scar diameter (222 μm), higher than the baseline measurement. Once more, all of the compounds incorporating $C_{13}H_{27}$-phosphate exhibit higher levels of wear than the majority of species tested, including the baseline additives, proving their unsuitability as components in anti-wear additives. However, in contrast to the engine oils conditions, shortening the alkyl chain to an *n*-butyl moiety does not impede anti-wear performance, as **[54]** exhibits a wear scar diameter of 163 μm, which is lower than that of **[56]** and both baseline additives.

It would appear that shortening the alkyl chain on the pyroborate moiety reduces the anti-wear activity of these species, as compounds **[69]**, **[71]** and **[72]** all exhibit larger wear scar diameters than **[56]** and the baseline additives (**[69]** 183 µm; **[71]** 257 µm; **[72]** 188 µm). However, additional variation of the ammonium alkylphosphate component leads to a subsequent reduction in wear scar diameter, with compounds **[70]**, **[73]** and **[74]** exhibiting lower levels of wear than **[56]** and the baseline additives (**[70]** 162 µm; **[73]** 152 µm; **[74]** 153 µm). This exemplifies the dramatic effect small alterations in structure have upon the resulting anti-wear properties of these species.

Generally, the samples tested performed better at the higher load of 300 g, with two thirds of the compounds outperforming the baseline additives DL AW1 (245 µm) and DL AW2 (242 µm). Similar trends may be observed as those noted for the lower load. PIB_{550}catechol once more performed well, exhibiting a wear scar diameter of

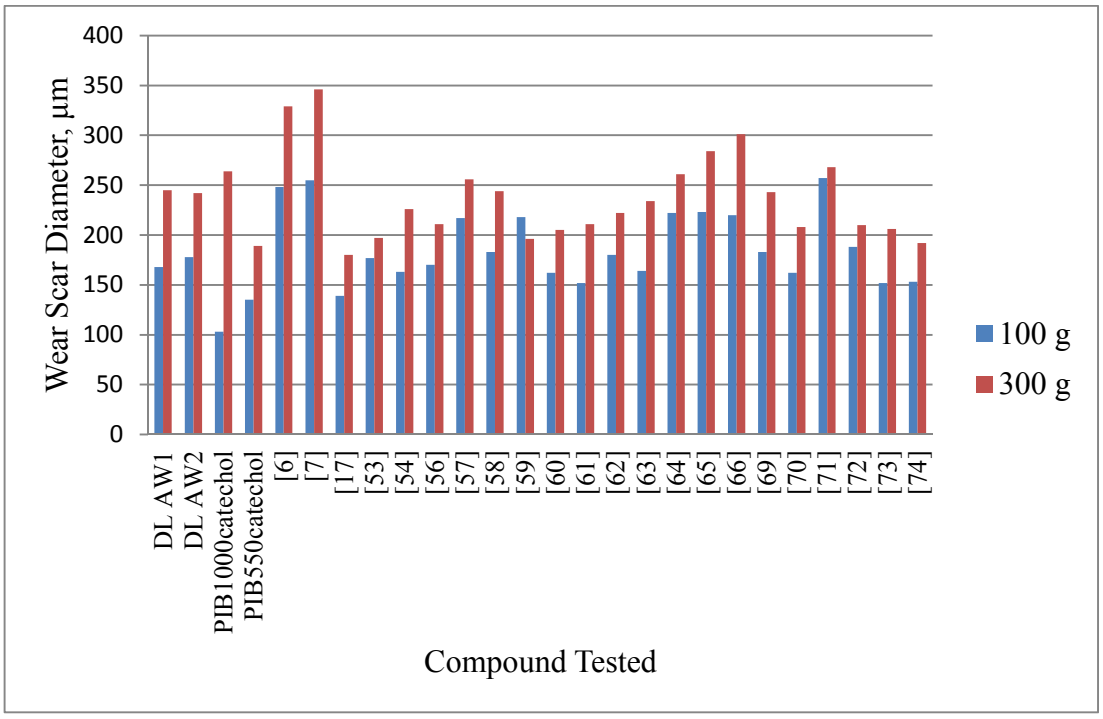


Figure 6.7 Average driveline wear scar diameter (µm) of tested compounds.

189 μm. However, PIB_{1000}catechol exhibits a higher level of wear than the baselines at 500 g (264 μm), suggesting the longer PIB chain may be too unstable to perform under these harsher conditions.

Again, the use of the primary 2-ethylhexylammonium counterion led to a reduction in anti-wear performance, as compound **[57]** exhibited a wear scar diameter of 256 μm. However, at 500 g dodecylammonium-containing **[59]** presented a smaller wear scar than the baseline (196 μm). This may indicate that it is not only the level of substitution on the nitrogen centre which affects performance, but the nature of the alkyl chain also.

At this higher load, the effect of increase in alkylphosphate chain length is less marked, with *n*-octylphosphate-containing compounds **[60]** and **[61]** only showing slight improvements on **[56]** (**[56]** 211 μm; **[60]** 205 μm; **[61]** 211 μm). Furthermore, oleylphosphate-containing **[63]** exhibited a larger wear scar than **[56]** of 234 μm, suggesting that the harsher conditions lessen the anti-wear contribution of the long-chain on the phosphate moiety. However, it must be noted that this sample still outperformed the two baselines additives.

Although shortening the alkyl chain on the pyroborate moiety has varying effects at this higher load, all three compounds containing the dodecylcatechol motif exhibit levels of wear lower than control compound **[56]** and the two baseline additives (**[72]** 210 μm; **[73]** 206 μm; **[75]** 192 μm). It is possible that the elevated levels of boron in these species lead to their enhanced performance.

6.3.2.2.2 Friction

At 100 g, eleven of the twenty four compounds tested had similar or lower average coefficients of friction than the baseline additives DL AW1 (0.159) and DL AW2 (0.151). Some similar trends may be observed as in the wear scar diameter results discussed above. The incorporation of primary ammonium counterions reduces the performance of the species, as 2-ethylhexylammonium compound **[57]** and dodecylammonium compound **[59]** both exhibited higher coefficients of friction than control compound **[56]** (**[56]** 0.167; **[57]** 0.173; **[59]** 0.174). However, unlike the wear results, changing to tris(2-ethylhexyl)ammonium species **[58]** had a beneficial impact on the resulting friction coefficient (0.162), suggesting that the anti-friction and anti-wear mechanisms of these species may differ with respect to involvement of the counterion.

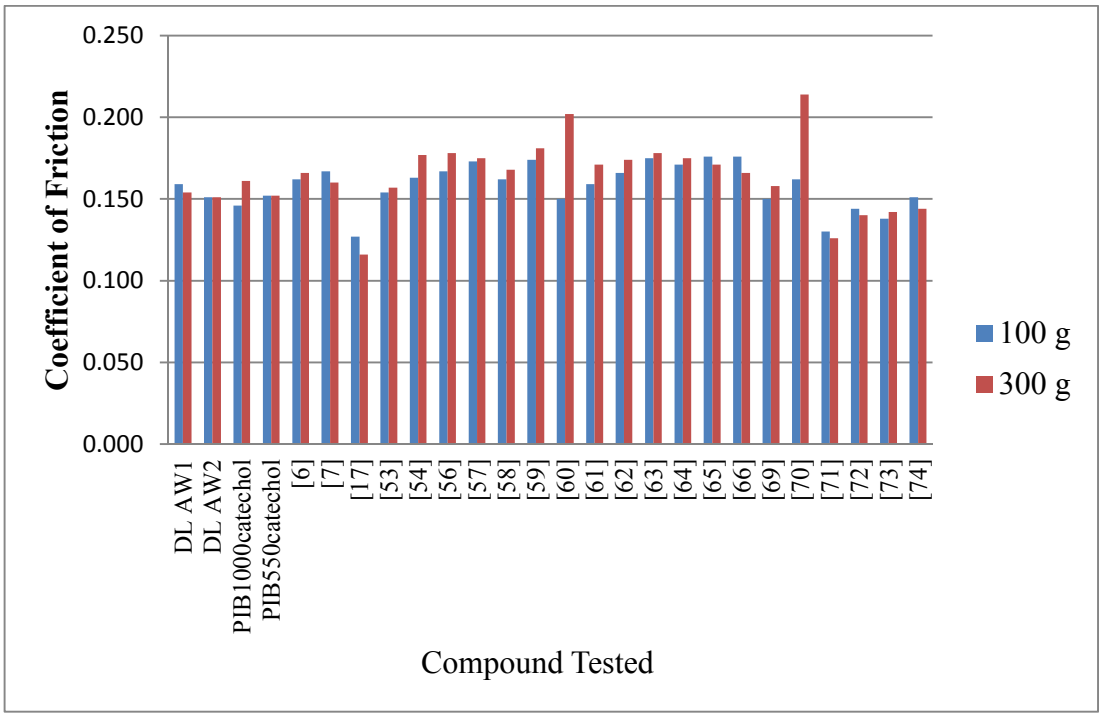


Figure 6.8 Average driveline coefficient of friction of tested compounds.

It would again appear that lengthening the alkylphosphate component improves the friction reducing performance of the compounds, as a friction coefficient of 0.159 is exhibited on changing from 2-ethylhexylphosphate to *n*-octylphosphate, bringing the compound in line with the baseline additives. However, the oleylphosphate-containing compound **[63]** exhibits a higher friction coefficient of 0.175, suggesting there is a limit to this improvement. Furthermore, shortening the alkylphosphate to an *n*-butyl chain lowers the level of friction to a greater degree than lengthening it (**[54]** 0.163), indicating that the relationship of the alkylphosphate in reducing the friction is more complex than simply the length of the alkyl chain. The highly branched $C_{13}H_{27}$-phosphate again increases the friction coefficient to 0.171, higher than the baseline measurement. Indeed, all of the compounds incorporating $C_{13}H_{27}$-phosphate exhibit higher coefficients of friction than the majority of species tested, including the baseline additives, proving their unsuitability as components in friction-reducing additives under driveline conditions.

Unlike the wear results discussed above, shortening the alkyl chain on the pyroborate component of the samples appears to directly improve their friction-lowering performance. Indeed, compounds **[69]**, **[71]** and **[72]** all exhibit lower friction coefficients than **[56]** and the baseline additives, with **[71]** outperforming all of the species tested (**[69]** 0.150; **[71]** 0.130; **[72]** 0.144). Further variation of **[71]** offered differing results, with lengthening of the alkylphosphate to oleylphosphate reducing the friction coefficient further (**[73]** 0.138), and reducing it to *n*-butylphosphate and increasing the substitution on the ammonium counterion to tris(2-ethylhexyl)ammonium slightly increasing the friction coefficient (**[74]** 0.151), but still providing similar performance to the baseline additives.

Generally, the samples tested did not reduce friction as efficiently at the higher 300 g load, with only a quarter of the species equalling or outperforming DL AW1 (0.154) and DL AW2 (0.151). This suggests many of these compounds would be inappropriate as anti-wear additives under harsher driveline conditions. However, the samples incorporating shorter-chain pyroborate components continued to perform well at the higher load, with compounds **[71]**, **[72]**, **[73]** and **[74]** exhibiting even lower coefficients of friction under these conditions (**[71]** 0.126; **[72]** 0.140; **[73]** 0.142; **[74]** 0.144). This may be due to the higher levels of boron in these samples, and exemplifies their viability as friction-reducing additives under harsh driveline conditions.

6.3.2.2.3 Contact Potential

Although none of the samples exhibited contact potentials as high as DL AW1 (99 %) and DL AW2 (98 %), every compound gave a contact potential of 72 % or above

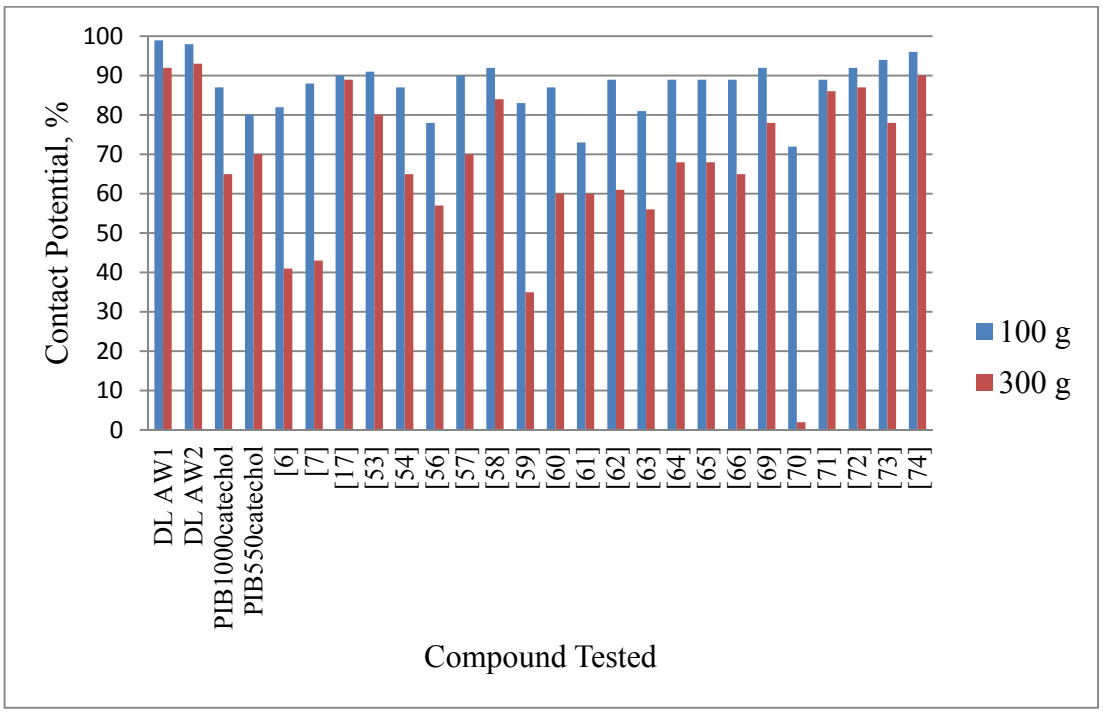


Figure 6.9 Average driveline contact potential (%) of tested compounds.

at 100 g, with more than two thirds giving contact potentials of above 85 % (Figure 6.9), indicating good levels of film formation between the two steel surfaces. Furthermore, inspection of the HFRR traces (see Appendix III) shows good film stability for the majority of species. A notable exception is PIB_{550}catechol, which shows intermittent drops in contact potential with concomitant spikes in friction coefficient, suggesting a patchy film is being formed. PIB_{1000}catechol gives a much more stable film, which may explain its superior performance over PIB_{550}catechol in the reduction of both wear and friction. However, at 300 g PIB_{1000}catechol exhibits a similar HFRR trace resembling that of a patchy film, suggesting that a similar layer is being formed on the surface under these harsher conditions, accounting for the poor anti-wear performance of this species at 300 g.

Surprisingly, the contact potentials of the poorly performing primary ammonium and $C_{13}H_{27}$-phosphate-containing compounds **[57]**, **[59]**, **[64]**, **[65]** and **[66]** are higher than that of control compound **[56]** at 100 g (**[56]** 78 %; **[57]** 90 %; **[59]** 83 %; **[64]** 89 %; **[65]** 89 %; **[66]** 85 %). In contrast to the engine oils results discussed above, this suggests that it is the nature of the film itself, not its efficient formation, which affects the resulting performance of these species under driveline conditions. This is further exemplified by the observation that *n*-octylphosphate-containing compound **[61]**, which exhibited good wear and friction-reducing properties, exhibits a contact potential of 73 %, lower than the baselines and control compound **[56]**.

There appears to be a more direct correlation between performance and contact potential for the compounds containing shorter-chain pyroborate components. Compounds **[69]**, **[71]**, **[72]**, **[73]** and **[74]**, which exhibited lower levels of wear and/or friction than the baselines and **[56]**, all exhibit higher contact potentials than **[56]** at 100 g (**[69]** 92 %; **[71]** 89 %; **[72]** 92 %; **[73]** 94 %; **[74]** 96 %). This suggests that the

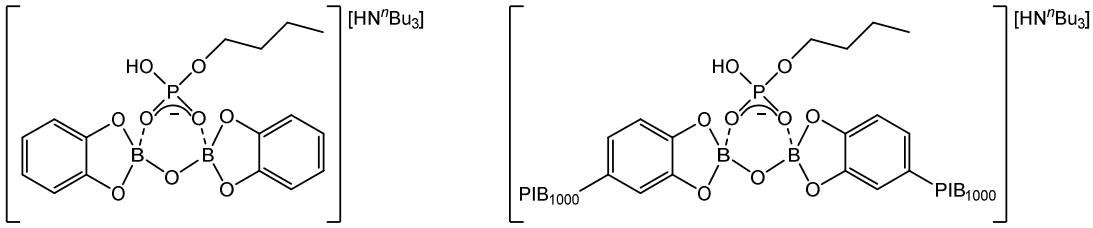
performance of these compounds may at least in some part be attributed to their highly efficient film formation.

As found under engine oils conditions, the compounds tested formed less efficient films under the heavier load, including the baseline additives, which exhibited contact potentials 7 and 5 % lower respectively than those found at 100 g (DL AW1 92 %; DL AW2 93 %). However, the novel alkylphosphate-bound additives generally showed greater drops in contact potential, with only five out of the twenty four compounds tested exhibiting contact potentials of above 85 %. Several compounds maintained reasonable films throughout the test, with PIB_{550}catechol, **[53]**, **[57]**, **[58]**, **[69]**, **[71]**, **[72]**, **[73]** and **[75]** exhibiting contact potentials of 70 % and above. Furthermore, inspection of the HFRR traces (see Appendix III) reveals that the majority of compounds were still able to successfully form films, with the only exceptions being **[60]** and **[70]**. Since both these compounds contain the tri-*n*-butylammonium counterion, it is possible that this is responsible for their poor film formation during this test. However, compound **[53]** also contains this counterion, and so the relationship between the ammonium counterion and the alkylphosphate may be key to whether a film is successfully formed or not under these harsher conditions.

With the exception of compound **[70]** discussed above, samples containing lower chain-length pyroborate components continued to perform well under the 300 g load, exhibiting contact potentials of 78 % and above (**[69]** 78 %; **[71]** 86 %; **[72]** 87 %; **[73]** 78 %; **[74]** 90 %). This highlights their promising performance as driveline additives under both loads, indicating their viability as additives for this application.

6.3.3 Further Engine Oils Testing

As compound **[53]** demonstrated promising early results in engine oils HFRR tests, further engine oils tests were carried out in order to probe the viability of this compound as an anti-wear additive for this application. The effect of **[53]** on the oxidative stability of the resulting lubricant was tested using pressure differential scanning calorimetry (PDSC) at 0.5 wt %. When compared with a traditional aminic antioxidant supplied by the Lubrizol Corporation, **[53]** does not perform as well, exhibiting an oxidation onset of 62.5 min compared to 124.2 min for the aminic species (Figure 6.11). However, being a potential anti-wear additive, this species is not required to function as an antioxidant, and simply must not promote oxidation. Indeed, **[53]** does not exacerbate oxidation, retarding it by 10.1 minutes when compared to a fluid containing no antioxidant.



[37] **[53]**

Figure 6.10 Structures of model compound [37] and its PIB_{1000} analogue [53].

Two tests were carried out on **[53]** in order to investigate its tendency to form deposits within the engine oils environment: microcoker and hot tube tests. Superior performance in one of these two tests is required before further engine oils testing of a compound may be carried out. Compound **[53]** exhibited excellent performance in the microcoker test, offering an improvement of 0.90 in average merit rating when compared to a typical Lubrizol dispersant (Figure 6.12), and outperforming the baseline by 1.21 (a difference of 0.40 or above is significant). Furthermore, the

temperature of the onset of deposit formation was 11 °C higher than the Lubrizol dispersant, and 21 °C higher than the baseline, showing that higher temperatures are required to produce deposits on metal surfaces when **[53]** is incorporated as an additive.

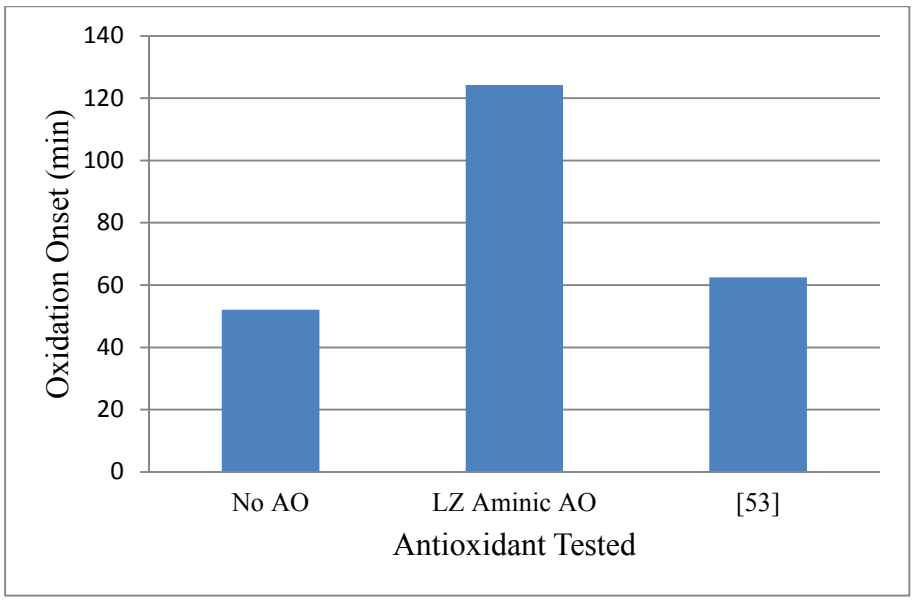


Figure 6.11 Antioxidancy of [53].

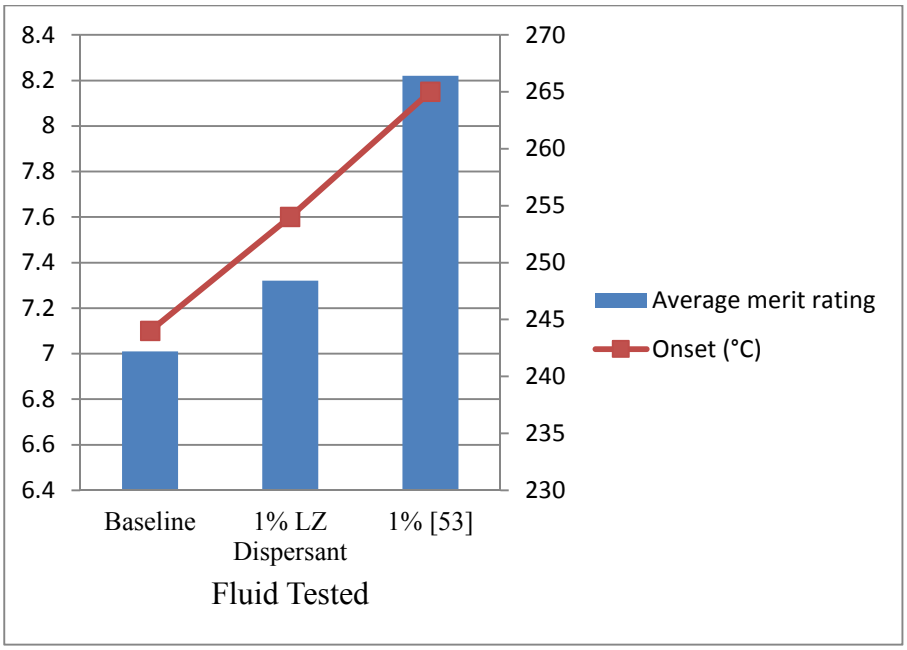


Figure 6.12 Microcoker test results for [53].

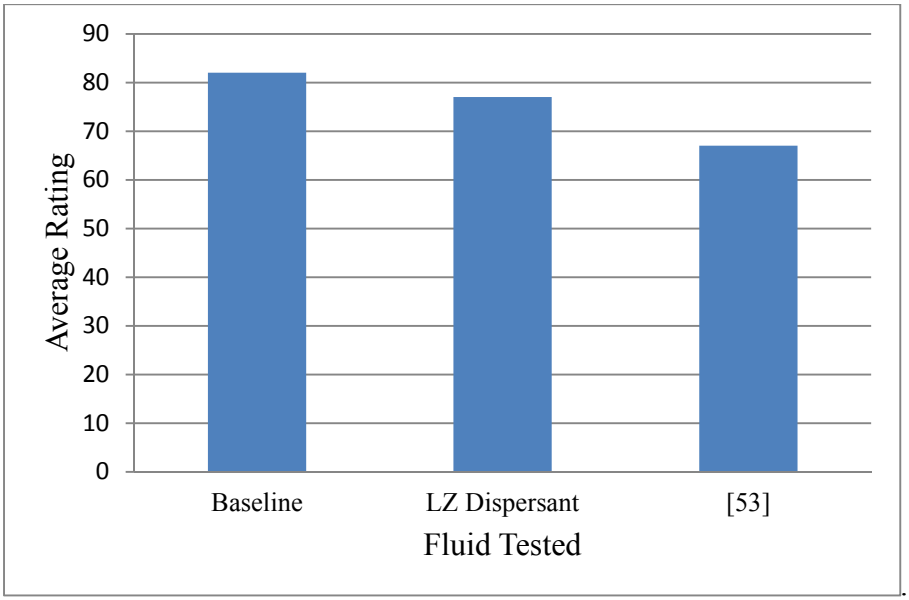


Figure 6.13 Hot tube test results for [53].

Compound **[53]** exhibited reduced performance in the hot tube test compared to a typical Lubrizol dispersant and the baseline (Figure 6.13). A rating of 67 was given, compared to the Lubrizol dispersant's rating of 77 (a difference of 10 or above is significant). This indicates that fluids containing this compound may present issues with the formation of deposits on glassy surfaces under engine oils conditions.

6.3.4 Fully Formulated Driveline HFRR Testing

As compound **[53]** demonstrated promising early results in single-component driveline HFRR tests, full oil formulations containing this species as the anti-wear additive component were tested as an indication of its future performance in a final lubricant package. As with the single-component tests, two loads of 100 and 300 g were tested. Additionally, two different treat rates were tested, which equated to 400 and 800 ppm levels of phosphorus in the overall formulation for each additive tested. These data are tabulated in Appendix III. At the lower treat rate, **[53]** exhibited a smaller wear scar than both baseline additives at both loads (Figure 6.14), indicating

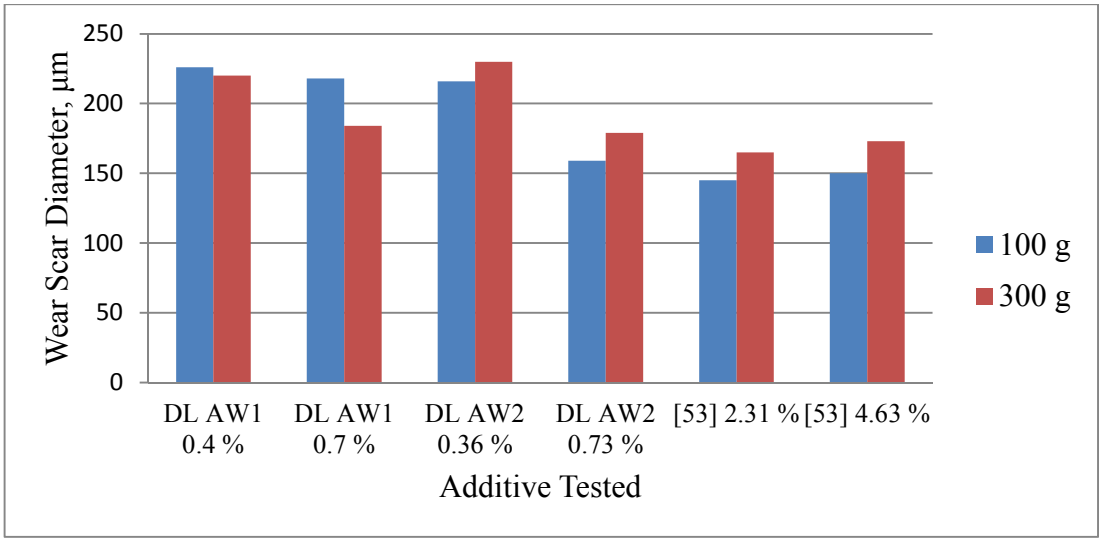


Figure 6.14 Average fully formulated driveline wear scar diameters (µm).

superior performance (**[53]** 100 g: 145 µm, 300 g 165 µm; DL AW1 100g: 226 µm, 300 g: 220 µm; DL AW2 100 g: 216 µm, 300 g: 230 µm). At the higher treat rate, **[53]** continues to outperform the two baseline additives, although the difference is less marked.

At the lower treat rate and 100 g load, **[53]** exhibits a much lower coefficient of friction than the two baseline additives (Figure 6.15), indicating superior

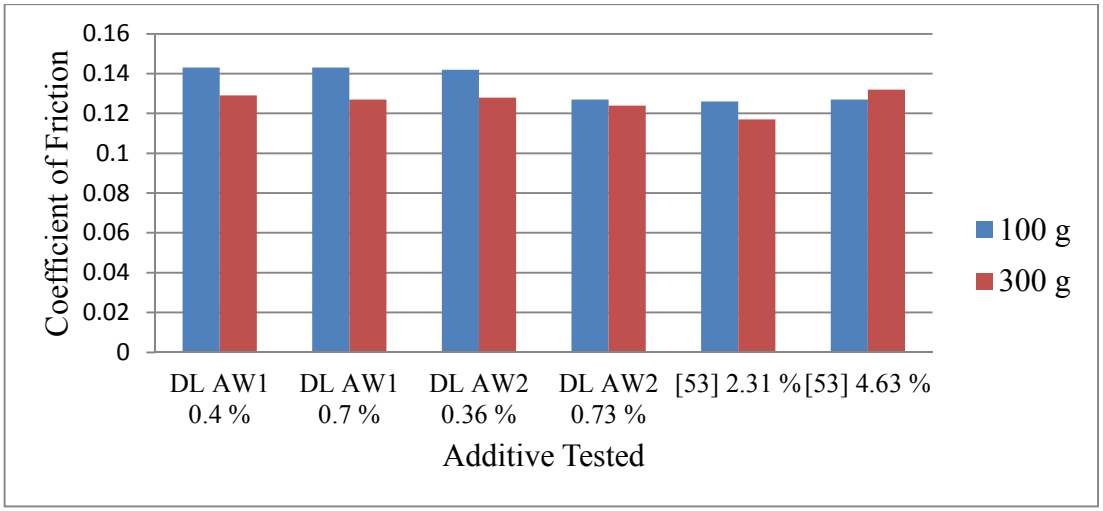


Figure 6.15 Average fully formulated driveline coefficients of friction.

performance under these conditions (**[53]** 0.126; DL AW1 0.143; DL AW2 0.142). At the higher treat rate at 100 g, **[53]** continues to outperform DL AW1, offering a coefficient of friction of 0.127 *vs* 0.143. However, DL AW2 and **[53]** exhibit the same coefficient of friction under these conditions.

At the higher load of 300 g, **[53]** exhibits superior performance over the two baseline additives at the lower treat rate (**[53]** 0.117; DL AW1 0.129; DL AW2 0.128) (Figure 6.15). However, at the higher treat rate **[53]** slightly underperforms, exhibiting a friction coefficient of 0.132 compared to DL AW1 and DL AW2 which offer friction coefficients of 0.127 and 0.124 respectively. It is possible that the higher weight percentage of **[53]** required to achieve the equivalent levels of phosphorus in the formulation leads to thickening of the fluid, which has a slight detrimental effect on the performance at the higher treat rate. This may be remedied *via* the use of lower molecular weight alkylphosphate-bound species such as **[74]**.

The contact potentials exhibited by **[53]** at 100 g are superior to those offered by the baseline additives at both treat rates (Figure 6.16). Indeed, **[53]** significantly outperforms DL AW1 at both treat rates, exhibiting contact potentials of 81 and 90 % compared to 32 and 43 %. At the higher treat rate, DL AW2 performs somewhat better, exhibiting a contact potential of 81 %, but **[53]** continues to outperform this baseline additive. At the higher load, **[53]** outperforms DL AW2 at the lower treat rate (**[53]** 78 %; DL AW2 31 %). However, at the higher treat rate, DL AW2 does show a slight improvement over **[53]**, offering a contact potential of 87 *vs* 84 %. Inspection of the HFRR traces (see Appendix III) shows that compound **[53]** offers more stable films than both DL AW1 and DL AW2 at both treat rates and loads, indicating superior film formation than both baseline additives under these conditions.

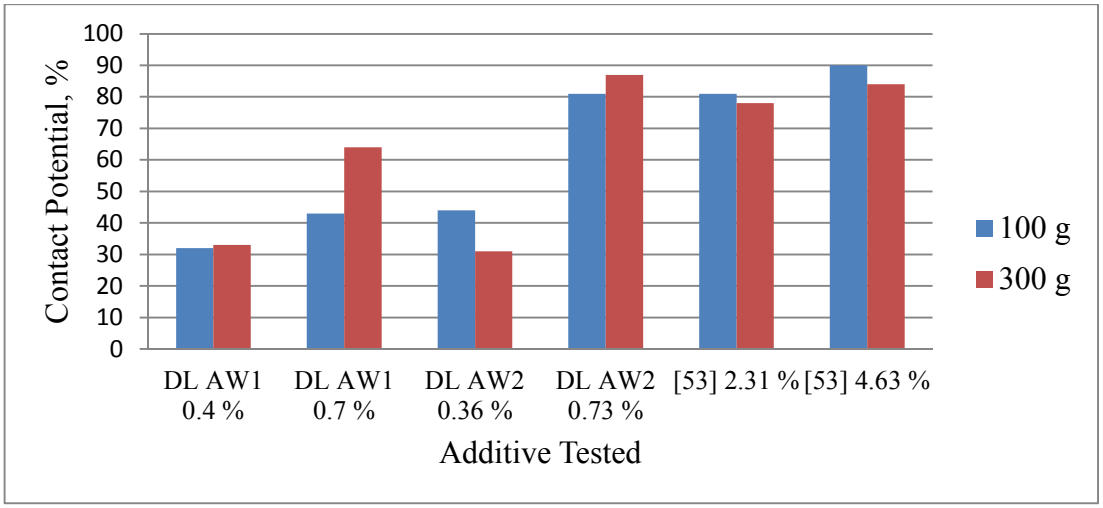


Figure 6.16 Average fully formulated driveline contact potentials (%).

6.4 Conclusions

A range of novel alkylphosphate-bound compounds **[53]**-**[75]** were screened for their lubricant additive suitability. Incorporation of PIB_{1000} chains into the pyroborate moiety successfully imparted hydrolytic stability and oil solubility in all cases. The molecular weight of the compounds was successfully reduced *via* the introduction of shorter-chain catechol pyroborate components, but the chain-length of the alkylphosphate and ammonium counterion components had to be lengthened in order to retain oil solubility of these species.

Many of the species tested exhibited superior performance to the baseline additives under both engine oils and driveline conditions, indicating their viability as a new family of anti-wear additives. Every species tested offered reduced levels of wear under engine oils conditions at higher loads, with **[73]** exhibiting particularly good anti-wear and anti-friction performance under harsher conditions, indicating promise as an engine oil EP additive. Furthermore, many compounds presented good anti-wear performance at higher temperatures during engine oils tests, unlike the baseline additive. Some PIB-containing compounds appeared to suffer film breakdown and reformation under engine oils conditions at higher temperatures, suggesting conversion to a decomposition product. However, this new film continued to provide friction-reducing performance until the end of the test.

HFRR testing of the suitable compounds offered insight into the structure-performance relationship of these species. PIBcatechols performed well during engine oils and driveline wear tests, implying these components may impart anti-wear performance on their derivative compounds. However, pyroborates **[6]** and **[7]** generally performed poorly, suggesting the entire complex contributes to performance. Increasing the chain length of the bound alkylphosphate enhanced the

anti-wear and anti-friction performance of compounds under both engine oils and driveline conditions. However, the highly branched $C_{13}H_{27}$-phosphate was consistently detrimental to performance. Similarly, the use of primary ammonium counterions typically increased levels of friction and wear under both engine oils and driveline conditions. This is despite the species containing these components exhibiting high contact potentials under driveline conditions, indicating that it may be the nature of the film formed, not its successful formation, which leads to poor performance. Lowering the molecular weight of the compounds *via* shortening of the alkyl chain on the pyroborate component generally led to an improvement in anti-wear and anti-friction performance under both engine oils and driveline conditions, with compounds **[70]**-**[74]** consistently outperforming other species and the baseline additives, even at higher loads. This may be due to the higher relative amounts of boron in these lower molecular weight species.

Compound **[53]** was taken forward for further engine oils tests. Although this species only offers very mild antioxidancy, it does not exacerbate oxidation of the base oil, slowing the process by 52 minutes. **[53]** performed very strongly in the microcoker deposit test, outperforming a current Lubrizol dispersant and increasing the onset temperature for deposit formation on a metal surface. However, **[53]** underperformed on the hot tube test, indicating the formation of deposits on glassy surfaces at high temperatures may present an issue.

Compound **[53]** performed very well in fully formulated driveline HFRR tests, exhibiting lower wear than both baseline additives at both 100 g and 300 g loads and treat rates of 400 ppm and 800 ppm phosphorus. **[53]** typically offered lower coefficients of friction than the baseline samples, the exception being under the 300 g load at the 800 ppm treat rate, when it slightly underperformed. This may be due to

the high molecular weight of the compound resulting in larger masses being required to give 800 ppm phosphorus, and so lower molecular analogues may perform better under these conditions. **[53]** offered superior contact potentials at both loads and treat rates and exhibited more stable films throughout the tests.

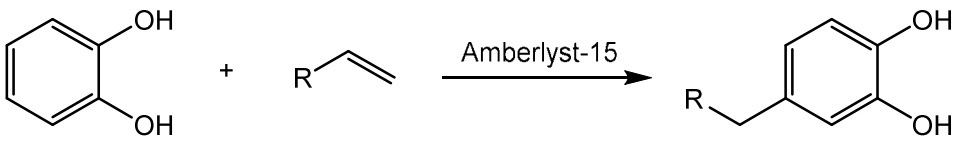
These results indicate the significant promise of **[53]** and its analogues as anti-wear additives for both engine oils and driveline conditions.

6.5 Future Work

In order to understand the nature of the films being formed during HFRR testing of these species, SEM-EDS surface analysis of the wear scars formed during the process would be carried out. This would not only give the elemental composition of the film, but also its thickness, offering insight into the anti-wear mechanism taking place. This would be particularly useful for the study of PIB_{1000}-containing species under engine oils conditions at high load, as the HFRR results suggest decomposition and reformation of the film between the two metal surfaces. SEM-EDS analysis would aid in the identification of the film composition both before and after this takes place. Furthermore, the presence or absence of each component of these compounds in the film may confirm the structure-performance relationship postulated by this study, and allow for more in-depth comparisons of these species and the model analogues discussed in Chapter V. The thermal stability of these additives may also be investigated by thermogravimetric analysis, in order to further probe the nature of any decomposition taking place during HFRR testing.

As lower molecular weight compounds **[70]-[74]** exhibited superior performance to the other species tested, future work would involve further testing of these species. This would include the additional engine oils tests and fully formulated driveline HFRR tests carried out on **[53]**. If the results of these tests are positive, further testing of the properties of these species may be carried out, such as corrosion tests, compatibility with other components (*e.g.* seals), and tests carried out in full automotive engines and driveline transmissions.

As the length of the pyroborate component appears to not only affect solubility but also performance, further attempts to lower the molecular weights of these species



Scheme 6.1 Synthesis of shorter-chain catechols, where R = n-octyl, n-heptyl, etc.

may be carried out, *via* the synthesis of shorter-chain alkyl catechols (Scheme 6.1). The alkylphosphate-bound pyroborates formed from these components would then be tested, in the hope of producing an additive possessing the ideal combination of low molecular weight, oil solubility, hydrolytic stability and anti-wear performance.

Chapter VII

Global Conclusions

7.1 Global Conclusions

Although the simple pyroborates **[1]**, **[10]** and **[13]** were known prior to this study, the synthetic methodology to produce such species has been expanded to provide an array of novel pyroborate esters from a variety of aryl and alkyl 1,2- and 1,3-diols.

The Lewis acidity of the pyroborate compounds was investigated *via* the Gutmann-Beckett method, revealing a significant drop in Lewis acidity as alkyl substituents are incorporated into the species. Furthermore, aromatic moieties were found to be crucial for imparting Lewis acidity. Calculation of the Acid Numbers of the compounds highlighted the high Lewis acidity of compounds **[1]-[3]** and **[10]**, suggesting their possible suitability as Lewis acid anion binders or catalysts. Perbrominated pyroborate **[5]** was found to be significantly less Lewis acidic than expected, with DFT calculations suggesting this may arise from significant twisting of the molecule due to the sterically-demanding bromide substituents, decoupling the π-electron networks of the two boron centres. Not only does this offer insight into the high Lewis acidity of these species having originated from the electron withdrawing effect of having two borates attached to one another, it indicates how this may be significantly disrupted by the choice of substituents on the aryl rings of the pyroborate moiety.

A series of four-coordinate bis-borate species **[18]-[33]** has been synthesised from a variety of aromatic 1,2- and 1,3-diols *via* a simple, industrially applicable, solvent-free methodology. This improved upon previously employed synthetic routes, which involve significant use of organic solvents for purification purposes. Furthermore, this route was extended for use with long-chain catechol derivates which could be exploited in future work in the preparation of anti-wear additives of this nature.

Compounds **[18]**, **[19]**, **[21]**, **[26]**, **[32]** and **[33]** were found to be highly crystalline, and so could be further analysed by X-ray crystallography. It was revealed that small variations in the substitution of the catechol rings had a significant degree of impact upon the solid state structure of these species. Hydrogen bond distances were found to be relatively long compared to related species, indicating weak hydrogen bonding interactions, and highlighting a great degree of separation between the ion pairs, which may require consideration in electrochemical applications.

Preliminary conductivity investigations were carried out for compounds **[26]**, **[27]**, **[33]**, **[34]**, **[35]** and **[36]**. These species were found to exhibit lower conductivities than similar bis-borates in the literature, which may be attributed to their lack of solubility and large ionic radii. Therefore, in their current form, these compounds are unsuitable for electrochemical applications, but with this knowledge in hand, steps may be made for further structural variation which may open up this avenue of research.

Through a combination of various pyroborates and anionic starting materials, short-chain species of the general formula $\{[RO_2B)_2O][EO_2X_n]\}\{NR_4\}$ were investigated as models for the longer-chain species to be tested as lubricant additives. This revealed a complex array of processes occurring in solution. Attempts to synthesise a dihydrogen-phosphate bound complex were unsuccessful, with four-coordinate bis-borate $[cat_2B][N^nBu_4]$ **[36]** being isolated. The formation of **[36]** was investigated using NMR spectroscopy, which revealed that borate-phosphate species may be formed, broken down and reformed, depending on the ratio of each starting material in solution. Furthermore, this process appears to be unique to pyroborate species, as binding did occur between $[N^nBu_4][H_2PO_4]$ and $B(OPh)_3$, which may open a new avenue of research into the synthesis of borate-phosphate species.

Investigations using alkylphosphate-bound species were more successful, with significant retention of the phosphate component being observed in each case. The binding of such species was exposed to consist of a collection of different interactions between the starting species, rendering calculation of the binding coefficients for these events impossible. Interestingly, it was also found that primary ammonium counterions led to mixtures which did not contain a four-coordinate bis-borate species, despite these compounds being synthetically accessible through other routes. A deeper delve into the species formed in these cases may serve to reveal even more about the processes taking place between pyroborate and ammonium phosphates in solution.

The binding interactions of pyroborates **[1]** and **[3]** with acetate, benzoate and methanesulfonate were revealed to be much more straight forward, with 1:1 binding dominating in each case. This allowed for the determination of the binding constants for these interactions using NMR titrations. Binding of acetate and benzoate is modest, and the Lewis acidity of the pyroborate receptor has some effect on the resulting binding strength with benzoate. **[1]** shows high affinity to methanesulfonate, which is unusual as receptors specific to anions such as this are rare and usually highly selective. It is possible that methanesulfonate binds in a different mode to the other oxoanions studied, resulting in much stronger binding.

This methodology was easily adapted to the synthesis of long-chain alkylphosphate-bound compounds, and a series of these species was synthesised, **[53]-[75]**. Long alkyl-chain substituents imparted sufficient hydrolytic stability for these reactions to be carried out under normal atmospheric conditions. Their NMR spectra matched the corresponding short-chain analogues, suggesting that, although binding of phosphates with pyroborates has been shown to be complex, short-chain species are indeed useful models for longer-chain derivatives. The synthesis of longer-chain analogues proved

to be easily scaled up, with no limit to reaction size being encountered thus far, indicating their viability to be commercially produced.

With achieving both hydrolytic stability and oil solubility in mind, the molecular weight of the long-chain compounds was successfully reduced *via* the introduction of shorter-chain catechol pyroborate components, providing desirable lower molecular weight species for testing.

Many of the species tested exhibited superior performance to the baseline additives under both engine oils and driveline conditions, indicating their viability as a new family of anti-wear additives. Furthermore, many compounds presented good anti-wear performance at higher temperatures during engine oils tests, unlike the baseline additive. Some PIB-containing compounds appeared to suffer film breakdown and reformation under engine oils conditions at higher temperatures, suggesting conversion to a decomposition product. However, this new film continued to provide friction-reducing performance until the end of the test, further exemplifying their superiority to additives currently employed for this application.

HFRR testing of the suitable compounds did offer some insight into the structure-performance relationship of these species. Increasing the chain length of the bound alkylphosphate generally enhanced the anti-wear and anti-friction performance of compounds under both engine oils and driveline conditions. However, the highly branched $C_{13}H_{27}$-phosphate was consistently detrimental to performance. Similarly, the use of primary ammonium counterions typically increased levels of friction and wear under both engine oils and driveline conditions. This is despite the species containing these components exhibiting high contact potentials under driveline conditions, indicating that it may be the nature of the film formed, not its successful

formation, which leads to poor performance. Lowering the molecular weight of the compounds *via* shortening of the alkyl chain on the pyroborate component generally led to an improvement in anti-wear and anti-friction performance under both engine oils and driveline conditions, with compounds **[70]**-**[74]** consistently outperforming other species and the baseline additives, even at higher loads. This may be due to the higher relative amounts of boron in these lower molecular weight species. These insights provide us with a strong starting point for the further development of these compounds to produce additives with optimum friction- and wear-reducing performance under both engine oil and driveline conditions.

Compound **[53]** was taken forward for further engine oils tests, offering a greater than expected level of anti-oxidancy and performing very strongly in the microcoker deposit test, outperforming a current Lubrizol dispersant and increasing the onset temperature for deposit formation on a metal surface. **[53]** did underperform on the hot tube test, indicating the formation of deposits on glassy surfaces at high temperatures may present an issue, but it has not been ruled out of further testing at present. This combination of results indicates the promise of not only compound **[53]** but this entire family of species as engine oil anti-wear additives, and it is antipicated that lower molecular derivatives such as **[70]**-**[74]** may perform even better.

Compound **[53]** performed very well in fully formulated driveline HFRR tests, exhibiting low wear and friction, and proving its efficiency as part of a full driveline oil package. Furthermore, **[53]** offered superior contact potentials at both loads and treat rates and exhibited more stable films throughout the tests. These testing results are a clear indication that there is a strong case for compounds of this nature to be taken forward as a new generation of lubricant additives. Their outperformance over

additives currently employed in both engine oil and driveline applications merits their continued investigation for this purpose.

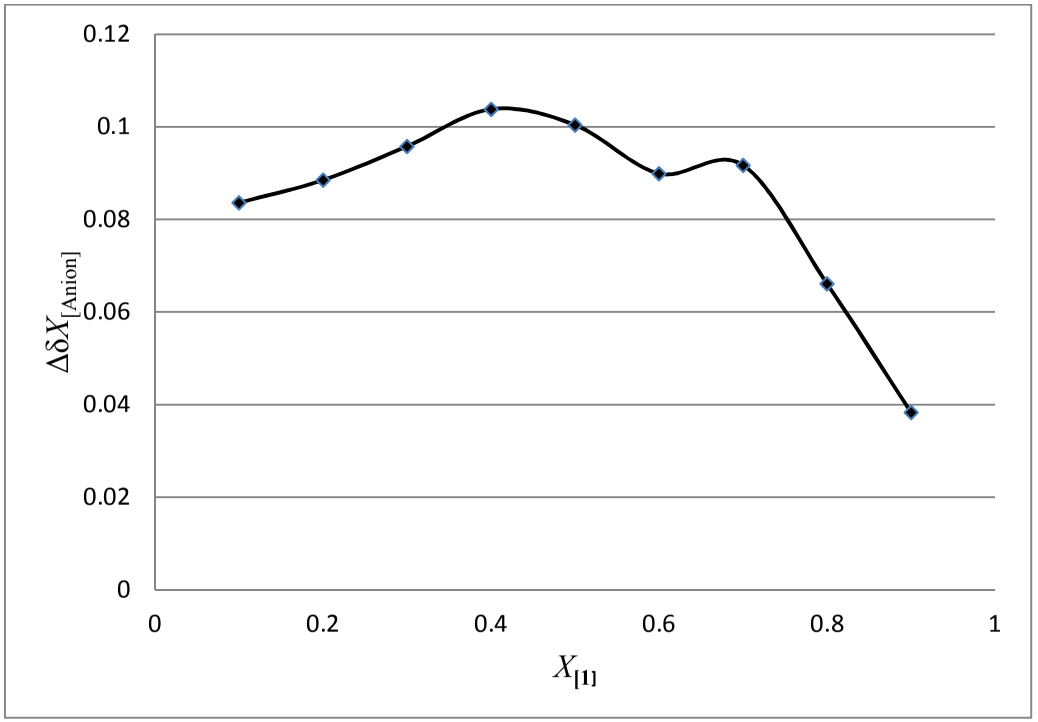
Appendix I. Crystallography Data Tables

	[3]	[26]	[18]	[28]	[19]	[32]	[21]	[33]
Internal Code	AGBDKC	CKMHMD	CKMHMJ	CKMHMO	CKMHMP	CKMHLX	CKMHMK	CKMHMB
Formula	$C_{14}H_{12}B_2O_7$	$C_{26}H_{40}BNO_6$	$C_{18}H_{24}BNO_4$	$C_{21.5}H_{20}BBr_8NO_4$	$C_{24}H_{36}BNO_4$	$C_{27}H_{30}BCl_2NO_4$	$C_{67}H_{86}B_4Cl_6N_4O_{16}$	$C_{32}H_{40}BNO_4$
M_w	313.86	473.40	329.19	1006.47	413.35	514.23	1459.33	513.46
Crystal system	Monoclinic	Monoclinic	Monoclinic	Monoclinic	Orthorhombic	Monoclinic	Triclinic	Monoclinic
Space Group	$P2_1/c$	$P2_1/n$	$P2_1/n$	C2/c	Pccn	C2/c	P-1	Cc
Crystal size/mm	0.13 × 0.07 × 0.06	0.32 × 0.19 × 0.13	0.27 × 0.26 × 0.13	0.08 × 0.03 × 0.02	0.06 × 0.01 × 0.01	0.95 × 0.54 × 0.31	0.12 × 0.07 × 0.04	0.61 × 0.45 × 0.18
a (Å)	8.2904(16)	10.8140(9)	8.7081(4)	27.225(3)	22.1052(16)	30.306(3)	15.6889(17)	8.0856(8)
b (Å)	17.4873(4)	17.2762(13)	10.0186(4)	10.8780(8)	25.289(2)	10.9282(8)	16.892(2)	31.352(3)
c (Å)	17.5806(4)	7.4854(6)	20.1456(9)	23.420(3)	8.433(6)	15.8481(13)	17.1227(14)	11.6986(13)
α (°)	90	90	90	90	90	90	88.532(8)	90
β (°)	90.7962(19)	103.299(7)	95.813(4)	123.224(15)	90	102.120(9)	66.515(9)	109.555(13)
γ (°)	90	90	90	90	90	90	64.747(11)	90
V (Å^3)	2548.54(10)	1360.95(19)	1748.53(13)	5802.3(12)	4714(3)	5131.7(7)	3706.8(8)	2794.5(5)
Z	4	2	4	8	8	8	2	4
T (K)	120(2)	120(2)	120(2)	120(2)	120(2)	120(2)	120(2)	120(2)
D_{calc} (g cm^{-3})	1.532	1.234	1.251	2.304	1.165	1.331	1.307	1.220
F_{000}	648.0	1024.0	704.0	3784.0	1792.0	2160.0	1532.0	1104.0
μ (mm^{-1})	1.022	0.691	0.701	13.481	0.075	2.550	2.657	0.620
θ range for data collection (°)	5.032 to 74.039	4.201 to 74.305	3.882 to 66.599	4.935 to 74.462	4.312 to 74.141	1.186 to 16.257	3.364 to 75.764	4.904 to 66.529
Max. and min. Transmission	0.825 and 0.929	0.989 and 0.997	0.789 and 0.491	0.875 and 0.936	0.583 and 0.240		0.977 and 0.958	0.908 and 0.748
reflns measd	10541	10341	15501	7199	10759	7896	28176	4772
independent reflns	4978	2578	5124	3461	5074	1326	14517	3219
R_{int}	0.026	0.048	0.0797	0.025	0.0326	0.2791	0.1214	0.0219
Final *GooF*	1.083	1.056	1.097	1.021	1.039	0.826	1.006	2.037
R_1, wR_2 [$I > 2\sigma(I)$]	0.0377, 0.1474	0.0439, 0.1124	0.0829, 0.2478	0.0363, 0.0905	0.0522, 0.1364	0.0784, 0.1631	0.1082, 0.2705	0.1288, 0.3816
R_1, wR_2 (all data)	0.0645, 0.1533	0.0617, 0.1247	0.1194, 0.2783	0.0420, 0.0952	0.0563, 0.1409	0.1801, 0.2056	0.1962, 0.3545	0.1292, 0.3825
min. and max. electron densities (e Å^{-3})	−0.28, 0.52	−0.32, 0.26	−1.30, 1.75	−0.20, 0.24	−0.74, 0.74	−0.19, 0.20	−0.81, 0.45	−0.61, 0.75

Appendix II. Job Plot and NMR Titration Data

Job plot data for the binding of $[H^nBuPO_4]^-$ to $(catB)_2O$ [1].

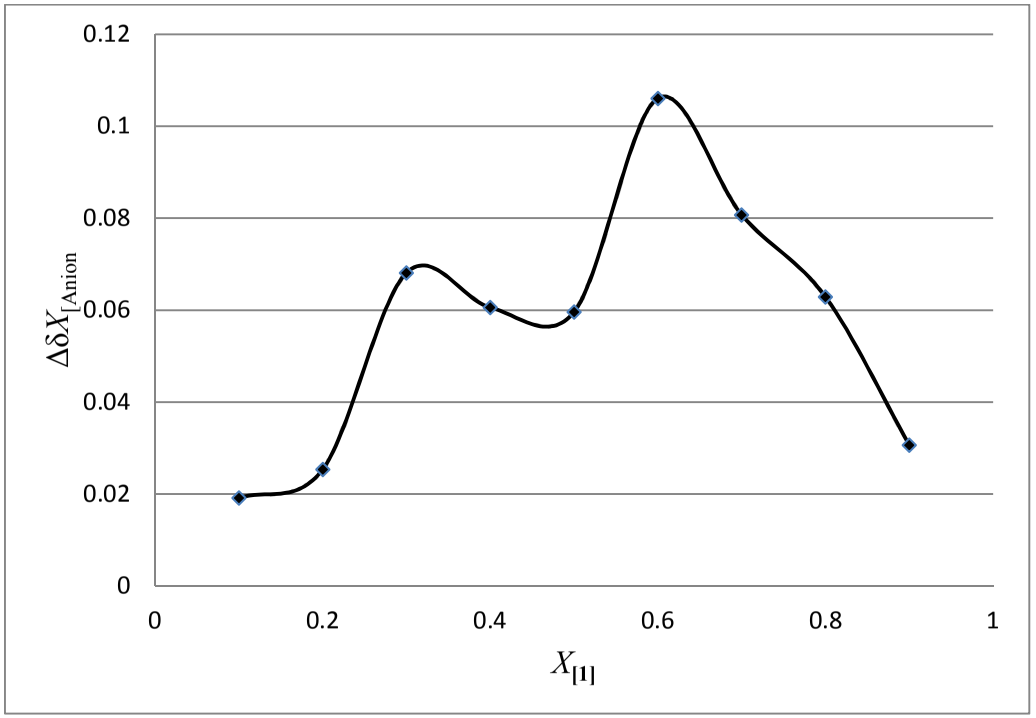
Volume **[1]** (μL)	Volume Anion (μL)	[**[1]**] (mM)	[Anion] (mM)	$X_{[1]}$	$X_{[Anion]}$	δ	Δδ	$X_{[Anion]}$
100	900	5	45	0.1	0.9	3.9129	0.0929	0.0836
200	800	10	40	0.2	0.8	3.9306	0.1106	0.0885
300	700	15	35	0.3	0.7	3.9569	0.1369	0.0958
400	600	20	30	0.4	0.6	3.9930	0.1730	0.1038
500	500	25	25	0.5	0.5	4.0209	0.2009	0.1004
600	400	30	20	0.6	0.4	4.0448	0.2248	0.0899
700	300	35	15	0.7	0.3	4.1258	0.3058	0.0917
800	200	40	10	0.8	0.2	4.1504	0.3304	0.0661
900	100	45	5	0.9	0.1	4.2034	0.3834	0.0383



Job plot for the binding of $[H^nBuPO_4]^-$ to $(catB)_2O$ [1].

Job plot data for the binding of $[H^{i}BuPO_4]^-$ to $(catB)_2O$ [1] following α-CH_2 proton.

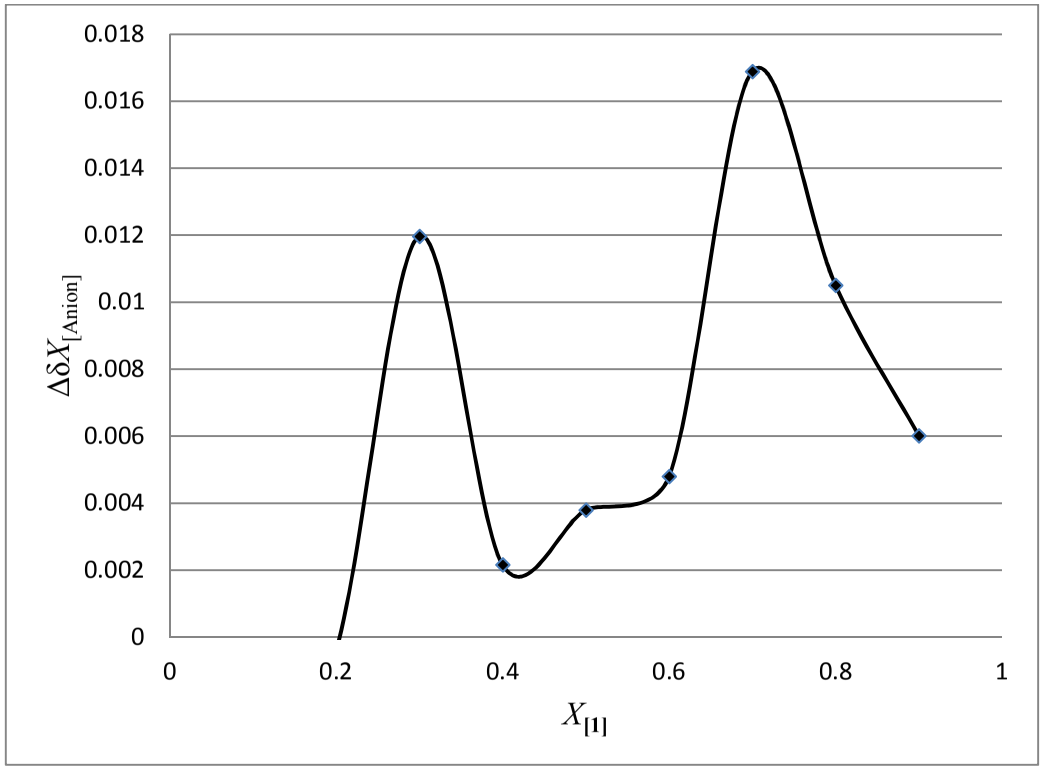
Volume **[1]** (μL)	Volume Anion (μL)	[**[1]**] (mM)	[Anion] (mM)	$X_{[1]}$	$X_{[Anion]}$	δ	Δδ	$X_{[Anion]}$
100	900	5	45	0.1	0.9	3.681	0.0213	0.0192
200	800	10	40	0.2	0.8	3.6914	0.0317	0.0254
300	700	15	35	0.3	0.7	3.757	0.0973	0.0681
400	600	20	30	0.4	0.6	3.7607	0.1010	0.0606
500	500	25	25	0.5	0.5	3.7789	0.1192	0.0596
600	400	30	20	0.6	0.4	3.9249	0.2652	0.1061
700	300	35	15	0.7	0.3	3.9288	0.2691	0.0807
800	200	40	10	0.8	0.2	3.9741	0.3144	0.0629
900	100	45	5	0.9	0.1	3.9666	0.3069	0.0307



Job plot for the binding of $[H^iBuPO_4]^-$ to $(catB)_2O$ [1] following α-CH_2 proton.

Job plot data for the binding of $[H^iBuPO_4]^-$ to $(catB)_2O$ [1] following β-CH proton.

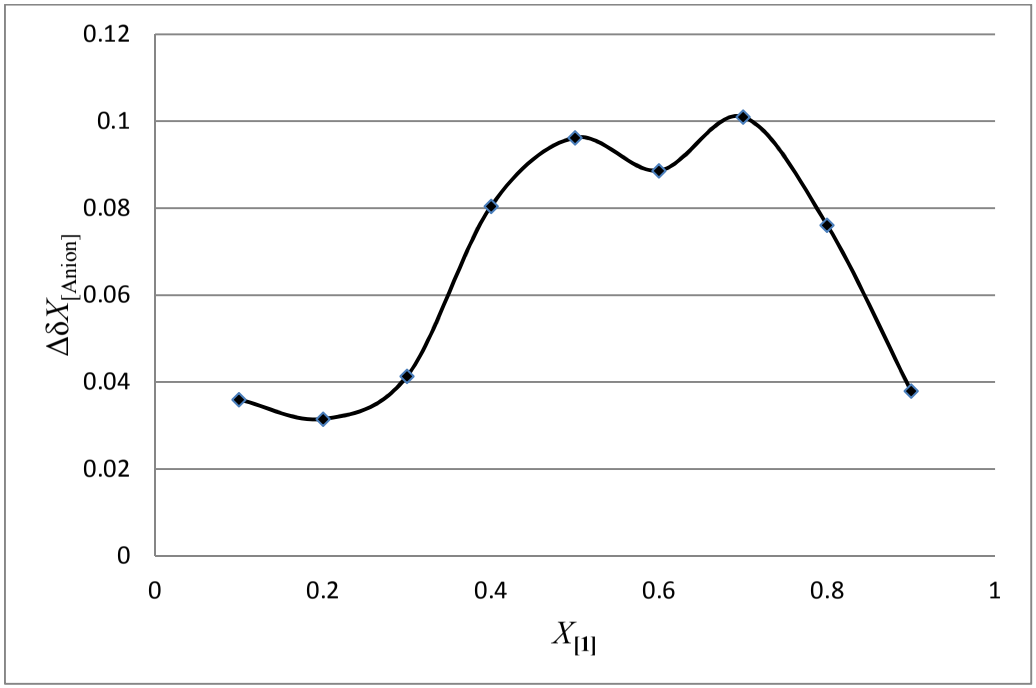
Volume **[1]** (μL)	Volume Anion (μL)	[**[1]**] (mM)	[Anion] (mM)	$X_{[1]}$	$X_{[Anion]}$	δ	Δδ	$X_{[Anion]}$
100	900	0.5	4.5	0.1	0.9	1.9007	-0.0055	−0.0050
200	800	1	4	0.2	0.8	1.9057	-0.0005	−0.0004
300	700	1.5	3.5	0.3	0.7	1.9233	0.0171	0.0120
400	600	2	3	0.4	0.6	1.9098	0.0036	0.0022
500	500	2.5	2.5	0.5	0.5	1.9138	0.0076	0.0038
600	400	3	2	0.6	0.4	1.9182	0.0120	0.0048
700	300	3.5	1.5	0.7	0.3	1.9625	0.0563	0.0169
800	200	4	1	0.8	0.2	1.9587	0.0525	0.0105
900	100	4.5	0.5	0.9	0.1	1.9663	0.0601	0.0060



Job plot for the binding of $[H^{i}BuPO_4]^-$ to $(catB)_2O$ [1] following β-CH proton.

Job plot data for the binding of [^{n}Bu$_2$PO$_4$]$^-$ to (catB)$_2$O [1].

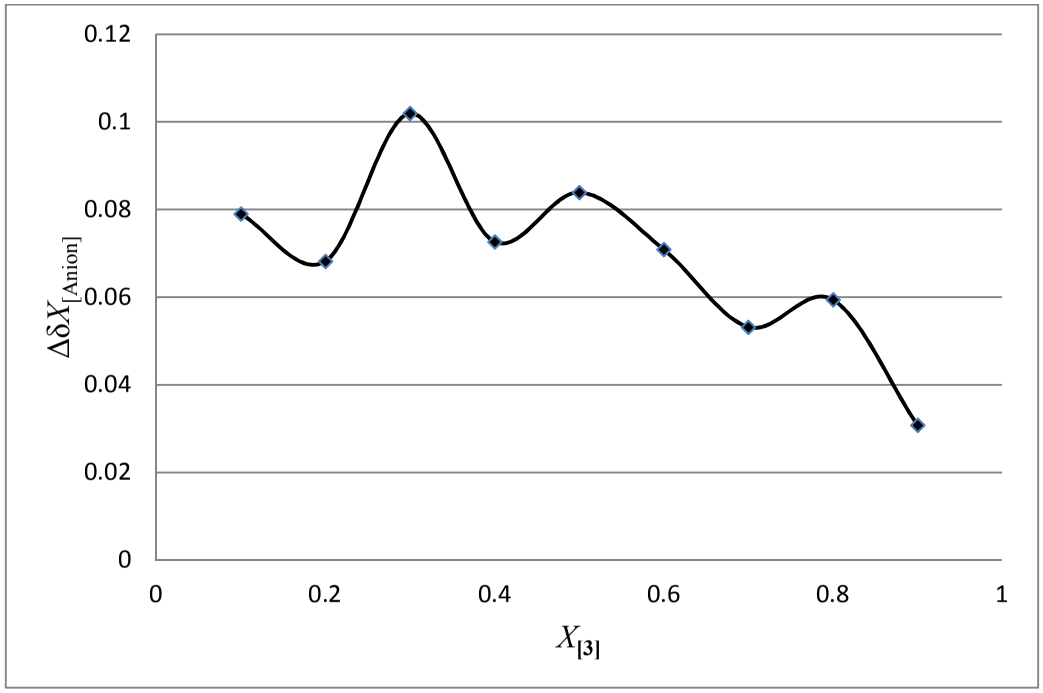
Volume **[1]** (μL)	Volume Anion (μL)	[**[1]**] (mM)	[Anion] (mM)	$X_{[1]}$	$X_{[Anion]}$	δ	Δδ	$X_{[Anion]}$
100	900	5	45	0.1	0.9	3.8924	0.0400	0.0360
200	800	10	40	0.2	0.8	3.8918	0.0394	0.0315
300	700	15	35	0.3	0.7	3.9115	0.0591	0.0414
400	600	20	30	0.4	0.6	3.9865	0.1341	0.0805
500	500	25	25	0.5	0.5	4.0448	0.1924	0.0962
600	400	30	20	0.6	0.4	4.0740	0.2216	0.0886
700	300	35	15	0.7	0.3	4.1890	0.3366	0.1010
800	200	40	10	0.8	0.2	4.2329	0.3805	0.0761
900	100	45	5	0.9	0.1	4.232	0.3796	0.0380



Job plot for the binding of [^{n}Bu$_2$PO$_4$]$^-$ to (catB)$_2$O [1].

Job plot data for the binding of $[H^nBuPO_4]^-$ to $(3\text{-MeOcatB})_2O$ [3].

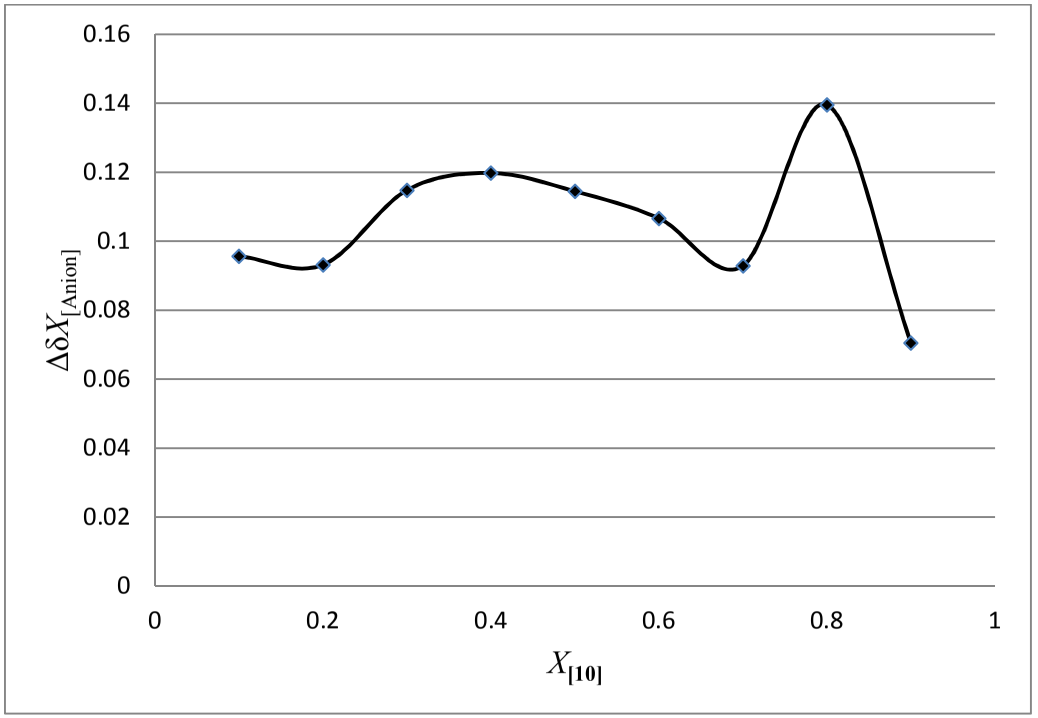
Volume **[3]** (μL)	Volume Anion (μL)	[**[3]**] (mM)	[Anion] (mM)	$X_{[3]}$	$X_{[Anion]}$	δ	Δδ	$X_{[Anion]}$
100	900	5	45	0.1	0.9	3.9078	0.0878	0.0791
200	800	10	40	0.2	0.8	3.9352	0.0852	0.0682
300	700	15	35	0.3	0.7	3.9956	0.1456	0.1019
400	600	20	30	0.4	0.6	3.9711	0.1211	0.0727
500	500	25	25	0.5	0.5	4.0178	0.1678	0.0839
600	400	30	20	0.6	0.4	4.0272	0.1772	0.0709
700	300	35	15	0.7	0.3	4.0272	0.1772	0.0532
800	200	40	10	0.8	0.2	4.1470	0.297	0.0594
900	100	45	5	0.9	0.1	4.1577	0.3077	0.0308



Job plot for the binding of $[H^nBuPO_4]^-$ to $(3\text{-}MeOcatB)_2O$ [3].

Job plot data for the binding of $[H^nBuPO_4]^-$ to $(Naph\text{-}1,2\text{-}O_2B)_2O$ [10].

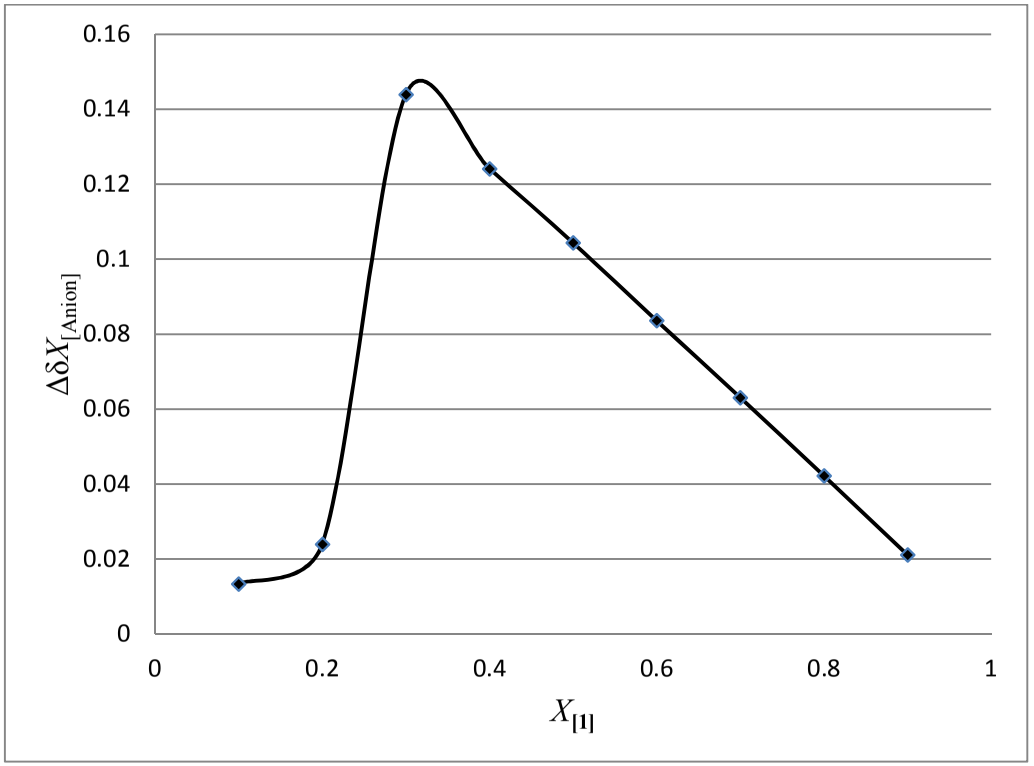
Volume **[10]** (μL)	Volume Anion (μL)	[**[10]**] (mM)	[Anion] (mM)	$X_{[10]}$	$X_{[Anion]}$	δ	Δδ	$X_{[Anion]}$
100	900	0.5	4.5	0.1	0.9	3.9263	0.1063	0.0957
200	800	1	4	0.2	0.8	3.9364	0.1164	0.0931
300	700	1.5	3.5	0.3	0.7	3.984	0.164	0.1148
400	600	2	3	0.4	0.6	4.0196	0.1996	0.1198
500	500	2.5	2.5	0.5	0.5	4.0489	0.2289	0.1145
600	400	3	2	0.6	0.4	4.0865	0.2665	0.1066
700	300	3.5	1.5	0.7	0.3	4.1296	0.3096	0.0929
800	200	4	1	0.8	0.2	4.5176	0.6976	0.1395
900	100	4.5	0.5	0.9	0.1	4.5252	0.7052	0.0705



Job plot for the binding of $[H^nBuPO_4]^-$ to $(Naph\text{-}1,2\text{-}O_2B)_2O$ [10].

Job plot data for the binding of $[AcO]^-$ to $(catB)_2O$ [1].

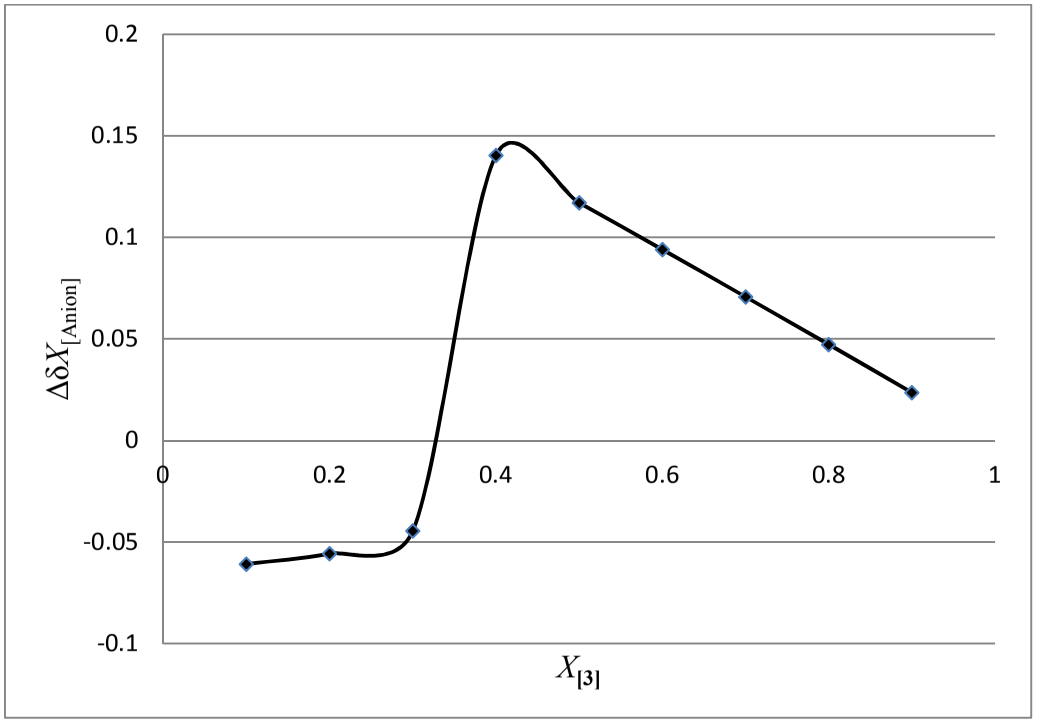
Volume **[1]** (μL)	Volume Anion (μL)	[**[1]**] (mM)	[Anion] (mM)	$X_{[1]}$	$X_{[Anion]}$	δ	Δδ	$X_{[Anion]}$
100	900	5	45	0.1	0.9	2.1691	0.0149	0.0134
200	800	10	40	0.2	0.8	2.1842	0.0300	0.0240
300	700	15	35	0.3	0.7	2.3598	0.2056	0.1439
400	600	20	30	0.4	0.6	2.3611	0.2069	0.1241
500	500	25	25	0.5	0.5	2.3629	0.2087	0.1044
600	400	30	20	0.6	0.4	2.3632	0.2090	0.0836
700	300	35	15	0.7	0.3	2.3645	0.2103	0.0631
800	200	40	10	0.8	0.2	2.3654	0.2112	0.0422
900	100	45	5	0.9	0.1	2.3654	0.2112	0.0211



Job plot for the binding of $[AcO]^-$ to $(catB)_2O$ [1].

Job plot data for the binding of [AcO]⁻ to (3-MeOcatB)$_2$O [3].

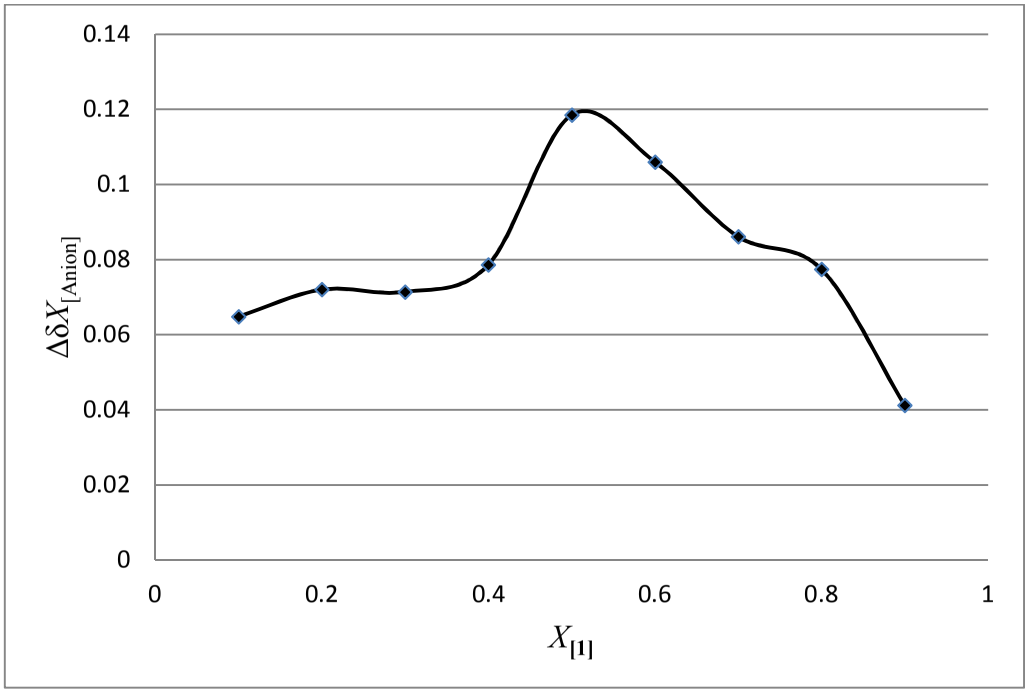
Volume **[3]** (μL)	Volume Anion (μL)	[**[3]**] (mM)	[Anion] (mM)	$X_{[3]}$	$X_{[Anion]}$	δ	Δδ	$X_{[Anion]}$
100	900	5	45	0.1	0.9	2.0592	-0.0680	−0.0608
200	800	10	40	0.2	0.8	2.0572	-0.0700	−0.0557
300	700	15	35	0.3	0.7	2.0632	-0.0640	−0.0445
400	600	20	30	0.4	0.6	2.3607	0.2339	0.1403
500	500	25	25	0.5	0.5	2.361	0.2342	0.1171
600	400	30	20	0.6	0.4	2.3617	0.2349	0.0940
700	300	35	15	0.7	0.3	2.3626	0.2358	0.0707
800	200	40	10	0.8	0.2	2.3632	0.2364	0.0473
900	100	45	5	0.9	0.1	2.3629	0.2361	0.0236



Job plot for the binding of $[AcO]^-$ to $(3\text{-MeOcatB})_2O$ [3].

Job plot data for the binding of $[PhCO_2]^-$ to $(catB)_2O$ [1].

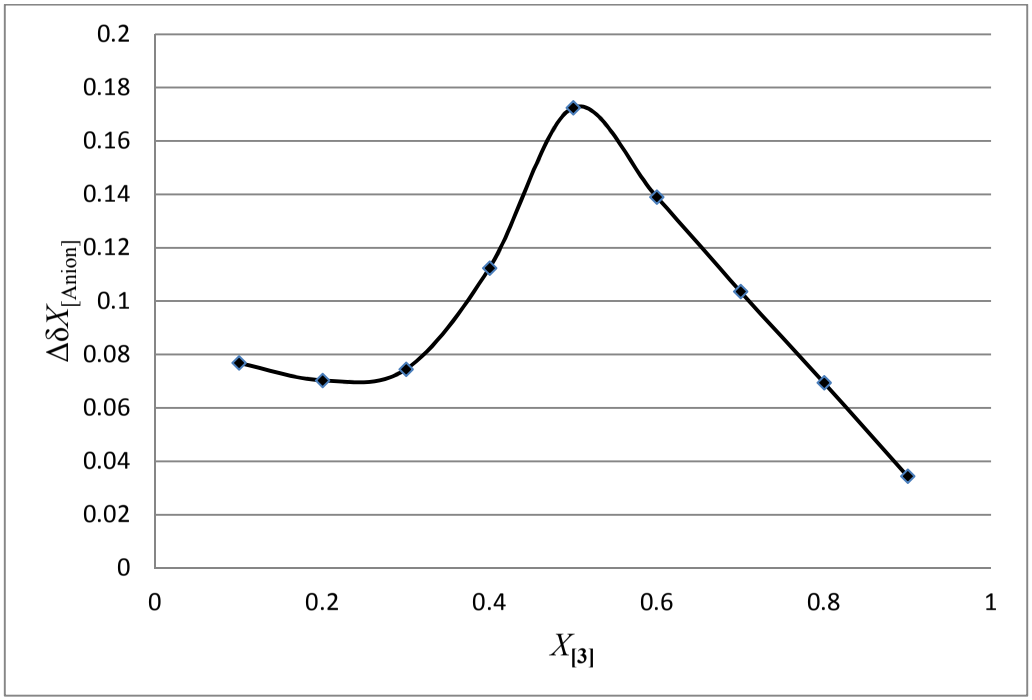
Volume **[1]** (μL)	Volume Anion (μL)	[**[1]**] (mM)	[Anion] (mM)	$X_{[1]}$	$X_{[Anion]}$	δ	Δδ	$X_{[Anion]}$
100	900	5	45	0.1	0.9	7.285	0.0720	0.0648
200	800	10	40	0.2	0.8	7.303	0.0900	0.0720
300	700	15	35	0.3	0.7	7.315	0.1020	0.0714
400	600	20	30	0.4	0.6	7.344	0.1310	0.0786
500	500	25	25	0.5	0.5	7.450	0.2370	0.1185
600	400	30	20	0.6	0.4	7.478	0.2650	0.1060
700	300	35	15	0.7	0.3	7.500	0.2870	0.0861
800	200	40	10	0.8	0.2	7.600	0.3870	0.0774
900	100	45	5	0.9	0.1	7.625	0.4120	0.0412



Job plot for the binding of $[PhCO_2]^-$ to $(catB)_2O$ [1].

Job plot data for the binding of $[PhCO_2O]^-$ to $(3\text{-MeOcatB})_2O$ [3].

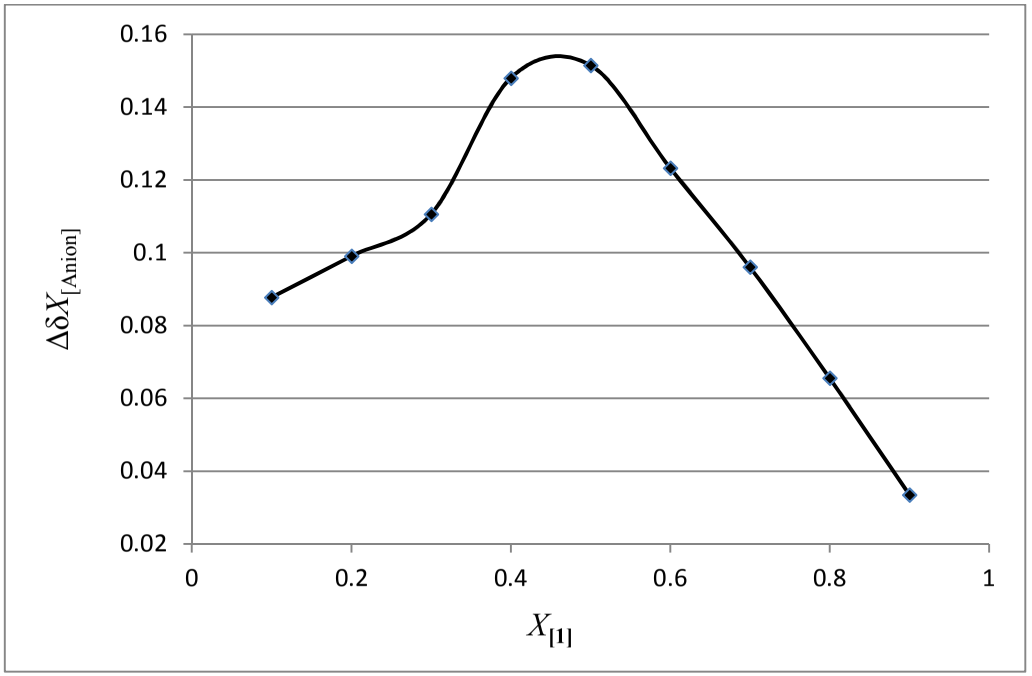
Volume **[3]** (μL)	Volume Anion (μL)	[**[3]**] (mM)	[Anion] (mM)	$X_{[3]}$	$X_{[Anion]}$	δ	Δδ	$X_{[Anion]}$
100	900	5	45	0.1	0.9	7.2860	0.0854	0.0769
200	800	10	40	0.2	0.8	7.2885	0.0879	0.0703
300	700	15	35	0.3	0.7	7.3070	0.1064	0.0745
400	600	20	30	0.4	0.6	7.3880	0.1874	0.1124
500	500	25	25	0.5	0.5	7.5456	0.3450	0.1725
600	400	30	20	0.6	0.4	7.5481	0.3475	0.1390
700	300	35	15	0.7	0.3	7.5462	0.3456	0.1037
800	200	40	10	0.8	0.2	7.5478	0.3472	0.0694
900	100	45	5	0.9	0.1	7.5456	0.3450	0.0345



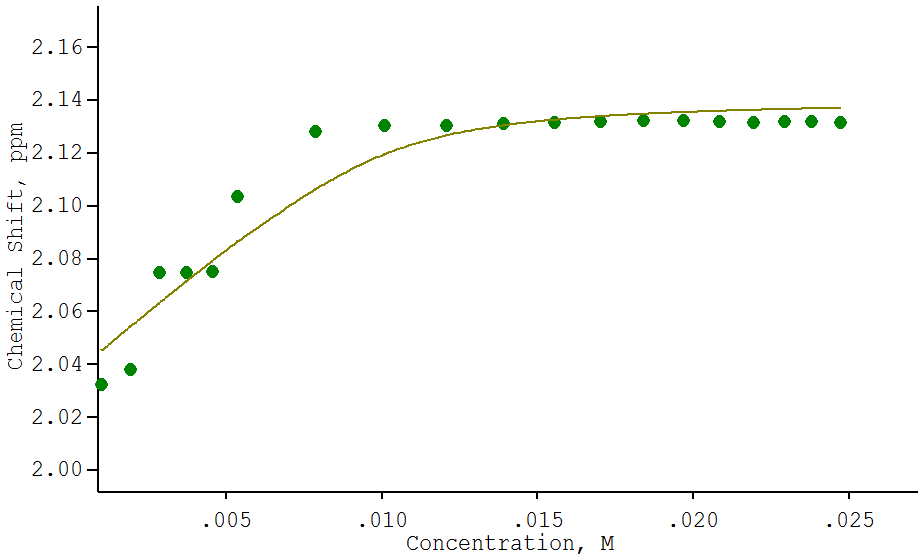
Job plot for the binding of $[PhCO_2]^-$ to $(3\text{-MeOcatB})_2O$ [3].

Job plot data for the binding of $[SO_3Me]^-$ to $(catB)_2O$ [1].

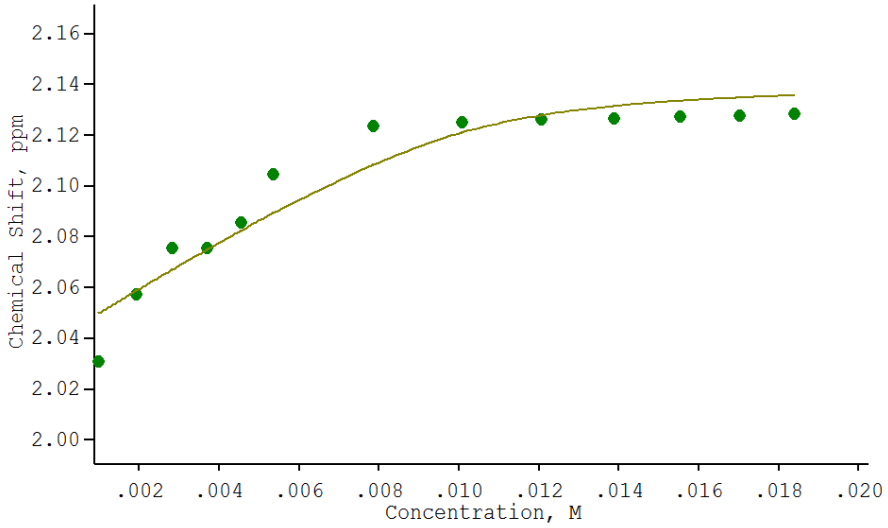
Volume **[1]** (μL)	Volume Anion (μL)	[**[1]**] (mM)	[Anion] (mM)	$X_{[1]}$	$X_{[Anion]}$	δ	Δδ	$X_{[Anion]}$
100	900	5	45	0.1	0.9	2.7928	0.0975	0.0878
200	800	10	40	0.2	0.8	2.8191	0.1238	0.0990
300	700	15	35	0.3	0.7	2.8533	0.1580	0.1106
400	600	20	30	0.4	0.6	2.9419	0.2466	0.1480
500	500	25	25	0.5	0.5	2.9982	0.3029	0.1515
600	400	30	20	0.6	0.4	3.0034	0.3081	0.1232
700	300	35	15	0.7	0.3	3.0154	0.3201	0.0960
800	200	40	10	0.8	0.2	3.0230	0.3277	0.0655
900	100	45	5	0.9	0.1	3.0303	0.3350	0.0335



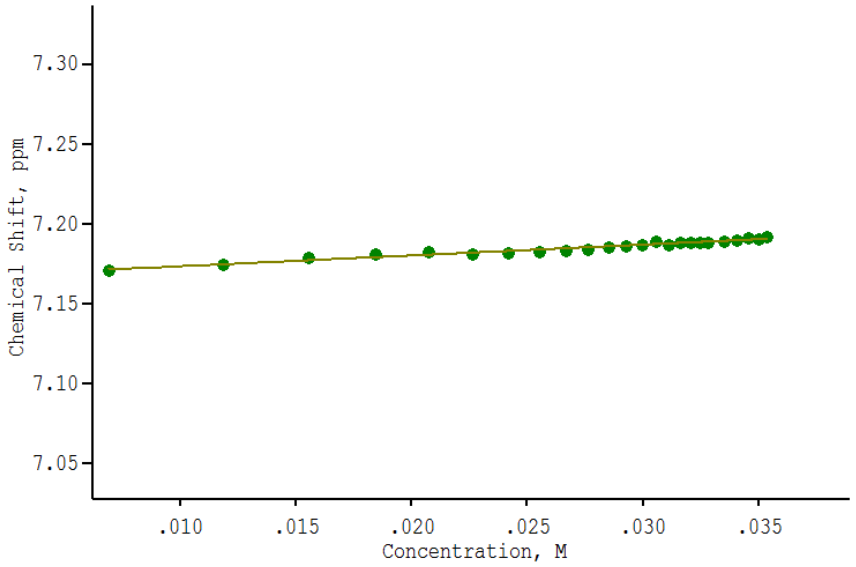
Job plot for the binding of $[SO_3Me]^-$ to $(catB)_2O$ [1].



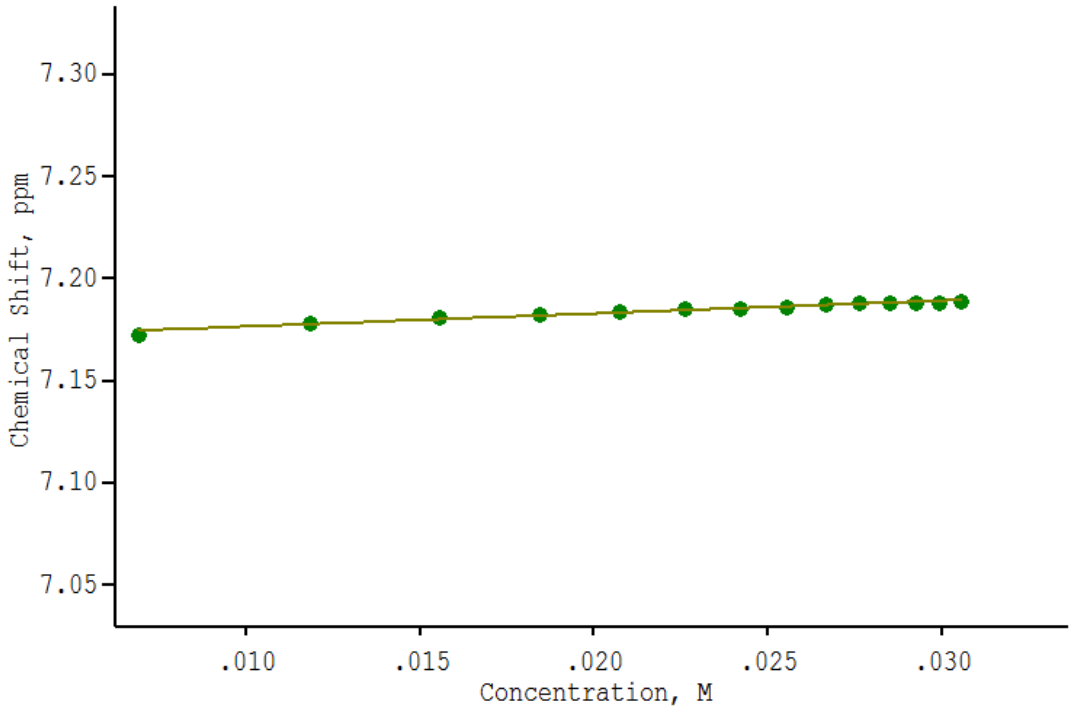
NMR titration curve for the binding of binding of [AcO]⁻ to (catB)₂O [1].



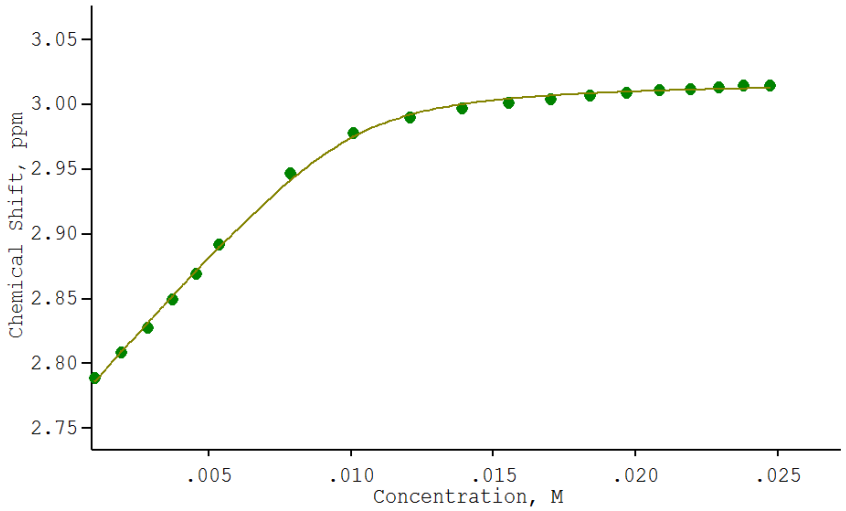
NMR titration curve for the binding of binding of [AcO]⁻ to (3-MeOcatB)₂O [3].



NMR titration curve for the binding of binding of $[PhCO_2]^-$ to $(catB)_2O$ [1].



NMR titration curve for the binding of binding of $[PhCO_2]^-$ to $(3\text{-}MeOcatB)_2O$ [3].



NMR titration curve for the binding of binding of $[SO_3Me]^-$ to $(catB)_2O$ [1].

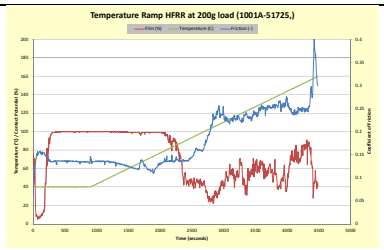
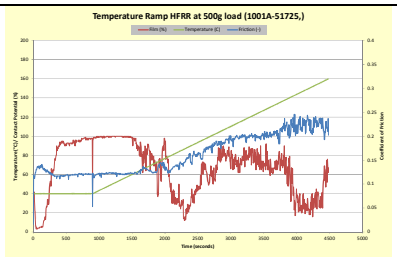
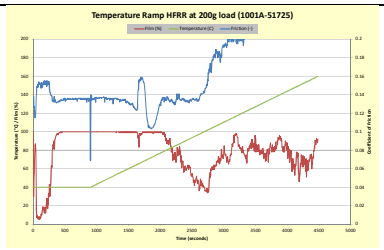
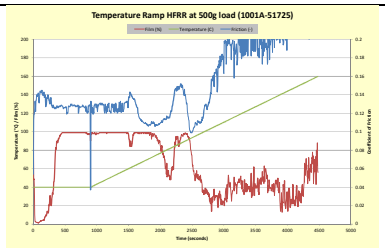
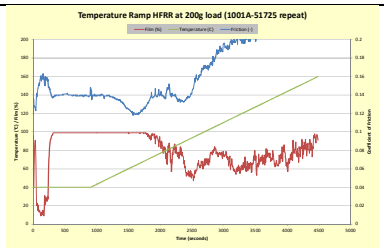
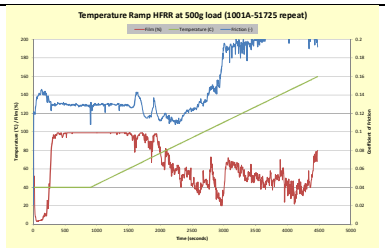
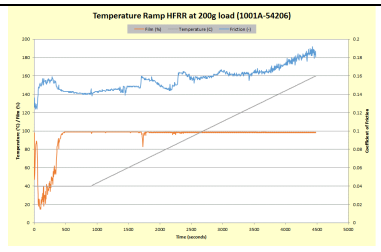
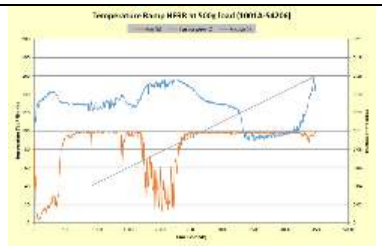
Appendix III. Anti-wear Testing Data

III.I Engine Oil Single-Component HFRR Testing

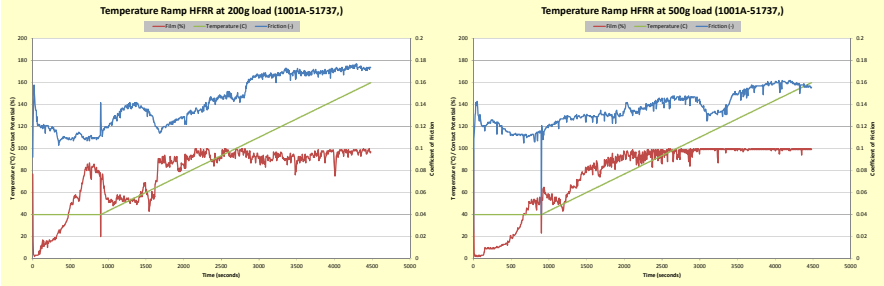
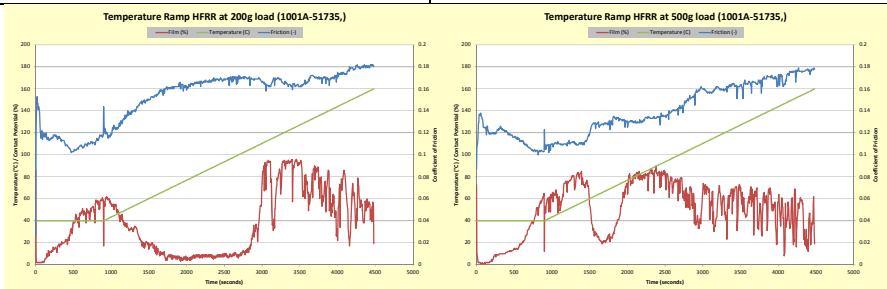
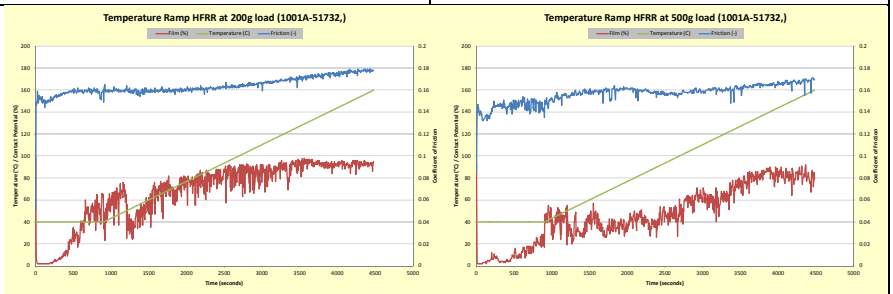
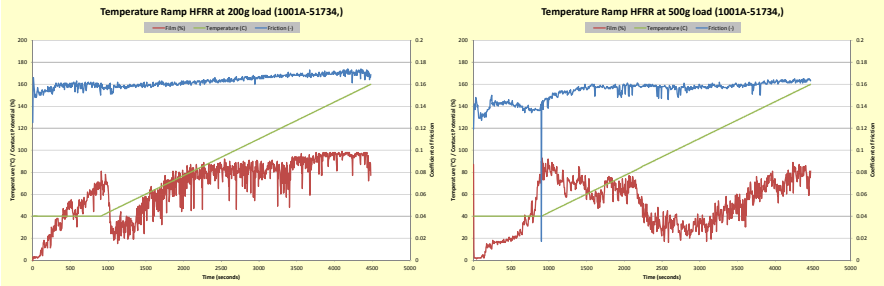
Average Engine Oils HFRR Results.

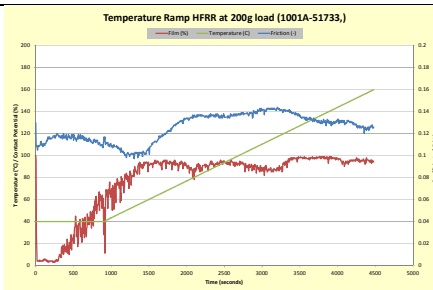
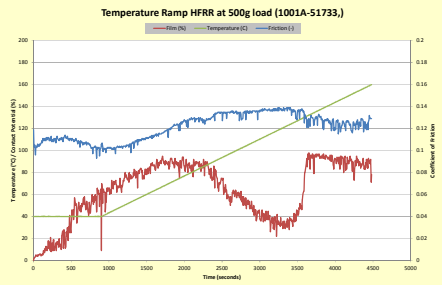
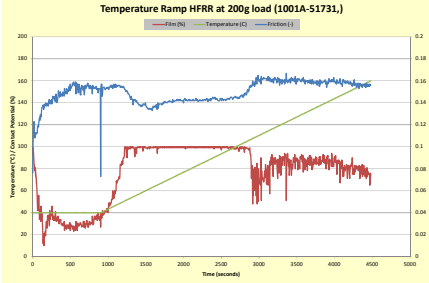
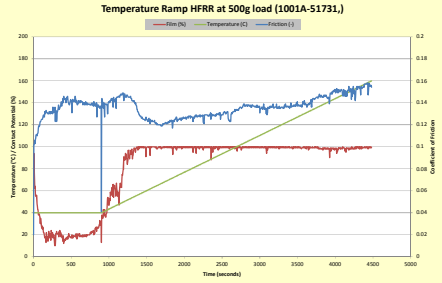
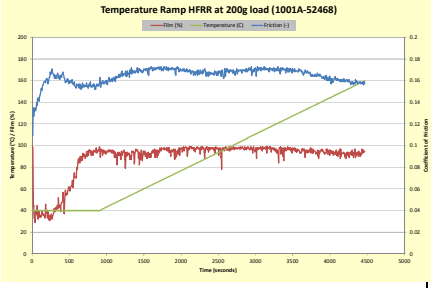
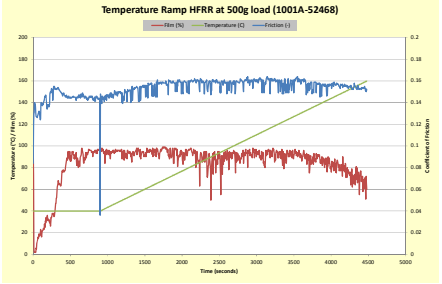
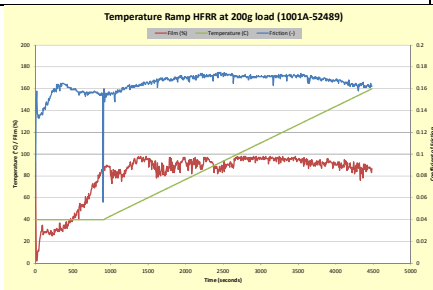
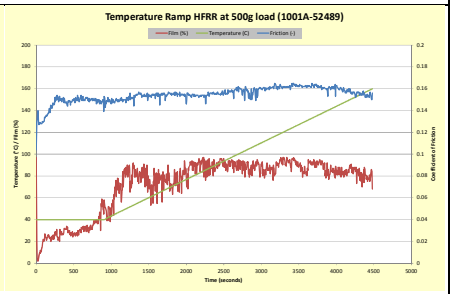
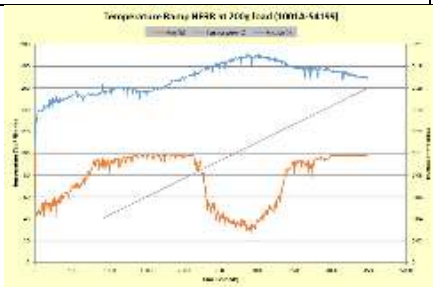
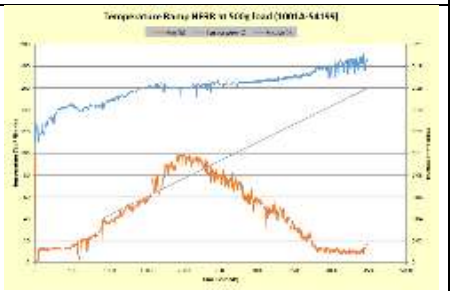
Compound	Wear Scar Diameter, μm		Coefficient of Friction		Contact Potential, %	
	200 g	500 g	200 g	500 g	200 g	500 g
EO AW1	202	265	0.166	0.153	83	71
PIB_{1000}catechol	125	173	0.150	0.141	85	90
PIB_{550}catechol	202	212	0.162	0.145	40	58
[6]	160	316	0.166	0.160	78	56
[7]	312	332	0.164	0.157	74	57
[17]	166	211	0.128	0.125	90	72
[53]	144	264	0.151	0.136	97	95
[54]	205	259	0.164	0.158	97	90
[56]	196	246	0.168	0.157	91	83
[57]	174	225	0.173	0.166	79	51
[58]	167	237	0.140	0.193	98	3
[59]	180	207	0.172	0.162	70	42
[60]	162	204	0.146	0.134	91	87
[61]	160	191	0.147	0.134	92	95
[62]	208	244	0.162	0.157	96	87
[63]	151	161	0.153	0.147	96	93
[64]	204	228	0.173	0.201	70	3
[65]	243	252	0.175	0.185	81	6
[66]	234	255	0.171	0.187	79	13
[69]	223	269	0.152	0.143	85	73
[70]	182	206	0.165	0.148	88	70
[71]	145	269	0.140	0.135	98	76
[72]	182	243	0.143	0.135	96	89
[73]	252	154	0.168	0.136	84	97
[74]	162	211	0.152	0.140	99	94

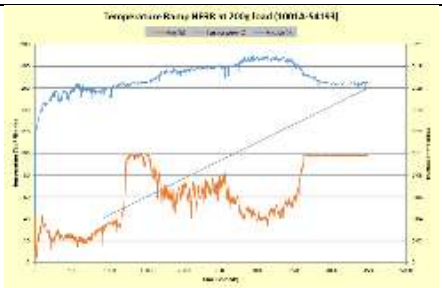
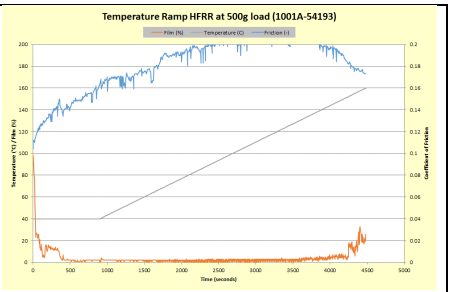
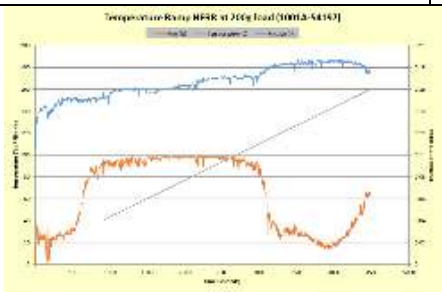
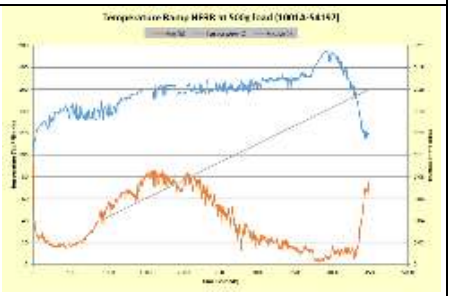
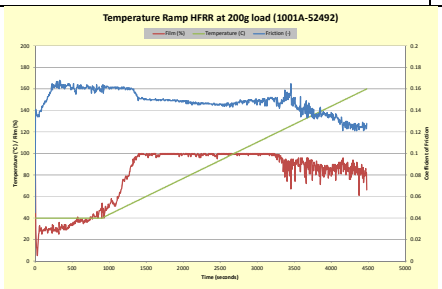
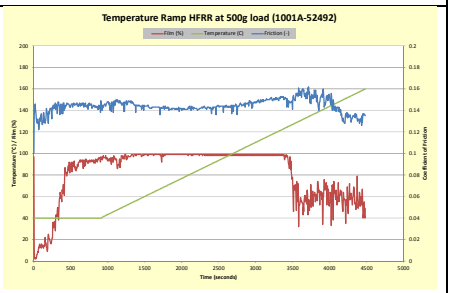
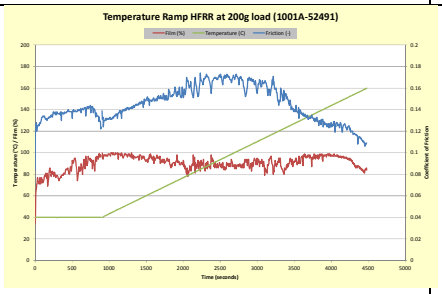
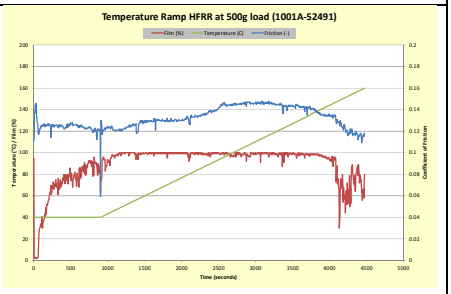
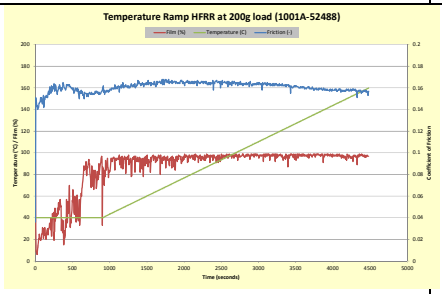
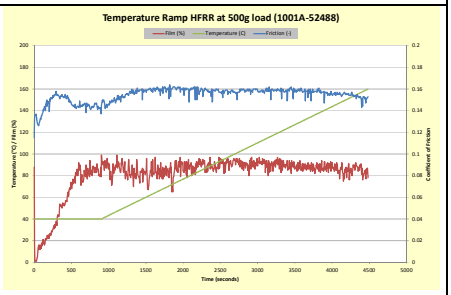
EO AW1 Baseline HFRR traces showing coefficient of friction (blue) and contact potential (red/orange).

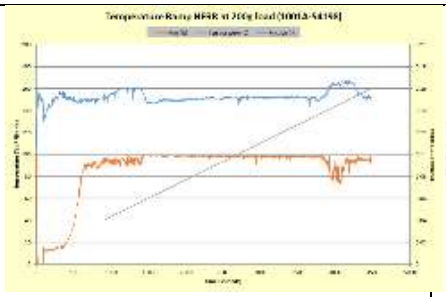
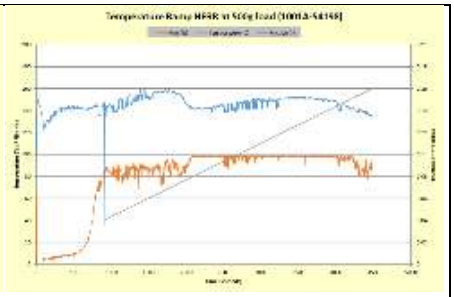
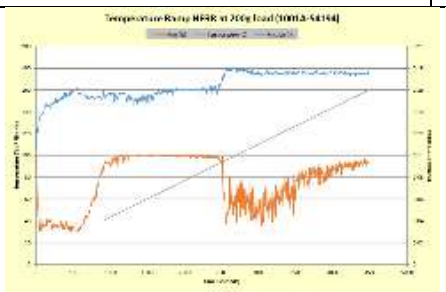
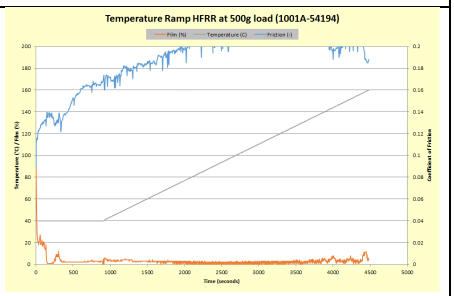
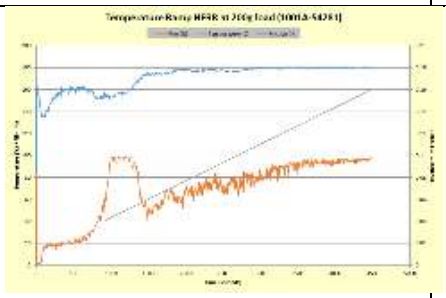
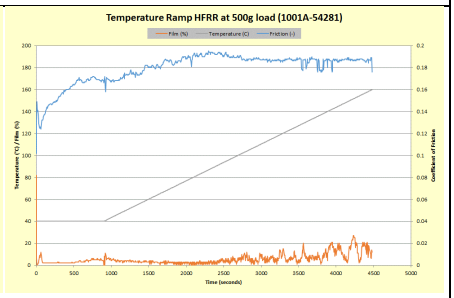
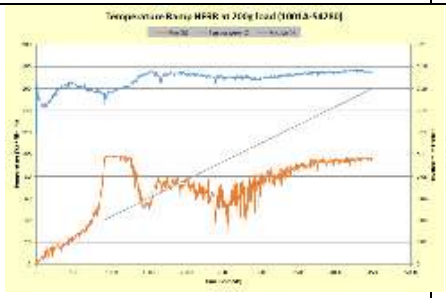
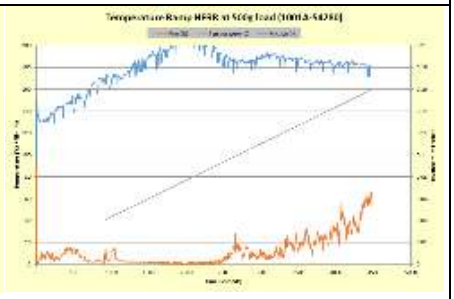
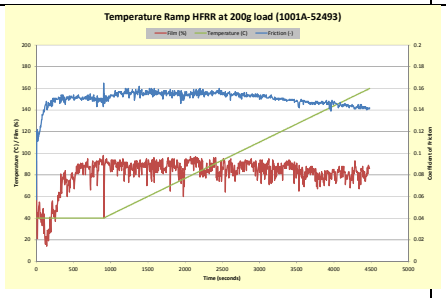
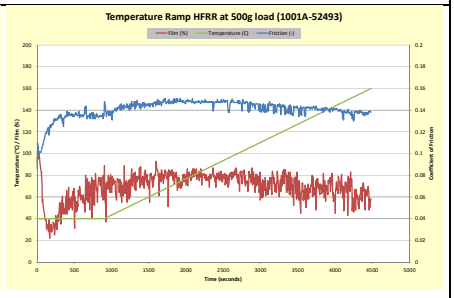
200 g	500 g
	
	
	
	

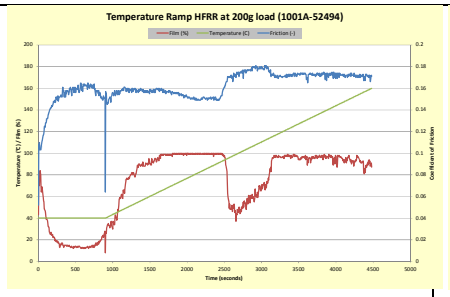
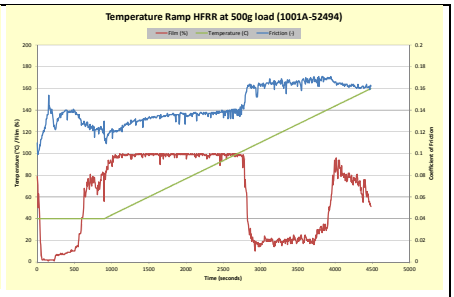
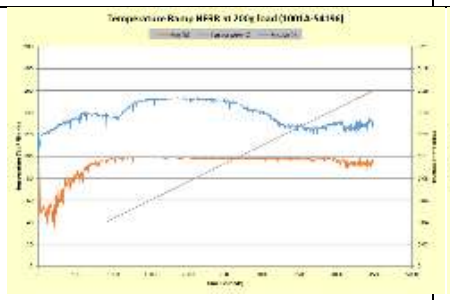
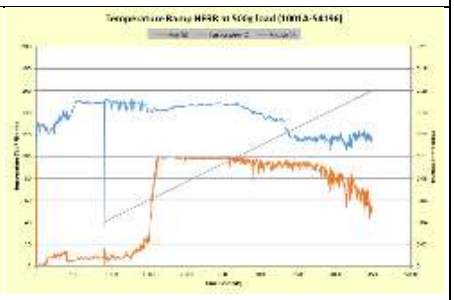
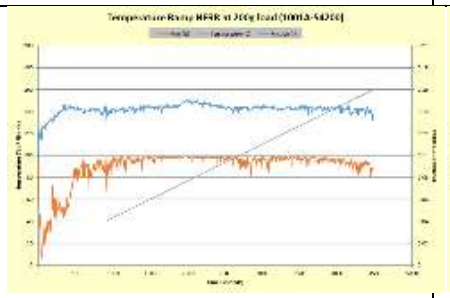
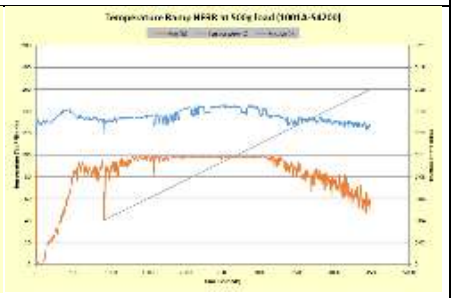
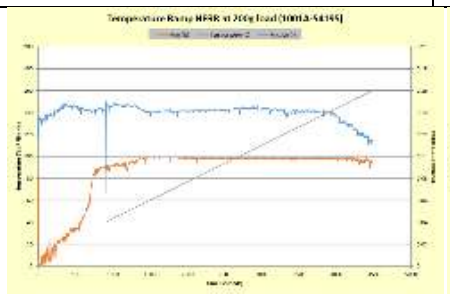
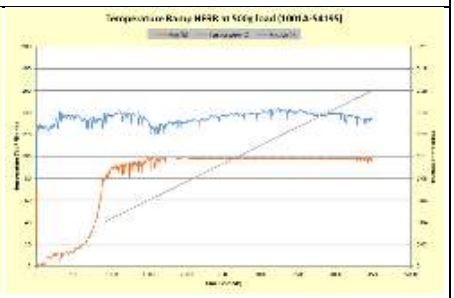
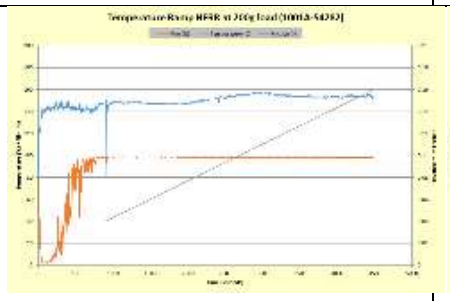
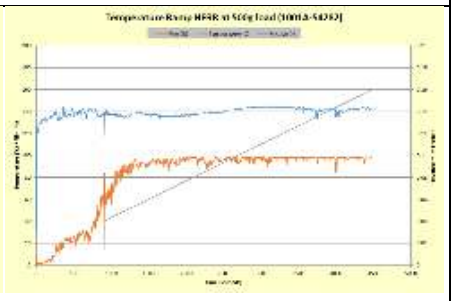
Engine Oil HFRR Traces showing coefficient of friction (blue) and contact potential (red/orange).

Compound	200 g	500 g
PIB_{1000}catechol		
PIB_{550}catechol		
[6]		
[7]		

[17]	 Temperature Ramp HFRR at 200g load (1001A-51733,)  Temperature Ramp HFRR at 500g load (1001A-51733,)
[53]	 Temperature Ramp HFRR at 200g load (1001A-51731,)  Temperature Ramp HFRR at 500g load (1001A-51731,)
[54]	 Temperature Ramp HFRR at 200g load (1001A-52468)  Temperature Ramp HFRR at 500g load (1001A-52468)
[56]	 Temperature Ramp HFRR at 200g load (1001A-52489)  Temperature Ramp HFRR at 500g load (1001A-52489)
[57]	 

[58]		 Temperature Ramp HFRR at 500g load (1001A-54193)
[59]		
[60]	 Temperature Ramp HFRR at 200g load (1001A-52492)	 Temperature Ramp HFRR at 500g load (1001A-52492)
[61]	 Temperature Ramp HFRR at 200g load (1001A-52491)	 Temperature Ramp HFRR at 500g load (1001A-52491)
[62]	 Temperature Ramp HFRR at 200g load (1001A-52488)	 Temperature Ramp HFRR at 500g load (1001A-52488)

[63]		
[64]		 Temperature Ramp HFRR at 500g load (1001A-54194)
[65]		 Temperature Ramp HFRR at 500g load (1001A-54281)
[66]		
[69]	 Temperature Ramp HFRR at 200g load (1001A-52493)	 Temperature Ramp HFRR at 500g load (1001A-52493)

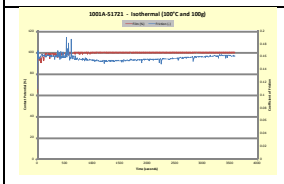
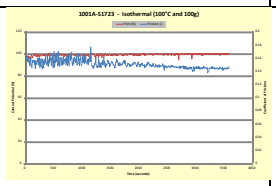
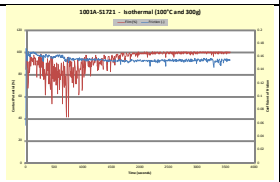
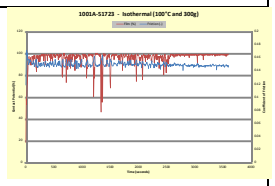
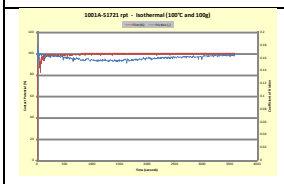
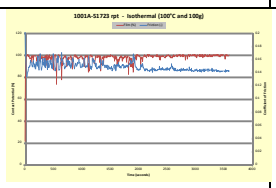
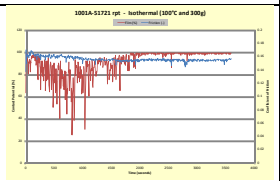
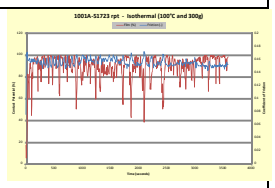
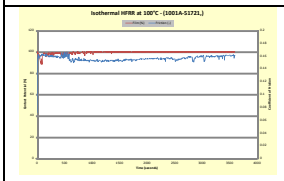
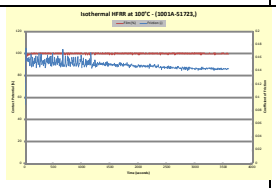
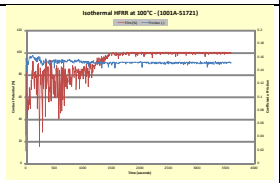
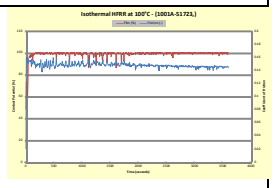
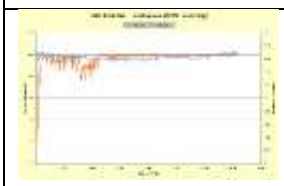
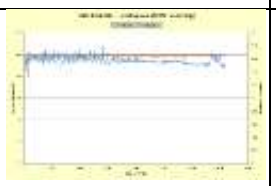
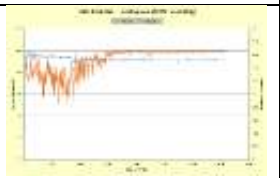
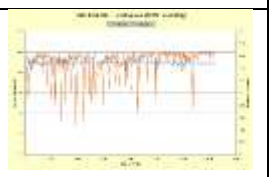
[70]	 Temperature Ramp HFRR at 200g load (1001A-52494)	 Temperature Ramp HFRR at 500g load (1001A-52494)
[71]		
[72]		
[73]		
[74]		

III.II Driveline Single-Component Testing

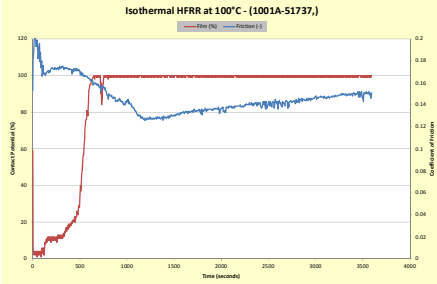
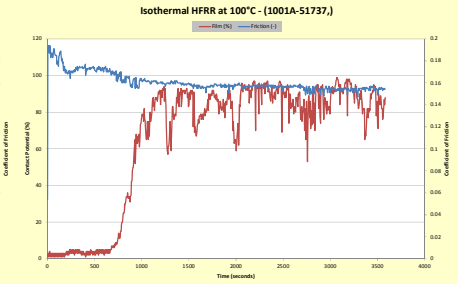
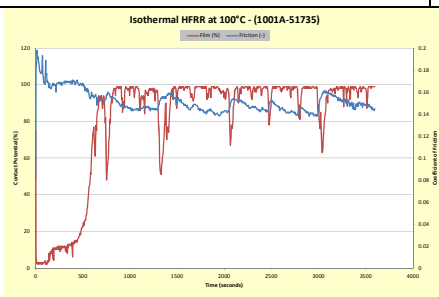
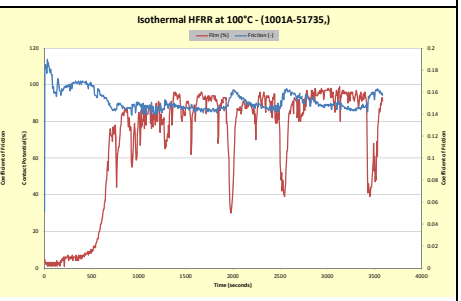
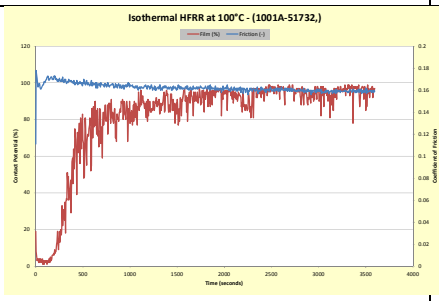
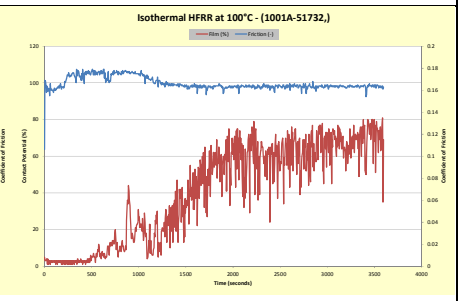
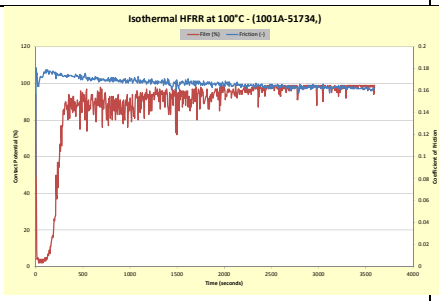
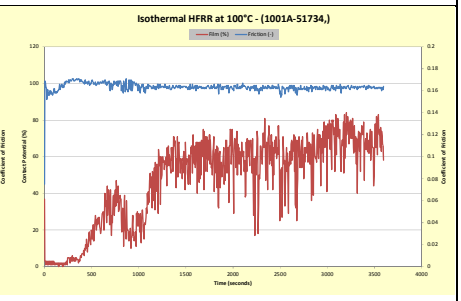
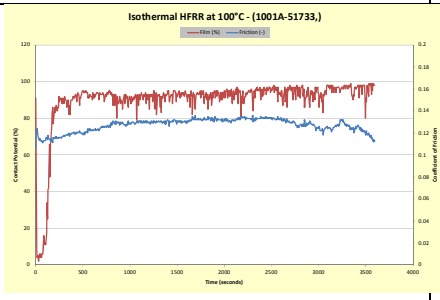
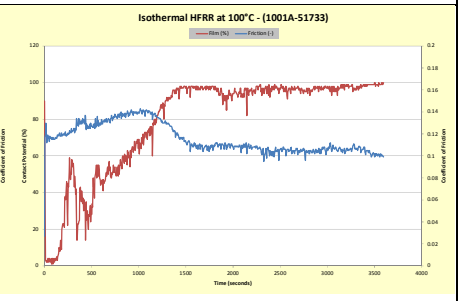
Average Driveline HFRR Results.

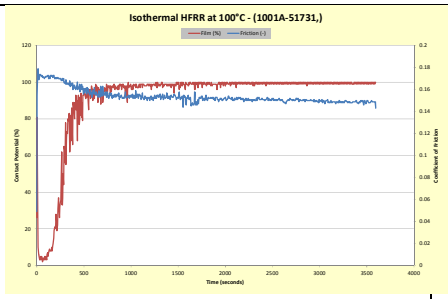
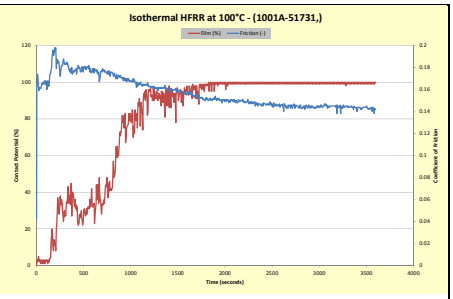
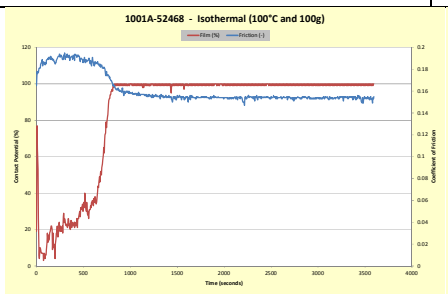
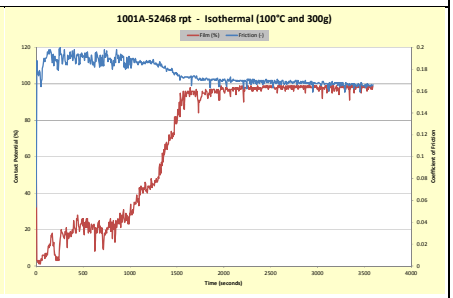
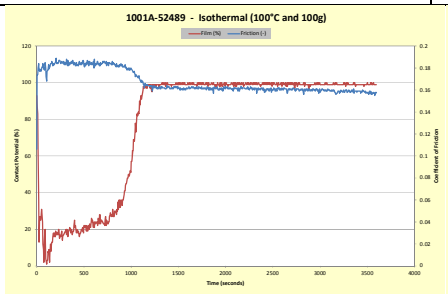
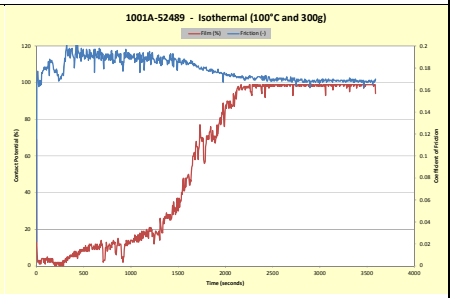
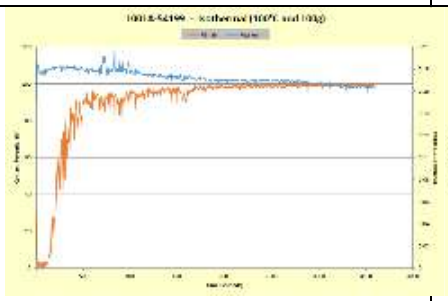
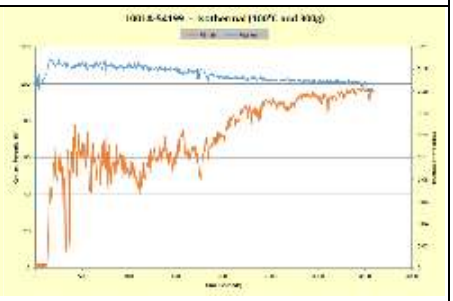
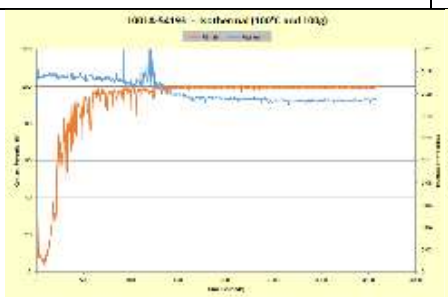
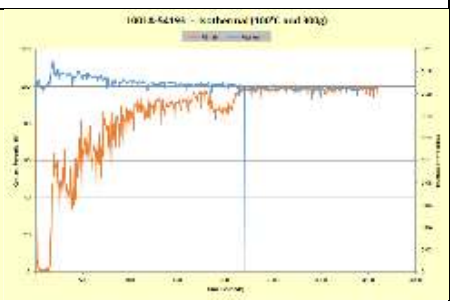
Compound	Wear Scar Diameter, µm		Coefficient of Friction		Contact Potential, %	
	100 g	300 g	100 g	300 g	100 g	300 g
DL AW1	168	245	0.159	0.154	99	92
DL AW2	178	242	0.151	0.151	98	93
PIB_{1000}catechol	103	264	0.146	0.161	87	65
PIB_{550}catechol	135	189	0.152	0.152	80	70
[6]	248	329	0.162	0.166	82	41
[7]	255	346	0.167	0.160	88	43
[17]	139	180	0.127	0.116	90	89
[53]	177	197	0.154	0.157	91	80
[54]	163	226	0.163	0.177	87	65
[56]	170	211	0.167	0.178	78	57
[57]	217	256	0.173	0.175	90	70
[58]	183	244	0.162	0.168	92	84
[59]	218	196	0.174	0.181	83	35
[60]	162	205	0.150	0.202	87	60
[61]	152	211	0.159	0.171	73	60
[62]	180	222	0.166	0.174	89	61
[63]	164	234	0.175	0.178	81	56
[64]	222	261	0.171	0.175	89	68
[65]	223	284	0.176	0.171	89	68
[66]	220	301	0.176	0.166	89	65
[69]	183	243	0.150	0.158	92	78
[70]	162	208	0.162	0.214	72	2
[71]	257	268	0.130	0.126	89	86
[72]	188	210	0.144	0.140	92	87
[73]	152	206	0.138	0.142	94	78
[74]	153	192	0.151	0.144	96	90

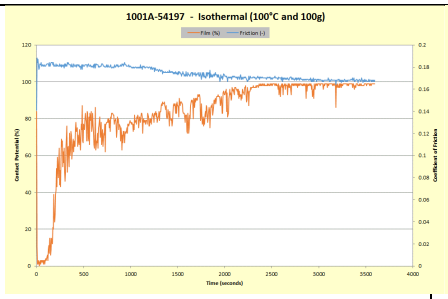
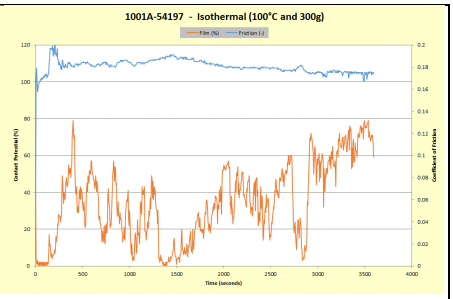
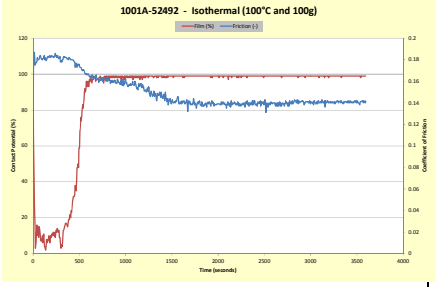
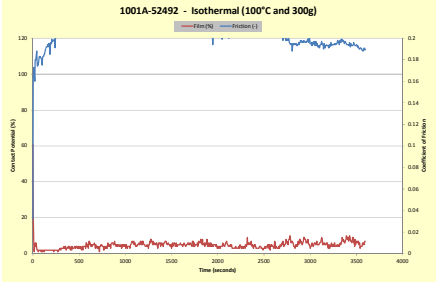
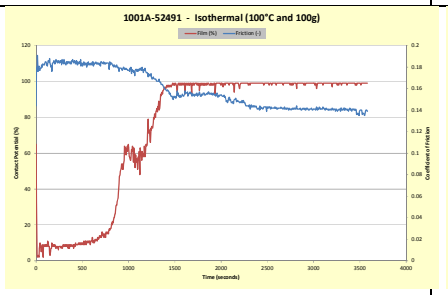
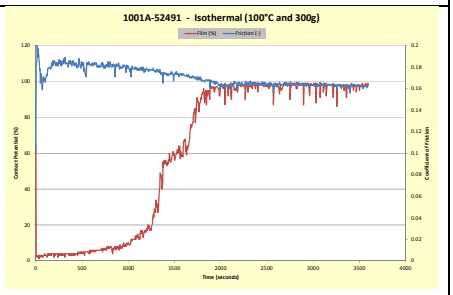
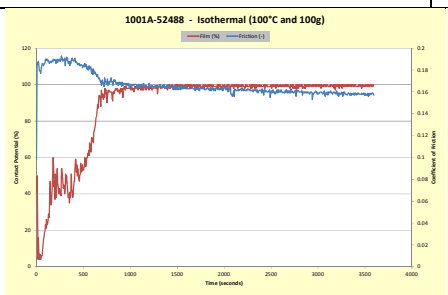
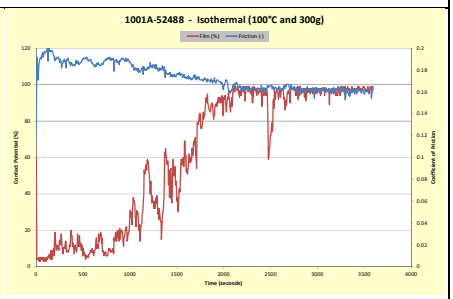
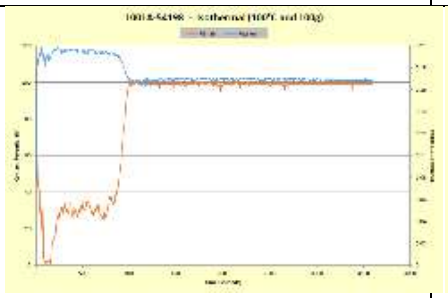
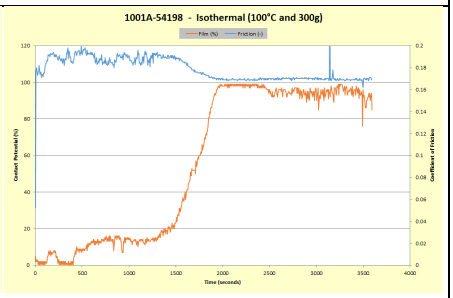
Driveline Baseline HFRR traces showing coefficient of friction (blue) and contact potential (red/orange).

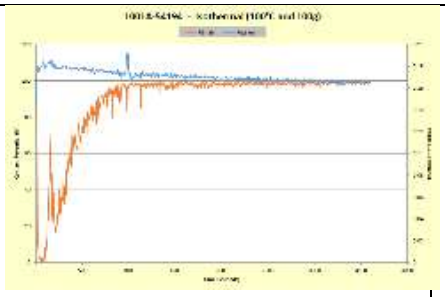
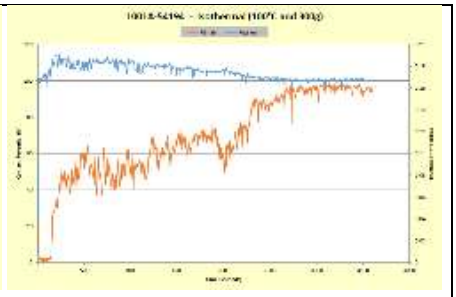
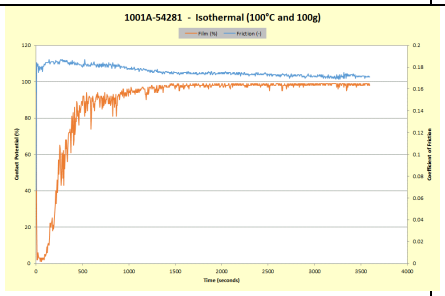
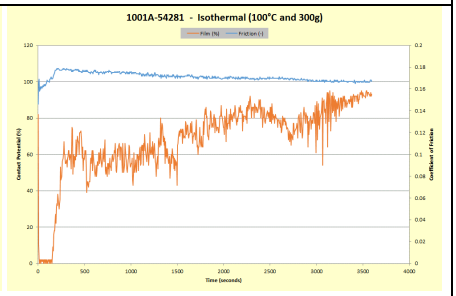
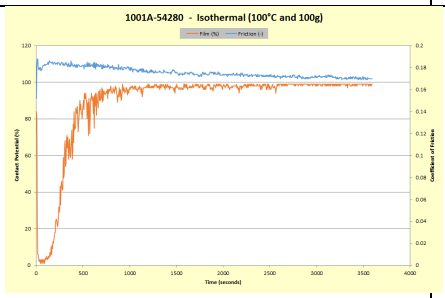
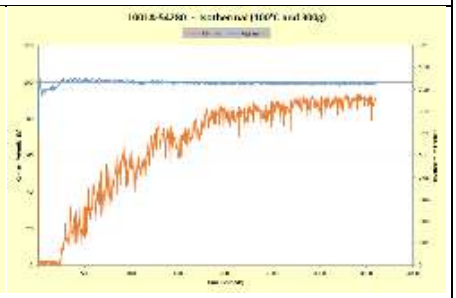
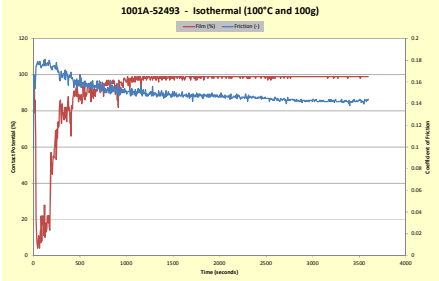
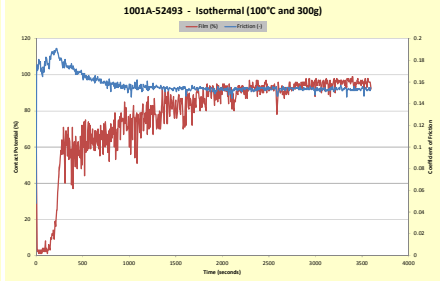
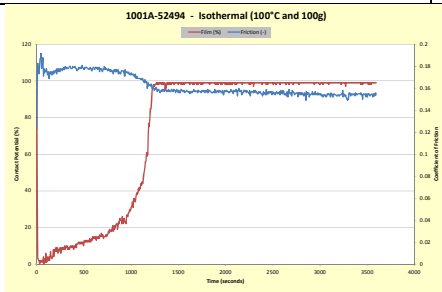
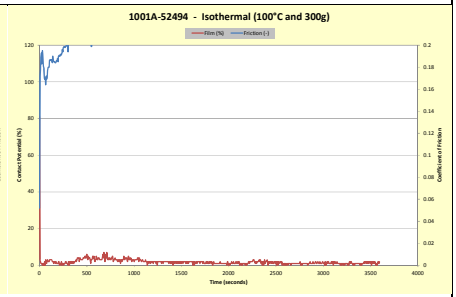
100 g		300 g	
AW1	AW2	AW1	AW2
			
			
			
			

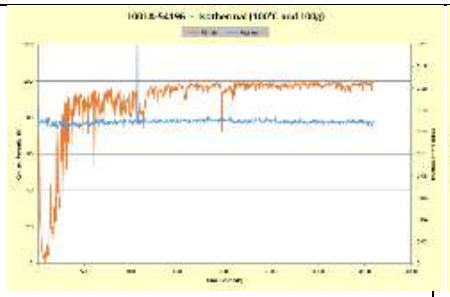
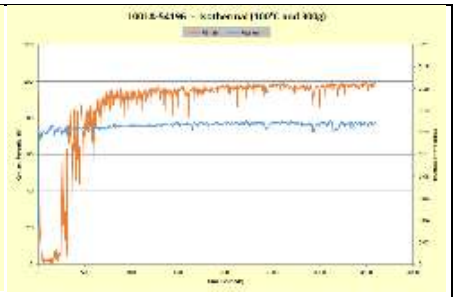
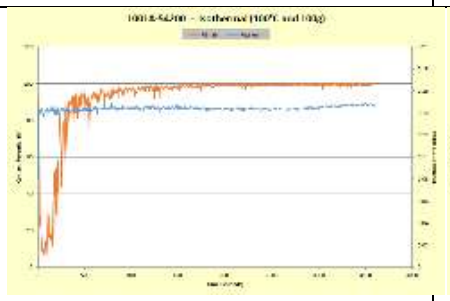
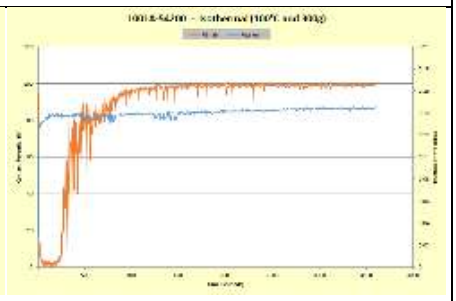
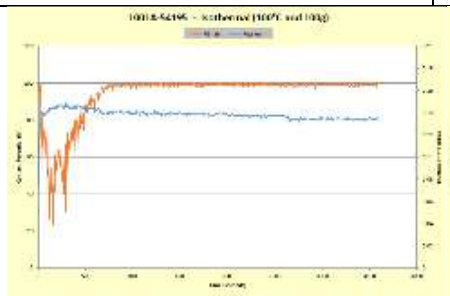
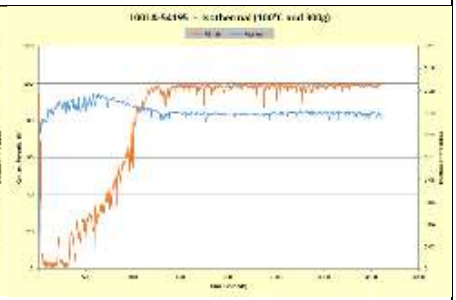
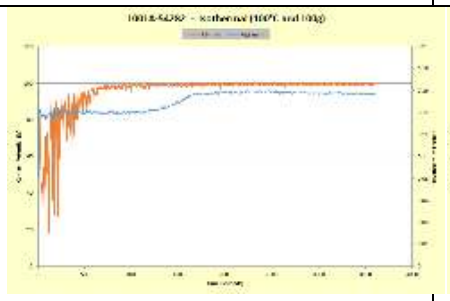
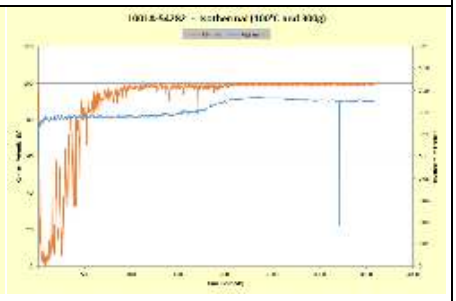
Driveline HFRR Traces showing coefficient of friction (blue) and contact potential (red/orange).

Compound	100 g	300 g
PIB_{1000}catechol		
PIB_{550}catechol		
[6]		
[7]		
[17]		

[53]	 Isothermal HFRR at 100°C - (1001A-51731,) Film (%) Friction (-) Contact Potential (%) Coefficient of Friction Time (seconds)  Isothermal HFRR at 100°C - (1001A-51731,) Film (%) Friction (-) Contact Potential (%) Coefficient of Friction Time (seconds)
[54]	 1001A-52468 - Isothermal (100°C and 100g) Film (%) Friction (-) Contact Potential (%) Coefficient of Friction Time (seconds)  1001A-52468 rpt - Isothermal (100°C and 300g) Film (%) Friction (-) Contact Potential (%) Coefficient of Friction Time (seconds)
[56]	 1001A-52489 - Isothermal (100°C and 100g) Film (%) Friction (-) Contact Potential (%) Coefficient of Friction Time (seconds)  1001A-52489 - Isothermal (100°C and 300g) Film (%) Friction (-) Contact Potential (%) Coefficient of Friction Time (seconds)
[57]	 
[58]	 

[59]	 1001A-54197 - Isothermal (100°C and 100g)	 1001A-54197 - Isothermal (100°C and 300g)
[60]	 1001A-52492 - Isothermal (100°C and 100g)	 1001A-52492 - Isothermal (100°C and 300g)
[61]	 1001A-52491 - Isothermal (100°C and 100g)	 1001A-52491 - Isothermal (100°C and 300g)
[62]	 1001A-52488 - Isothermal (100°C and 100g)	 1001A-52488 - Isothermal (100°C and 300g)
[63]		 1001A-54198 - Isothermal (100°C and 300g)

[64]		
[65]	 1001A-54281 - Isothermal (100°C and 100g)	 1001A-54281 - Isothermal (100°C and 300g)
[66]	 1001A-54280 - Isothermal (100°C and 100g)	
[69]	 1001A-52493 - Isothermal (100°C and 100g)	 1001A-52493 - Isothermal (100°C and 300g)
[70]	 1001A-52494 - Isothermal (100°C and 100g)	 1001A-52494 - Isothermal (100°C and 300g)

[71]		
[72]		
[73]		
[74]		

III.III Further Engine Oils Testing

Antioxidancy of [53].

Antioxidant	No AO	LZ Aminic AO	**[53]**
Oxidation Onset (min)	52.1	124.2	62.5

Microcoker test results for [53].

Fluid Tested	Baseline	1% LZ Dispersant	1% **[53]**
Average merit rating	7.01	7.32	8.22
Onset (°C)	244	254	265

Hot tube test results for [54].

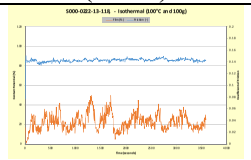
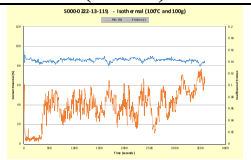
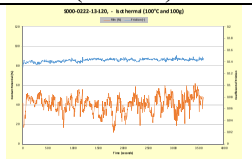
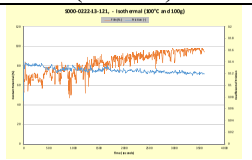
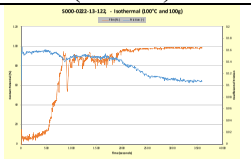
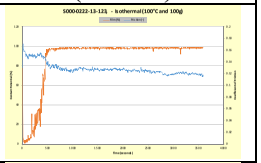
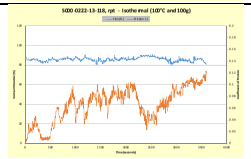
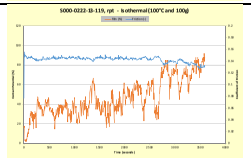
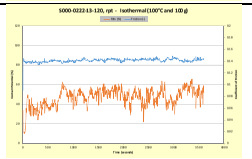
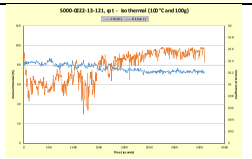
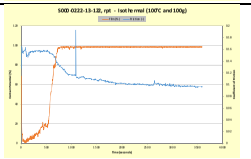
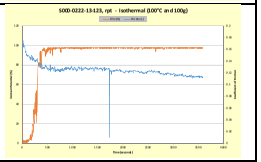
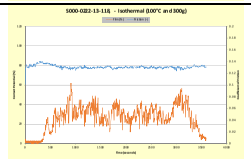
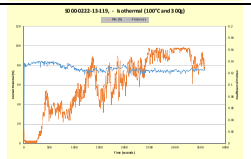
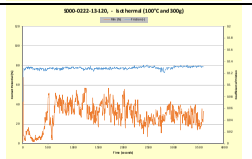
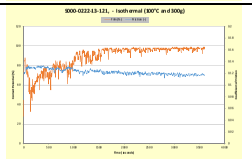
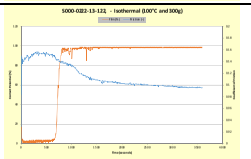
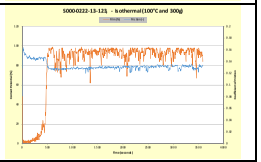
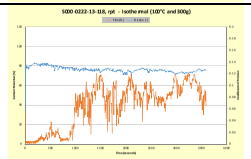
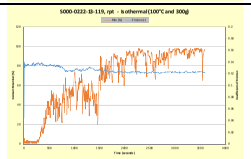
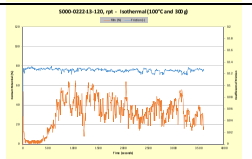
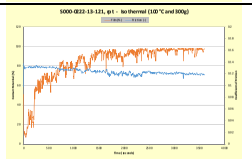
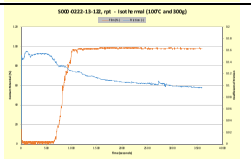
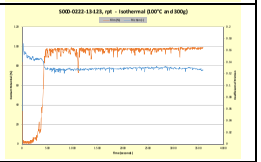
Sample	Baseline	LZ Dispersant	**[53]**
Average rating	82	77	67

III.IV Fully Formulated Driveline HFRR Testing

Average fully formulated HFRR results for [53].

Compound	Treat Rate	Wear Scar Diameter, µm		Coefficient of Friction		Contact Potential, %	
		100 g	300 g	100 g	300 g	100 g	300 g
DL AW1	0.40	226	220	0.143	0.129	32	33
DL AW1	0.70	218	184	0.143	0.127	43	64
DL AW2	0.36	216	230	0.142	0.128	44	31
DL AW2	0.73	159	179	0.127	0.124	81	87
[53]	2.31	145	165	0.126	0.117	81	78
[53]	4.63	150	173	0.127	0.132	90	84

Driveline HFRR traces showing coefficient of friction (blue) and contact potential (orange).

	DL AW1 (0.4%)	DL AW1 (0.7%)	DL AW2 (0.36%)	DL AW2 (0.73%)	**[53]** (2.31%)	**[53]** (4.63%)
100g (Run 1)						
100g (Run 2)						
300g (Run 1)						
300g (Run 2)						

References

[1] S. K. Basu, S. N. Sengupta, B. B. Ahuja, *Fundamentals of Tribology*, Prentice - Hall of India, New Delhi, **2005**.

[2] E. Great Britain. Department of, Science, H. P. Jost, *Lubrication-Tribology. Education and research. A report on the present position and industry's needs*, London, **1966**.

[3] Q. J. Que, Y. Z. Zhang, J. Li, *Tribol. Online* **2007**, *2*, 10-13.

[4] D. Dowson, *History of tribology*, 2nd ed., Professional Engineering Publishing, London, **1998**.

[5] R. M. Mortier, M. F. Fox, S. T. Orszulik, *Chemistry and Technology of Lubricants*, 3rd ed., Springer, London, **2010**.

[6] O. Reynolds, *Philos. Trans. R. Soc. London* **1886**, *177*, 157-234.

[7] F. P. Bowden, D. Tabor, *The Friction and Wear of Solids*, Clarendon Press, Oxford, **1964**.

[8] D. Dowson, G. F. Higginson, *Elasto-hydrodynamic Lubrication*, Pergamon Press, Oxford, **1977**.

[9] S. P. Srivastava, *Developments in Lubricant Technology*, John Wiley & Sons, New Jersey, **2014**.

[10] a) H. Zhang, M. Hua, G. Dong, D. Zhang, K. Chin, *Tribol. Int.* **2016**, *93*, 583-592; b) M. Scaraggi, B. N. J. Persson, *Tribol. Int.* **2014**, *72*, 118-130.

[11] a) A. Moshkovich, V. Perfilyev, I. Lapsker, L. Rapoport, *Wear* **2014**, *320*, 34-40; b) A. Rosenkranz, B. Martin, S. Bettscheider, C. Gachot, H. Kliem, F. Mücklich, *Wear* **2014**, *320*, 51-61; c) M. M. Maru, R. M. Trommer, K. F. Cavalcanti, E. S. Figueiredo, R. F. Silva, C. A. Achete, *Energy* **2014**, *69*, 673-681.

[12] M. Cai, R. Guo, F. Zhou, W. Liu, *Sci. Chin. Tech. Sci.* **2013**, *56*, 2888-2913.

[13] A. Jackson, in *International Tribology Conference*, Melbourne, Australia, **1987**.

[14] F. W. Sullivan, V. Voorhees, A. W. Neeley, R. V. Shankland, *Ind. Eng. Chem.* **1931**, *23*, 604-611.

[15] S. Boyde, *Green Chem.* **2002**, *4*, 293-307.

[16] S. Ray, P. V. C. Rao, N. V. Choudary, *Lubr. Sci.* **2012**, *24*, 23-44.

[17] B. Wilson, *Ind. Lubr. Tribol.* **1994**, *46*, 3-6.

[18] G. E. Totton, *Fuel and Lubricants Handbook*, ASTM, Pennsylvania, USA, **2003**.

[19] M. R. Greaves, *Tribol. Lubr. Technol.* **2013**, 35-39.

[20] D. C. Hone, B. H. Robinson, D. C. Steytler, R. W. Glyde, J. R. Galsworthy, *Langmuir* **2000**, *16*, 340-346.

[21] N. S. Ahmed, A. M. Nassar, A. A., *Int. J. Polymer. Mater.* **2007**, *57*, 114-124.

[22] L. K. Hudson, J. Eastoe, P. J. Dowding, *Adv. Colloid Interface Sci.* **2006**, *123–126*, 425-431.

[23] D. Uy, A. E. O'Neill, S. J. Simko, A. K. Gangopadhyay, *Lubr. Sci.* **2010**, *22*, 19-36.

[24] R. G. Anderson, A. Y. Drummond, F. A. Stuart, US3361673, **1968**.

[25] Y. Shen, J. Duhamel, *Langmuir* **2008**, *24*, 10665-10673.

[26] S. K. Naidu, E. E. Klaus, J. L. Duda, *Ind. Eng. Chem. Prod. Res. Dev.* **1984**, *23*, 613-619.

[27] P. Mousavi, D. Wang, C. S. Grant, W. Oxenham, P. J. Hauser, *Ind. Eng. Chem. Res.* **2006**, *45*, 15-22.
[28] V. J. Gatto, W. E. Moehle, T. W. Cobb, E. R. Schneller, *J. Synth. Lubr.* **2007**, *24*, 111-124.
[29] G40-01, in *ASTM Standard Terminology Relating to Wear and Erosion*, West Conshohocken, PA, **2001**.
[30] G. W. Stachowiak, *Wear - materials, mechanisms and practice*, John Wiley & Sons, Chichester, UK, **2005**.
[31] Z. Jun, S. Robab, B. A. James, *J. Phys. D: Appl. Phys.* **2013**, *46*, 055307.
[32] X. Yin, K. Komvopoulos, *Int. J. Solids Struct.* **2010**, *47*, 912-921.
[33] J. T. Burwell, C. D. Strang, *J. Appl. Phys.* **1952**, *23*, 18-28.
[34] H. Mishina, A. Hase, *Wear* **2013**, *308*, 186-192.
[35] T. E. Fischer, *Annu. Rev. Mater. Sci.* **1988**, *18*, 303-323.
[36] P. A. Asseff, US2261047, **1941**.
[37] H. Spikes, *Tribol. Lett.* **2004**, *17*, 469-489.
[38] M. Fuller, Z. Yin, M. Kasrai, G. M. Bancroft, E. S. Yamaguchi, P. R. Ryason, P. A. Willermet, K. H. Tan, *Tribol. Int.* **1997**, *30*, 305-315.
[39] L. R. Rudnick, *Lubricant Additives: Chemistry and Applications*, 2nd ed., CRC Press, New York, **2009**.
[40] N. J. Mosey, M. H. Muser, T. K. Woo, *Science* **2005**, *307*, 1612-1615.
[41] J. M. Martin, C. Grossiord, T. Le Mogne, S. Bec, A. Tonck, *Tribol. Int.* **2001**, *34*, 523-530.
[42] E. S. Ferrari, K. J. Roberts, D. Adams, *Wear* **1999**, *236*, 246-258.
[43] a) M. J. Rokosz, A. E. Chen, C. K. Lowe-Ma, A. V. Kucherov, D. Benson, M. C. P. Peck, R. W. McCabe, *Appl. Catal. B-Environ.* **2001**, *33*, 205-215; b) H. Q. Hu, X. Y. Wei, G. L. Dai, Y. W. Fei, F. Xie, Z. M. Zong, *Tribol. Int.* **2008**, *41*, 549-555.
[44] A. P. Institute, *Engine Oil Licensing and Certification System*, 17 ed., **2012**.
[45] M. T. Devlin, J. Guevremont, R. Sheets, J. Loper, G. Guinther, K. Thompson, T. C. Jao, *Lubr. Sci.* **2008**, *20*, 151-161.
[46] O. Beeck, J. W. Givens, E. C. Williams, *Proc. R. Soc. London, Ser. A* **1940**, *177*, 103-118.
[47] H. Spikes, *Lubr. Sci.* **2008**, *20*, 103-136.
[48] T. Sakurai, K. Sato, *A S L E Trans.* **1970**, *13*, 252-261.
[49] H. B. Ma, J. Li, H. Chen, G. Z. Zuo, Y. Yu, T. H. Ren, Y. D. Zhao, *Tribol. Int.* **2009**, *42*, 940-945.
[50] I. Minami, S. Mitsumune, *Tribol. Lett.* **2002**, *13*, 95-101.
[51] Z. He, W. Rao, T. Ren, W. Liu, Q. Xue, *Tribol. Lett.* **2002**, *13*, 87-93.
[52] D. Qiao, H. Wang, D. Feng, *Lubr. Sci.* **2014**, *26*, 1-11.
[53] G. Zhao, X. Wu, W. Li, X. Wang, *Ind. Eng. Chem. Res.* **2013**, *52*, 7419-7424.
[54] X. Wu, X. Wang, W. Liu, *RSC Adv.* **2014**, *4*, 6074-6082.
[55] X. Wu, G. Zhao, X. Wang, W. Liu, W. Liu, *RSC Adv.* **2016**, *6*, 47824-47832.
[56] R. Schumacher, H. Zinke, *Tribol. Int.* **1997**, *30*, 199-208.
[57] M. N. Najman, M. Kasrai, G. M. Bancroft, *Tribol. Lett.* **2004**, *17*, 217-229.
[58] S. Y. Jiang, S. F. Yang, *Wear* **2010**, *268*, 777-783.
[59] Z. Li, X. Hou, L. Yu, Z. Zhang, P. Zhang, *Appl. Surf. Sci.* **2014**, *292*, 971-977.
[60] V. I. Kolesnikov, S. F. Ermakov, A. P. Sychev, N. A. Myasnikova, M. A. Savenkova, E. I. Luneva, *J. Frict. Wear* **2009**, *30*, 182-187.

[61] N. Kong, A. K. Tieu, Q. Zhu, H. Zhu, S. Wan, C. Kong, *Wear* **2015**, *330–331*, 230-238.
[62] V. Sharma, N. Doerr, P. B. Aswath, *RSC Adv.* **2016**, *6*, 22341-22356.
[63] X. Fan, Y. Xia, L. Wang, J. Pu, T. Chen, H. Zhang, *Tribol. Lett.* **2014**, *53*, 281-291.
[64] V. Sharma, C. Gabler, N. Doerr, P. B. Aswath, *Tribol. Int.* **2015**, *92*, 353-364.
[65] Y. Zhou, J. Dyck, T. W. Graham, H. Luo, D. N. Leonard, J. Qu, *Langmuir* **2014**, *30*, 13301-13311.
[66] A. Hernández Battez, M. Bartolomé, D. Blanco, J. L. Viesca, A. Fernández-González, R. González, *Tribol. Int.* **2016**, *95*, 118-131.
[67] X. Fu, L. Sun, X. Zhou, Z. Li, T. Ren, *Tribol. Lett.* **2015**, *60*, 1-12.
[68] G. W. Rowe, *Wear* **1960**, *3*, 274-285.
[69] R. S. Pease, *Nature* **1950**, *165*, 722-723.
[70] Y. Kimura, T. Wakabayashi, K. Okada, T. Wada, H. Nishikawa, *Wear* **1999**, *232*, 199-206.
[71] Z. Pawlak, T. Kaldonski, M. Lisewski, W. Urbaniak, A. Oloyede, *Ind. Lubr. Tribol.* **2012**, *64*, 84-89.
[72] B. Pan, N. Li, G. Chu, F. Wei, J. Liu, J. Zhang, Y. Zhang, *Tribol. Lett.* **2014**, *54*, 161-170.
[73] B. M. Chen, Q. L. Bi, J. Yang, Y. Q. Xia, J. C. Hao, *Tribol. Int.* **2008**, *41*, 1145-1152.
[74] W. Chen, Y. M. Gao, C. Chen, J. D. Xing, *Wear* **2010**, *269*, 241-248.
[75] S. T. Zhang, J. S. Zhou, B. G. Guo, H. D. Zhou, Y. P. Pu, J. M. Chen, *Advanced Tribology* **2009**, 442-442.
[76] R. Tyagi, D. S. Xiong, J. L. Li, J. H. A. Da, *Wear* **2010**, *269*, 884-890.
[77] X. F. Wei, R. C. Wang, Y. Feng, C. Q. Peng, X. W. Zhu, *J. Cent. South Univ. T.* **2011**, *18*, 1334-1339.
[78] B. Dikici, I. Ozdemir, *Anti. Corros. Method. M.* **2012**, *59*, 246-254.
[79] S. Miyake, M. Wang, J. Kim, *Nanotechnology* **2006**, *17*, 1607-1614.
[80] S. Miyake, *J. Vac. Sci. Technol. B* **2003**, *21*, 785-789.
[81] Y. M. Chen, Z. X. Zeng, S. R. Yang, J. Y. Zhang, *Diam. Relat. Mater.* **2009**, *18*, 20-26.
[82] Z. Pawlak, R. Pai, E. Bayraktar, T. Kaldonski, A. Oloyede, *Biosystems* **2008**, *94*, 202-208.
[83] M. Alvarez-Vera, J. A. Ortega-Saenz, M. A. L. Hernandez-Rodríguez, *Wear* **2013**, *301*, 175-181.
[84] T. Ugurlu, M. Turkoglu, *Int. J. Pharm.* **2008**, *353*, 45-51.
[85] F. Shah, S. Glavatskih, O. Antzutkin, *Tribol. Lett.* **2013**, *51*, 281-301.
[86] M. R. Lovell, M. A. Kabir, P. L. Menezes, C. F. Higgs, *Philos. Trans. R. Soc. London, Ser. A* **2010**, *368*, 4851-4868.
[87] P. Deshmukh, M. Lovell, W. G. Sawyer, A. Mobley, *Wear* **2006**, *260*, 1295-1304.
[88] M. Lovell, C. F. Higgs, P. Deshmukh, A. Mobley, *J. Mater. Process. Technol.* **2006**, *177*, 87-90.
[89] Z. S. Hu, J. X. Dong, *Wear* **1998**, *216*, 87-91.
[90] J. X. Dong, Z. S. Hu, *Tribol. Int.* **1998**, *31*, 219-223.
[91] S. A. Savrik, D. Balkose, S. Ulku, *J. Therm. Anal. Calorim.* **2011**, *104*, 605-612.

[92] V. Normand, J. M. Martin, L. Ponsonnet, K. Inoue, *Tribol. Lett.* **1998**, *5*, 235-242.
[93] K. Masenelli-Varlot, M. Kasrai, G. M. Bancroft, G. De Stasio, B. Gilbert, E. S. Yamaguchi, P. R. Ryason, *Tribol. Lett.* **2003**, *14*, 157-166.
[94] J. B. Yao, Q. L. Wang, S. Q. Chen, J. Z. Sun, J. X. Dong, *Lubr. Sci.* **2002**, *14*, 415-423.
[95] K. L. Kreuz, R. S. Fein, M. Dundy, *A S L E Trans.* **1967**, *10*, 67-76.
[96] J. B. Yao, *Tribol. Int.* **1997**, *30*, 387-389.
[97] Z. Zheng, G. Shen, Y. Wan, L. Cao, X. Xu, Q. Yue, T. Sun, *Wear* **1998**, *222*, 135–144.
[98] J. Li, Z. Li, T. Ren, X. Zeng, E. van der Heide, *Tribol. Int.* **2014**, *73*, 101-107.
[99] Z. Jia, Y. Xia, X. Pang, J. Hao, *Tribol. Lett.* **2010**, *41*, 247-256.
[100] J. Li, B. Fan, T. Ren, Y. Zhao, *Tribol. Int.* **2015**, *88*, 1-7.
[101] Y. Zhang, X. Zeng, H. Wu, Z. Li, T. Ren, Y. Zhao, *Tribol. Lett.* **2014**, *53*, 533-542.
[102] B. S. Chen, N. Zhang, J. Wu, J. Wang, J. H. Fang, K. Liang, *Green Chem.* **2013**, *15*, 738-743.
[103] Z. Li, X. Li, Y. Zhang, T. Ren, Y. Zhao, X. Zeng, E. van der Heide, *Appl. Surf. Sci.* **2014**, *308*, 91-99.
[104] Y. G. Wang, J. S. Li, T. H. Ren, *Proc. Inst. Mech. Eng., Part J* **2007**, *221*, 553-559.
[105] J. Wang, J. Wang, C. Li, G. Zhao, X. Wang, *Tribol. Lett.* **2011**, *43*, 235-245.
[106] Y. B. Sun, L. T. Hu, Q. J. Xue, *Ind. Lubr. Tribol.* **2010**, *62*, 70-77.
[107] X. B. Ji, Y. X. Chen, X. B. Wang, W. M. Liu, *Ind. Lubr. Tribol.* **2012**, *64*, 315-320.
[108] F. U. Shah, S. Glavatskih, O. N. Antzutkin, *Tribol. Lett.* **2012**, *45*, 67-78.
[109] R. Gusain, P. Gupta, S. Saran, O. P. Khatri, *ACS Appl. Mater. Interfaces* **2014**, *6*, 15318-15328.
[110] N. Antzutkin, WO2012128714 (A1), **2012**.
[111] K. G. Stanulov, H. N. Harhara, G. S. Cholakov, *Tribol. Int.* **1998**, *31*, 257-263.
[112] K. Varlot, J. M. Martin, C. Grossiord, R. Vargiolu, B. Vacher, K. Inoue, *Tribol. Lett.* **1999**, *6*, 181-189.
[113] C. Grossiord, J.-M. Martin, K. Varlot, B. Vacher, T. Le Mogne, Y. Yamada, *Tribol. Lett.* **2000**, *8*, 203-212.
[114] F. U. Shah, S. Glavatskih, O. N. Antzutkin, *ACS Appl. Mater. Interfaces* **2009**, *1*, 2835-2842.
[115] F. U. Shah, S. Glavatskih, E. Hoglund, M. Lindberg, O. N. Antzutkin, *ACS Appl. Mater. Interfaces* **2011**, *3*, 956-968.
[116] W. Li, Y. Wu, X. Wang, W. Liu, *Tribol. Lett.* **2012**, *47*, 381-388.
[117] F. U. Shah, S. Glavatskih, D. R. MacFarlane, A. Somers, M. Forsyth, O. N. Antzutkin, *Phys. Chem. Chem. Phys.* **2011**, *13*, 12865-12873.
[118] V. Totolin, I. Minami, C. Gabler, J. Brenner, N. Dörr, *Tribol. Lett.* **2014**, *53*, 421-432.
[119] J. Cosier, A. M. Glazer, *J. Appl. Crystallogr.* **1986**, *19*, 105-107.
[120] CrysAlisPRO, Oxford Diffraction/Agilent Technologies UK Ltd, Yarnton, UK.
[121] a) G. M. Sheldrick, *Acta Crystallogr. Sect. A* **2008**, *64*, 112-122; b) G. Sheldrick, *Acta Crystallogr. Sect. A* **2015**, *71*, 3-8.

[122] L. Palatinus, G. Chapuis, *J. Appl. Crystallogr.* **2007**, *40*, 786-790.
[123] a) O. V. Dolomanov, L. J. Bourhis, R. J. Gildea, J. A. K. Howard, H. Puschmann, *J. Appl. Crystallogr.* **2009**, *42*, 339-341; b) O. V. Dolomanov, A. J. Blake, N. R. Champness, M. Schroder, *J. Appl. Crystallogr.* **2003**, *36*, 1283-1284.
[124] G. Winter, Diamond Light Source, **2009**.
[125] a) M. J. Frisch, G. W. Trucks, H. B. Schlegel, G. E. Scuseria, M. A. Robb, J. R. Cheeseman, G. Scalmani, V. Barone, B. Mennucci, G. A. Petersson, H. Nakatsuji, M. Caricato, X. Li, H. P. Hratchian, A. F. Izmaylov, J. Bloino, G. Zheng, J. L. Sonnenberg, M. Hada, M. Ehara, K. Toyota, R. Fukuda, J. Hasegawa, M. Ishida, T. Nakajima, Y. Honda, O. Kitao, H. Nakai, T. Vreven, J. A. Montgomery Jr., J. E. Peralta, F. Ogliaro, M. J. Bearpark, J. Heyd, E. N. Brothers, K. N. Kudin, V. N. Staroverov, R. Kobayashi, J. Normand, K. Raghavachari, A. P. Rendell, J. C. Burant, S. S. Iyengar, J. Tomasi, M. Cossi, N. Rega, N. J. Millam, M. Klene, J. E. Knox, J. B. Cross, V. Bakken, C. Adamo, J. Jaramillo, R. Gomperts, R. E. Stratmann, O. Yazyev, A. J. Austin, R. Cammi, C. Pomelli, J. W. Ochterski, R. L. Martin, K. Morokuma, V. G. Zakrzewski, G. A. Voth, P. Salvador, J. J. Dannenberg, S. Dapprich, A. D. Daniels, Ö. Farkas, J. B. Foresman, J. V. Ortiz, J. Cioslowski, D. J. Fox, Gaussian, Inc., Wallingford, CT, USA, **2009**; b) C. Lee, W. Yang, R. G. Parr, *Physical Review B* **1988**, *37*, 785-789.
[126] a) P. Flukiger, H. P. Luthi, S. Portmann, J. Weber, Swiss Center for Scientific Computing, Switzerland, **2000**; b) S. Portmann, H. P. Luthi, *CHIMIA International Journal for Chemistry* **2000**, *54*, 766-770.
[127] Y. Aihara, A. Sonai, M. Hattori, K. Hayamizu, *J. Phys. Chem. B.* **2006**, *110*, 24999-25006.
[128] a) E. W. Abel, W. Gerrard, M. F. Lappert, *J. Chem. Soc.* **1957**, 3833-3838; b) W. Gerrard, M. F. Lappert, R. Shafferman, *J. Chem. Soc.* **1957**, 3828-3833; c) R. L. Letsinger, I. H. Skoog, *J. Am. Chem. Soc.* **1955**, *77*, 5176-5177.
[129] a) S. S. Barnes, C. M. Vogels, A. Decken, S. A. Westcott, *Dalton Trans.* **2011**, *40*, 4707-4714; b) Y. Cui, F. Li, Z.-H. Lu, S. Wang, *Dalton Trans.* **2007**, 2634-2643.
[130] E. Januszewski, A. Lorbach, R. Grewal, M. Bolte, J. W. Bats, H.-W. Lerner, M. Wagner, *Chem. Eur. J.* **2011**, *17*, 12696-12705.
[131] C. M. King, M. T. Musser, US3864380, **1975**.
[132] W. G. Whittingham, K. R. Lawson, R. A. Lyon, GB2314080, **1997**.
[133] a) S. M. Darling, P. S. Fay, US2741548, **1956**; b) P. S. Fay, L. S. Szabo, US2767069, **1956**; c) C. Liao, US2848312, **1958**; d) C. Liao, D. D. Emrick, US3011880, **1961**; e) R. J. d. Gray, US2931714, **1960**; f) R. J. d. Gray, US2956869, **1960**; g) G. E. Irish, US3009798, **1961**.
[134] G. E. Irish, US2931774, **1960**.
[135] a) D. D. Emrick, US3009791, **1961**; b) D. D. Emrick, US3080403, **1963**.
[136] C. Liao, US3150157, **1964**.
[137] J. M. K. A.G. Horodysky, US005407451, **1995**.
[138] E. L. Kay, E. C. Knowles, US3100221, **1963**.
[139] a) C. Martín, J. C. Ronda, V. Cádiz, *J. Polym. Sci., Part A: Polym. Chem.* **2006**, *44*, 1701-1710; b) C. Martín, J. C. Ronda, V. Cádiz, *Polym. Degrad. Stabil.* **2006**, *91*, 747-754.
[140] T. Knauber, F. Arikan, G.-V. Röschenthaler, L. J. Gooßen, *Chem. Eur. J.* **2011**, *17*, 2689-2697.

[141] M. Ito, M. Itazaki, H. Nakazawa, *J. Am. Chem. Soc.* **2014**, *136*, 6183-6186.
[142] S. Hawkeswood, D. W. Stephan, *Dalton Trans.* **2005**, 2182-2187.
[143] X. Zhao, D. W. Stephan, *Chem. Commun.* **2011**, *47*, 1833-1835.
[144] N. Fey, M. Garland, J. P. Hopewell, C. L. McMullin, S. Mastroianni, A. G. Orpen, P. G. Pringle, *Angew. Chem. Int. Ed.* **2012**, *51*, 118-122.
[145] Y. Zhang, A. Desai, Z. J. Lu, G. Hu, Z. S. Ding, W. D. Wulff, *Chem.-Eur. J.* **2008**, *14*, 3785-3803.
[146] W. Zhao, X. Yin, A. K. Gupta, X. Zhang, W. D. Wulff, *Synlett* **2015**, *26*, 1606-1614.
[147] Z. Shan, Y. Xiong, W. Li, D. Zhao, *Tetrahedron: Asymmetry* **1998**, *9*, 3985-3989.
[148] D. J. Harrison, N. C. Tam, C. M. Vogels, R. F. Langler, R. T. Baker, A. Decken, S. A. Westcott, *Tetrahedron Lett.* **2004**, *45*, 8493-8496.
[149] N. D. Coombs, S. Aldridge, G. Wiltshire, D. L. Kays, C. Bresner, L. L. Ooi, *J. Organomet. Chem.* **2005**, *690*, 2725-2731.
[150] G. J. P. Britovsek, J. Ugolotti, A. J. P. White, *Organometallics* **2005**, *24*, 1685-1691.
[151] A. Lang, J. Knizek, H. Noth, S. Schur, M. Thomann, *Z. Anorg. Allg. Chem.* **1997**, *623*, 901-907.
[152] V. Montiel-Palma, M. Lumbierres, B. Donnadieu, S. Sabo-Etienne, B. Chaudret, *J. Am. Chem. Soc.* **2002**, *124*, 5624-5625.
[153] a) I. M. Malkowsky, R. Fröhlich, U. Griesbach, H. Pütter, S. R. Waldvogel, *Eur. J. Inorg. Chem.* **2006**, *2006*, 1690-1697; b) A. Budanow, T. Sinke, H.-W. Lerner, M. Bolte, *Acta Crystallogr. Sect. C* **2014**, *70*, 662-667.
[154] R. C. Neu, E. Y. Ouyang, S. J. Geier, X. Zhao, A. Ramos, D. W. Stephan, *Dalton Trans.* **2010**, *39*, 4285-4294.
[155] A. Lang, H. Nöth, M. Thomann-Albach, *Chem. Ber.* **1997**, *130*, 363-370.
[156] a) S.-i. Tabata, T. Hirakimoto, H. Tokuda, M. A. B. H. Susan, M. Watanabe, *J. Phys. Chem. B.* **2004**, *108*, 19518-19526; b) R. J. Chein, Y. Y. Yeung, E. J. Corey, *Org. Lett.* **2009**, *11*, 1611-1614; c) S. Bontemps, L. Vendier, S. Sabo-Etienne, *Angew. Chem. Int. Ed.* **2012**, *51*, 1671-1674; d) A. Peschiulli, V. Smout, T. E. Storr, E. A. Mitchell, Z. Elias, W. Herrebout, D. Berthelot, L. Meerpoel, B. U. W. Maes, *Chem.-Eur. J.* **2013**, *19*, 10378-10387.
[157] a) B. Wrackmeyer, O. L. Tok, *Z. Naturforsch.* **2006**, *61b*, 949-955; b) B. R. Groves, S. M. Crawford, T. Lundrigan, C. F. Matta, S. Sowlati-Hashjin, A. Thompson, *Chem. Commun.* **2013**, *49*, 816-818; c) G. Hu, L. Huang, R. H. Huang, W. D. Wulff, *J. Am. Chem. Soc.* **2009**, *131*, 15615-15617.
[158] P. Király, *Magn. Reson. Chem.* **2012**, *50*, 620-626.
[159] a) J. M. Carr, P. J. Duggan, D. G. Humphrey, E. M. Tyndall, *Aust. J. Chem.* **2005**, *58*, 21-25; b) J. M. Carr, P. J. Duggan, D. G. Humphrey, J. A. Platts, E. M. Tyndall, *Aust. J. Chem.* **2005**, *58*, 901-911.
[160] M. Braid, US4547302, **1985**.
[161] M. A. Beckett, G. C. Strickland, J. R. Holland, K. Sukumar Varma, *Polymer* **1996**, *37*, 4629-4631.
[162] U. Mayer, V. Gutmann, W. Gerger, *Monatshefte für Chemie / Chemical Monthly*, *106*, 1235-1257.
[163] G. C. Welch, L. Cabrera, P. A. Chase, E. Hollink, J. D. Masuda, P. Wei, D. W. Stephan, *Dalton Trans.* **2007**, 3407-3414.
[164] C. Hansch, A. Leo, R. W. Taft, *Chem. Rev.* **1991**, *91*, 165-195.

[165] P. R. Weider, L. S. Hegedus, H. Asada, S. V. Dandreq, *J. Org. Chem.* **1985**, *50*, 4276-4281.
[166] W. Lowe, US002883412, **1959**.
[167] a) G. L. Heise, B. K. Sharma, S. Z. Erhan, WO2012044681, **2012**; b) B. K. Sharma, K. M. Doll, G. L. Heise, M. Myslinska, S. Z. Erhan, *Ind. Eng. Chem. Res.* **2012**, *51*, 11941-11945.
[168] J. Dale, *J. Chem. Soc.* **1961**, 910-322.
[169] K. Ishihara, M. Miyata, K. Hattori, T. Tada, H. Yamamoto, *J. Am. Chem. Soc.* **1994**, *116*, 10520-10524.
[170] D. B. Llewellyn, D. Adamson, B. A. Arndtsen, *Org. Lett.* **2000**, *2*, 4165-4168.
[171] R. R. Santway, US3403305, **1968**.
[172] J. Barthel, A. Schmid, H. J. Gores, *J. Electrochem. Soc.* **2000**, *147*, 21-24.
[173] W. Xu, A. J. Shusterman, R. Marzke, C. A. Angell, *J. Electrochem. Soc.* **2004**, *151*, A632-A638.
[174] Z.-M. Xue, J.-F. Zhao, J. Ding, C.-H. Chen, *J. Power Sources* **2010**, *195*, 853-856.
[175] H. Danjo, K. Hirata, S. Yoshigai, I. Azumaya, K. Yamaguchi, *J. Am. Chem. Soc.* **2009**, *131*, 1638-1639.
[176] H. Danjo, K. Hirata, M. Noda, S. Uchiyama, K. Fukui, M. Kawahata, I. Azumaya, K. Yamaguchi, T. Miyazawa, *J. Am. Chem. Soc.* **2010**, *132*, 15556-15558.
[177] N. Kameta, K. Hiratani, *Tetrahedron Lett.* **2006**, *47*, 4947-4950.
[178] B. F. Abrahams, D. J. Price, R. Robson, *Angew. Chem. Int. Ed.* **2006**, *45*, 806-810.
[179] R. Pizer, L. Babcock, *Inorg. Chem.* **1977**, *16*, 1677-1681.
[180] a) S. A. Westcott, N. J. Taylor, T. B. Marder, R. T. Baker, N. J. Jones, J. C. Calabrese, *J. Chem. Soc., Chem. Commun.* **1991**, 304-305; b) I. A. I. Mkhalid, R. B. Coapes, S. N. Edes, D. N. Coventry, F. E. S. Souza, R. L. Thomas, J. J. Hall, S. W. Bi, Z. Y. Lin, T. B. Marder, *Dalton Trans.* **2008**, 1055-1064.
[181] S. H. Chikkali, D. Gudat, F. Lissner, M. Nieger, T. Schleid, *Dalton Trans.* **2007**, *0*, 3906-3913.
[182] a) M. J. Geier, E. G. Bowes, G. M. Lee, H. Li, T. O'Neill, A. Flewelling, C. M. Vogels, A. Decken, C. A. Gray, S. A. Westcott, *Heteroat. Chem* **2013**, *24*, 116-123; b) J. M. Carr, P. J. Duggan, D. G. Humphrey, J. A. Platts, E. M. Tyndall, *Aust. J. Chem.* **2011**, *64*, 495-502.
[183] T. Alaviuhkola, J. Bobacka, M. Nissinen, K. Rissanen, A. Ivaska, J. Pursiainen, *Chem.-Eur. J.* **2005**, *11*, 2071-2080.
[184] a) S. H. Chikkali, D. Gudat, F. Lissner, M. Nieger, T. Schleid, *Dalton Trans.* **2007**, 3906-3913; b) N. R. Halcovitch, M. J. Geier, C. M. Vogels, A. Decken, S. A. Westcott, *Cent. Eur. J. Chem.* **2011**, *9*, 386-390; c) C. Dai, T. B. Marder, E. G. Robins, D. S. Yufit, J. A. K. Howard, T. B. Marder, A. J. Scott, W. Clegg, *Chem. Commun.* **1998**, 1983-1984.
[185] J. A. Raskatov, J. M. Brown, A. L. Thompson, *CrystEngComm* **2011**, *13*, 2923-2929.
[186] R. Balz, U. Brändle, E. Kämmerer, D. Köhnlein, O. Lutz, A. Nolle, in *Zeitschrift für Naturforschung A, Vol. 41*, **1986**, p. 737.
[187] a) W. P. Griffith, A. J. P. White, D. J. Williams, *Polyhedron* **1996**, *15*, 2835-2839; b) E. Voisin, T. Maris, J. D. Wuest, *Cryst. Growtth Des.* **2007**, *8*, 308-

318; c) T. Tu, T. Maris, J. D. Wuest, *Cryst. Growtth Des.* **2008**, *8*, 1541-1546; d) W. Clegg, A. J. Scott, F. J. Lawlor, N. C. Norman, T. B. Marder, C. Dai, P. Nguyen, *Acta Crystallogr. Sect. C* **1998**, *54*, 1875-1880; e) J. A. Mosseler, J. A. Melanson, E. G. Bowes, G. M. Lee, C. M. Vogels, F. J. Baerlocher, A. Decken, S. A. Westcott, *J. Mol. Struct.* **2011**, *1002*, 24-27.

[188] a) R. J. Gillespie, I. Bytheway, E. A. Robinson, *Inorg. Chem.* **1998**, *37*, 2811-2825; b) Z. Xu, C. Zhao, Z. Lin, *J. Chem. Soc., Perk. Trans. 2* **2000**, 2319-2323; c) N. Narasimhamurthy, H. Manohar, A. G. Samuelson, J. Chandrasekhar, *J. Am. Chem. Soc.* **1990**, *112*, 2937-2941; d) N. C. Norman, A. G. Orpen, M. J. Quayle, E. G. Robins, *Acta Crystallogr. Sect. C* **2000**, *56*, 50-52.

[189] S. S. Batsanov, *Inorg. Mater.*, *37*, 871-885.

[190] R. Goddard, C. M. Niemeyer, M. T. Reetz, *Acta Crystallogr. Sect. C* **1993**, *49*, 402-404.

[191] a) J. Barthel, R. Buestrich, E. Carl, H. J. Gores, *J. Electrochem. Soc.* **1996**, *143*, 3572-3575; b) M. Finkelstein, E. A. Mayeda, S. D. Ross, *J. Org. Chem.* **1975**, *40*, 804-805; c) V. Prakash Reddy, M. Blanco, R. Bugga, *J. Power Sources* **2014**, *247*, 813-820; d) U. Heider, US2001/0033964A1, **2001**.

[192] in *A Guide to Conductivity Measurement* (Ed.: Mettler-Toledo), Schwerzenbach, **2013**, p. 25.

[193] a) A. Bianchi, K. Bowman-James, E. García-España, *Supramolecular Chemistry of Anions*, Wiley-VCH, New York, **1997**; b) K. Bowman-James, *Acc. Chem. Res.* **2005**, *38*, 671-678; c) N. H. Evans, P. D. Beer, *Angew. Chem. Int. Ed.* **2014**, *53*, 11716-11754.

[194] A. E. Hargrove, S. Nieto, T. Zhang, J. L. Sessler, E. V. Anslyn, *Chem. Rev.* **2011**, *111*, 6603-6782.

[195] C. F. Mason, *Biology of Freshwater Pollution*, Longman, New York, **1991**.

[196] A. J. P. Smolders, E. C. H. E. T. Lucassen, R. Bobbink, J. G. M. Roelofs, L. P. M. Lamers, *Biogeochemistry* **2010**, *98*, 1-7.

[197] N. Benjamin, *Ann. Zootech.* **2000**, *49*, 207-216.

[198] a) A. J. Wolfe, *Microbiol. Mol. Biol. Rev.* **2005**, *69*, 12-50; b) A. J. Wolfe, *J. Bacteriol.* **2008**, *190*, 5735-5737.

[199] M. Hannuksela, T. Haahtela, *Allergy* **1987**, *42*, 561-575.

[200] a) J. R. Aranzaes, C. Belin, D. Astruc, *Angew. Chem. Int. Ed.* **2006**, *45*, 132-136; b) P. D. Beer, A. R. Graydon, A. O. M. Johnson, D. K. Smith, *Inorg. Chem.* **1997**, *36*, 2112-2118; c) Y. Willener, K. M. Joly, C. J. Moody, J. H. R. Tucker, *J. Org. Chem.* **2008**, *73*, 1225-1233; d) V. Amendola, M. Boiocchi, B. Colasson, L. Fabbrizzi, E. Monzani, M. J. Douton-Rodriguez, C. Spadini, *Inorg. Chem.* **2008**, *47*, 4808-4816.

[201] a) B. Schazmann, N. Alhashimy, D. Diamond, *J. Am. Chem. Soc.* **2006**, *128*, 8607-8614; b) Z. Xu, N. J. Singh, J. Lim, J. Pan, H. N. Kim, S. Park, K. S. Kim, J. Yoon, *J. Am. Chem. Soc.* **2009**, *131*, 15528-15533; c) M. S. Vickers, K. S. Martindale, P. D. Beer, *J. Mater. Chem.* **2005**, *15*, 2784-2790; d) J. M. Engle, C. N. Carroll, D. W. Johnson, M. M. Haley, *Chemical Science* **2012**, *3*, 1105-1110; e) B. W. Tresca, L. N. Zakharov, C. N. Carroll, D. W. Johnson, M. M. Haley, *Chem. Commun.* **2013**, *49*, 7240-7242.

[202] a) F. Sancenón, R. Martínez-Máñez, M. A. Miranda, M.-J. Seguí, J. Soto, *Angew. Chem.* **2003**, *115*, 671-674; b) D. Jiménez, R. Martínez-Máñez, F. Sancenón, J. V. Ros-Lis, A. Benito, J. Soto, *J. Am. Chem. Soc.* **2003**, *125*, 9000-9001; c) S. Sole, F. P. Gabbai, *Chem. Commun.* **2004**, 1284-1285; d) F.

Sancenón, R. Martínez-Máñez, M. A. Miranda, M.-J. Seguí, J. Soto, *Angew. Chem. Int. Ed.* **2003**, *42*, 647-650; e) K. N. Farrugia, D. Makuc, A. Podborska, K. Szacilowski, J. Plavec, D. C. Magri, *Org. Biomol. Chem.* **2015**, *13*, 1662-1672.
[203] D. Curiel, A. Cowley, P. D. Beer, *Chem. Commun.* **2005**, 236-238.
[204] T. H. Kwon, K.-S. Jeong, *Tetrahedron Lett.* **2006**, *47*, 8539-8541.
[205] P. D. Beer, A. R. Graydon, L. R. Sutton, *Polyhedron* **1996**, *15*, 2457-2461.
[206] B. H. M. Snellink-Ruël, M. M. G. Antonisse, J. F. J. Engbersen, P. Timmerman, D. N. Reinhoudt, *Eur. J. Org. Chem.* **2000**, *2000*, 165-170.
[207] V. Král, H. Furuta, K. Shreder, V. Lynch, J. L. Sessler, *J. Am. Chem. Soc.* **1996**, *118*, 1595-1607.
[208] K. Choi, A. D. Hamilton, *Angew. Chem. Int. Ed.* **2001**, *40*, 3912-3915.
[209] a) K. Choi, A. D. Hamilton, *J. Am. Chem. Soc.* **2001**, *123*, 2456-2457; b) K. Choi, A. D. Hamilton, *J. Am. Chem. Soc.* **2003**, *125*, 10241-10249.
[210] S. P. Mahanta, B. S. Kumar, P. K. Panda, *Chem. Commun.* **2011**, *47*, 4496-4498.
[211] M. J. Langton, P. D. Beer, *Chem. Commun.* **2014**, *50*, 8124-8127.
[212] M. J. Langton, P. D. Beer, *Chem. Eur. J.* **2012**, *18*, 14406-14412.
[213] M. J. Langton, L. C. Duckworth, P. D. Beer, *Chem. Commun.* **2013**, *49*, 8608-8610.
[214] K. Worm, F. P. Schmidtchen, A. Schier, A. Schäfer, M. Hesse, *Angew. Chem. Int. Ed.* **1994**, *33*, 327-329.
[215] G. T. Spence, C. Chan, F. Szemes, P. D. Beer, *Dalton Trans.* **2012**, *41*, 13474-13485.
[216] W. T. Gong, B. Gao, S. Bao, J. W. Ye, G. L. Ning, *J. Incl. Phenom. Macrocycl. Chem.* **2012**, *72*, 481-486.
[217] D. M. Rudkevich, W. Verboom, Z. Brzozka, M. J. Palys, W. P. R. V. Stauthamer, G. J. van Hummel, S. M. Franken, S. Harkema, J. F. J. Engbersen, D. N. Reinhoudt, *J. Am. Chem. Soc.* **1994**, *116*, 4341-4351.
[218] a) X. Yang, C. B. Knobler, M. F. Hawthorne, *J. Am. Chem. Soc.* **1992**, *114*, 380-382; b) J. D. Wuest, B. Zacharie, *Organometallics* **1985**, *4*, 410-411.
[219] A. A. Zinn, C. B. Knobler, D. E. Harwell, M. F. Hawthorne, *Inorg. Chem.* **1999**, *38*, 2227-2230.
[220] a) D. W. Stephan, *J. Am. Chem. Soc.* **2015**, *137*, 10018-10032; b) D. W. Stephan, G. Erker, *Angew. Chem. Int. Ed.* **2015**, *54*, 6400-6441.
[221] T. W. Hudnall, F. P. Gabbaï, *J. Am. Chem. Soc.* **2007**, *129*, 11978-11986.
[222] R. Tirfoin, S. Aldridge, *Dalton Trans.* **2013**, *42*, 12836-12839.
[223] a) H. E. Katz, *J. Am. Chem. Soc.* **1985**, *107*, 1420-1421; b) H. E. Katz, *Organometallics* **1987**, *6*, 1134-1136; c) H. E. Katz, *J. Org. Chem.* **1985**, *50*, 5027-5032.
[224] M. Melaimi, F. P. Gabbaï, *J. Am. Chem. Soc.* **2005**, *127*, 9680-9681.
[225] H. Zhao, F. P. Gabbaï, *Nat. Chem.* **2010**, *2*, 984-990.
[226] W. Uhl, T. Spies, W. Saak, *Z. Anorg. Allg. Chem.* **1999**, *625*, 2095-2102.
[227] W. Uhl, T. Spies, W. Saak, *Eur. J. Inorg. Chem.* **1998**, *1998*, 1661-1665.
[228] W. Uhl, F. Hannemann, W. Saak, R. Wartchow, *Eur. J. Inorg. Chem.* **1998**, *1998*, 921-926.
[229] a) L. Fielding, *Tetrahedron* **2000**, *56*, 6151-6170; b) V. M. S. Gil, N. C. Oliveira, *J. Chem. Educ.* **1990**, *67*, 473.
[230] M. J. Hynes, *J. Chem. Soc., Dalton Trans.* **1993**, 311-312.

[231] W. Strojek, C. M. Fehse, H. Eckert, B. Ewald, R. Kniep, *Solid State Nucl. Magn. Reson.* **2007**, *32*, 89-98.
[232] M. J. Duer, *Solid State NMR Spectroscopy*, Wiley-Blackwell, **2008**.
[233] a) M. Pollard, K. Klimke, R. Graf, H. W. Spiess, M. Wilhelm, O. Sperber, C. Piel, W. Kaminsky, *Macromolecules* **2004**, *37*, 813-825; b) D. Olčák, V. Hronský, O. Fričová, M. Kovaľaková, P. Duranka, I. Chodák, *Journal of Polymer Research* **2013**, *20*, 1-9.
[234] R. K. Sharma, J. L. Fry, *J. Org. Chem.* **1983**, *48*, 2112-2114.
[235] C. Rijksen, L. Ott, K. Sievert, J. Harloff, A. Schulz, S. Ellinger, WO, **2014**.
[236] a) D. Cao, H. Zhao, F. P. Gabbai, *New J. Chem.* **2011**, *35*, 2299-2305; b) S. Aldridge, C. Bresner, I. A. Fallis, S. J. Coles, M. B. Hursthouse, *Chem. Commun.* **2002**, 740-741; c) K. M. K. Swamy, Y. J. Lee, H. N. Lee, J. Chun, Y. Kim, S.-J. Kim, J. Yoon, *J. Org. Chem.* **2006**, *71*, 8626-8628; d) S. Yamaguchi, S. Akiyama, K. Tamao, *J. Am. Chem. Soc.* **2001**, *123*, 11372-11375.
[237] a) C. Bresner, J. K. Day, N. D. Coombs, I. A. Fallis, S. Aldridge, S. J. Coles, M. B. Hursthouse, *Dalton Trans.* **2006**, 3660-3667; b) C. Bresner, S. Aldridge, I. A. Fallis, C. Jones, L.-L. Ooi, *Angew. Chem. Int. Ed.* **2005**, *44*, 3606-3609.
[238] H. Yamaguchi, H. Takahashi, M. Kato, J. Arai, *J. Electrochem. Soc.* **2003**, *150*, A312-A315.
[239] a) N. V. V. S. S. Raman, A. V. S. S. Prasad, K. Ratnakar Reddy, K. Ramakrishna, *J. Phsrm. Anal.* **2012**, *2*, 314-318; b) C. Lee, R. Helmy, C. Strulson, J. Plewa, E. Kolodziej, V. Antonucci, B. Mao, C. J. Welch, Z. Ge, M. A. Al-Sayah, *Org. Process Res. Dev.* **2010**, *14*, 1021-1026.
[240] a) J. V. Gavette, N. S. Mills, L. N. Zakharov, C. A. Johnson, D. W. Johnson, M. M. Haley, *Angew. Chem. Int. Ed.* **2013**, *52*, 10270-10274; b) J. H. Lee, J. Park, M. S. Lah, J. Chin, J.-I. Hong, *Org. Lett.* **2007**, *9*, 3729-3731; c) W.-X. Liu, Y.-B. Jiang, *J. Org. Chem.* **2008**, *73*, 1124-1127; d) A. Ojida, I. Takashima, T. Kohira, H. Nonaka, I. Hamachi, *J. Am. Chem. Soc.* **2008**, *130*, 12095-12101.
[241] a) J. L. Sessler, E. Katayev, G. D. Pantos, Y. A. Ustynyuk, *Chem. Commun.* **2004**, 1276-1277; b) S. K. Kim, D. Seo, S. J. Han, G. Son, I.-J. Lee, C. Lee, K. D. Lee, J. Yoon, *Tetrahedron* **2008**, *64*, 6402-6405.
[242] F. Chu, L. S. Flatt, E. V. Anslyn, *J. Am. Chem. Soc.* **1994**, *116*, 4194-4204.
[243] Y. Kubo, M. Kato, Y. Misawa, S. Tokita, *Tetrahedron Lett.* **2004**, *45*, 3769-3773.
[244] J. Lehr, T. Lang, O. A. Blackburn, T. A. Barendt, S. Faulkner, J. J. Davis, P. D. Beer, *Chem. Eur. J.* **2013**, *19*, 15898-15906.
[245] K. Ariga, E. V. Anslyn, *J. Org. Chem.* **1992**, *57*, 417-419.
[246] a) H. Maeda, Y. Ito, *Inorg. Chem.* **2006**, *45*, 8205-8210; b) S.-i. Kondo, T. Suzuki, Y. Yano, *Tetrahedron Lett.* **2002**, *43*, 7059-7061; c) C. Caltagirone, A. Mulas, F. Isaia, V. Lippolis, P. A. Gale, M. E. Light, *Chem. Commun.* **2009**, 6279-6281; d) F.-Y. Wu, Z. Li, L. Guo, X. Wang, M.-H. Lin, Y.-F. Zhao, Y.-B. Jiang, *Org. Biomol. Chem.* **2006**, *4*, 624-630.
[247] W. Huang, H. Lin, H. Lin, *Sens. Actuators, B* **2011**, *153*, 404-408.
[248] M. Schnopp, S. Ernst, G. Haberhauer, *Eur. J. Org. Chem.* **2009**, *2009*, 213-222.

[249] a) M. J. Chmielewski, J. Jurczak, *Chem. Eur. J.* **2005**, *11*, 6080-6094; b) H. A. Jeong, E. J. Cho, H. M. Yeo, B. J. Ryu, K. C. Nam, *Bull. Korean. Chem. Soc.* **2007**, *28*, 851-854.
[250] K. Ghosh, I. Saha, A. Patra, *Tetrahedron Lett.* **2009**, *50*, 2392-2397.
[251] a) M. J. Chmielewski, J. Jurczak, *Chem. Eur. J.* **2006**, *12*, 7652-7667; b) M. J. Langton, O. A. Blackburn, T. Lang, S. Faulkner, P. D. Beer, *Angew. Chem. Int. Ed.* **2014**, *53*, 11463-11466.
[252] N. G. White, H. G. Lovett, P. D. Beer, *RSC Adv.* **2014**, *4*, 12133-12147.
[253] D. P. Cormode, S. S. Murray, A. R. Cowley, P. D. Beer, *Dalton Trans.* **2006**, 5135-5140.
[254] ASTM G99-05, **2010**.
[255] ASTM D4172-94, **2016**.
[256] B. Wilson, *Ind. Lubr. Tribol.* **1996**, *48*, 10-14.
[257] G. Knothe, *Lubr. Sci.* **2008**, *20*, 35-45.
[258] a) ISO 12156-1, **2016**; b) ASTM D6079-99, **2000**.
[259] Y. F. Suen, EP2643440, **2013**.
[260] M. R. Grimbley, R. S. Lehrle, *Polym. Degrad. Stabil.* **1995**, *48*, 441-455.